2008

SPATIAL VARIABILITY IN FOREST FUELS: SIMULATION MODELING AND EFFECTS ON FIRE BEHAVIOR

Russell Andrew Parsons
The University of Montana

SPATIAL VARIABILITY IN FOREST FUELS: SIMULATION MODELING AND EFFECTS ON FIRE BEHAVIOR

By

Russell Andrew Parsons

B.S., University of California, Berkeley, 1992
M.S., University of Idaho, Moscow, 1999

Dissertation

presented in partial fulfillment of the requirements
for the degree of

Doctor of Philosophy
in Forestry

The University of Montana
Missoula, MT

Autumn 2007

Approved by:

Dr. David A. Strobel, Dean
Graduate School

Dr. Ronald H. Wakimoto,Chair
Department of Ecosystem & Conservation Sciences

Dr. Hans Zuuring
Department of Forest Management

Dr. Jesse V. Johnson
Department of Computer Science

Dr. Rodman R. Linn
Los Alamos National Laboratory
Division of Environmental Sciences

Dr. Elizabeth Reinhardt
Affiliate faculty, College of Forestry and Conservation
USDA Forest Service
Fire Sciences Laboratory

Parsons, Russell, Ph.D., Autumn 2007, Forestry

SPATIAL VARIABILITY IN FOREST FUELS: SIMULATION MODELING AND EFFECTS ON FIRE BEHAVIOR

Chair: Dr. Ronald H. Wakimoto

Abstract:
Forests in the western United States and elsewhere face a growing crisis arising from global warming, changes in fuel beds and an increasing human population. Fire management policy emphasizes fuel treatments, such as thinning and prescribed burning, to remedy this situation because fuels are the one component of the problem that we can directly affect through management action. At present, however, the tools we have for the evaluation of fuel treatments are inadequate because they do not describe the fuel bed, or effects of modifications to the fuel bed on fire behavior in sufficient detail. The work described here presents a system that has potential to address the shortcomings of current approaches. In the first chapter, to improve our ability to represent wildland fuels, a three dimensional spatially explicit fuel model, FUEL3D, is presented which represents fuels at a level of detail comparable to what we can actually measure: stands as collections of individual trees, with branches and foliage. In conjunction with new, physical fire models, detailed fire behavior simulations can be carried out using fuels represented with FUEL3D as inputs. This system thus comprises a simulation laboratory which will greatly enhance our capabilities to evaluate fuel treatments and strengthen our understanding of fire and fuel interactions.

In the second chapter, this system is demonstrated in an exploratory simulation study which examines the impact of spatial variability within an individual tree crown on fire behavior. Results demonstrate that the distribution of fuel within a tree crown significantly affects the rate of fuel consumption, as well as the timing, duration and magnitude of heat produced. This suggests that modeling of both crown fire initiation and propagation would benefit from more detailed description of crown fuels.

In third chapter a replicated series of stand scale fire simulations is carried out to examine variability in forward spread rate; accelerated spread rates endanger fire fighters. Substantial variability is observed to arise from fine scale fuel-atmosphere-fire interactions which are not easily predicted beforehand. A new strategy is proposed in which physical fire models are used to quantify the potential drivers of variability in fire behavior.

DEDICATION

I dedicate this dissertation to my parents, Tory Parsons, and Noelle and Ron Anderson, who always encouraged me to follow my passions and strive for new heights, to my wife, Shannon, who has been there for me throughout this long journey, and without whom I certainly could not have persevered, and to my children, Leila and Claire, who have saved (and threatened) my sanity on countless occasions.

ACKNOWLEDGEMENTS

I will always be grateful for the depth and breadth of support that I have received from the USDA Forest Service, Fire Sciences Laboratory throughout my doctoral studies. Over the course of this period I have had many interactions and discussions with a great many people at the Fire Lab. As my mentor, Bob Keane has been a constant source of inspiration and has challenged me to grow professionally in many ways. I will forever be in his debt. Elizabeth Reinhardt, Jim Reardon, Mick Harrington, Emily Heyerdahl, Mark Finney, Jack Cohen, Matt Jolly and Colin Hardy have all taught me different aspects of what it means to be a scientist. Many others assisted me in field work and data entry: Wayne Langholm, Laurie Dickenson, Curtis Johnson, Aaron Wilson, Greg Cohn, Violet Holley. Karen Iverson, Wendy Zarbolias, Trina Kreyenhagen and Jan Bixler all helped to somehow keep me in order administratively.

At the University of Montana I am deeply appreciative of the commitment and interest my committee members have shown me. During the first two years of my doctoral studies, I spent much of my time at the computer science department, where Jesse Johnson's intense instruction and deeply sincere interest in his students changed the way I think and greatly expanded my skills. Hans Zuuring and Ron Wakimoto both gave me stalwart support and provided very helpful advice on many occasions. Their interest in my work has helped motivate me. Elizabeth Reinhardt provided data, advice and challenged me to think in new directions. From Rod Linn I have learned to think about wildland fire in a completely different way than I had thought before. His support was critical to the success of this undertaking. To all these, and to those I may not have listed, please know that I am deeply grateful for your help.

TABLE OF CONTENTS

LIST OF TABLES

LIST OF FIGURES

CHAPTER I : FUEL3D, A SPATIALLY EXPLICIT FUEL MODEL

ABSTRACT

Forests in the western United States and elsewhere face a growing crisis arising from global warming, changes in fuel beds and an increasing human population. Fire management policy emphasizes fuel treatments, such as thinning and prescribed burning, to remedy this situation because fuels are the one component of the problem that we can directly affect through management action. At present, however, the tools we have for the evaluation of fuel treatments are inadequate because they do not describe the fuel bed, or effects of modifications to the fuel bed on fire behavior in sufficient detail. The work described here presents a system that has potential to address the shortcomings of current approaches. To improve our ability to represent wildland fuels, a three dimensional spatially explicit fuel model, FUEL3D, is presented. Using standard forest inventory data as inputs, this model is designed to represent fuels at a level of detail comparable to what we can actually measure: stands as collections of individual trees, with branches and foliage. A key component of the model is that, in conjunction with new, physical fire models, detailed fire behavior simulations can be carried out using fuels represented with FUEL3D as inputs. This system thus comprises a simulation laboratory which will greatly enhance our capabilities to evaluate fuel treatments and strengthen our understand of fire and fuel interactions.

INTRODUCTION

Background

In many parts of the western United States, forests are in a state of crisis. Nearly every year this decade so far (2000, 2002, 2003, 2004, 2005, 2006, and 2007) has been characterized by large and catastrophic fires in which the number of acres burned, and associated economic and environmental impacts, are unprecedented in recent history (Graham et al 2004, Westerling et al 2006, Robichaud et al 2003, Pierce et al 2004, GAO 2007). The size and intensity of these fires has stretched fire fighting resources and budgets to their limits and has compromised the ability of federal agencies to carry out their other responsibilities (GAO 2007, GAO 2004). These increases in area burned and burn severity reflect both the climatic influences of global warming, such as earlier snowmelt and hotter summer temperatures (IPCC 2007, Westerling et al. 2006), and changes in the nature, composition and condition of wildlands, such as increased forest density and fuel continuity (Covington and Moore 1994, Graham et al 2004). The magnitude and drivers of changes in fuels vary with location and vegetation type (Graham et al 2004) but generally have come about as a result of different factors, including management suppression of fires, effects of past land use such as grazing (Heyerdahl et al 2006), as well as a diminished influence of native American ignitions on the landscape in some areas (Pyne 1982, Lewis 1985, Arno 1985).

This crisis is expected to get worse as time progresses, for several reasons. Climate models predict continuing trends of higher temperatures and more persistent drought

conditions, leading to longer fire seasons, characterized by larger and more intense fires (Westerling et al 2006, Gillet et al 2004, Wotton and Flannigan 1993, Flannigan et al 2005). Because CO_2 released by forest fires accumulates in the atmosphere, increases in area burned may accelerate global warming, resulting in yet more area burned (Running 2006). Similarly, increases in incidence and severity of insect attacks associated with warmer climate are expected to make forests more susceptible to fire (Fleming and Candau 1998, Fleming et al 2002). At the same time, a rapidly growing Wildland Urban Interface, or WUI (a mixture of housing and wildland vegetation) translates to increasing risk to life and property, as well as increased fire suppression costs (GAO 2007), as more and more houses face potential destruction from fire (Radeloff et al 2005, Hammer et al 2007). The juxtaposition of global warming, changes in fuels and increasing population density in wildland areas represents a growing fire management crisis which will likely dominate federal agency policy and expenditures for the foreseeable future (GAO 2007). In an arena in which the stakes are high, and time is short, there is a desperate need for accurate information to aid fire managers in strategic decision-making.

Decades of on the ground fire management and related fire research have established a strong knowledge base about wildland fire (Agee 1993). Fundamentally, the behavior of wildland fire is determined by three main factors, often referred to as the 'fire behavior triangle', consisting of weather, terrain, and fuel, all of which influence fire behavior in multiple ways. The occurrence of large fires and the total area burned is driven primarily by climate, such as drought (Strauss 1989, Swetnam and Betancourt 1990, Westerling et al 2006, Gillet et al 2004, Cary et al 2006). Terrain modifies climate (such as differences

in solar radiation by aspect) as well as fire behavior (such as preheating of fuels upslope of a fire). However, current fire management strategies and policy emphasize modification of the fuels, through fuel treatments such as thinning and prescribed burning, because fuels are the only component of the problem that can be addressed directly through management action (Graham et al 2004).

While fuel treatments may be the only component we can affect directly, they are not without limitations. Short of permanent conversion to a non-flammable surface (i.e. pavement), modification of fuel beds does not prevent fire from occurring (Graham et al. 2004, Finney and Cohen 2003). Fuel treatments may not have much effect under extreme weather conditions (Finney and Cohen 2003). However, empirical evidence and qualitative observation suggest that, under some range of conditions, fuel modification can significantly change *how* fires burn, by reducing either the amount of fuel, or the continuity within the fuel bed (Graham et al 1999, Graham et al 2004). For example, reduction in the quantity of surface fuels, such as needles and dead fine woody fuels on the forest floor, has been shown to reduce fire intensity (heat released over area and time) (Weaver 1955, Cooper 1960, Biswell 1960). Similarly, the potential for crown fire (fires which burn through the tree crowns) can be reduced through elimination of ladder fuels (small such as small trees and shrubs which vertically connect surface fuels and the base of the foliage canopy), and by thinning, which reduces both horizontal continuity and quantity of crown fuels (Van Wagner 1977, Graham et al 1999, Scott and Reinhardt 2001). Fuel treatments thus comprise a suite of different alternative actions which can be employed to modify how fires burn.

In many locations there is a compelling need for fuel treatments, and large scale fuel treatment projects are already underway in different parts of the country. At present, however, three key knowledge gaps limit our ability to reliably and quantitatively predict the effect that a given fuel treatment will have on fire behavior. First, we lack a detailed understanding of fine scale fire and fuel interactions. The propagation of fire is a fundamentally fine scale, spatial process, dependent on the size, shape, composition and arrangement of fuel particles (Burrows 2001) and, particularly, distance between fuel particles (Fons 1946, Vogel and Williams 1970, Weber 1990, Bradstock and Gill 1993). Wildland fuels are spatially clumped at multiple scales, with gaps between needles, between branches and between trees. At present we have no way of either adequately describing these properties of real fuels, or accounting for the potential effects of these properties on how fire spreads through a natural fuel bed. This in turn leads to our second knowledge gap: threshold behaviors. Fire spread through trees and shrubs is characterized by abrupt thresholds in fire behavior (Cohen et al 2006), where a surface fire may rapidly grow to a crown fire, or, vice versa, in the space of a few meters and within a several seconds. The nature and drivers of these thresholds are not well understood. Finally, fuel treatments such as thinning can be expected to modify the microclimate in a given site, changing the solar radiation regime on the forest floor and within the stand (Reifsnyder and Lull 1965, North 1996; Govaerts and Verstraete,1998) and the interception of rain by the canopy (Helvey and Patric 1965), both of which influence fuel moisture (Fosberg and Deeming, 1971; Nelson 2002). The canopy structure also influences winds within a stand (Jensen 1983, Oke 1978, Brandle 1984). These changes likely represent important

potential feedback relationships between fire and fuel which complicate fuel treatment assessments. For example, is the reduction in fuel continuity achieved with a particular thinning strategy compensated for by an increased effective wind speed and drier surface fuels within that stand? At present we do not have the tools to address these issues.

Fuel treatments must generally be implemented at one time, and actually tested (by a wildfire passing through or near them) at a different time. As substantial resources must be committed to carry out fuel treatments, and conditions at the time the treated area burns are unknown, fuel treatment assessments rely heavily on predictions from computer models. The accuracy of predictions from such models is dependent on the detail with which they represent the main components of the problem, namely, wildland fuels and their interactions with fire.

The architecture and scope of current management tools used in the United States to predict fire behavior, such as BehavePlus (Andrews 2005) and FARSITE (Finney 1998) , limits the degree to which they can be used to assess these issues. These models assume that fuels are homogeneous and continuous and are thus intrinsically inappropriate for dealing with the potential effects of spatial variability within the fuel bed on fire behavior. Fuel treatments can only be assessed with such models as a comparison of average conditions (e.g. Van Wagtendonk 1996). This is problematic because the complex and dynamic nature of fire-fuel and fire-atmosphere interactions may result in cases in which the average conditions either do not actually occur (such as mean crown base height in a two storied tree stand) or do not result in average fire behavior.

In recent years more advanced physics-based, numerical fire behavior models have emerged such as FIRETEC (Linn et al 2002, Linn and Cunningham 2005), and the Wildland Fire Dynamic Simulator (WFDS) (Mell et al.2005). Unlike current operational models, which assume a stead state rate of fire spread (Rothermel 1972), these models are self-determining and are thus capable of addressing fire-fuel interactions arising from spatial variability within the fuel bed, and fire-atmosphere interactions. The detail with which these models address fundamental drivers of fire behavior, as well as the underlying physics basis of the models, facilitates robust modeling of fire behavior and related analyses of fuel treatments at multiple scales.

One of the key limitations in the application of these models is that they require fine scale spatially explicit fuels inputs which are difficult to directly measure in the field, such as 3-D cells describing the distribution of fuel within a tree. While the fire behavior models are very sophisticated in their treatment of the physics of fire spread and heat transfer, fuels information for wildland fuels of commensurate detail is extremely rare or non-existent. At present no procedures exist by which fuels data measured in the field can be used to develop these inputs or test the accuracy with which fuels are represented. Perhaps even more importantly, no tool exists by which the fundamental properties of wildland fuels can be assessed, quantified and evaluated as to their importance across a range of spatial scales. Wildland fire science will not be able to take full advantage of the advancements that have been made in fire modeling until these knowledge gaps are addressed.

The objective of this endeavor is to develop a spatially explicit fuel model, FUEL3D, which can be used to better describe the complexities of wildland fuels than current fuel models, and, in conjunction with detailed fire behavior models, to improve our understanding of fundamental fire and fuel interactions.

Theoretical background

Spatially explicit models of trees and shrubs have been developed with different levels of detail. The most common applications of such models are light dynamics and plant growth models (see Brunner 1998 and Busing and Mailly 2004 for reviews of several such models, respectively). A common approach is to represent trees and shrubs crowns as simple geometric forms, such as cylinders, cones or ellipsoids (e.g. Canham et al. 1999, Kuuluvainen and Pukkala.1987, Pukkala et al. 1993). Such representations are limited to particular scales because detail within the tree crown is not modeled. A much more accurate approach represents plants as fractal objects (Mandelbrot 1983, Godin 2000) and model plant architecture in detail, sometimes extending as far as individual branches, twigs and leaves (Berezovskava et al. 1997, Ozier-Lafontaine et al 1999, Richardson and zu Dohna 2003, Godin et al 2004). Such approaches are particularly relevant to representation of canopy fuels because they successfully capture the natural pattern of clumps of fuel separated by gaps, such as those between needles and between branches.

The capacity to branch out and occupy space is a defining characteristic of vascular plants which tends to represent an optimization in which photosynthesis is maximized while constraints such as mechanical support (Morgan and Cannell 1988, McMahon

1973, McMahon and Kronauer 1976) and hydrodynamic resistance (Tyree and Ewers 1991) are minimized (Niklas and Kerchner 1984, West et al. 1997, West et al. 1999). As different species occupy different ecological niches and thus face different sets of constraints, there is no single universal optimum. Nevertheless, the vast majority of species can be classified into a surprisingly small number of plant architectural forms (Halle and Oldemann 1970, Halle et al 1978). These commonalities suggest that despite the diversity of conditions in which plants are found they are obligated to observe the same general set of "rules" governing their form and function.

The pipe model theory theory (Shinozaki et al 1964) is the first broad theory which attempts to explain these "rules" of plant structure and function. It is a conceptual model of plant structure in which trees are envisioned as a collection of "unit pipes", where a unit pipe transports water to a unit of foliage. This proportional relationship based on the functional balance between water supply and demand provides for a straightforward and generally accurate estimation of biomass quantities; for this reason, despite criticism of its simplistic portrayal of plant function such as hydrodynamics (Tyree and Ewers 1991) the pipe model plays a key role in numerous contemporary forest models and is widely cited in the literature (Grace 1997).

One of the main "rules" that plants seem to have to follow is that fundamental properties of both their structure and function are governed by size. Plant size influences nearly all biological functions, controlling rates of metabolism, reproduction and many other functions (Peters 1983). Such size dependent relationships can be described mathematically with allometric scaling relationships of the form

$$M = aD^b$$

Eqn. 1- 1

where M is the biomass, D is basal diameter (a dimensional measurement which relates to size), a is an empirical scaling constant and b is the scaling exponent (Huxley 1932). While allometric equations can be successfully fit to data for nearly all species, in general an explanation of why this was the case has been lacking.

In recent years, the WBE model (West et al. 1997, West et al. 1999, Enquist 2002) has emerged as a comprehensive theory attempting to explain why allometric scaling relationships exist and the role they play in the structure and function of living things. The WBE model proposes that quarter power based (i.e. 3 / 4, 3 / 8) allometric scaling relationships, which have been broadly observed across species(Niklas and Enquist 2001, Cheng and Niklas 2007), can be explained by the hierarchical, fractal-like, space-filling branching networks which minimize the energy and material costs and hydrodynamic resistance associated with transport within the network.

The WBE model has been criticized on the grounds that allometric exponents observed in many cases do not appear to conform to the universal quarter power scaling relationships predicted (White et al 2007, Kozlowski and Konarzewski 2004 Agutter and Wheatley 2004, Li et al. 2005). It has also been criticized because the allometric scaling relationships described do not necessarily have to arise because of the assumptions made by the WBE model, but can be shown to be simply intrinsic properties of systems in which materials must be distributed in space (Banavar 1999, Banavar et al 2002 ,Dreyer

2001). If these latter arguments are correct, then the quarter power scaling relationships represent an ideal case in which no further constraints impede the efficiency of the network. This is likely the case in non living systems such as rivers (Leopold 1971). It seems likely though that, in living systems such as vascular plants, departures from the ideal case can be explained as a loss in efficiency of branching resulting from some constraint imposed on the system. Perhaps the true value of the WBE model is that it is capable of suggesting an explanation for those cases in which allometric relationships do not conform to its predictions.

Makela and Valentine(2006) combined elements of the pipe model with elements of the WBE model, with modifications, to address some of the ways in which allometric scaling relationships for trees do not strictly conform to the predictions of the WBE model. They demonstrated that allometric scaling relationships are dependent not just on the total woody biomass, as stated in the WBE model, but also on the crown ratio, which measures the length of the contiguous live crown relative to the total tree height:

$$M_f \propto \left(R^2 M_T\right)^{z/(za+1)}$$

Eqn. 1- 2

where M_f is total foliar biomass, R is the crown ratio, M_T is total woody biomass, z is the fractal dimension, and *a* is a parameter describing change in the sum cross sectional area throughout the branching structure of the crown. When z = 3 and *a* = 1, the scaling relationship reduces to the 3 / 4 scaling predicted by the WBE model. The inclusion of

the fractal dimension of the crown, z, accounts for the cavity which arises in the interior of the crown due to self-shading, while the parameter *a* accounts for accumulation of non-conducting heartwood in the stem and coarse branches, which change the cross sectional area. Since the crown ratio is influenced by the growth history of the tree, the scaling relationships that arise are not universal but variable and context dependent. An important outcome of their approach is that the fractal-like properties of the tree do not apply to the stem below the base of the live crown because the length of the stem below the crown base is not necessarily proportional to the total length, but rather, determined by the crown ratio, R, which is dependent on the growth history of the tree. For this reason the stem below the crown base is dealt with separately from the tree above the crown base.

The underlying theory behind the FUEL3D model derives from the pipe model, the WBE model and the work of Makela and Valentine 2006. However, all three of these sources are theoretical and general in nature and therefore do not actually attempt to model biomass realistically in space. To bridge the gaps between general aspatial theory and spatially explicit distribution of biomass in three dimensions FUEL3D must necessarily traverse many aspects of plant structure which are not explicitly dealt with by the theoretical models listed above. Chief among these are specific geometry, variability in form and architecture, and the challenge of incorporation of field measurable inputs into the model. The manner in which FUEL3D addresses these issues is driven largely by the intended concept and scope of the model, discussed below.

MODEL DESCRIPTION

Ancillary Materials

The development of the FUEL3D model comprises more material than fits easily within a single chapter. To enhance the readability of this chapter, a number of related components are presented in appendices, listed in the table below.

Table 1- 1 List of appendices related to the FUEL3D model.

Appendix	Content
A	List of symbols and their meaning, for the FUEL3D model
B	Analytical solution for the determination of the coefficients of the quadratic polynomial function describing the radius of the tree bole above the crown base as a tapering column.
C	Field and image processing based measurement of geometric parameters
D	Parameterization of the FUEL3D model for ponderosa pine

Model concept and scope

Trees are complex organisms. The growth of trees is determined by their interaction with their environment (availability of light, water and nutrients) and their immediate surroundings (competition with other trees etc) over time. Given this complexity, it is not surprising that computer modeling has played a key role in the advancement of our understanding of plant structure and function, and numerous plant architecture models exist which span a spectrum of detail. The most detailed plant architecture models are dynamic and explicitly deal with the response of trees to these environmental factors; due to their complexity and the long periods of time typically modeled they are often limited in the number of trees which can be modeled.

Although the processes of plant growth and change over time, and their interaction with the environment are clearly relevant to certain aspects of wildland fire science, such as

longer term fuel dynamics, these processes occur at broader time scales than are relevant to fire behavior, which typically occurs over time scales of a few seconds to several days, during which the structure of the fuel is reasonably constant. For this reason FUEL3D is not intended to study dynamic plant processes such as growth or response to the environment over time, but rather to simply provide a realistic static representation of the fuel that a fire might encounter at a particular moment in time. FUEL3D thus provides a compromise to the limitations of more complex plant architecture models by using an empirical, field data driven approach rather than a dynamic mechanistic approach. The chief purpose of the model is to provide a means by which the properties of biomass (living and dead) which constitute forest fuels can be quantitatively represented in three dimensional arrays, both to enhance our understanding of these properties and also as inputs to numerical fire behavior models or other models. There are several central requirements underlying the concept of the model. First, because the interactions of fire and fuels span a range of spatial scales from micrometers to hundreds of meters, the model must facilitate consideration of these properties across spatial scales. Second, as many key processes involved in fire and fuel interactions are not yet completely understood, as a research model, FUEL3D must provide a means of exploration of fundamental crown fuel properties by ensuring flexibility in the type and nature of fuels that can be modeled. Third, the model must be able to run with a relatively small list of inputs, of which the majority must be measurable in the field.

As the first three dimensional plant model developed explicitly for the purpose of modeling wildland fuels, FUEL3D is admittedly somewhat simplistic; it is expected that additional refinements will be implemented as time goes on.

Model Inputs

The model requires information at three levels: tree, species and site. A complete list of all symbols used in the model is presented in **Appendix A**. Specific values obtained for model parameterization are presented in **Appendix D**. Tree inputs are simply a list of one or more trees with commonly measured attributes, such as height, diameter at breast height and height to crown base. This tree list may come from forest inventory data or may itself be simulated. Species parameters largely describe the geometry and branching habit of trees. Measurements include angles, both between the main stem and lateral branches, and between branches in a branching node, as well as numbers and dimensions of child branch segments at branching nodes. These are more detailed measurements that are not typical of standard forest inventory, but it is expected that once collected the same general set of species parameters can be used to represent all trees of that species. Site parameters are a small set of inputs that allow the model to incorporate climatic influences and site productivity into biomass estimates. **Figure 1-1** presents an overview of the architecture of the model.

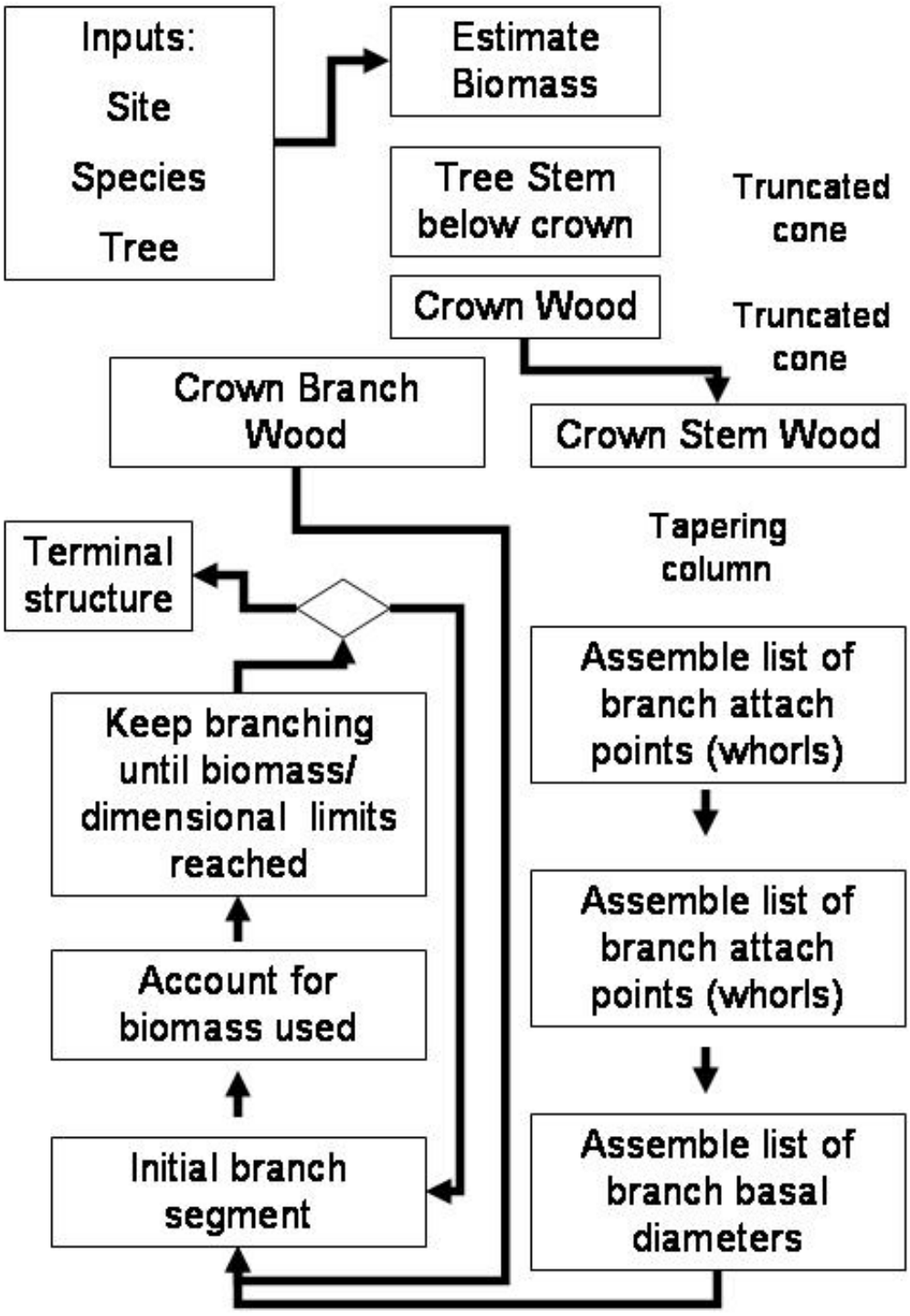

Figure 1- 1 Overview of the FUEL3D model

Model formulation

The process by which fuels are modeled in FUEL3D consists of three main steps. First biomass quantities are estimated using allometric relationships largely based on the work of Makela and Valentine (2006 REF). These quantities are then distributed in space according to fractal branching rules and species specific geometry parameters. The distributed quantities are then summarized to discrete volume cells for inputs to fire behavior models. Each of these processes is detailed below.

Biomass estimation

A small set of basic tree measurements are the main inputs: diameter at breast height D_1, where breast height, H_1, is 1.37m; the height to base of the contiguous live crown, H_2, the total tree height H_T, and a minimum diameter (**Figure 1-2**).

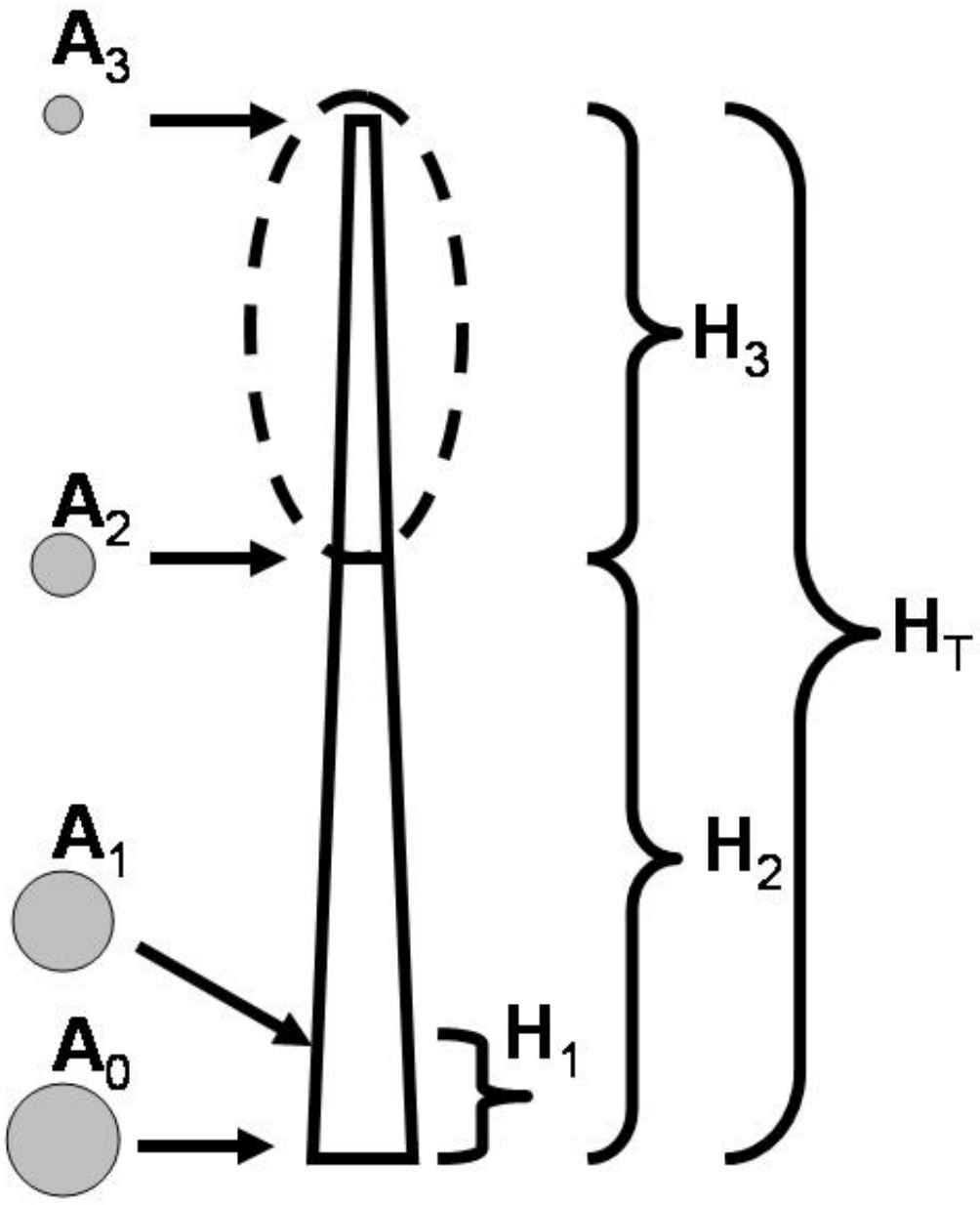

Figure 1- 2 Schematic diagram of a tree and symbols used in the model

From these tree measurements a few basic calculations are made. These include the crown length, H_3, the crown ratio, $_R$, and the cross sectional area at breast height, A_1:

$$H_3 = H_T - H_2$$

Eqn. 1- 3

$$R = \frac{H_3}{(H_T - H_1)}$$

Eqn. 1- 4 (Valentine et al. 1994)

$$A_1 = \pi(\frac{D_1}{2})^2$$

Eqn. 1- 5

Valentine et al. 1994 determined from analysis of tree stem taper (Gray 1956) that the cross sectional area at the base of the live crown, A_2, (**Figure 1-2**) can be reliably predicted by the simple relationship:

$$A_2 = A_1 R$$

Eqn. 1- 6

The stem below the crown presents a problem in the fractal modeling of the tree because the length of the stem below the crown base is not necessarily proportional to the total length, but rather, determined by the crown ratio, R, which is dependent on the growth history of the tree. For this reason, the stem below the crown base does not scale in a

manner consistent with the wood and foliage within the crown. Following Makela and Valentine 2006, FUEL3D assumes that the stem below the crown can be represented as a truncated cone. The cross sectional area of the base of the tree, A_0 is thus estimated as

$$A_0 = \frac{H_2(A_1 - A_2)}{(H_2 - H_1)} + A_2$$

Eqn. 1- 7

The wood volume in the stem below the crown base is modeled as a truncated cone. The volume of a truncated cone is calculated with the general equation for the volume of a pyramid as

$$V_1 = \frac{\left(H_2\left(A_0 + A_2 + (A_0 A_2)^{\frac{1}{2}}\right)\right)}{3}$$

Eqn. 1- 8

in which A_0 is the stem cross sectional area at the base of the tree, A_2 is the stem cross sectional area at the base of the crown, H_2 is the height to crown base. The woody biomass of the stem below the live crown base is then

$$M_1 = \rho V_1$$

Eqn. 1- 9

The pipe model (Shinozaki et al. 1964) predicts that the foliar dry biomass is proportional to the cross sectional area at the base of the live crown, A_2 (**Figure 1-2**). From the pipe model, foliar biomass, M_F, is then predicted as:

$$M_F = C_1 A_2$$

Eqn. 1- 10

where C_1 is an empirical constant which is determined by the site productivity, and particularly, by the evaporative demands of the environment in which the tree is found (Callaway et al. 1994, Mencuccini and Grace 1995, Berninger et al 1995, Kaufmann et al 1981, Grier and Waring 1984); more arid sites require more cross sectional area to produce the same foliar biomass because the evaporative demand of the foliage is higher. The evaporative demands of the environment are described quantitatively as the vapor pressure deficit; this quantity can be modeled across landscapes using biogeochemical models which describe plant physiological interactions with the environment (Keane and Holsinger 2006). Such modeling approaches are termed 'gradient modeling' in the ecological literature, and form the underlying theory behind current efforts to map fuels and vegetation across the conterminous United States (Keane et al 2007). The incorporation of parameters sensitive to these gradients in FUEL3D is intended to provide a linkage between fine scale, tree level properties, and the coarser scale environmental factors which influence tree properties.

Similarly, from the pipe model the total branch basal cross sectional area available should be proportionate to the cross sectional area of the tree stem at the base of the live crown, A_2 (**Figure 1-2**).

$$A_{BT} = \sum_{1}^{n} A_{Bi} = C_2 A_2$$

Eqn. 1- 11

where A_{BT} is the total branch basal cross sectional area available, which equals the sum of individual branch cross sectional areas A_{Bi} .. A_{Bn}, A_2 is the cross sectional area of the stem at the base of the live crown, and C_2 is an empirical coefficient determined for the site. C_2 is similar to another site level parameter, C_1, in that both relate to the evaporative demands of the environment in which the tree is found but C_1 addresses foliar biomass (and thus implicitly sapwood cross sectional area relations) and C_2 addresses branch wood cross sectional area relations.

Following the pipe model, crown wood can be considered as a combination of conducting tissue (sapwood) and non-conducting tissue (heartwood). As sapwood cross sectional area is considered to be conserved, if there is no heartwood within the crown, the volume of wood within the crown, $V_{wc,}$ which consists of both the main stem above the crown base and all branch wood, can be modeled as a simple cylinder, with circular base A_2 and length H_3. However, as studies have shown that there is heartwood within the crown (Vanninen et al. 1996, Meinzer et al. 2005), this volume necessarily tapers, resulting in a truncated cone, described as

$$V_2 = C_3 A_2 H_3$$

Eqn. 1- 12

in which C_3 is an empirical coefficient; if $C_3 = 1$ the crown wood volume is that of a cylinder (with no heartwood) with a value < 1 which

With the wood volume within the crown known, the crown woody biomass is then

$$M_2 = \rho V_2$$

Eqn. 1- 13

where ρ is an empirical value for the average wood density for the species in question. A single constant wood density value is used throughout the FUEL3D model for the sake of simplicity.

At this point the woody biomass, above and below the base of the crown, and foliar biomass are all quantified. However, before FUEL3D can proceed to distribute the biomass in space it is necessary to partition the woody biomass within the crown, M_2, into stem, M_{2s} and branchwood components, M_{2b}. This partitioning facilitates modeling of variability in branch size and geometry. This flexibility is essential in enabling the model to represent different species as well as within-species variability in crown structure. The model first calculates the biomass in the stem above the crown base and then determines the branch wood by subtraction.

Stem wood above the live crown base is modeled as a tapering column (**Figure 1-3**) in which the change in radius over its length (from the base to the top) is described with a

quadratic polynomial equation (Kozak et al 1969, Goulding and Murray 1975) of the form:

$$r = p_1 x^2 + p_2 x + p_3$$

Eqn. 1- 14

where r is the radius of the tree bole, x represents height above height of the crown base and p_1, p_2, and p_3 are coefficients of the polynomial.

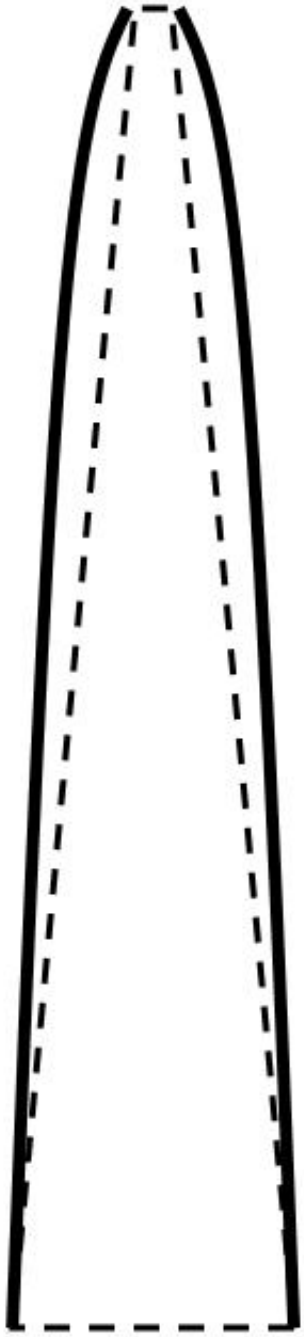

Figure 1- 3 The stem wood portion of the woody biomass within the crown is modeled as a tapering column with a volume that is referenced to that of a truncated cone.

The volume of stem wood above the crown base is then estimated as

$$V_{2s} = \frac{C_4(H_3(A_3 + A_3 + (A_2A_3)^{0.5}))}{3}$$

Eqn. 1- 15

where A_2 is the cross sectional area at the base of the live crown, A_3 is the cross sectional area corresponding to a measured minimum diameter, D_3, and C_4 is a taper form coefficient determined empirically or from the literature. The portion of the equation on the right hand side which is multiplied by C_4 represents the volume of a truncated cone, as is used for the volume of the tree stem below the crown base. Thus, if C_4 is equal to 1, the stem top is modeled as a truncated cone. However, generally taper within the stem top results in a volume that is larger than the truncated cone, so C_4 is generally larger than 1. The specific polynomial coefficients for any given tree can be determined analytically because the volume, or left hand side of the equation, is known (**Appendix B**). Modeling the stem within the crown with a polynomial results in a suitably realistic tree bole (Goulding and Murray 1975) which, due to its continuously differentiable form, facilitates calculation of the cross sectional area at any point above the crown base as well as the woody biomass occupied by any particular section along its length. These calculations are essential to the accounting of biomass used within the tree and to ensure

that modeled biomass quantities are consistent with theory and observation while still providing the flexibility required by the design criteria for the FUEL3D model.

We determine the volume of branch wood biomass, by subtraction, as

$$V_{2b} = V_2 - V_{2s}$$

Eqn. 1- 16

and the woody biomass corresponding to the crown stem wood, M_{2s} and branch wood, V_{2b}, are simply the product of the volume and a constant wood density value.

$$M_{2s} = \rho V_{2s}$$
$$M_{2b} = \rho V_{2b}$$
$$M_{2s} = \rho V_{2s}$$

Eqn. 1- 17

and the volume of branch woody biomass is determined by subtraction

$$M_{2b} = M_2 - M_{2s}$$

Eqn. 1- 18

Once all key biomass components are quantified, the model then proceeds to distribute this biomass in space, beginning with the tree stem and then adding branches. Strict accounting of biomass throughout the process; biomass is distributed until no biomass remains.

Distributing biomass in space

FUEL3D models the distribution of biomass in space as one or more lists of primitive geometric units; similar objects are listed together. At present two types of fundamental geometric units are used to describe a plant. The first is a tree branch segment, which is modeled as a cylinder or a frustum of a cone. Cylinders are also used for conifer needles. The other primitive geometric unit is a planar polygon. This unit can be used to represent a hardwood or shrub leaf or a portion of a leaf.

Primitive units such as cylinders are grouped into larger structures referred to as 'objects' to construct more complex branching and leaf structures in which species specific architectures can be assembled (**Figure 1-4**). In this manner it is possible to use the model to represent a wide variety of particular plant features. For deciduous trees or shrubs with leaves, an object might contain both segments and leaf polygon elements. For conifers, in which no planar polygon primitives are included, such objects typically consist of a series of cylindrical or truncated cone segments which together constitute a branching node.

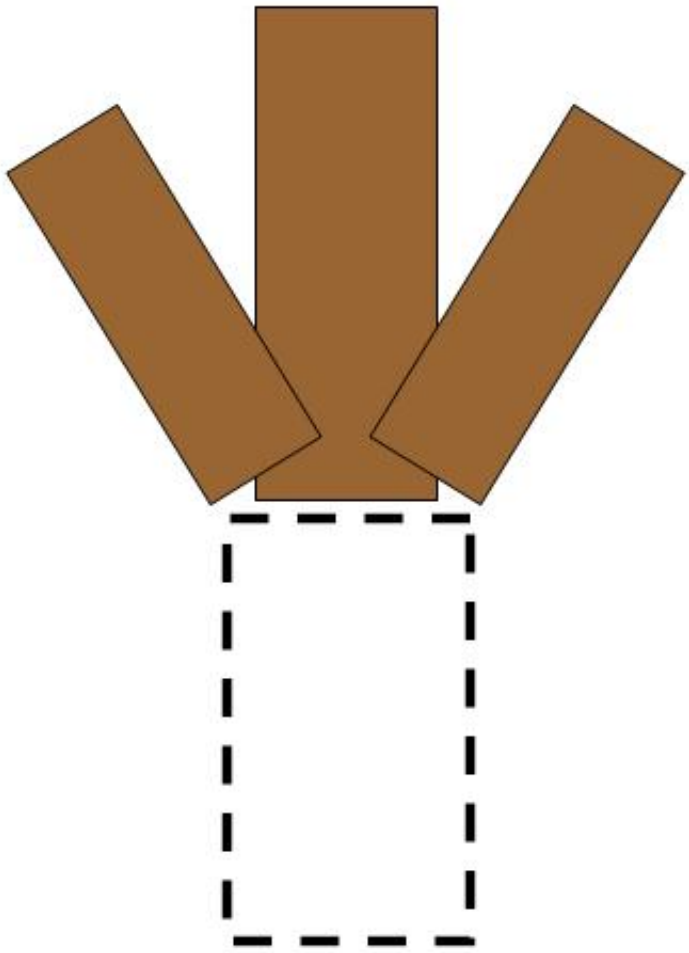

Figure 1- 4 A branching 'object' in the FUEL3D model is the set of child segments extending out from the end of the parent segment.

A central concept in the implementation of the FUEL3D model is that species can be associated with different types of objects, and that these objects can be generated from parameterized statistical distributions such that variability in the branching structure, observed in nature, can be incorporated into the geometric structure of the tree or shrub. Thus, at each point where a branching node is needed, the number of child segments, their orientations, their relative proportions of biomass and corresponding dimensions can all be drawn from appropriate distributions determined from field observation.

The first object in the list is the truncated cone which represents the tree stem below the crown base. Coordinates in x,y and z, at the bottom and top of the truncated cone, and the radii at those positions are recorded in the list. In addition to this basic spatial information other quantities of interest are calculated, including the volume, biomass and the surface area:

$$\sigma = \pi(r_1 + r_2)\sqrt{\left((r_1 - r_2)^2 + h^2\right)}$$

Eqn. 1- 19

In addition to the coordinates, dimensions and properties (such as calculated volume, surface area and mass), other descriptors are stored in the list which serve to link this object to others when appropriate, such as a common tree identity. Elsewhere in the tree, a common branch identity number will be assigned for all branch segments which form

part of the same larger branch. These descriptors provide a capability of extracting subsets of a tree on the basis of a simple query, such as a particular branch identity number, and also facilitate analysis and post-processing of model outputs, such as visualization and summarization.

Once the tree stem below the crown base is complete, FUEL3D proceeds to assemble the crown, beginning with the stem wood within the crown.

Using the polynomial coefficients specific to this tree and determined analytically (**Appendix B**), FUEL3D produces the tapering curve of the stem within the crown. The stem is then divided up into a series of sections in which the length of each section is drawn from a distribution parameterized by data collected on whorl length (a site level parameter).

At each of these locations, a branching object, consisting of a portion of the stem within the crown, and one or more potential branching points, is constructed according to species parameters. Each of these sections then represents a whorl, or a location on the bole from which branches might extend.

Species parameters describe the numbers of branches in a whorl and angles associated with their orientation. A branch is not actually attached at this point but the location where a branch might attach as well as its initial orientation is stored in a temporary list. This process continues until the model has arrived at the top of the tree. At this point the tree consists of a whole stem and a series of locations from which branches might extend.

To facilitate modeling of a diversity of tree architectures, several simple controls are implemented at this stage which control overall whole tree patterns. These include crown form, initial controls on branch angles, and the use of a statistical probability distribution function to provide for variability in branch size. The crown form control enables a coarse control over the whole tree crown form by providing a link between branch diameter and vertical position within the crown. If a conical form is desired, for example, larger branch diameters will be assigned to the lower portions of the crown, while an ellipsoidal form can be achieved by assigning larger branch diameters to the center of the crown. A less regular overall crown geometry can be achieved by imposing no preference on the relationship between branch basal diameter and position within the tree crown. In general, although some trees have highly consistent crown form (such as subalpine fir), many trees, and particularly Ponderosa pine, exhibit a significant variability in crown form, varying with light conditions and stand density (Horn 1971, Osada et al 2004).

Branching out

FUEL3D adds one branch at a time. Each branch is assigned a basal diameter drawn from a statistical probability distribution (the Beta distribution, shown below), and an initial segment length. Together these measurements constitute a cylindrical branch segment. Both the probability distribution and the initial segment length are parameterized from field data.

The Beta distribution is a flexible, positive distribution function. Because the distribution is bounded on the interval 0 <= x <= 1, it is useful in representing data which are proportions of some quantity. The probability density function of the Beta distribution is

$$f(x \mid v, w) = \frac{x^{v-1}(1-x)^{w-1}}{\beta(v, w)}$$

Eqn. 1- 20 (Evans et al. 1993)

where β(v,w) is the Beta function with two shape parameters v and w, (v > 0, w >0)

$$\beta(v, w) = \int_0^1 u^{v-1}(1-u)^{w-1}\, du$$

Eqn. 1- 21

depending on the values of the shape parameters v and w, the beta distribution can exhibit a wide variety of forms (**Figure 1-5**).

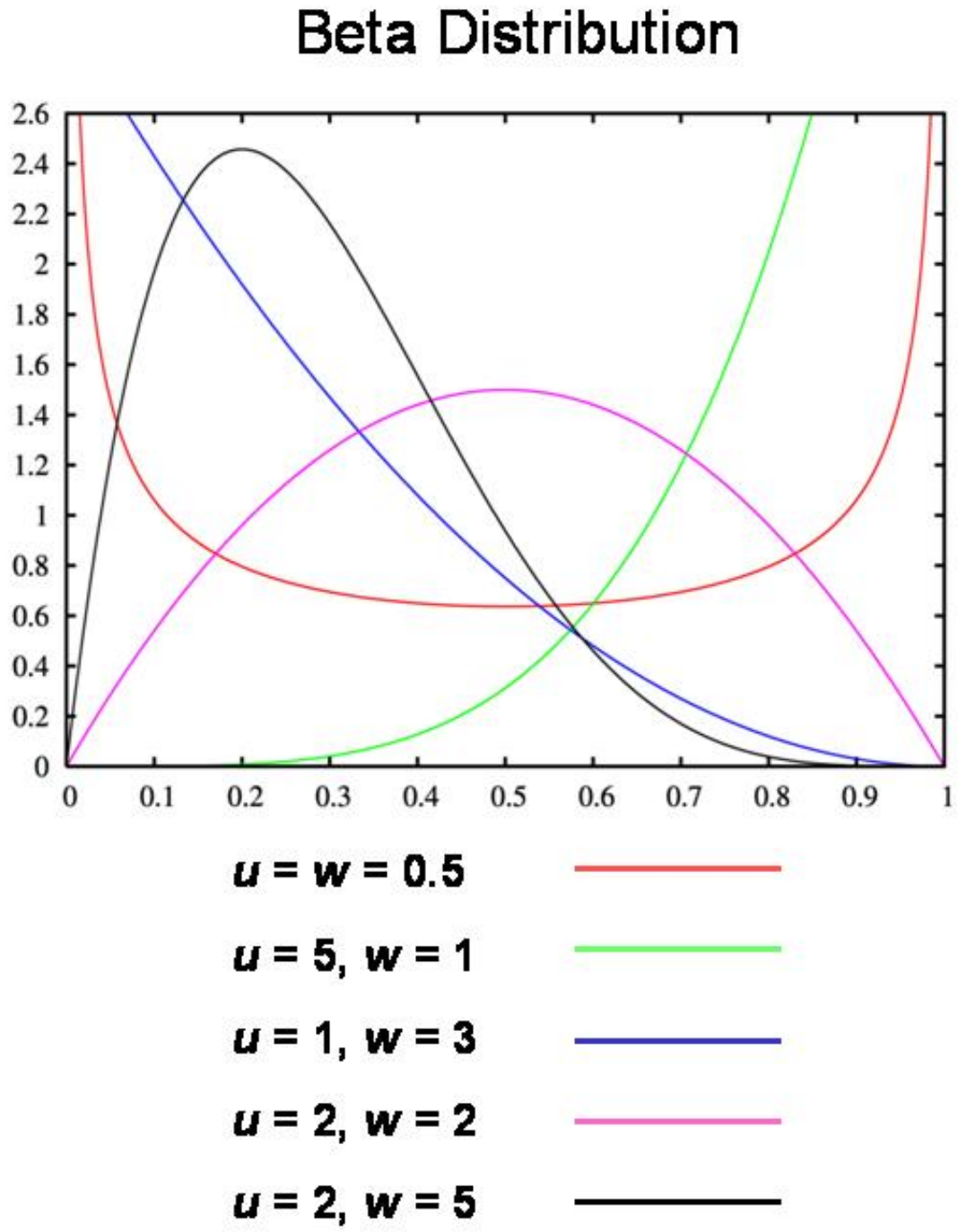

Figure 1- 5 Figure demonstrating the flexibility of the Beta distribution, used in FUEL3D to model the size distribution of branch basal diameters.

The Beta distribution is used here in FUEL3D largely because its flexibility permits a wide range of tree forms to be easily implemented. For example, one set of parameters for the Beta distribution might result in a tree with many small branches, while another might result in a tree with a small number of larger branches. It is important to be able to represent a range of different kinds of branch size distributions because the form of a tree crown is highly dependent on the light conditions and competition with other trees (Horn 1971).

The number drawn from the distribution represents a proportion. This proportion is multiplied by the total branch basal cross sectional area available, A_{BT} (described below), to determine the cross sectional area for a particular branch as:

$$A_{Bp} = A_{BT}\beta$$

Eqn. 1- 22

where A_{Bp} is the cross sectional area at the base of a particular branch. Later in the process the label A_{Bp} will refer to the cross sectional area of any parent segment. A_{BT} is the total branch cross sectional area available, and β is a proportion, specific to this branch, drawn from the Beta distribution.

The initial segment length is set as a proportion expected total branch length, L_T, as follows:

$$\ell_0 = L_T C_5$$

Eqn. 1- 23

where L_T is total branch length predicted empirically from branch diameter, D_B, and C_5 is an empirically measured value calculated as the length from the branch base to the first live second order branch divided by the total branch length.

The total woody biomass, and associated foliar biomass to be distributed in this branch is determined on the basis of its proportion of branch cross sectional area, as follows:

$$M_{2bi} = \beta_i M_{2b}$$
$$M_{fi} = \beta_i M_f$$

Eqn. 1- 24

where M_{2bi} and M_{fi} are the woody and foliar biomass, respectivelym for branch i, β_i is the proportion from the Beta distribution for this branch and M_{2b} and M_f are the total branch wood biomass and foliar biomass quantities for the tree.

Once dimensions (length and diameter), locations (coordinates of the midpoint of the proximal and distal ends), orientation (theta and phi angles), and associated biomass quantities (woody and foliar biomass for this branch) for the initial branch segment are defined, the model has all the information it needs to distribute biomass within the branch. This is done with a recursive (self-referencing) algorithm, similar to other fractal

tree models (Berezovskava et al 1997, Niklas 1986, Van Noordwijk and Mulia 2002). The algorithm extends itself, splits into smaller branches, which themselves split into smaller branches, and so on until the biomass quantities allocated to the branch are used up (**Figure 1-6**).

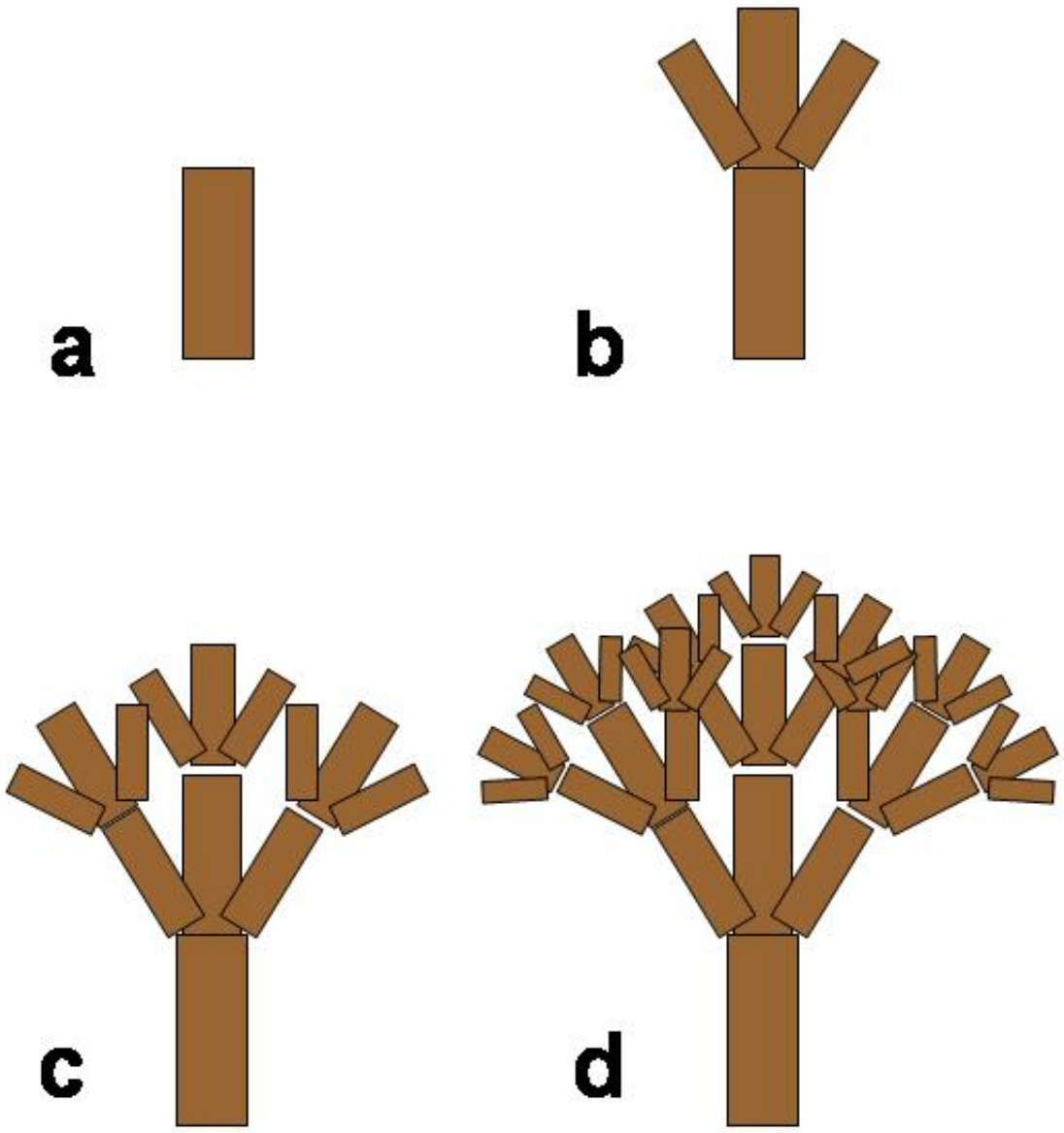

Figure 1- 6 Figure illustrating the process by which branching objects are built on to the ends of previous branching objects until biomass apportioned to the branch is depleted.

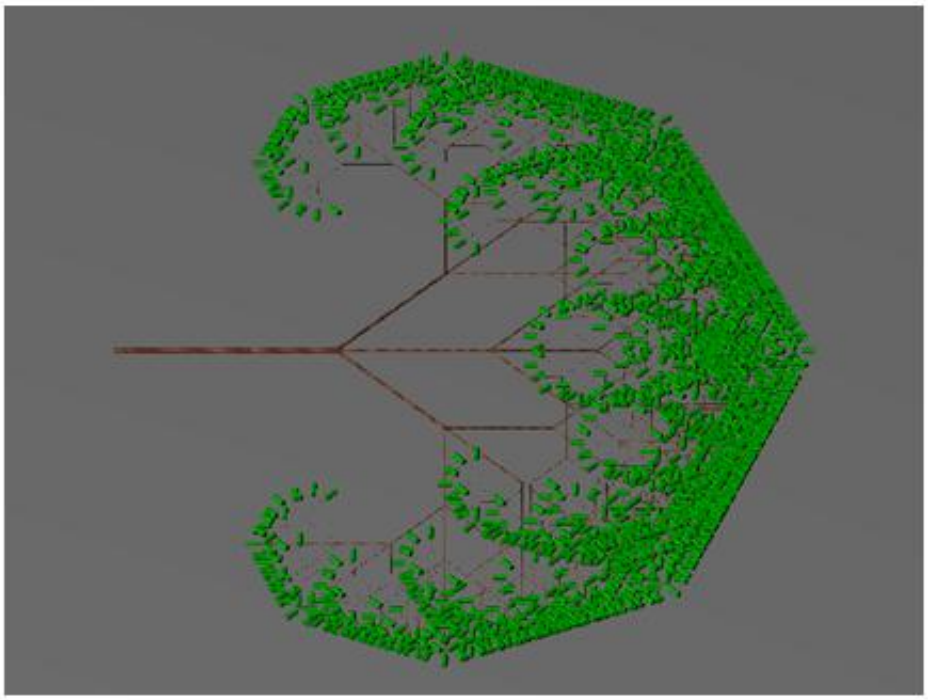

Figure 1- 7 A prototypical fractal branch, with no variability in dimensions or angles.

An example of a prototypical fractal branch, with no variability in dimensions or angles is shown in **Figure 1-7**. This process is described below:

At the beginning of the recursive algorithm, the program accesses, through a lookup table, all relevant tree, species and site parameters. For example, all species parameters (which describe geometry and properties of branching nodes) are accessed via an integer code for species identification in the tree input parameters). The algorithm then determines the orientation of the segment in question. This is done by determining the x,y and z components of the distance between the x,y,z coordinate at the center of one end of the segment and the x,y,z, coordinate at the other end:

$$\Delta x = x_2 - x_1$$
$$\Delta y = y_2 - y_1$$
$$\Delta z = z_2 - z_1$$

Eqn. 1- 25

where coordinate (x_1,y_1,z_1) is the proximal end of the segment and (x_2,y_2,z_2) is the distal end. The orientation of the segment is then calculated by conversion of cartesian coordinates to spherical coordinates as follows

$$\theta = \arctan(\Delta y, \Delta x)$$
$$\phi = \arctan(\Delta z, \sqrt{(\Delta x^2 + \Delta y^2)})$$

Eqn. 1- 26

where arctan refers to the four quadrant inverse tangent. The orientation of the segment is used when child segments are built off of an existing segment. A simple species level parameter for incremental angle changes can also be used here to modify the branching habit. For example, a branch could be initially oriented perpendicular to the tree but could then angle slightly upward at each successive branching to provide an upward curve.

The length of the segment is calculated as

$$\ell = \sqrt{\left(\Delta x^2 + \Delta y^2 + \Delta z^2\right)}$$

Eqn. 1- 27

The model then evaluates whether the biomass allocated to this branch is sufficient to continue branching (based on a theshold value of biomass) . If there is sufficient biomass for branching to continue, the model produces a branching node consisting of two or more child segments from a template based on species level parameters. Variability is explicitly incorporated into this process such that each branching node may have a different number of child segments and angles between them may vary, with the numbers being drawn from distributions parameterized from field data.

Following the pipe model, the sum cross sectional area across all child segments is preserved, according to the relationship

$$\sum_{i=1}^{m} A_{Bi} = C_6 A_{Bp}$$

Eqn. 1- 28

where A_{Bp} is the cross sectional area of the parent branch, A_{Bi} is the cross sectional area of a particular child segment, *m* is the number of child segments in this particular branching node and C_6 is a parameter describing change in the sum cross sectional area which allows for the presence of non-conducting tissue within the wood. The parameter C_6 must be greater than or equal to 1.

In FUEL3D, the proportion of the sum cross sectional area assigned to the various child segments may vary, such that child branch segments may be of different size. This enables FUEL3D to account in a simple manner for apical control, in which the main, usually central portion, of the branch is larger and longer than the smaller branches which extend off of it (**Figures 1-8 and 1-9**).

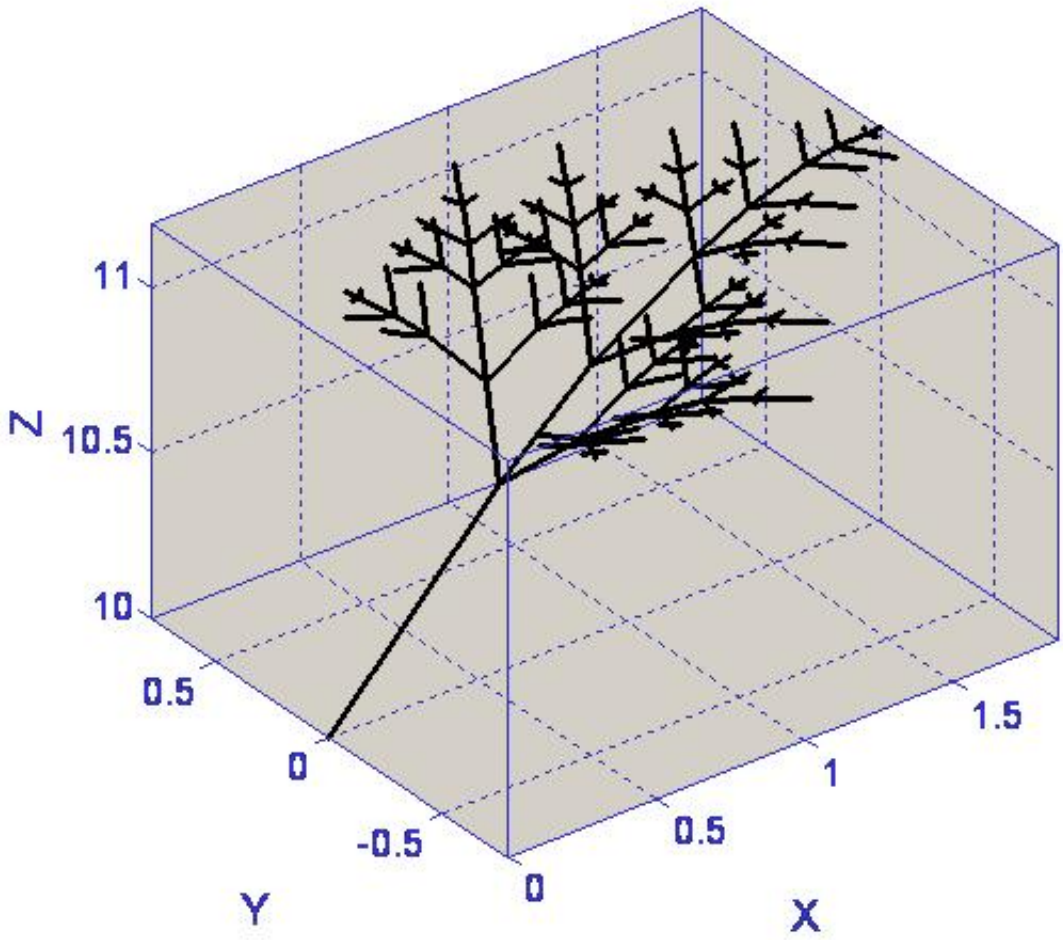

Figure 1- 8 An example branch, shown as a line figure.

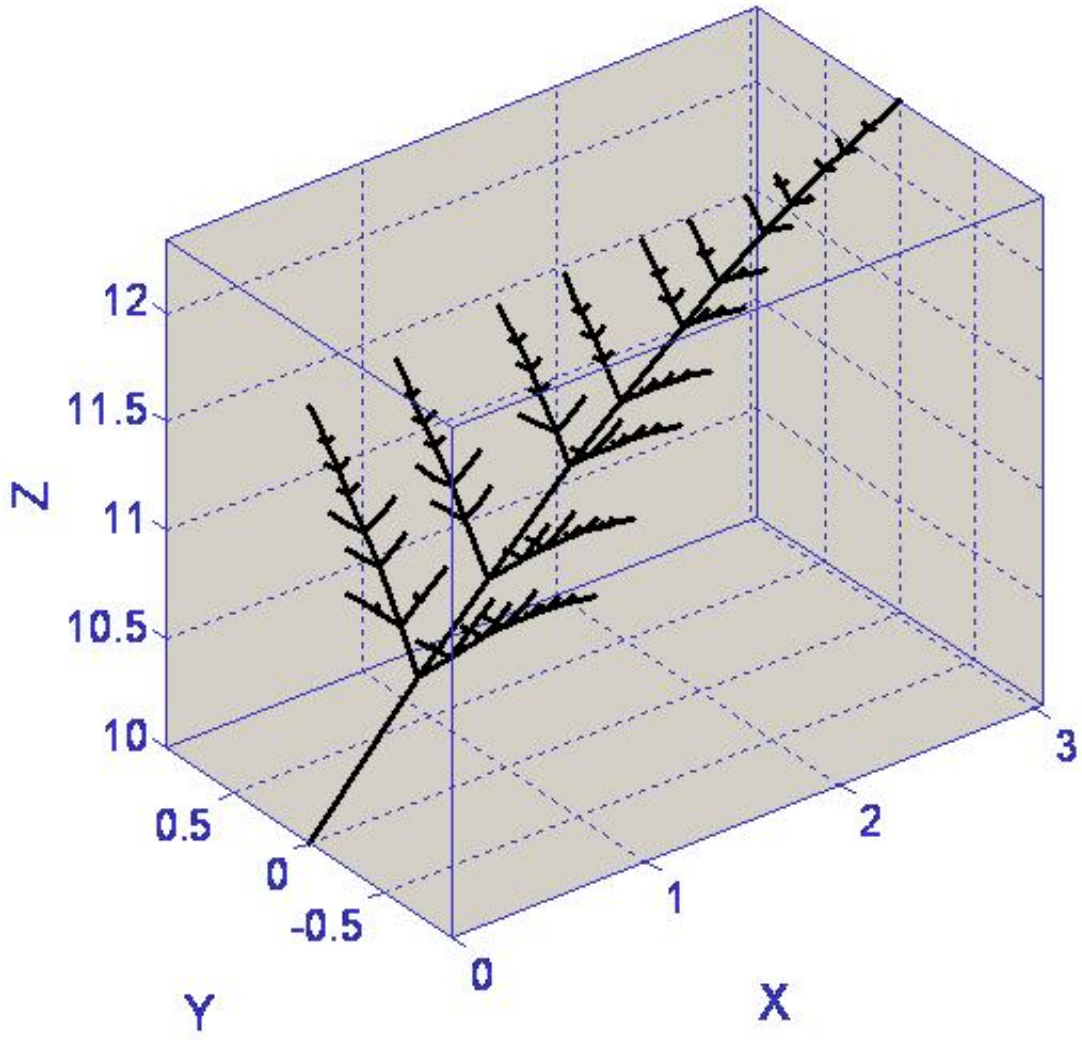

Figure 1- 9 A different branch, shown as a line figure. A change in the allocation of biomass to the dominant branch segment has resulted in a longer branch and a different geometry.

This variability in cross sectional area also allows for patterns which reflect natural variability in plant growth. This variability in cross sectional area, and corresponding proportion of biomass quantities, is implemented as an array of coefficients p_1 .. p_n, where *n* is the number of child segments in a particular branching node;

$$\sum_{i=1}^{n} p_i = 1$$
$$A_{Bi} = p_i C_6 A_{Bp}$$

Eqn. 1- 29

the array is required to sum to 1, and the cross sectional area of a given child branch, A_{bi}, is its proportion, p_i, multiplied by the sum cross sectional area.This is similar to the approach used in other static fractal models in which child segments can be of unequal size (Richardson and zu Dohna 2003,Ozier-Lafontaine et al. 1999).

A particular branching node is created with orientations between child segments but generic dimensions. Its position is also generic, with the base at the origin (x=0,y=0,and z = 0), with the main segment (which would typically serve as the continuing extension of the parent branch segment) oriented along the z axis. For this branching node to become part of the larger tree structure in space its dimensions must be scaled properly and its position must be rotated such that its orientation is consistent with the parent segment, and translated such that it extends from the distal end of the parent segment.

Following the WBE model (West et al. 1997), when all child segments are of the same size, the lengths of child segments scale with the parent segment length as:

$$\gamma = n^{-\frac{1}{3}}$$

Eqn. 1- 30

where γ is the ratio of the child segment length to the parent segment length, *n* is the number of child segments. In FUEL3D, where child segments may be of different size, this scaling relationship is modified to

$$\gamma = \left(\frac{1}{p}\right)^{-\frac{1}{3}}$$

Eqn. 1- 31

where *p* is the proportion of the sum cross sectional area for a particular child segment. Note that when all children are of the same size, their proportions are equal, and this equation resolves to the same as the preceding one.

Throughout the process, FUEL3D makes strict accounting of the biomass available. If the biomass allocated to a particular child segment is not sufficient to construct a segment of the specified dimensions, the algorithm will build a segment within the limits of the biomass available while reserving sufficient biomass to build a terminal structure, described some paragraphs below. In no case is a segment allowed to be constructed with

more biomass than is available for that construction. FUEL3D is sensitive to the wood density, a species level constant. A higher density material will result in smaller dimensions for the same biomass. The reduction in dimensions in branches is done in length rather than diameter.

Once the appropriate dimensions are determined for all child segments, the algorithm then updates the position of the end point of each child segment such that its positions are in accord with the new dimensions.

Each child segment is then rotated such that the overall structure of the branching node (which is a collection of child segments) is oriented to fit on the distal end of the parent segment. This rotation essentially involves a mapping of positions in the local coordinate system of the branching node (i.e. at the origin and oriented along its z axis) to the global coordinate system in which the tree and its component branches are found. This is done with standard coordinate system transformations, which consist of rotations around the x axis (referred to as the "roll angle"), y axis (referred to as the "pitch angle") and the z axis (referred to as the "yaw angle"):

$$\Re_x(\theta_x)=\begin{bmatrix}1 & 0 & 0\\ 0 & \cos\theta_x & -\sin\theta_x\\ 0 & \sin\theta_x & \cos\theta_x\end{bmatrix}$$

$$\Re_y(\theta_y)=\begin{bmatrix}\cos\theta_y & 0 & \sin\theta_y\\ 0 & 1 & 0\\ -\sin\theta_y & 0 & \cos\theta_y\end{bmatrix}$$

$$\Re_z(\theta_z)=\begin{bmatrix}\cos\theta_z & -\sin\theta_z & 0\\ \sin\theta_z & \cos\theta_z & 0\\ 0 & 0 & 1\end{bmatrix}$$

Eqn. 1- 32

At this point the complete branch node is oriented properly with its parent segment but is not in the correct position. The correct position is achieved by translating the branching node to the distal end of the parent segment.

Biomass quantities (foliar biomass and woody biomass associated with a particular branch segment) are updated such that the biomass that was used in the construction of each segment is accounted for and subtracted from the amount of biomass allocated to that segment (and its eventual child segments).

A list containing all pertinent information for all geometric structures in the tree is updated each time a new segment is added. The list is assembled primarily for the purpose of developing three dimensional inputs for 3D fire behavior models, but other uses for this list arise as well, such as post processing and analyses and detailed visualization.

At this point the recursive nature of the algorithm comes into play as the sequence is then repeated for each of the child segments. Each segment continues to branch, producing a new branching node consisting of some number of child segments, until the amount of biomass left is insufficient for continued branching. When this occurs the algorithm stops branching and constructs a terminal structure.

Terminal structures are another kind of species specific branching node. Similar to the branching nodes described above, terminal structures have particular aspects that are defined, and others that are assembled 'to order'. For conifers, a terminal structure consists of one or more branches supporting clumps of needles. Foliar biomass is divided up into needles, and needles are arranged in clumps which are arranged on the terminal branches. Measurements of needle dimensions and angles are part of the detailed data collection used to parameterize a species; here this information is put to use. An important feature of FUEL3D is that it provides for two levels of detail with respect to terminal structures. In either case the same calculations are made, but the difference lies in what level of detail is explicitly written to the list. In the more detailed case, each individual needle is described with explicit coordinates and dimensions and related calculations such as mass, volume and surface area.

The positions and orientation of needles are assembled much in the same manner as the branching structure within the rest of the tree crown: by assembly of smaller geometric objects (**Figure 1-10**). The total number of needles is calculated by dividing the foliar

biomass by the mass per needle; needles are then assembled in clumps, with dimensions and patterns described in the detailed species terminal parameters. Clumps are assembled in needle whorls; gaps between needle whorls are described in species parameters as well.

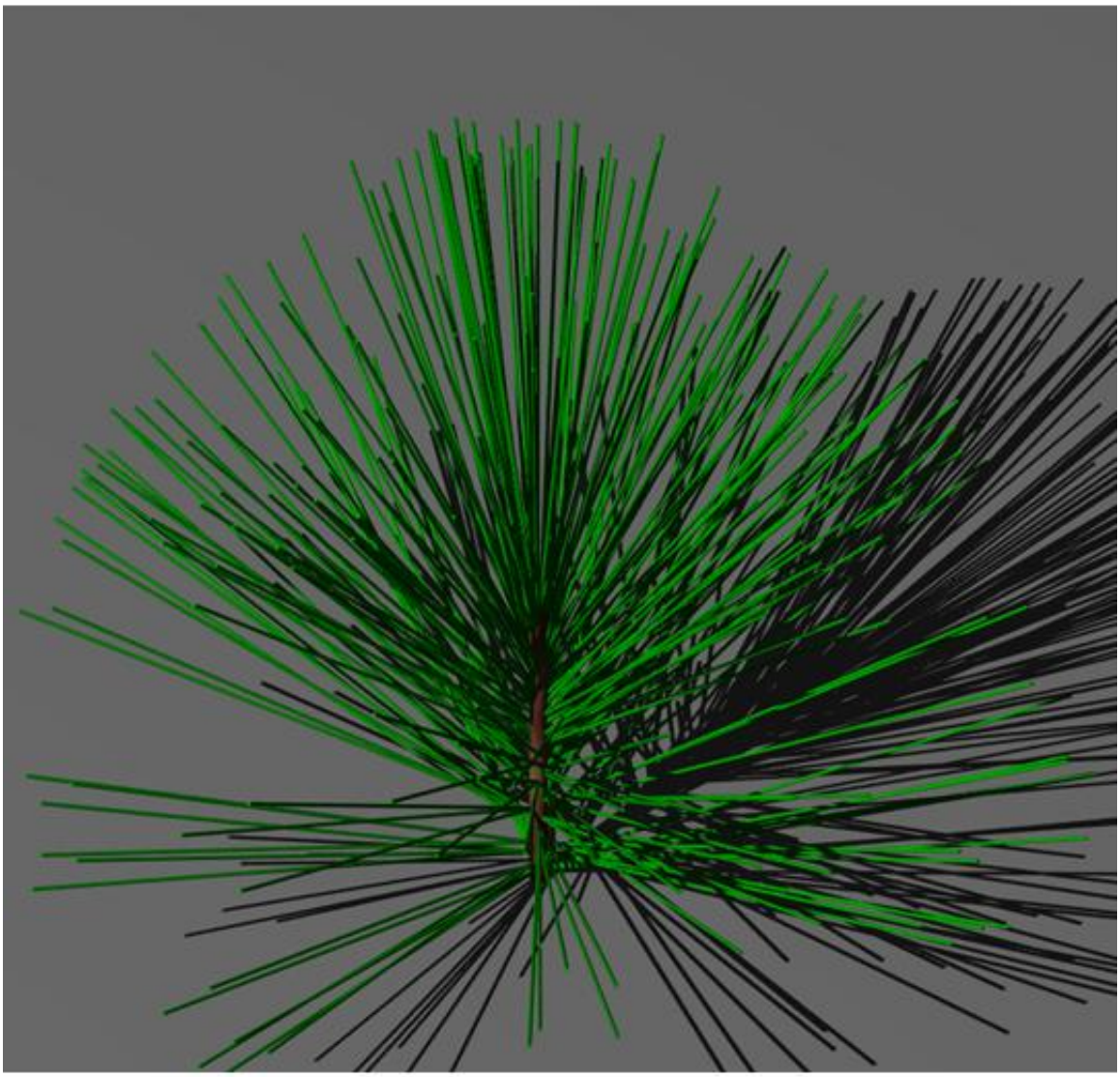

Figure 1- 10 An example terminal structure consisting of a terminal branch segment and associated foliar biomass.

One of the most straightforward uses of the geometric objects output by FUEL3D is in visualization. As a standard output of the model a file is written which can be used by an external ray tracing software for detailed photorealistic visualizations. Ray tracing is a spatially explicit approach for light modeling which samples beams of light between the light source (such as the sun) and a given object and back to a specified viewpoint. Ray tracing thus is capable of representing shadows and other behaviors related to light with great detail, both in space and in time. **Figure 1-11** illustrates an example tree shown via ray tracing visualization, without foliage; the same tree is shown with foliage in **Figure 1-12**. **Figure 1-13** presents a more detailed view of the same tree.

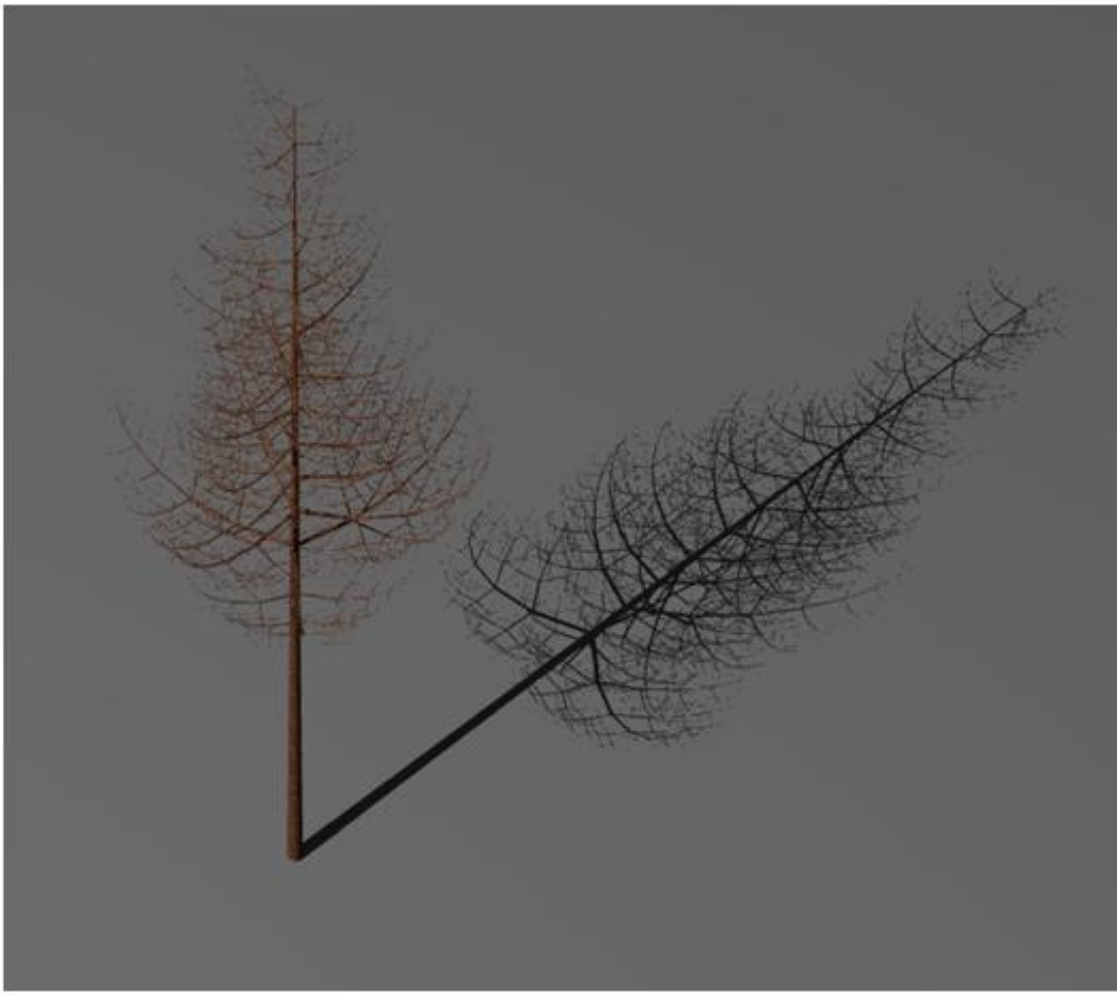

Figure 1- 11 A three dimensional tree modeled with FUEL3D and visualized with ray tracing procedures. The tree is shown here without foliage to illustrate the branching structure within the crown.

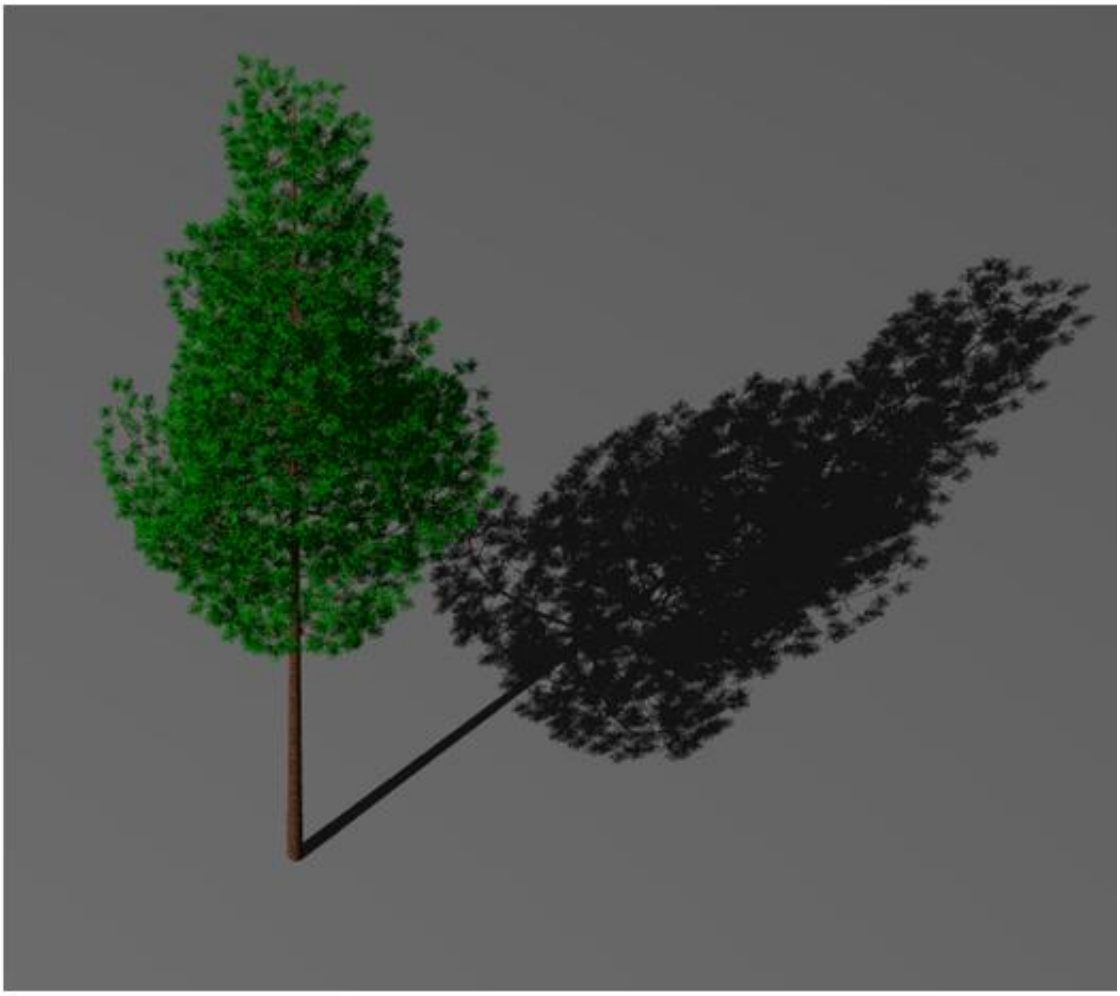

Figure 1- 12 A three dimensional tree modeled with FUEL3D and visualized with ray tracing procedures.

Figure 1- 13 A three dimensional tree modeled with FUEL3D. The tree is visualized with ray tracing procedures and the view perspective is closer to the tree, revealing more detail.

Figure 1- 14 Foliage of a tree modeled with FUEL3D has been summarized to "container" objects which retain all the information of the finer detail structures within them. Containers facilitate quantitative modeling across a range of spatial scales.

As might be imagined, this results in a very large number of geometric objects, with correspondingly larger file sizes and lengthier processing in summarization of fuel information to volume cells. For most purposes this is not necessary, although it is useful when there is need for a highly detailed description of a small volume. In most cases, though, what is written to the list is a "container", which is a cylindrical bounding volume which includes a summary of its contents; the summary is built from the list of needles and fine twigs which are found within it (**Figure 1-14**). This use of containers facilitates much faster processing and analysis. Extending the concept further, for coarser scale analyses, an entire branch, portion of the crown or even a whole tree, could be described as a container. **Figure 1-15** illustrates two different stands in which each tree was summarized to a minimal number of containers. This is an important mechanism in FUEL3D which facilitates analyses across a range of spatial scales.

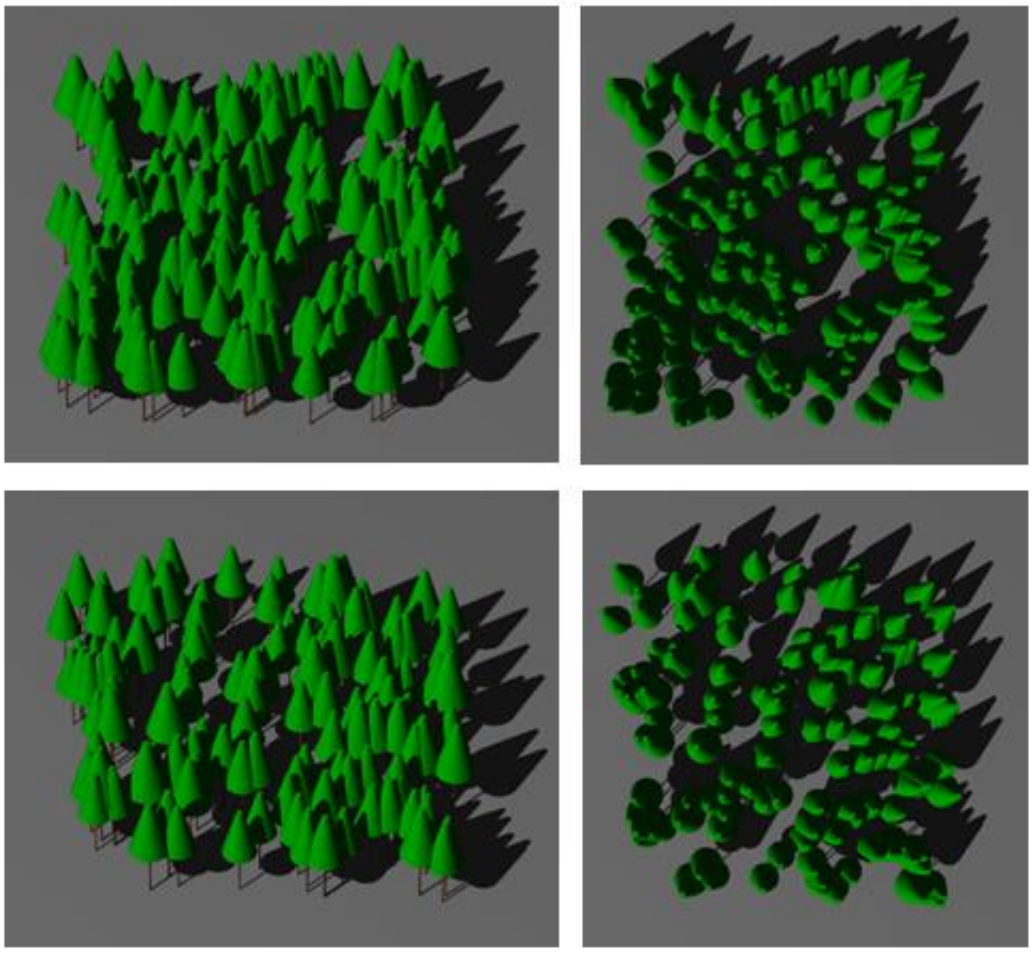

Figure 1- 15 An example use of large "container" objects to represent two stands of trees. The two figures on the left side are oblique perspectives on each of the two stands while the two figures on the right show a view from directly overhead.

Summarization to discrete volumes

In order for the collection of branch segments and foliage which compose the simulated tree to be used in a numerical fire model it is necessary to convert the data to values associated with three-dimensional grid cells, or voxels. To do this, each branch segment, or other spatial structure output by the biomass distribution process above, must be juxtaposed on the boundary lines of the mesh which defines the three dimensional array.

If volume cells are large relative to the branching segments it is often the case that the branch segment is wholly contained by a particular volume cell. In this case, the appropriate quantities in the segment needed by the fire model for that cell, such as its total woody mass, are simply added to the existing quantity for that cell. In this way the quantities in each cell volume reflect all the component segments which fall within their bounding coordinates.

However, in many cases the branch segment will cross boundaries between one or more volume cells. In this case, the branch segment must be divided into portions between all cells which contain part of it. While this may not seem difficult it is a process which, if not deftly handled, may become computationally demanding. This is particularly true as the discrete cells approach the size of the branch segments. A tree may have several hundred thousand segments (many more if biomass distribution is done at the level of individual needles rather than terminal "containers"); likewise, if the size of discrete cells is small there may be a great number of such cells even within a relatively small volume. For example, in one cubic meter there are one thousand volume cells of a decimeter on a side, and one million volume cells of a centimeter on a side. To evaluate the intersection

of all branch segments by all cells in such a case would be prohibitive in computational demands.

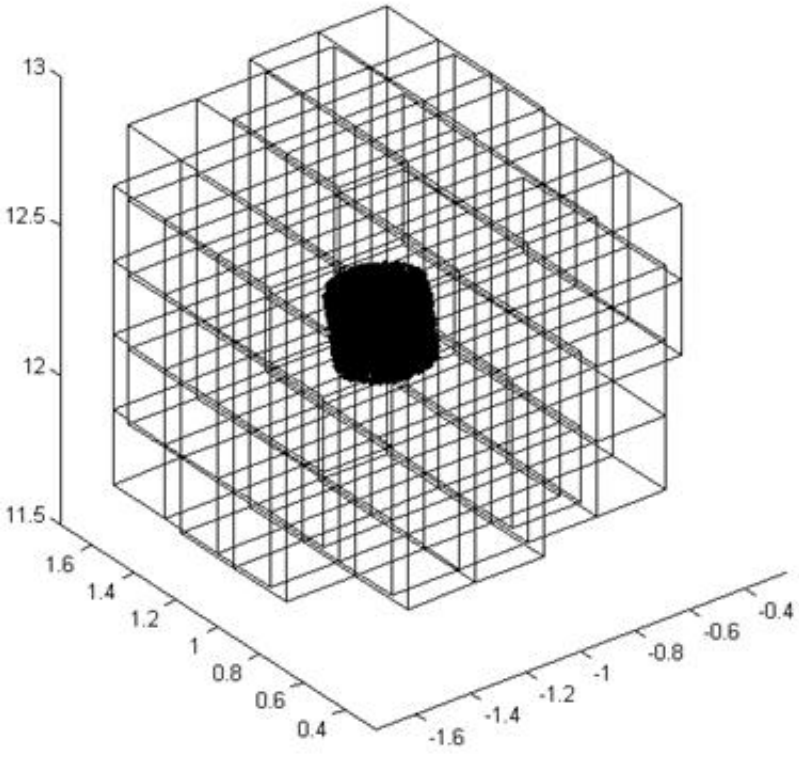

Figure 1- 16 Example of a spatial search in the vicinity of a cylinder. The spatial search is used to improve the efficiency of the process of summarization of fuel quantities to three dimensional volume cells.

FUEL3D eliminates some of this potential computational demand through the use of a spatial search to identify potential cells which might intersect a branch segment before carrying out more involved calculations (**Figure 1-16**). A search radius is set to a particular length; the appropriate length depends on the relative sizes of the boxes and the objects to be summarized. The search radius defines a sphere centered on the midpoint of the cylinder. The program identifies those boxes for which any vertex falls within the search distance. Only those boxes whose midpoints fall within the search radius are considered for assignment of some portion of the mass of the cylinder. To determine the portion of the cylinder's volume (and thus its mass) occupied by each potential volume cell, the program then performs a rather simple montecarlo integration. Monte carlo integration is a numerical technique typically used to integrate over irregular areas or volumes. The general procedure involves sampling a known, regular, bounding volume, (such as a box) which intersects the more complex volume, with a series of random points, and then evaluating each point as to whether it lies inside or outside the irregular volume. In the specific case here, both the bounding volume (the cell box) and the branch segment (cylinder) are regular shapes with known properties, so the procedure is somewhat simpler. FUEL3D samples the cylinder volume with a series of random points; each point is evaluated as to whether it falls within the bounding coordinates of each box and points are tallied by box. The proportion of those points which fall inside a particular volume cell is the proportion of mass assigned to that box. Parts of a branch segment that fall outside of one cell will be accounted for in an adjacent cell. In this manner the total quantities are preserved across whatever spatial scale is desired.

As the total mass of the cylinder is known, differences between the sum of mass apportioned and the known mass, which may arise from sampling are divided evenly among those boxes which had a non-zero proportion.

Figures 1-17, 1-18 and 1-19 illustrate the volume summarization of a small tree at three cell sizes. In each figure the tree was collapsed to a single horizontal layer (summing all fuel load quantities by vertical columns).

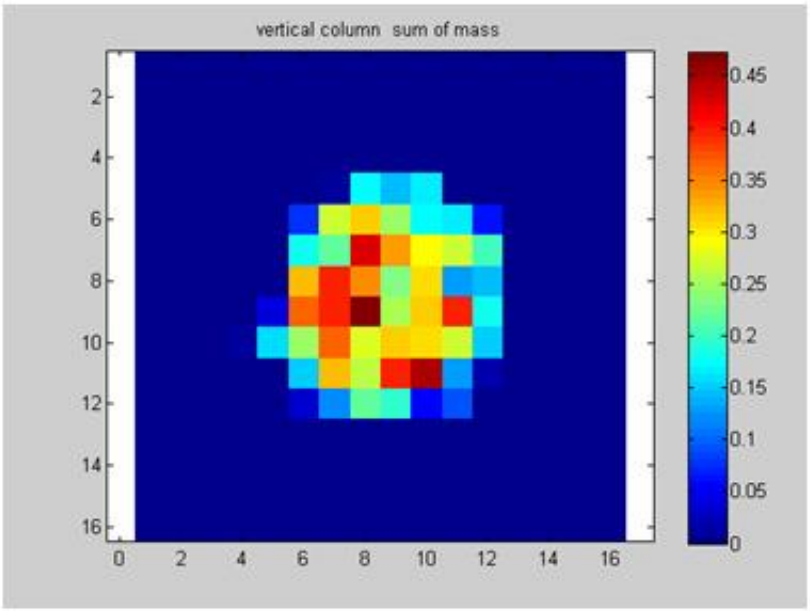

Figure 1- 17 Demonstration of spatial pattern in fuels within the crown of a small tree at cell resolution of 0.5 m. For this figure all fuels were summarized in vertical columns to produce a single layer.

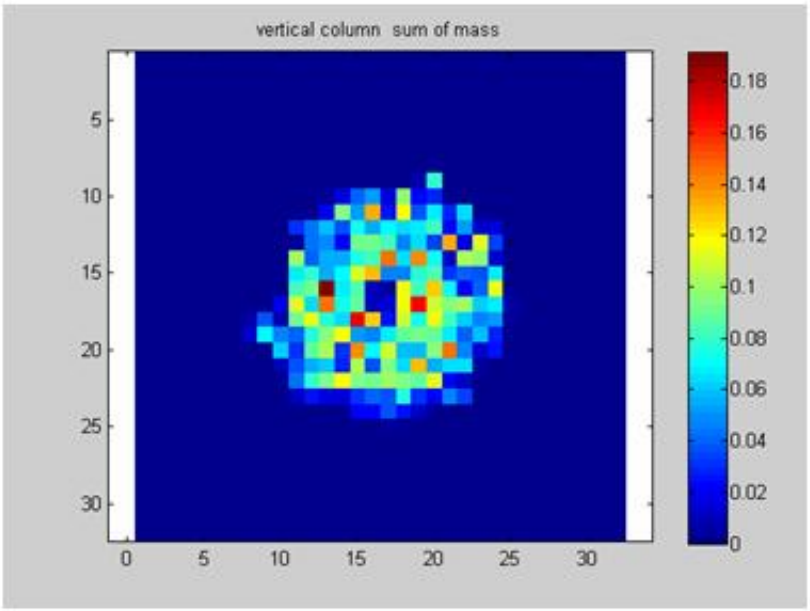

Figure 1- 18 Demonstration of spatial pattern in fuels within the crown of a small tree at cell resolution of 0.25 m. For this figure all fuels were summarized in vertical columns to produce a single layer.

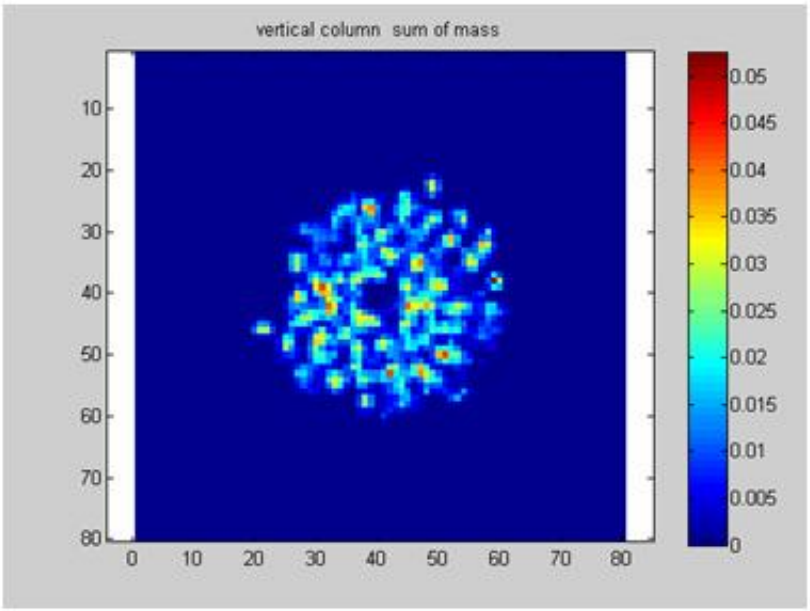

Figure 1- 19 Demonstration of spatial pattern in fuels within the crown of a small tree at cell resolution of 0.1 m. For this figure all fuels were summarized in vertical columns to produce a single layer.

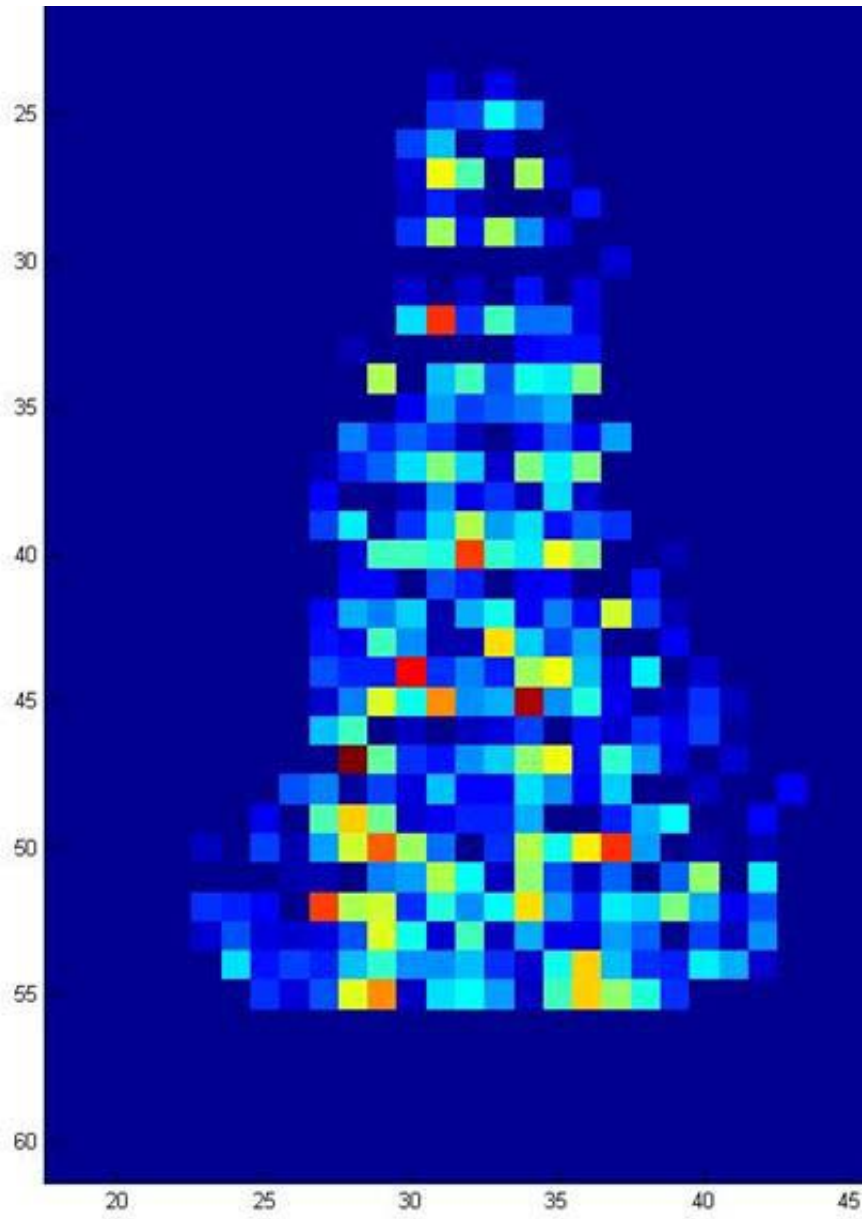

Figure 1- 20 View of the crown of a tree collapsed horizontally to a single vertical layer.

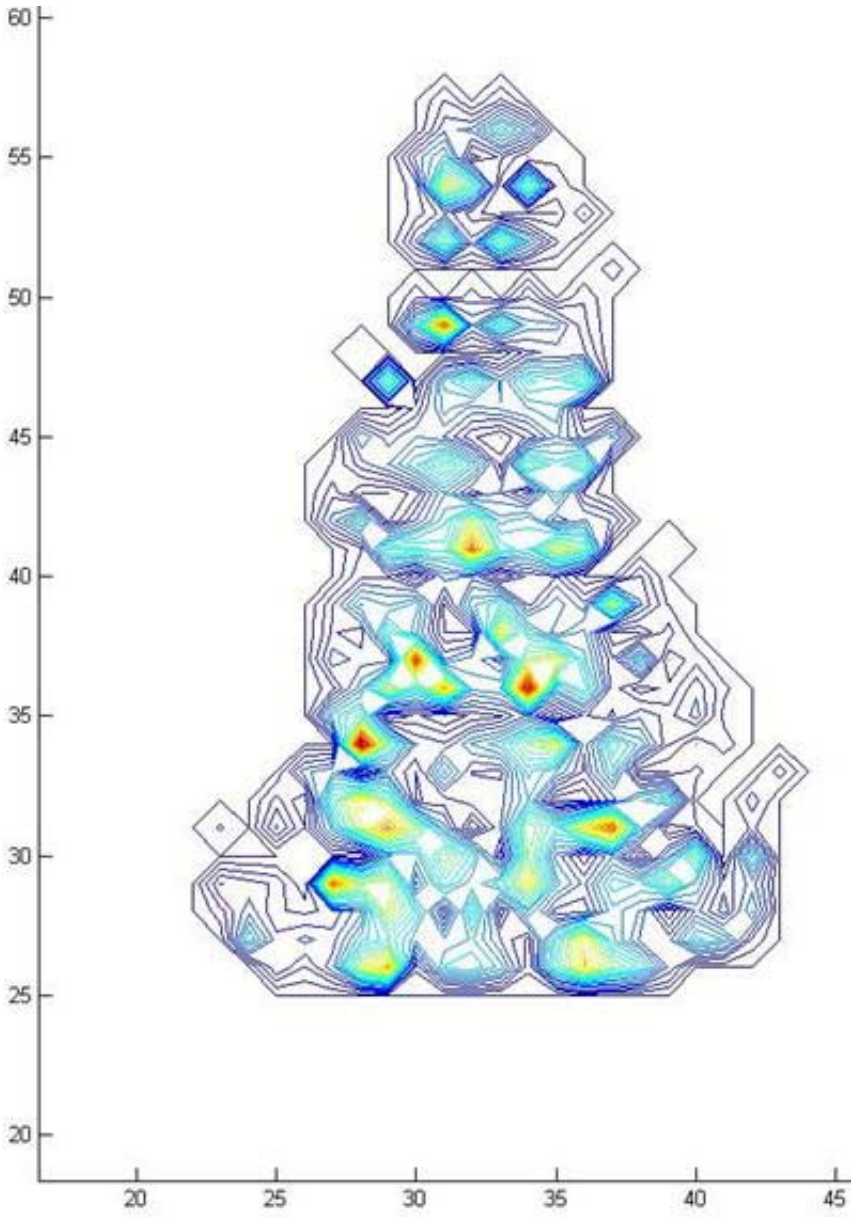

Figure 1- 21 View of the crown of a tree collapsed horizontally to a single vertical layer, shown here as contours indicating the quantity of fuel.

Figure 1- 22 Demonstration of the extraction of particular components of a fuel array for a specified sub volume: a 1 m wide swath, consisting of foliage only, was extracted from a tree. A perspective view with shadows is made using ray tracing procedures.

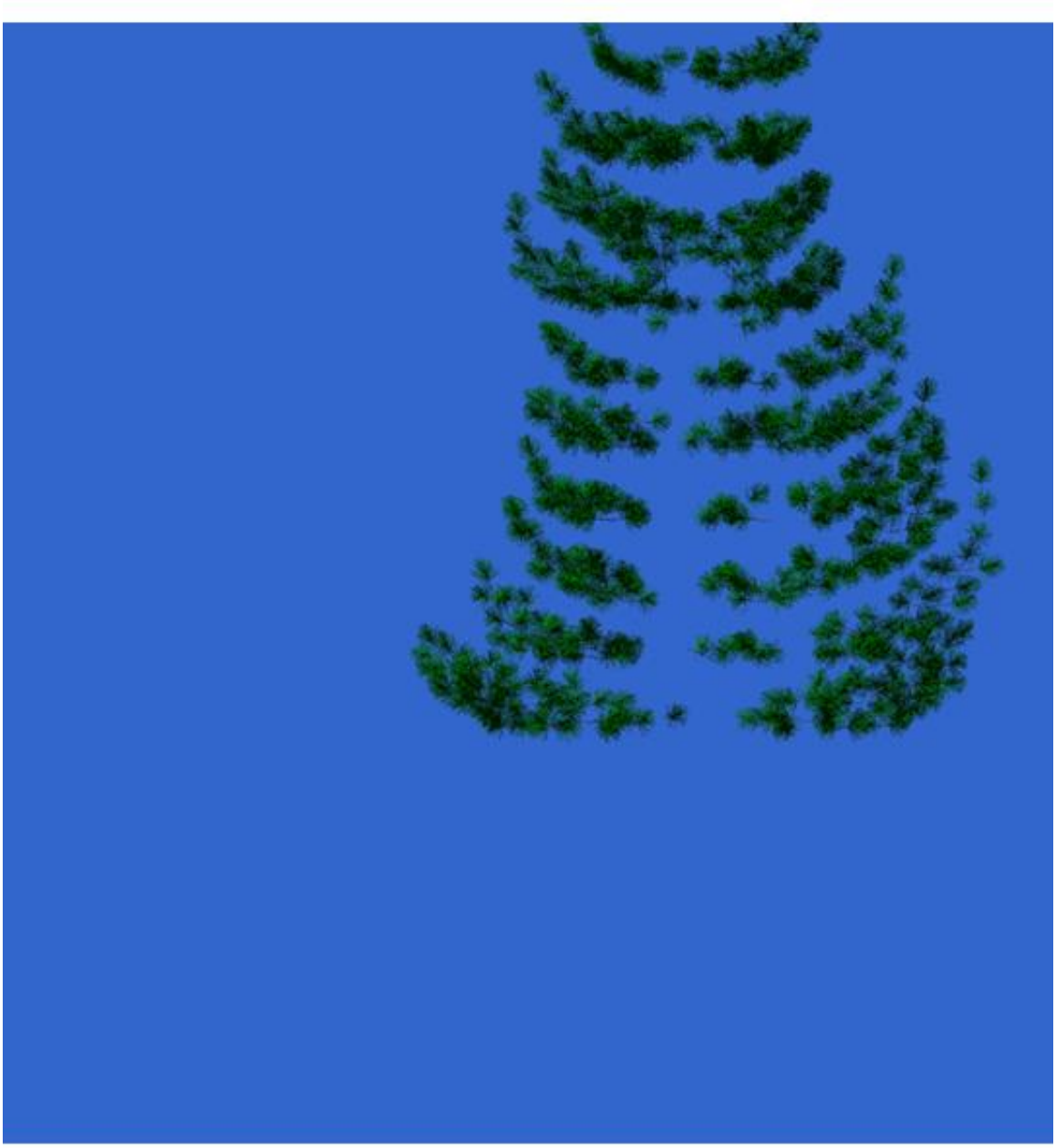

Figure 1- 23 Demonstration of the extraction of particular components of a fuel array for a specified sub volume: a 1 m wide swath, consisting of foliage only, was extracted from a tree. Here a side view is shown.

Figures 1-20 and 1-21 illustrate a similar process but where a tree was collapsed by horizontal arrays. A useful feature of the spatially explicit representation of crown fuels is that fuels can be described for a particular portion of a tree crown; this is accomplished by a simple query on the output file. **Figures 1-22 and 1-23** illustrate perspective and side views, respectively, of a 1m wide portion of a tree crown.

Assignment of other fuels attributes

FUEL3D deals with the spatial structure of fuels. However, other aspects of fuels may vary in time while the spatial structure remains the same. A key example is fuel moisture, which can change within a tree over the course of a season, or in response to drought or insect or pathogen attack. To accommodate this important characteristic of fuel variability, each individual branch segment, terminal container or even needle can be assigned its own fuel moisture, as well as other attributes. This facilitates explorations of changes in fire behavior arising from insect outbreaks or other forest health issues.

MODEL APPLICATIONS

The detailed outputs of the FUEL3D model can be used in number of ways. Here, I briefly demonstrate two important applications: fire and fuel interactions, and light dynamics.

Fire –Fuels interactions

To demonstrate how model output from FUEL3D can be used in conjunction with detailed fire behavior models to explore fire and fuel interactions, foliar biomass from a tree simulated with FUEL3D was summarized to 0.25 m cells and used as input to the Wildland Fire Dynamics Simulator (WFDS), a physical fire behavior model (Mell et al 2005). This model is described in greater detail in Chapter II, so here it is presented in brief only. WFDS is a Computational Fluid Dynamics (CFD) physical fire model in which different modes of heat transfer (i.e. radiation and convection) are dealt with explicitly in a time and space dependent simulation. A key aspect of this model, as well as other CFD fire models such as FIRETEC (Linn 1997, Linn et al 2005), is that they are capable of simulating fire behavior in heterogeneous and discontinuous fuel beds in three

dimensions. This makes them ideal for exploring complex fire and fuel interactions. Figure 1-24 shows a fire burning under a single tree crown at a particular moment in time (t = 21.5 seconds). The tree shown in this figure was assigned high foliar fuel moistures (100%) typical of a live tree. In contrast, Figure 1-25 shows the same tree, at the same point in time, with the same ignition pattern, but with fuel moistures typical of a dead tree (30%). The differences in fire behavior arising from this single factor are probably best viewed as animations: live_tree_fire, dead_tree_fire.

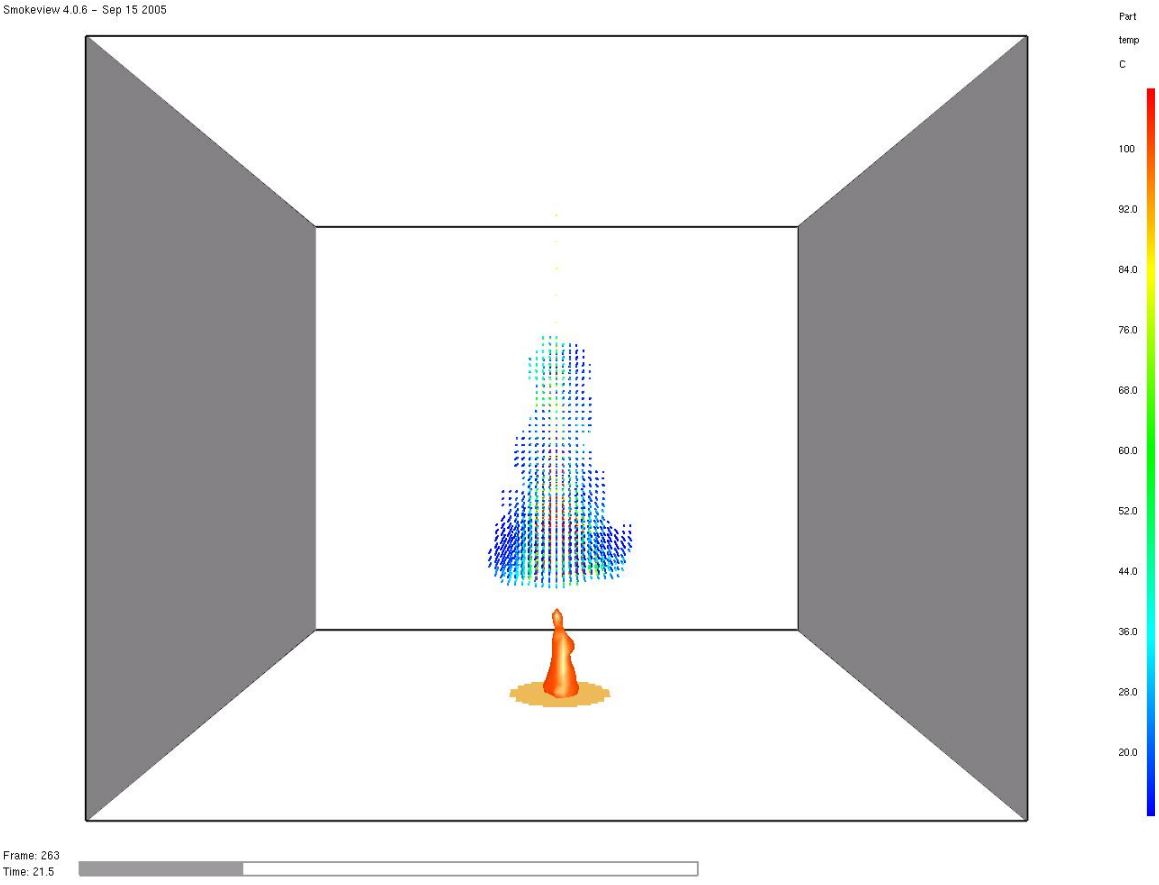

Figure 1- 24 Detailed fire simulation, using output from the FUEL3D model as input to the physical fire model, WFDS. The image shows a fire burning below a tree crown. The tree has a height to crown base of 4m, and foliar biomass is parameterized as live, with 100% fuel moisture. At t = 21.5 seconds, the fire has heated a portion of the tree crown but has not ignited it.

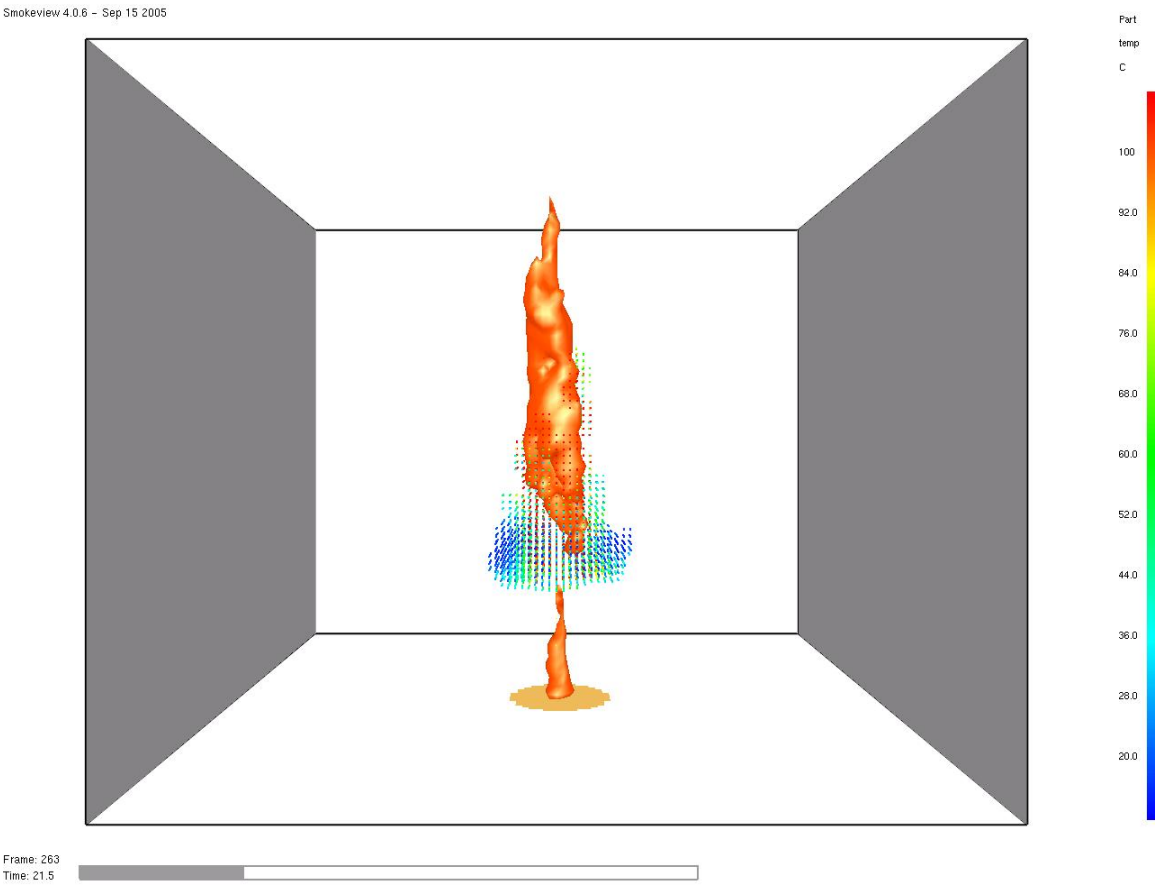

Figure 1- 25 Detailed fire simulation, using output from the FUEL3D model as input to the physical fire model, WFDS. The image shows a fire burning below a tree crown. The tree has a height to crown base of 4m, and foliar biomass is parameterized as dead, with 30% fuel moisture. At t = 21.5 seconds, the fire is actively torching the tree crown.

Light dynamics

Solar radiation has a significant drying effect on dead fine fuel moisture (Nelson 2002) and a fire burning through sun lit fuels can burn hotter and faster than one in the shade. Light dynamics on the forest floor thus both impacts fuel moisture dynamics and can affect fire behavior. To demonstrate the application of fine scale spatial representation in assessing impacts to the microclimate I used ray tracing procedures (North 1996, Govaerts and Verstraete,1998, Brunner 1998) to simulate the shadows cast by a single tree modeled with FUEL3-D. Ray tracing is a spatially explicit approach for light modeling which samples beams of light between the light source (the sun) and a given object and thus is capable of representing shadows and other behaviors related to light with great detail, both in space and in time. The tree, represented as a series of branches and terminal containers, is located in Missoula, Montana., at a point in space (Latitude 46.5 North, Longitude 114.0 degrees West, Missoula, Montana) and at five different points in time over the course of a single day (June 21, 2007, local time) (**Figures 1-26 to 1-30)**. The sequence can also be viewed as an animation: Tree_sun_simulation

Figure 1- 26 View of a single tree with shadows, on the morning of June 21, 2007, in Missoula Montana. The sun-earth-shadow geometry is accurate. Visualization is done with ray tracing.

Figure 1- 27 View of a single tree with shadows, on the morning of June 21, 2007, in Missoula Montana. The sun-earth-shadow geometry is accurate. This image represents a point in time about an hour later than the previous one.

Figure 1- 28 View of a single tree with shadows, in the afternoon, on June 21, 2007, in Missoula Montana. The sun-earth-shadow geometry is accurate. This image represents a point in time about an hour later than the previous one.

Figure 1- 29 View of a single tree with shadows, in the afternoon, on June 21, 2007, in Missoula Montana. The sun-earth-shadow geometry is accurate. This image represents a point in time about an hour later than the previous one.

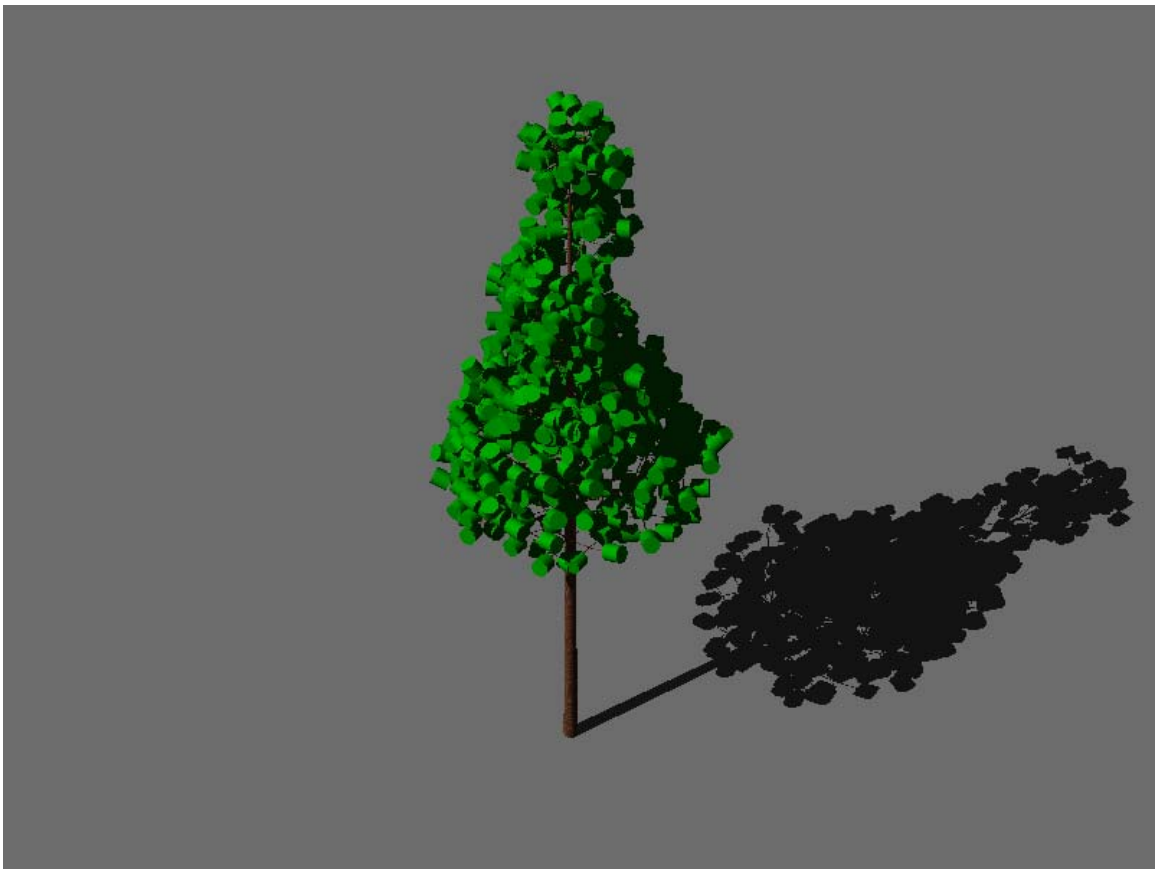

Figure 1- 30 View of a single tree with shadows, in the afternoon, on June 21, 2007, in Missoula Montana. The sun-earth-shadow geometry is accurate. This image represents a point in time about an hour later than the previous one.

DISCUSSION

The ability to represent the spatial structure of vegetation in detail across a range of scales will facilitate improvements in our understanding of fundamental fuels science. Fuel beds can be constructed describing any configuration of trees and shrubs of any size. By building fuel beds from fine scale components of individual trees and shrubs (and associated surface fuels), loss of relevant detail, and potential scale-dependent pitfalls associated with fuel classifications (e.g. Sandberg et al. 2001) can be avoided. At present there is no way that fundamental wildland fuel properties, such as the size distribution of particles or distribution of mass within a tree crown, can be easily calculated. With FUEL3-D these quantities can be calculated from the simulated structure, tested and calibrated. The flexibility with which FUEL3-D can represent the architecture of trees and shrubs makes it possible to develop species-specific fuel models. Differences in crown architecture between species likely play key roles in how fire burns through a stand and how that stand responds to fuel treatment over time. This provides stronger linkages between silviculture, ecosystem function and fuel management such that fuel treatments can be considered not only in terms of their potential impacts on fire behavior but also on other ecosystem components.

A rather simple, but important, feature of the FUEL3D model is that, due to explicit incorporation of coefficients C_1 and C_2 linking fine scale fuel properties to biophysical and climatic conditions for a given site, FUEL3D is designed to take advantage of recent mapping efforts which currently use an ecosystem process modeling approach to map these gradients over large areas. Development of simple correlative relationships linking

these gradients to FUEL3D inputs will enable detailed fuels inputs to be developed with FUEL3D for any location.

By quantitatively describing fuels at higher detail, FUEL3-D will promote an improved understanding of fire and fuels interactions. As seen in the significant differences in fire behavior between the live tree and the dead tree, detailed modeling can be very informative in identifying thresholds in fire behavior. In conjunction with numerical fire behavior models such as FIRETEC or WFDS it will be possible to more precisely study transitions from surface to crown fire and develop species-specific thinning spacing guidelines. Analyses across scales will help to systematically identify conditions when greater complexity in modeling is required, and simpler conditions in which it is not. Correlative relationships observed through more intense numerical studies may be used to refine existing operational models. One advantage of FUEL3-D is its independence from any specific fire behavior model and its assumptions and limitations. At present the model is being designed to work with two numerical fire models, FIRETEC (Linn et al 2002) and WFDS (Mell et al 2005). As other models appear or as these models change FUEL3-D will be able to provide the needed inputs. The independence of the fuel model from particular fire behavior models provides flexibility and facilitates comparisons between models.

Finally, modeling fuel-fire interactions at fine scales will aid in a tighter coupling between fire behavior and fire effects. Most fire effects calculations are carried out as point calculations, where fuel consumption at a point or mortality of an individual tree

are considered (Reinhardt et al 2001). At present it is difficult to rectify the homogeneous stand-based fire behavior calculations from operational fire behavior models with point level fire effects predictions. Incorporation of finer detail in representation of fuels with FUEL3-D, and detailed spatially explicit fire behavior models will provide a basis for linkages between fire behavior, fuels and fire effects than has been possible before. This will improve our ability to define burn window prescriptions and anticipate the consequences of treatments or wildfire.

LITERATURE CITED

Agee, J. K. 1993. Fire ecology of Pacific Northwest forests. Island Press, Washington DC USA.

Agutter, P. S., and D. N. Wheatley. 2004. Metabolic scaling: consensus or controversy? Theoretical Biology and Medical Modelling **1**:11.

Andrews, P. L., C. D. Bevins, and S. R. C. 2005. BehavePlus fire modeling system, version 3: User's guide. General Technical Report. USDA Forest Service, Rocky Mountain Research Station, Fort Collins, CO.

Arno, S. F. 1985. Ecological Effects and Management Implications of Indian Fires. Pages 81-86 in James E. Lotan, et al., ed. *Proceedings, Symposium and Workshop on Wilderness Fire: Missoula, Montana, November 15-18, 1983*. USDA Forest Service, Intermountain Forest and Range Experiment Station. p. 82-83

Banavar, J. R., J. Damuth, A. Maritan, and A. Rinaldo. 2002. Supply-demand balance and metabolic scaling. Proceedings of the National Academy of Sciences **99**:10506-10509.

Banavar, J. R., A. Maritan, and A. Rinaldo. 1999. Size and form in efficient transportation networks. Nature **399**:130-131

Berezovskava, F. S., G. P. Karev, Kisliuk O. S., Khlebopros R. G., and Y. L. Tsel'niker. 1997. A fractal approach to computer-analytical modelling of tree crowns. Trees **11**:323-327.

Berninger, F., M. Mencuccini, E. Nikinmaa, J. Grace, and P. Hari. 1995. Evaporative demand determines branchiness in Scots pine. Oecologia **102**:164-168.

Biswell, H. H. 1960. Danger of wildfire reduced by prescribed burning in ponderosa pine. California Agriculture **1410**:5-6.

Bradstock, R. A., and A. M. Gill. 1993. Fire in Semi-arid, Mallee Shrublands: Size of flames from discrete fuel arrays and their role in the spread of fire. International Journal of Wildland Fire **3**:3-12.

Brandle, J. R., B. B. Johnson, and D. D. Dearmont. 1984. Windbreak economics: the case of winter wheat production in eastern Nebraska. Journal of Soil and Water Conservation **39**:339-343.

Brunner, A. 1998. A light model for spatially explicit forest stand models. Forest Ecology and Management **107**.

Burrows, N. D. 2001. Flame residence times and rates of weight loss of eucalypt forest fuel particles. International Journal of Wildland Fire **10**:137-143.

Busing, R. T. , and Mailly, D. 2004. Advances in spatial, individual-based modelling of forest dynamics. Journal of Vegetation Science **15**:831-842.

Callaway, R. M., E. H. Delucia, and W. H. Shlesinger. 1994. Biomass allocation of montane and desert ponderosa pine: an analog for response to climate change. Ecology **75**:1474-1481.

Cary, G. J., R. E. Keane, R. H. Gardner, S. Lavorel, M. D. Flannigan, I. D. Davies, C. Li, J. M. Lenihan, T. S. Rupp, and F. Mouillot. 2006. Comparison of the sensitivity of landscape-fire-succession models to variation in terrain, fuel pattern and climate. Landscape Ecology **21**:121-137.

Cheng, D.-L., and K. J. Niklas. 2007. Above- and below- ground biomass relationships across 1534 forested communities. Annals of Botany **99**:95-102.

Cohen, J., M. Finney, and K. Yedinak. 2006. Active Spreading Crown Fire Characteristics: Implications for modeling in D. X. Viegas, editor. V International Conference on Forest Fire Research, Coimbra, Portugal.

Cooper, C. F. 1960. Changes in vegetation, structure and growth of southwestern pine forest since white settlement. Ecological Monographs **30**:129-164.

Covington, W. W., and M. M. Moore. 1994. Southwestern ponderosa forest structure: changes since Euro-American settlement. Journal of Forestry **42**:39-47.

Dreyer, O. 2001. Allometric Scaling and Central Source Systems. The American Physical Society **87**(3)**:**.38101

Enquist, B. J. 2002. Universal scaling in tree and vascular plant allometry: toward a general quantitative theory linking plant form and function from cells to ecosystems. Tree Physiology **22**:1045-1064.

Evans, M., N. Hastings, and B. Peacock 1993. Statistical Distributions. John Wiley and Sons, New York.

Finney, M. A. 1998. FARSITE: Fire Area Simulator -- model development and evaluation. Page 47. United States Department of Agriculture, Forest Service Rocky Mountain Research Station, Ft. Collins, CO USA.

Finney, M. A., and J. D. Cohen. 2003. Expectation and evaluation of fuel management objectives. Pages 353-366 in P. N. Omi, editor. Fire, Fuel Treatments and Ecological Restoration. USDA Forest Service RMRS-P-29.

Flannigan, M. D., B. D. Amiro, K. A. Logan, B. J. Stocks, and B. M. Wotton. 2005. Forest fires and climate change in the 21st century. Mitigation and Adaptation Strategies for Global Change **11**:847-859.

Fleming, R. A., Candau, J.-N., and R. S. McAlpine. 2002. Landscape-scale analysis of interactions between insect defoliation and forest fire in central Canada. Climatic Change 55:251-272

Fleming, R.A., and Candau, J.-N. 1998. Influences of climatic change on some ecological processes of an insect outbreak system in Canada's boreal forest and the implications for biodiversity. Environmental Monitoring and Assessment 49:235-249

Fons, W. L. 1946. Analysis of fire spread in light forest fuels. Journal of Agricultural Research **72**:93-121.

Fosberg, M. A., and J. E. Deeming. 1971. Derivation of the 1- and 10- hour timelag fuel moisture calculations for fire-danger rating. Research Note. USDA Forest Service, Rocky Mountain Forest and Range Experiment Station, Fort Collins, CO.

GAO. 2004. Wildfire suppression:funding transfers cause project cancellations and delays, strained relationships, and management disruptions. United States Government Accountability Office GAO-04-612.

GAO. 2007. Wildland Fire Management: A cohesive strategy and clear cost-containment goals are needed for federal agencies to manage wildland fire activities effectively. United States Government Accountability Office GA-07-1017T.

Gillett, N. P., A. J. Weaver, F. W. Zwiers, and M. D. Flannigan. 2004. Detecting the effect of climate change on Canadian forest fires. Geophysical Research Letters **31**:1-4.

Godin, C. 2000. Representing and encoding plant architecture: A review. Annals of Forest Science **57**:413-438.

Goulding, C. J., and J. C. Murray. 1975. Polynomial taper equations that are compatible with tree volume equations. New Zealand Journal of Forest Science **5**:313-322.

Govaerts, Y. M., and M. M. Verstaete. 1998. Raytran: a Monte Carlo ray -tracing model to compute light scattering in three dimensional media. IEEE Transactions on Geoscience and Remote Sensing **36**:493-505.

Grace, J. 1997. Plant water relations. Pages 28-50 in M. J. Crawley, editor. *Plant Ecology*. Blackwell Science, Cambridge.

Graham, R. T., A. E. Harvey, T. B. Jain, and J. R. Tonn. 1999. The effects of thinning and similar stands treatments on fire behavior in western forests. USDA Forest Service, PNW-GTR-463, Portland, OR.

Graham, R. T., S. McCaffrey, and T. B. Jain, Editors. 2004. Science basis for changing forest structure to modify wildfire behavior and severity. USDA Forest Service,Rocky Mountain Research Station.

Gray, H. R. 1956. *The Form And Taper Of Forest-Tree Stems*. Oxford University Press, Oxford.

Grier, C. C., and R. H. Waring. 1974. Conifer foliage mass related to sapwood area. Forest Science **20**:205-206.

Halle, F., and R. A. A. Oldeman 1970. *Essai Sur L'architecture Et La Dynamique De Croissance Des Arbres Tropicaux.* Masson et Cie, Paris.

Halle, F., R. A. A. Oldeman, and P. B. Tomlinson 1978. *Tropical Trees And Forests: An Architectural Analysis*. Springer-Verlag, New York.

Hammer, R. B., V. C. Radeloff, J. S. Fried, and S. I. Stewart. 2007. Wildland-urban interface housing growth during the 1990s in California,Oregon and Washington. International Journal of Wildland Fire **16**:255-265.

Helvey, J. D., and J. H. Patric. 1965. Canopy and litter interception by hardwoods of eastern United States. Water Resources Research **1**:193-206.

Heyerdahl, E. K., R. F. Miller, and R. A. Parsons. 2006. History of fire and Douglas-fir establishment in a savanna and sagebrush-grassland mosaic, southwestern Montana, USA. Forest Ecology and Management **230**:107-118.

Horn, J. S. 1971. The adaptive geometry of trees. Princeton University Press, Princeton, NJ.

Huxley, J. S. 1932. *Problems Of Relative Growth*. Methuea, Methuea.

IPCC. 2007. Climate change 2007: The Physical Science Basis. Summary for Policymakers. Intergovernmental Panel on Climate Change, Geneva, Switzerland.

Jensen, A. M. 1983. Shelterbelt effects in tropical and temperate zones. Page 61. Agriculture, Food and Nutrition Sciences Program, International Development Research Centre, Ottowa, Canada.

Kaufmann, M. R., and C. A. Troendle. 1981. The relationship of leaf area and foliage biomass to sapwood conducting area in four subalpine forest tree species. Forest Science **23**:477-482.

Keane, R. E., and L. Holsinger. 2006. Simulating biophysical environment for gradient modeling and ecosystem mapping using the WXFIRE program: Model documentation and application. Page 61. USDA Forest Service Rocky Mountain Research Station, Fort Collins, Co, USA.

Keane, R. E., M. Rollins, and Z.-L. Zhu. 2007. Using simulated historical time series to prioritize fuel treatments on landscapes across the United States: the LANDFIRE prototype project. Ecological Modelling **204**:485-502.

Kozak, A., D. Munro, and J. H. G. Smith. 1969. Taper functions and their application in forest inventory. Forestry Chronicals **45**:278-283.

Kozlowski, J., and M. Konarzewski. 2004. Is West, Brown and Enquist's model of allometric scaling mathematically correct and biologically relevant? Functional Ecology **18**:283-289.

Kuuluvainen, T. P., T. 1987. Effect of crown shape and tree distribution of shade. Agricultural and Forest Meterology **40**:215-231.

Leopold, L. B. 1971. Trees and Streams: The Efficiency of Branching Pattens. Journal of Theoretical Biology **31**:339-354.

Lewis, H. T. 1985. Why Indians burned: Specific versus general reasons. Pages 75-80 in James E. Lotan et al., ed. *Proceedings, Symposium and Workshop on Wilderness Fire: Missoula, Montana, November, 15-18, 1983*. USDA Forest Service, Intermountain Forest and Range Experiment Station, p. 79.

Li, H.-T., X.-G. Han, and J.-G. Wu. 2005. Lack of Evidence for 3/4 Scaling of Metabolism in Terrestrial Plants. Journal of Integrative Plant Biology **47**:1173-1183.

Linn, R., and Cunningham, P. 2005. Numerical simulations of grass fires using a coupled atmoshphere--fire model: Basic fire behavior and dependence on wind speed. Journal of Geophysical Research **110**:19.

Linn, R., J. N. Reisner, J. Colman, and J. Winterkamp. 2002. Studying wildfire behavior using FIRETEC. International Journal of Wildland Fire **11**:233-246.

Linn, R., J. Winterkamp, J. Colman, C. Edminster, and J. Bailey. 2005. Modeling interactions between fire and atmosphere in discrete element fuel beds. International Journal of Wildland Fire **14**:37-48.

Linn, R. R. 1997. Transport model for prediction of wildfire behavior. Scientific Report LA-13334-T, 195pp. Los Alamos National Laboratory, Los Alamos, NM.

Makela, A., and H. T. Valentine. 2006. Crown ratio influences allometric scaling in trees. Ecology **87**:2967-2972.

Mandelbrot, B. B. 1983. *The Fractal Geometry Of Nature*. W. H. Freeman and Company, New York, New York, USA.
McMahon, T. A. 1973. Size and shape in biology. Science **179**:1201-1204.
McMahon, T. A., and R. E. Kronauer. 1976. Tree Structures: Deducing the Principle of Mechanical Designs. Journal of Theoretical Biology **59**:443-466.
Meinzer, F. C., B. J. Bond, J. M. Warren, and D. R. Woodruff. 2005. Does water transport scale universally with tree size? Functional Ecology **14**:49-62.
Mell, W., J. J. Charney, M. A. Jenkins, P. Cheney, and J. Gould. 2005. Numerical simulations of grassland fire behavior from the LANL-FIRETEC and NIST-WFDS models. In Proceedings, EastFIRE Conference, George Mason University, Fairfax, VA. May 11-13, 2005.
Mencuccini, M., and J. Grace. 1995. Climate influences the leaf area-sapwood relationship in Scots pine (Pinus sylvestris L.). Plant, Cell and Environment **15**.
Morgan, J., and M. G. R. Cannell. 1988. Support costs of different branch designs: effects of position, number, angle and deflection of laterals. Tree Physiology **4**:303-313.
Nelson, R. M., jr. 2002. Prediction of diurnal change in 10-h fuel stick moisture content. Can. J. For. Res. **30**:1071-1087.
Niklas, K. J. 1986. Computer simulated plant evolution. Scientific American **254**.
Niklas, K. J., and B. J. Enquist. 2001. Invariant scaling relationships for interspecific plant biomass production rates and body size. Pages 2922-2927.
Niklas, K. J., and V. Kerchner. 1984. Mechanical and photosynthetic constraints on the evolution of plant shape. Palebiology **10**:79-101.
North, P. R. J. 1996. Three-dimensional forest light interaction model using a Monte Carlo method. IEEE Transactions on Geoscience and Remote Sensing **34**:946-956.
Oke, T. R. 1978. *Boundary Layer Climates*. Methuen, London.
Osada, N., R. Tateno, F. Hyodo, and H. Takeda. 2004. Changes in crown architecture with tree height in two deciduous tree species: developmental constraints or plastic response to the competition for light? Forest Ecology and Management **188**:337-347.
Ozier-Lafontaine, H., F. Lecompte, and J. Francois Sillon. 1999. Fractal analysis of the root architecture of *Gliricidia sepium* for the spatial prediction of root branching, size and mass: model development and evaluation in agroforestry. Plant and Soil **209**:167-180.
Peters, R. H. 1983. *The Ecological Implications Of Body Size*. Cambridge University Press, Cambridge.
Pierce, J. L., G. A. Meyer, and A. J. Jull. 2004. Fire-induced erosion and millennial-scale climate change in northern ponderosa pine forests. Nature **432**:87-90.
Pukkala, T., Kuuluvainen, T. and P. Stenberg. 1993. Below canopy distribution of photosynthetically active radiation and its relation to seedling growth in a boreal Pinus sylvestris stand: a simulation approach. Scand. J. Forest Research. 8:313-325
Pyne, Stephen J. 1982. *Fire in America: A Cultural History of Wildland and Rural Fire*. Princeton, NJ: Princeton University Press.

Radeloff, V. C., R. B. Hammer, S. I. Stewart, J. S. Fried, S. S. Holcomb, and J. S. McKeefry. 2005. The Wildland-Urban Interface in the United States. Ecological Applications **15**:799-805.

Reifsnyder, W. E., and H. W. Lull. 1965. Radient energy in relation to forests. Page 111. Technical Bulletin. USDA Forest Service.

Reinhardt, E. D., R. E. Keane, and J. K. Brown. 2001. Modeling fire effects. International Journal of Wildland Fire **10**:373-380.

Richardson, A. D., and H. zu Dohna. 2003. Predicting root biomass from branching patterns of Douglas-fir root systems. Oikos **100**:96-104.

Robichaud, P. R., L. MacDonald, J. Freeouf, D. Neary, D. Martin, and L. Ashmun. 2003. Postfire rehabilitation of the Hayman fire. In: Graham, Russell T. Tech. Ed. Hayman Fire Case Study. General Technical Report RMRS-GTR-114. Pages 293-313. USDA Forest Service, Rocky Mountain Research Station, Ogden, UT.

Rothermel, Richard C. 1972. A mathematical model for predicting fire spread in wildland fuels. Res. Pap. INT-115. Ogden, UT: U.S. Department of Agriculture, Forest Service, Intermountain Forest and Range Experiment Station. 40 p.

Running, S. W. 2007. Is global warming causing more, larger wildfires? Science **313**:927-928.

Sandberg, D. V., R. D. Ottmar, and G. H. Cushon. 2001. Characterizing fuels in the 21st century. International Journal of Wildland Fire **10**:381-387.

Scott, J. H., and E. D. Reinhardt. 2001. Assessing crown fire potential by linking models of surface and crown fire behavior. Research Paper. USDA Forest Service,Rocky Mountain Research Station, Fort Collins, CO.

Shinozaki, K., K. Yoda, K. Hozumi, and T. Kira. 1964. A quantitative analysis of plant form: the pipe model theory. I. Basic analysis. Japanese Journal of Ecology **14**:97-105.

Strauss, D., L. Bednar, and R. Mees. 1989. Do one percent of forest fires cause ninety-nine percent of the damage? Forest Science **35**:319-328.

Swetnam, T. W., and J. L. Betancourt. 1990. Fire-southern oscillation relations in the southwestern United States. Science **249**:1017-1020.

Tyree, M. T., and F. W. Ewers. 1991. Tansley Review No. 34. The Hydraulic Architecture of Trees and Other Woddy Plants. New Phytologist **119**:345-360.

Vainenen, P., H. Ylitalo, R. Sievanen, and A. Makela. 1996. Effects of age and site quality on the distribution of biomass in Scots pine. Trees **10**.

Valentine, H. T., V. C. Baldwin, T. G. Gregoire, and H. E. Burkhart. 1994a. Surrogates of foliar dry matter in Loblolly pine. Forest Science **40**:576-585.

Valentine, H. T., A. R. Ludlow, and G. M. Furnival. 1994b. Modeling crown rise in even-aged stands of Sitka spruce or loblolly pine. Forest Ecology and Management **69**:189-197.

van Noordwijk, M., and R. Mulia. 2002. Functional branch analysis as tool for fractal scaling above- and belowground trees for their additive and non-additive properties. Ecological Modelling **149**:41-51.

Van Wagner, C. E. 1977. Conditions for the start and spread of crown fire. Canadian Journal of Forest Research **7**:23-34.

Van Wagtendonk, J. W. 1996. Use of a deterministic fire growth model to test fuel treatments. Pages 1155-1165. Sierra Nevada Ecosystem Project final report to

Congress : status of the Sierra Nevada. Volume II, Assessment and scientific basis for management options. Davis CA : Centers for Water and Wildland Resources University of California Davis 1996.
Vogel, M., and F. A. Williams. 1970. Flame Propagation Along Matchstick Arrays. Combustion Science and Technology **1**:429-436.
Weaver, H. 1955. Fire as an enemy, friend and tool in forest management. Journal of Forestry **53**:499-504.
Weber, R. O. 1990. A model for fire propagation in arrays. Mathl Comput. Modelling **13**:95-102.
West, G. B., J. H. Brown, and B. J. Enquist. 1997. A general model for the origin of allometric scaling laws in biology. Science **276**:122-126.
West, G. B., J. H. Brown, and B. J. Enquist. 1999. A general model for the structure, function and allometry of plant vascular systems. Nature **400**:664-667.
Westerling, A. L., H. G. Hidalgo, D. R. Cayan, and T. W. Swetnam. 2006. Warming and earlier spring increase western U.S. forest wildfire activity. Science **313**:940-943.
White, C. R., P. Cassey, and T. M. Blackburn. 2007. Allometric exponents do not support a universal metabolic allometry. Ecology **88**:315-323.
Wotton, B. M., and M. D. Flannigan. 1993. Length of the fire season in a changing climate. Forestry Chronicals **69**:187-192.

CHAPTER II: EXPLORATION OF FINE SCALE FIRE AND FUEL INTERACTIONS WITH FUEL3D AND THE PHYSICAL FIRE MODEL, WFDS

ABSTRACT

Current operational predictions of crown fire initiation rely on the assumption that crown fuels can be reasonably represented as a homogeneous layer which will burn if enough heat is introduced at its base. However, this assumption has never been tested. In this study, the effect of heterogeneity within the crown of a tree on fire behavior is investigated. Three trees with the same fuel quantities but different spatial configurations are simulated with the spatial fuel model, FUEL3D. For each spatial configuration, four different scenarios are assembled representing combinations of height to crown base (HI, 7m and LO, 4m) and inclusion / exclusion of woody biomass within the crown, for a total of twelve different cases spanning three factors. Fires are then simulated under these tree crowns with the physical fire model, WFDS. All three factors appear to influence outcomes, with differences in fuel consumption, timing, duration and intensity of temperature and in flow dynamics; height to crown base generally had less effect than the spatial configuration of the fuels. These fine scale interactions between the fire and the fuel suggest that the initiation of crown fire may depend on the distribution, configuration and properties of fuel within the crown.

INTRODUCTION

Crown fires, once initiated, are extremely difficult to suppress (Albini and Stocks 1986), in part due to an increased likelihood of spotting behavior, as firebrands are lofted ahead of the flaming front from high in the canopy (Wade and Ward 1973). Crown fires burn with greater intensity and faster spread than surface fires (Rothermel 1983), so firefighters need larger safety zones to protect themselves from crown fires than from surface fires (Butler and Cohen 1998). Given that the onset of crown fire behavior can jeopardize fire fighters and typically necessitates a significant change in suppression

strategies, prediction of the conditions under which crown fire initiates is of primary concern in fire management.

Similarly, from an ecological standpoint, crown fires may result in severe impacts to ecosystems. Hydrologic functions within burned watersheds, such as whole system water storage, flow rates and timing of runoff events, are affected mainly through changes in the interception of rain by forest canopies and by water storage in the vegetation, both of which are affected when a crown fire kills trees. Changes in species composition may arise due to large scale changes in forest microclimates following severe fires, and often due to the destruction of trees which could serve as seed source for new regeneration. A key factor in the severity of crown fire ecological impacts is tree mortality. Thus, prediction of the degree of tree mortality that might be expected from a given fire is of paramount interest to researchers and ecosystem managers.

Current models used operationally for prediction of crown fire initiation (Finney 1998, Scott and Reinhardt 2001, Forestry Canada Fire Danger Group 1992) all rely on a common theoretical background developed (Van Wagner 1977), which states that,

$$I_0 = (Czh)^{(3/2)}$$

Eqn. 2- 1

where I_0 is the critical surface intensity needed for a crown fire to initiate, C is an empirical constant describing the ratio of the ambient temperature to the temperature

required for ignition , h is the ignition energy, and z is the height to the base of the crown fuel layer. Van Wagner's approach assumes that the crown fuel to be burned consists of a single homogeneous layer and that crown fire will be initiated provided that the base of this layer is heated to a sufficient temperature; the spread of the fire upward through the crown fuel is thus considered to occur without regard for the bulk density, or other properties of the crown. Other models have been developed with more complex configurations (e.g. Cruz et al 2006) but which still assume that crown fuels are a homogenous and continuous layer; this assumption is common to all of the operational models. Similarly, models used to predict fire induced tree mortality assume a homogeneous crown volume extending from the crown base to the top of the tree and intersect that volume with a predicted scorch height (Van Wagner 1973) (Ryan and Reinhardt 1988, Reinhardt et al. 2001, Keyser et al. 2006); the likelihood that a tree will be killed increases with the proportion of the crown volume burned.

The assumption of a homogeneous crown layer is thus a central component in current models used to predict the initiation of crown fires and tree mortality arising from fires. While it may be reasonable to assume a homogeneous crown layer in forest types characterized by dense, continuous trees of very similar size and age, typified by the stands used in Van Wagner's analysis (Van Wagner 1964, Van Wagner 1968), such an assumption is increasingly tenuous when applied to stands characterized by variability in size and numbers of trees. At present Van Wagner's model is used in operational models for all forest types, regardless of the composition, structure and stocking of the stand; it is likewise applied in stands that have been thinned or affected by disease (Reinhardt and

Crookston 2003). To date, however, the potential implications of crown fuel heterogeneity for crown fire initiation and tree mortality have not been explored.

In general, the only models which are capable of addressing variability in crown fuels are numerical physical models (Linn 1997, Linn et al 2002, Mell et al. 2005, Mell et al 2006a Dupuy and Morvan 2005, Morvan and Dupuy 2001). To date, however, applications of such models have been largely focused at scales larger than an individual tree (Linn et al 2002, Linn et al 2005, Cunningham and Linn 2007); those modeling experiments which have been done at individual tree scales have not dealt with gaps or other fine-scale fuel variability (< 1 m scale) within the tree crown (Mell et al 2006b, Linn et al. 2005).

Heterogeneity exists in a forest at several scales. At a landscape scale differences in productivity, aspect (sun exposure) and other factors lead to differences between stands. Within stands, heterogeneity arises in the spacing between trees and in differences in tree size and species. At the still finer scale of an individual tree, heterogeneity exists within a tree crown in the distribution of fuel in space, the gaps between branches and clumps of foliage.

This premise of this study is that, since crown fires consist of many burning trees, insights relevant to crown fire initiation and to tree mortality may arise from consideration of the rather simpler case of a single burning tree. In real fires, whether an individual tree crown burns or not is often highly dependent on the specific flame-crown

geometry (**Figure 2-1**). To avoid unnecessary complexity the basic scenario is that of a single tree, exposed to flame from below, with no ambient wind (**Figure 2-2**).

Figure 2- 1 Example photo illustrating the geometry-specific nature of fire burning through a tree crown. In this case the portion of the tree crown that is burning is directly in line with the heat source below.

Figure 2- 2 Photo of a single tree burning from below. This is the situation being modeled in this study. Unlike the simulations presented in this study there is some ambient wind influencing the fire plume at the top of the tree.

Objectives

The purpose of this experiment was to explore fine scale interactions between fire and fuels at the scale of an individual live tree. In this exploratory study three initial factors are considered: 1) differences in spatial configuration of the fuels, 2) differences in the height to crown base (4 m or 7 m), and 3) and whether or not larger diameter woody material within the crown, which does not itself burn but may alter certain aspects of the fire, is included in the simulation.

METHODS

The WFDS Model

The Wildland Fire Dynamics Simulator (WFDS) model is a recent adaptation of the Fire Dynamics Simulator (FDS), a detailed Computational Fluid Dynamics (CFD) model designed for structural fire (burning buildings) applications. WFDS was modified from FDS to handle wildland fuels that are unlike fuels in structure fires. WFDS is a physical numerical fire behavior model which solves the Navier-Stokes fluid dynamics equations appropriate for low Mach numbers (when the rates of change at which processes are occurring are significantly lower than the speed of sound). In such modeling, the simulation is confined within a defined volume, or spatial domain, within which quantities are required to be accounted for according to equations for the conservation of mass, momentum, energy and species (quantities of gasses). In WFDS, the spatial domain is a three-dimensional rectilinear grid. The use of a rectilinear grid facilitates the use of a Poisson flow solver, which can significantly speed up calculations, but also makes it difficult to deal with non-flat topography. In this fine scale experiment, however, topographic variability is not a concern.

The simulations

A total of thirteen simulations were carried out in the course of this study.

no tree simulation

The first simulation had no crown fuels and was designed to characterize the fire behavior arising from the ignitor rings (described below) alone without any potential interactions with the crown fuels. This initial simulation was then followed by twelve individual tree simulations, described below.

Tree simulations

Three live trees with the same biomass quantities and overall crown dimensions (crown length, crown radius and height to crown base) were simulated with FUEL3D. Each tree had a different crown form, or overall habit of the tree, as well as correspondingly different fine scale configuration of the fuels within the crown. Foliar moisture was held constant at 100% (dry weight basis). The first tree was simulated with a conical form, the second with a cylindrical form, and the third with an ellipsoidal form (**Figure 2-3**).

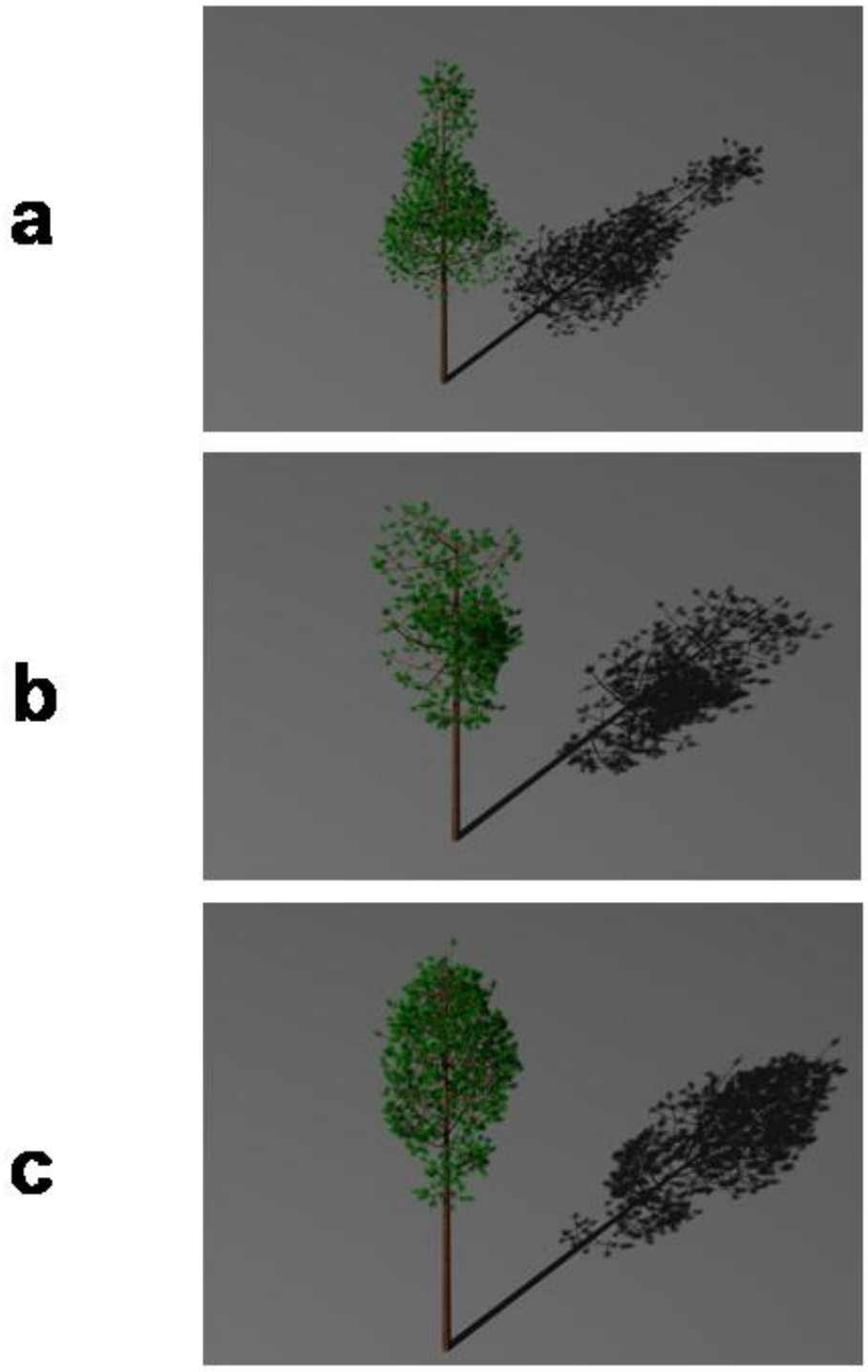

Figure 2- 3 The three trees simulated with the FUEL3D model and used in these experiments with the WFDS fire model. Tree A has a conical form, Tree B has a random crown form and Tree C has an elliptical crown form.

The three tree crowns were thus identical but had different spatial configurations. Each of these tree crowns was then translated down from its original position to create two, otherwise identical, crowns with different height to crown base. Each crown was then summarized to three dimensional arrays to be used as fuel inputs to the numerical fire behavior model WFDS, in two ways. In the first volume summarization only the thermally thin foliage fuel elements were included. Foliage and small twigs are considered to be "thermally thin" because heat transfer into the particle occurs essentially instantaneously because the particle size is very small. In the second volume summarization, larger woody components of the tree were also included (**Figure 2-4**). The larger diameter woody material is considered "thermally thick", meaning that there is a time dependent radial heat transfer into the particle. The thermally thick biomass was parameterized with a very high heat of vaporization (9999 degrees) so it would not burn up itself. The inclusion or exclusion of that biomass thus does not change the amount of fuel that can burn, but might affect how the thermally thin biomass burned or other aspects of the fire's behavior.

Altogether the tree simulations represents all combinations of three cases of spatial configuration, two cases of height to crown base, and two cases of woody biomass (with and without), for a total of twelve tree simulations scenarios.

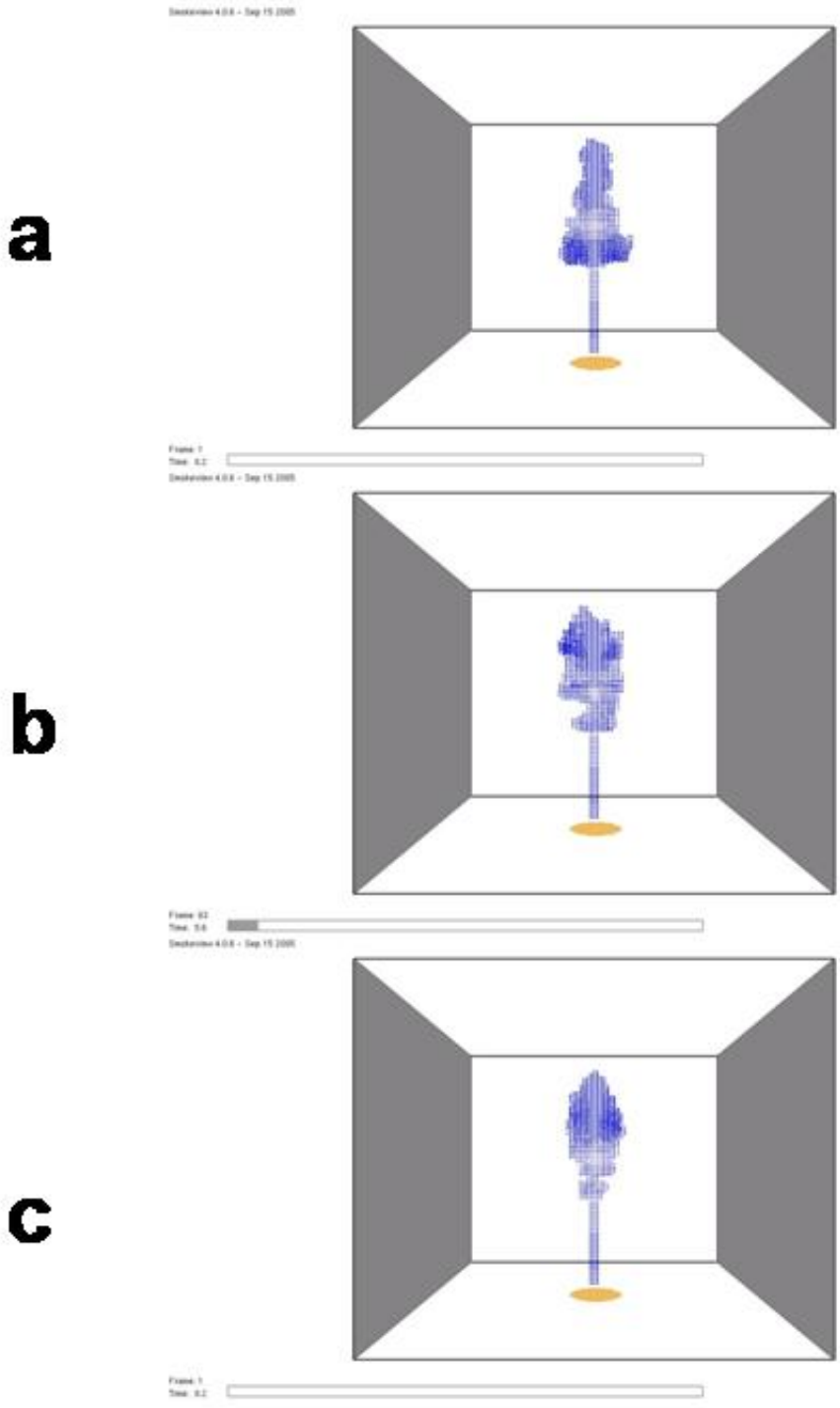

Figure 2- 4 Three trees simulated with FUEL3D after summarization to 0.25m cell volumes, shown here as a series of blue dots representing the center of a each cell. Each cell has a unique quantity of fuel associated with it as well as other properties.

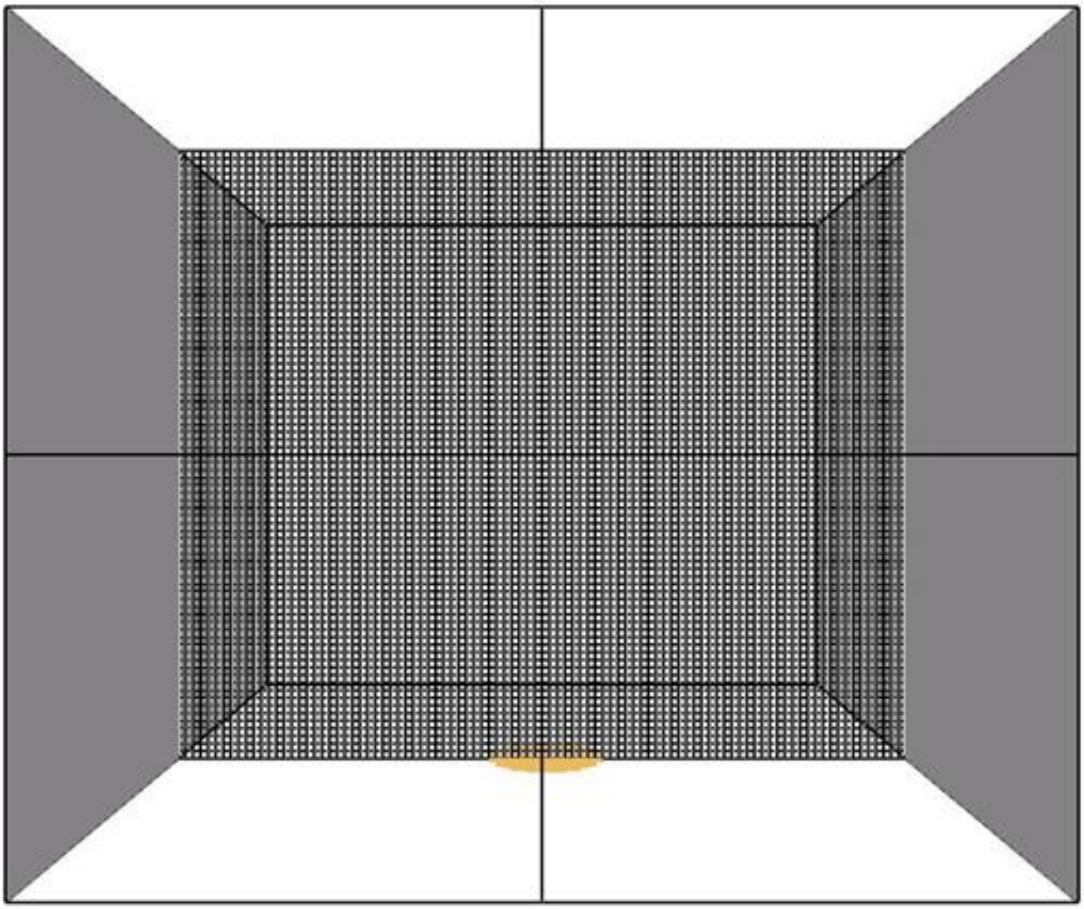

Figure 2- 5 The spatial domain used in WFDS simulations consisted of 96x96x80 cells.

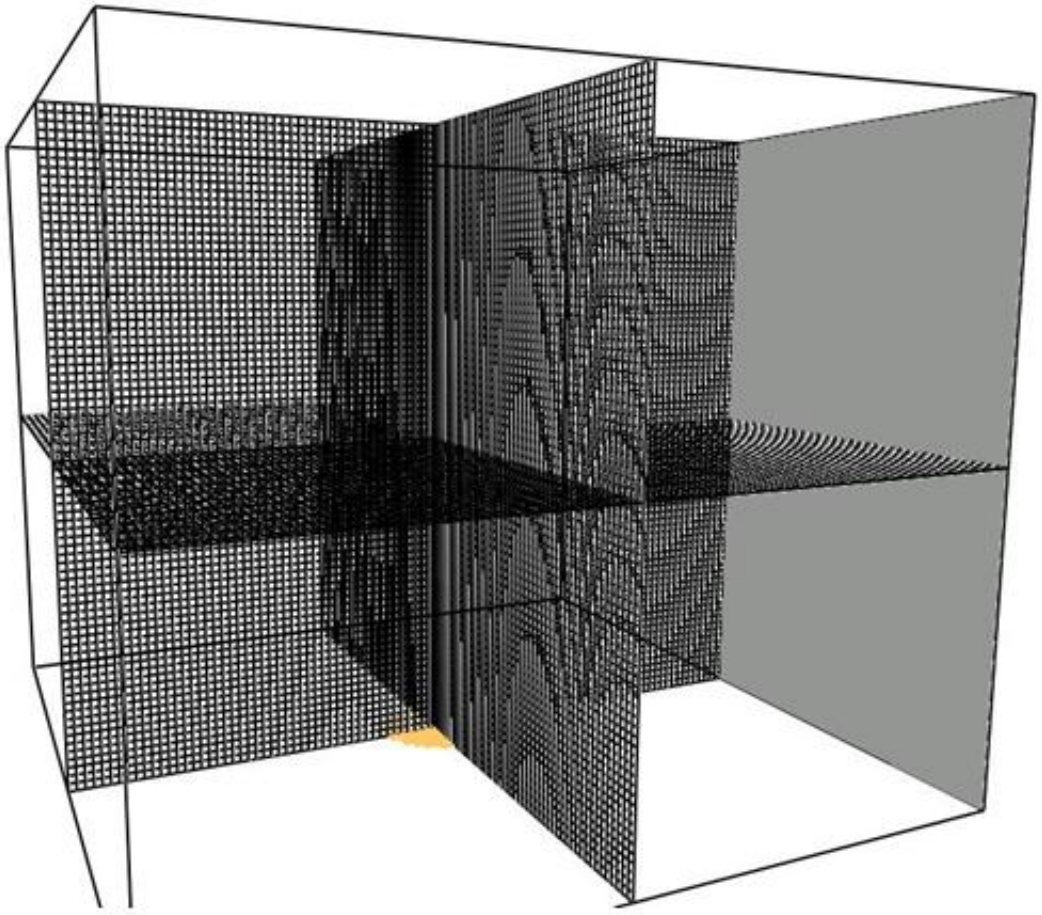

Figure 2- 6 An oblique view of the spatial domain, measuring 96x96x80 cells.

Each simulation was run with the numerical physical fire behavior model WFDS for 80 seconds of simulation time.

Spatial domain, boundary conditions and cell resolution

A rectangular spatial domain, measuring 24 meters x 24 meters in the x and y axes and 20 meters in the z axis (height) was used for the simulations. Cell size in all dimensions was 0.25 m; this resulted in a total numerical grid of 96x96x80 cells. Simulated trees were positioned at the origin (x=0, y=0) such that they were centered within the domain. Boundary conditions were open, with no external inertia, such that gasses and heat are permitted to leave the volume; for conservation however the quantities which leave are accounted for (**Figure 2-5 and 2-6**). These boundary conditions are straightforward but somewhat simplistic; in a real fire burning in the forest, winds outside the immediate area of the burning tree would have a good deal of inertia that would likely entrain the wind flows within the domain.

Ignition

Ignition with the WFDS model is a special, time dependent case of a boundary condition for a particular region. The ignition area is defined with a maximum heat output rate (heat release rate per unit area, in kW/m^2) and time specifications indicating the duration for which this heat output will be maintained. This is similar to a gas burner with a specified flow rate of gas. All simulations presented here had the same ignition setup, which consisted of a series of four concentric circles radiating out from the origin, each 0.5 m wide. The ignitor circles were set up on individual timers such that as one finished the next one began. This resulted in a pattern of fire ignition intended to mimic a fire being started from a small area in a grass fuel bed with no wind.

The heat release rate per unit area (kW/m^2) used for ignition is a calculated as follows

$$hrrpua = \frac{\left(r(1-c)w_f h_c\right)}{D}$$

Eqn. 2- 2

where r is the rate of spread in m/s, c is the char fraction,w_f is the fuel load (kg), h_c is the heat of combustion (kJ/kg) and D is the fireline depth. The values used in these simulations were r = 0.0333, c= 0.2,w_f = 0.7,h_c = 15600 and D = 0.2909. Altogether these yield a straightforward heat release per unit area of 1000 kW/m^2. This is approximately equivalent to the Anderson fuel model 3 (tall grass) burning in a no wind scenario (Anderson 1982). The value of r is set from the distance and time sequence of the ignitor rings. The value of w_f is consistent with recent grass fire experiments in Australia (Cheney et al 1993, Cheney and Gould 1995) and related numerical fire model tests (Mell et al. 2006a), while the values of h_c and c are from the literature (Susott 1982). Each ignitor ring was set to output the heat release rate per unit area of 1000 (kW/m^2)for 15 seconds following a 2 second ramp up period, and ending with a 2 second ramp down period. Rates of change in ignition ramps are linear in nature.

Analysis of model output

Types of model output

Interpretation of output from CFD models can be difficult because the data is dynamic in space and time. Output from the WFDS model is made accessible to the user through the

Smokeview program, a program produced by the developers of WFDS that reads in output from WFDS and which produces high quality graphic output (Forney and McGrattan 2004). Smokeview can be set up to provide a number of different forms of quantitative output, ranging from point measurements to 2 dimensional volume slices to complete three dimensional volumes (Forney and McGrattan 2004). For the most part desired outputs must be specified before the simulation is run. For these simulations four types of different model outputs were used to compare different simulations: total mass loss over time, vertical slices, individual cell temperature records, and animations generated from images showing the progression of the fire over time. These outputs, as well as related post processing and analysis carried out on those data are described below.

mass loss data

The first model output examined was the mass loss data, which refers to the overall fuel consumption over time. This is a global quantity tracked at each time step, so the data is formatted as a single array of mass loss values along with the corresponding points in time.

Two dimensional slice data

Two dimensional slice data are often used for visualizing flow and other dynamics of simulations in three dimensions. To aid in analysis of the simulations, two dimensional slices at y=0, (the plane along the centerline of the spatial domain and parallel to the x axis), were output for two quantities: the vertical component of the wind flow, and temperature.

The first quantity was the vertical, or W, component of the flow, or wind field. Winds in CFD models (and any other three dimensional application) are described as velocity vector fields with U,V and W components, where the U component measures the velocity in the direction of the x axis, V measures and velocity in the y axis and W measures the velocity along the z axis. In these experiments, in which there is no ambient wind, the source of wind is buoyancy from the heat of the fire, so the W component of the wind field describes the expected direction of movement, as well as reductions in velocity that might occur as a result of drag from the fuels.

The second quantity output as a two dimensional slice was temperature. While temperature is an obvious output to consider in comparisons between fire simulations, here the expectation was that the spatial pattern of the temperatures within the slice averaged over the thirty second period would provide insights about how the spatial pattern of the fuels might influence the fire, particularly with respect to reductions in temperature arising from either radiative shielding or absorption of heat by the thermally thick material.

Over the course of the simulation the values in all cells are constantly changing and can be quite ephemeral, with particular conditions lasting only for a fraction of a second. To provide a stable basis for comparison, the slices extracted from the simulation output were averaged over a 30 second period from t=30s to t=60s. This serves as a record of the overall pattern of what occurred during this period. The particular time window was selected because it captured the bulk of the fire-fuel interactions in these simulations.

To facilitate comparisons between simulations, the time averaged two dimensional slices for the temperature and wind data for each run were used to extract contours. For the temperature slices contours were extracted for temperatures of 300, 400 and 500 degrees while for the W component of the wind field contours were extracted at 3, 6 and 9 m/s. As all contours were closed figures, the area for each contour the area was then calculated. Similar to how the perimeter of a fire serves as a useful measure of how a fire spreads over time, the area of the contour at each value represents a succinct measure of difference between simulations.

Individual cell records over time

The third type of output used to compare simulations was from individual cell records of temperature over time. Temperature data were extracted at a series of cells located at the origin and extending vertically, at 1 m intervals, to a height of 18 m. For comparisons between runs I examined both the maximum temperature for each of these cells for each simulation and the progression of temperature recorded over time at each cell.

Animations

To illustrate the configuration of the fuels and behavior of the fire for each simulation, a series of one thousand images were output from the Smokeview software. These images were then used to make animations in standard .AVI file format using MATLAB. The view of the spatial domain was rotated incrementally during the image output such that each animation provides a full 360 degree view of the simulation.

RESULTS

Summary of fire behavior

As the simulations are highly dynamic, they are best viewed first via the animations. The table below presents links to animations for selected simulations:

Table 2- 1 Animations of selected individual tree fire simulations carried out with FUEL3D and WFDS.

Hyperlink to File
Conical_Hi_no_woody
Conical_Lo_no_woody
Elliptical_Hi_no_woody
Elliptical_Lo_no_woody
Conical_Hi_w_woody
Conical_Lo_w_woody
Elliptical_Hi_w_woody
Elliptical_Lo_w_woody

The narrative presented below, however, may be useful in interpreting the animations.

No Tree run

The behavior of the fire in the initial simulation, in which no tree was burned, is illustrative of the complex dynamics which occur in fires in three dimensions. Here I refer to three figures which show the no tree simulation at three particular moments in time. A more comprehensive view can be seen in the animation file. In these figures two features of the fire are displayed. The first is an orange isosurface, or three dimensional contour, of the stoichiometric value of the mixture fraction, which describes the mixture of fuel gas and oxygen necessary for flaming combustion. The spatial resolution in this simulation, and in most simulations, is too large to actually represent the true flame structure, but such an isosurface is commonly used to represent the flames of the fire. The second feature of the fire shown is a slice of the W component of the wind field. This is represented by the colored surface facing the viewer.

The chief behavior observed in this simulation is the formation of a smooth, laminar, candle like flame structure which occurs because there is no external ambient wind influencing the flames. This can be seen in the progression described below.

At t = 8.5 s, the flames are just beginning to develop at the center of the domain. The W wind component shown in color is very symmetrical, tall and smooth. An area near the top of the heat column (colored a deeper orange) shows a relatively higher vertical velocity from the buoyancy of a heat pulse from the initiation of the fire (**Figure 2-7**).

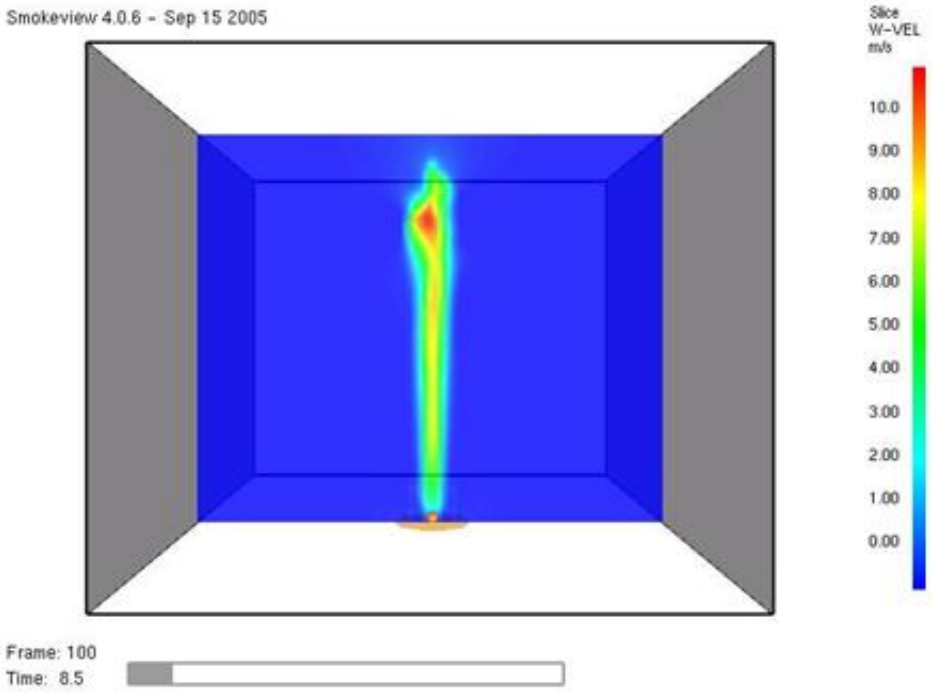

Figure 2- 7 W (vertical) component of the flow at y=0 at t=8.5 for the no tree simulation.

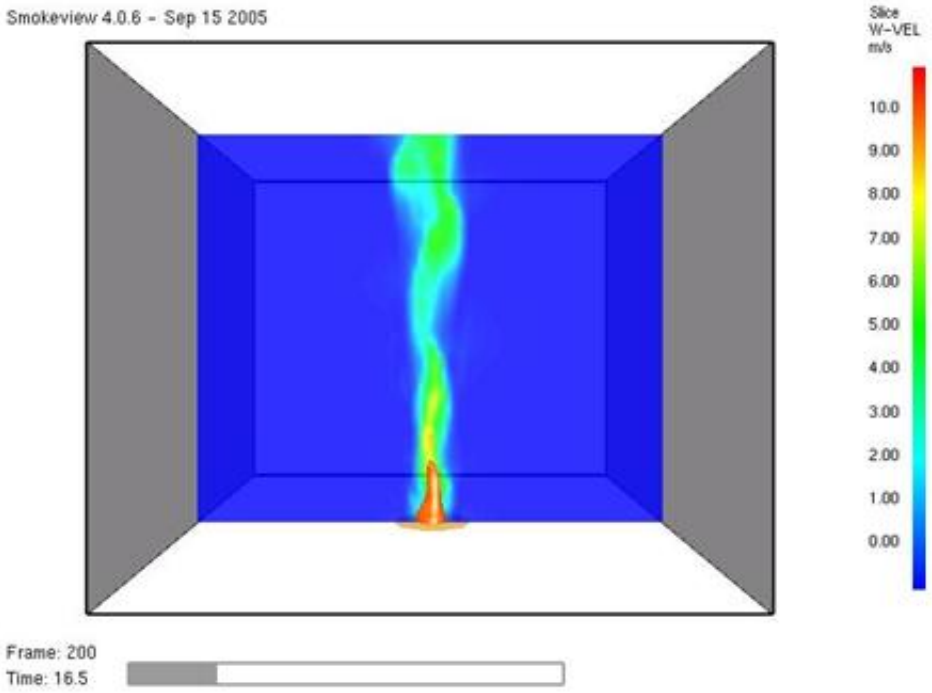

Figure 2- 8 W (vertical) component of the flow at y=0 at t=16.5 s for the no tree simulation run.

At t = 16.5 s, the flame surface has expanded outward radially and is now a cone like shape (**Figure 2-8**). The wind W component shown in color is fairly homogeneous in magnitude and has developed some waves in its profile as turbulent eddies start to form. These eddies are evident in the corresponding wind U component (**Figure 2-9**); in this figure the light blue colors to the right of the flame indicate a negative flow (going backwards in the x direction) associated with a convective in draft. By t=32.5, the flame surface has expanded radially again and is taller (**Figure 2-10**). Although there is some wave like movement in the flame at the particular moment in time shown, the overall shape is still very smooth and largely symmetrical. Above the flame surface the wind W component is broken up into distinct regions of lower velocity (green) , medium velocity (yellow) and higher velocity (red). These regions arise due to the turbulent eddies in the wind flow, which can be seen in the corresponding wind U component (**Figure 2-11**). Although the geometry of the flame structure at a particular moment in time is difficult to predict, the fire atmosphere interaction of the heat and the air tends to maintain an underlying pattern which is fairly stable. This can be seen in **Figure 2-12** which shows a similar flame structure for the no tree simulation at t = 30 and t=45.

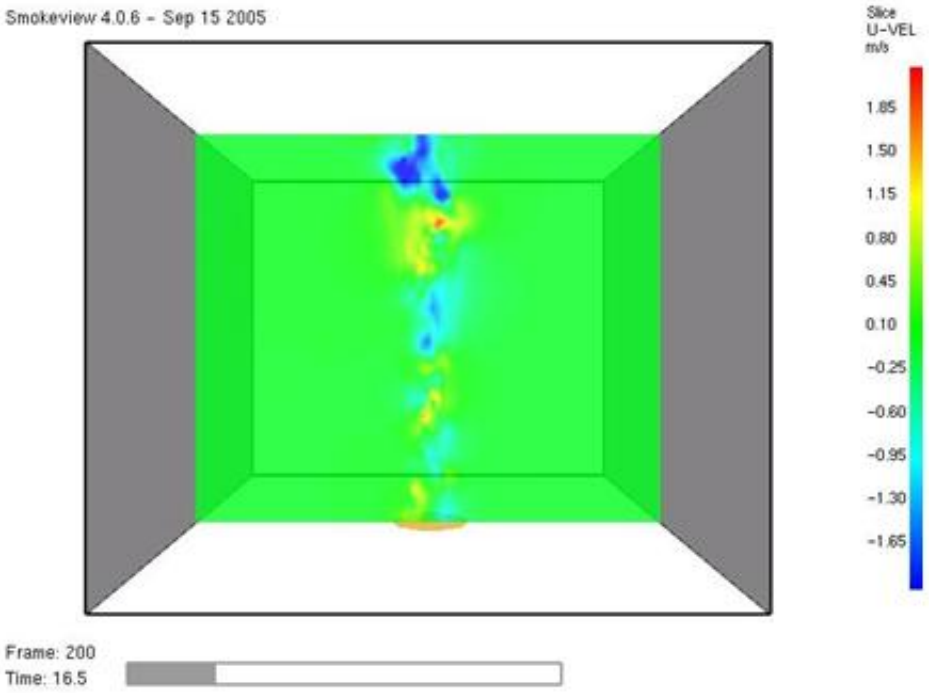

Figure 2- 9 A slice of the U (horizontal, along x axis) component of the wind flow at t=16.5 w.

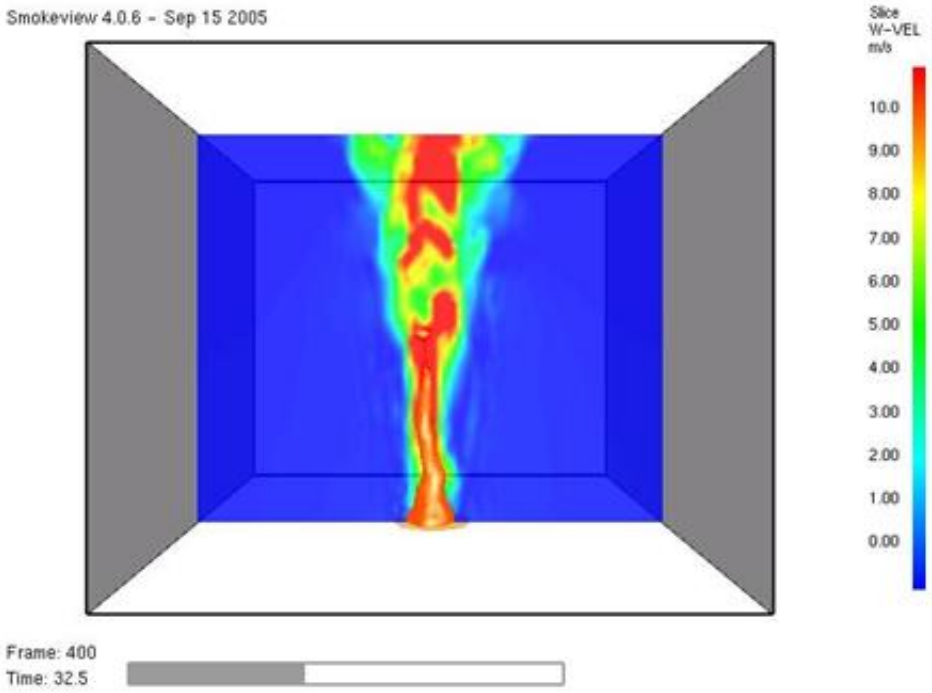

Figure 2- 10 W (vertical) component of the flow at t = 32.5s for the no tree simulation run.

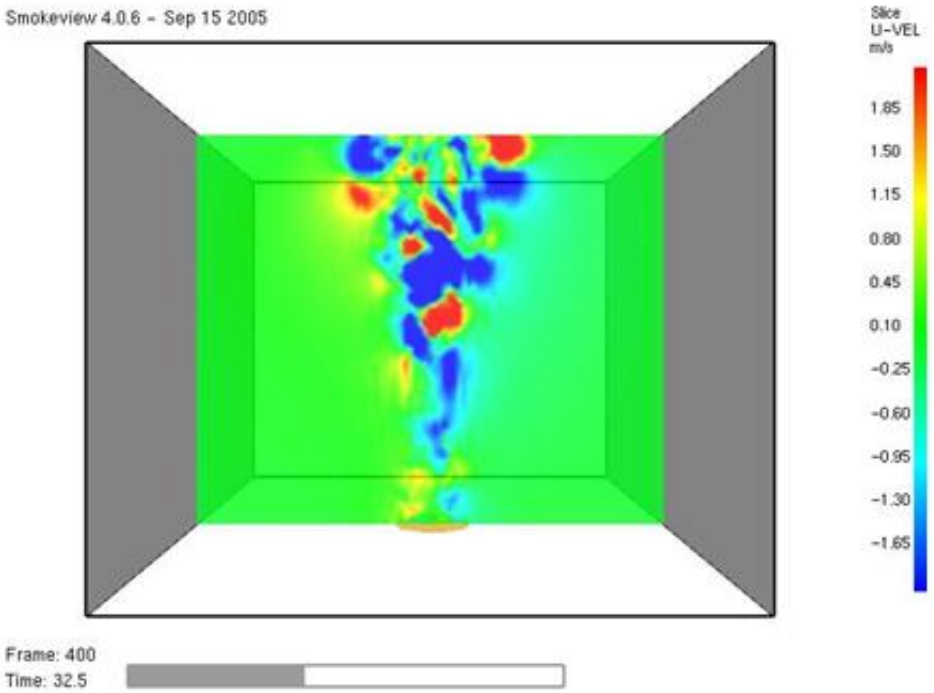

Figure 2- 11 U (horizontal, along x axisl) component of the flow at t=32.5 s for the no tree simulation run.

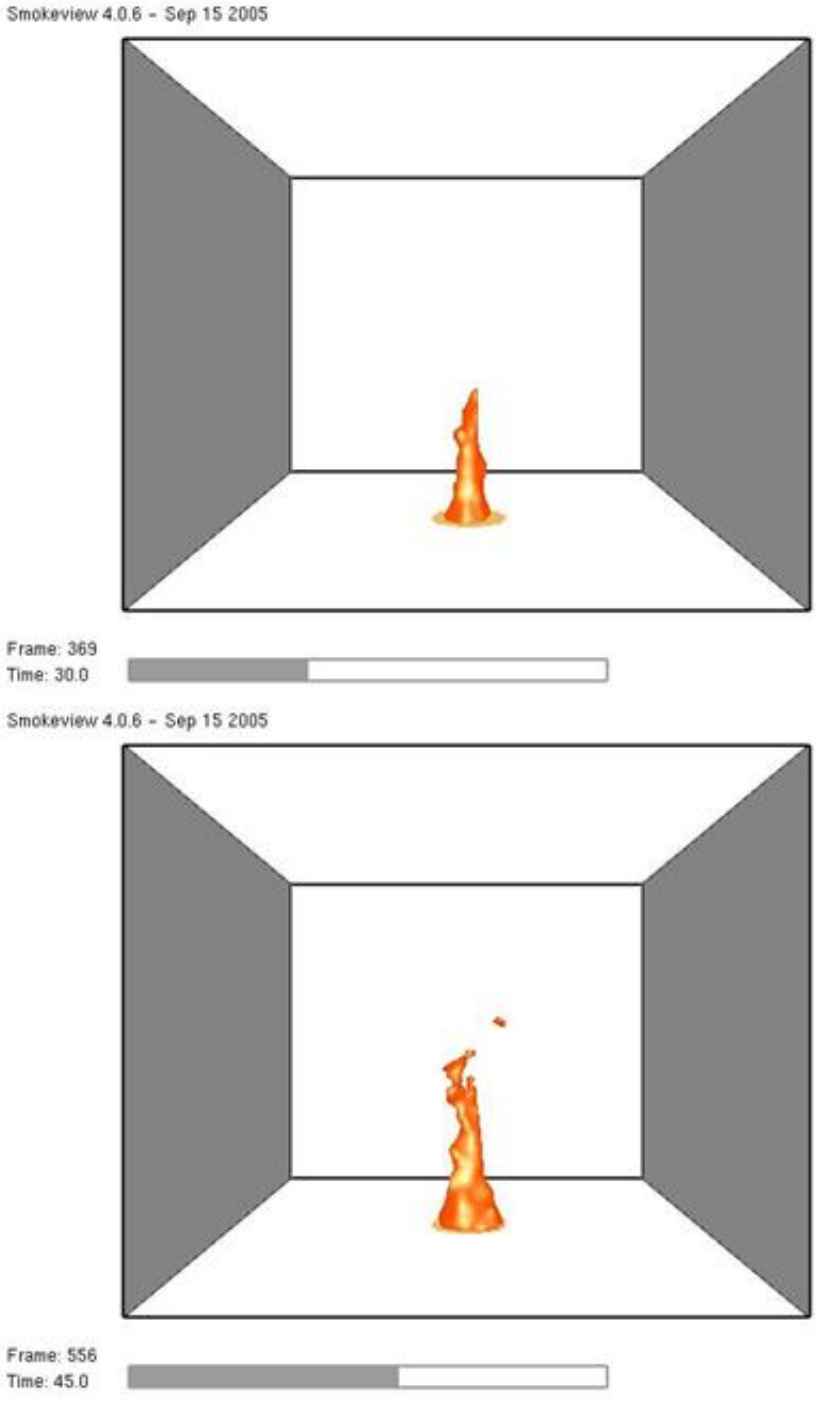

Figure 2- 12 Isosurfaces (three dimensional contours) on the mixture fraction, which is used to represent the flame structure in WFDS, at t=30 s(top) and t=45 s(bottom).

Tree simulations fire behavior description

Figures 2-13, 2-14 and 2-15 illustrate that addition of a tree crown to the simulation (conical, random and elliptical tree crowns, respectively, all with 7 m height to crown base and no woody mass), modifies the flame structure somewhat, producing a taller and thinner structure, but this structure is still fairly consistent over time. In these figures the top frame shows the fire at t= 30 and the bottom frame shows the fire at t = 45. In addition to the orange isosurface which represents the flame, the figures show a series of dots which indicate the location of cells with fuel, and for which the color shows the fuel temperature at that location. The figures show differences in the degree to which the tree crowns are heated between the two moments in time, with the cone tree and the elliptical tree generally hotter than the random tree. At t = 45 the base of the elliptical tree has burned off and the dots for those cells are no longer present.

While a more complete view of the simulations can be seen in the animations, these figures are representative of the fire behavior observed in the tree simulations. In general, while the tree crowns were all partially burned, no pronounced torching events, in which a large portion of the crown ignites rapidly were observed. This is consistent with field observation, where trees with high foliar moisture content do not easily ignite without a substantial heat source.

Fuel consumption within the crown was dependent on flame contact, which varied over time both as the ignitor rings successively turned on, and as turbulent eddies formed in the flow. In all simulations portions of the crown were left at the end of the

simulation. In most cases the remaining crown fuel was at the outer edges of the tree crown where flame contact was less consistent.

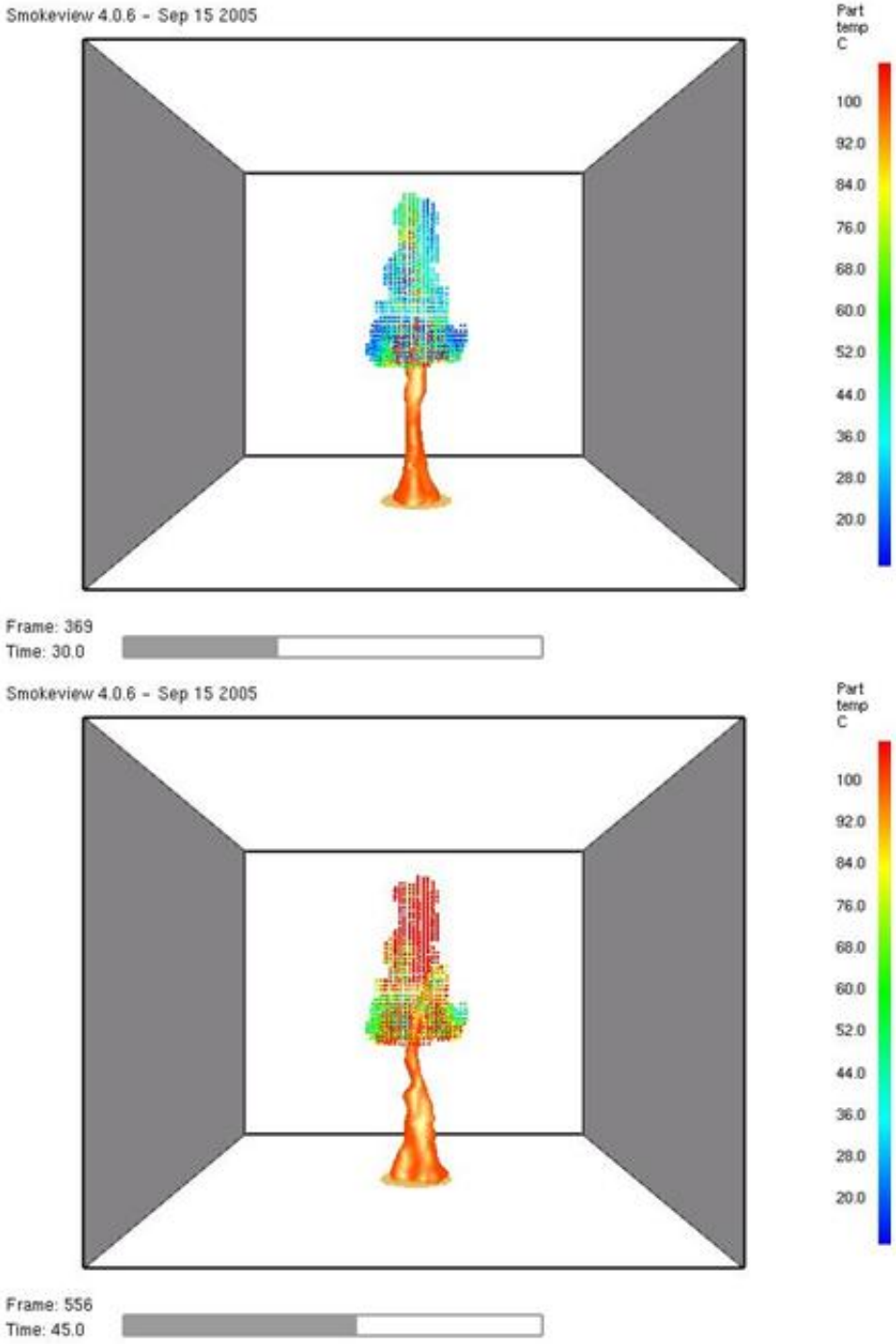

Figure 2- 13 Isosurfaces (three dimensional contours) on the mixture fraction, which is used to represent the flame structure in WFDS, at t=30 s(top) and t=45 s(bottom), along with the representation of the fuel elements, for the cone crown form tree.

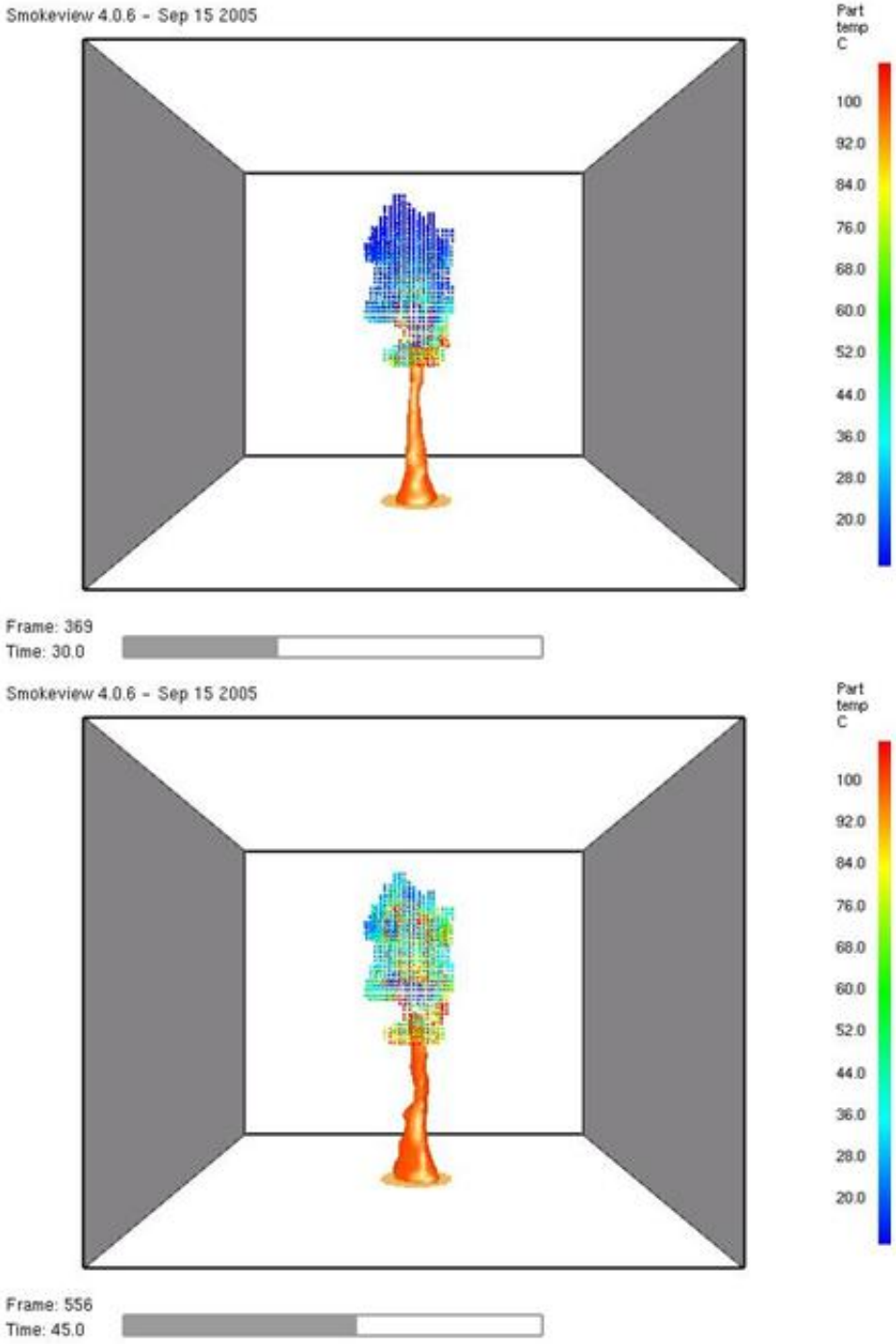

Figure 2- 14 Isosurfaces (three dimensional contours) on the mixture fraction, which is used to represent the flame structure in WFDS, at t=30 s(top) and t=45 s(bottom), along with the representation of the fuel elements, for the random crown form tree.

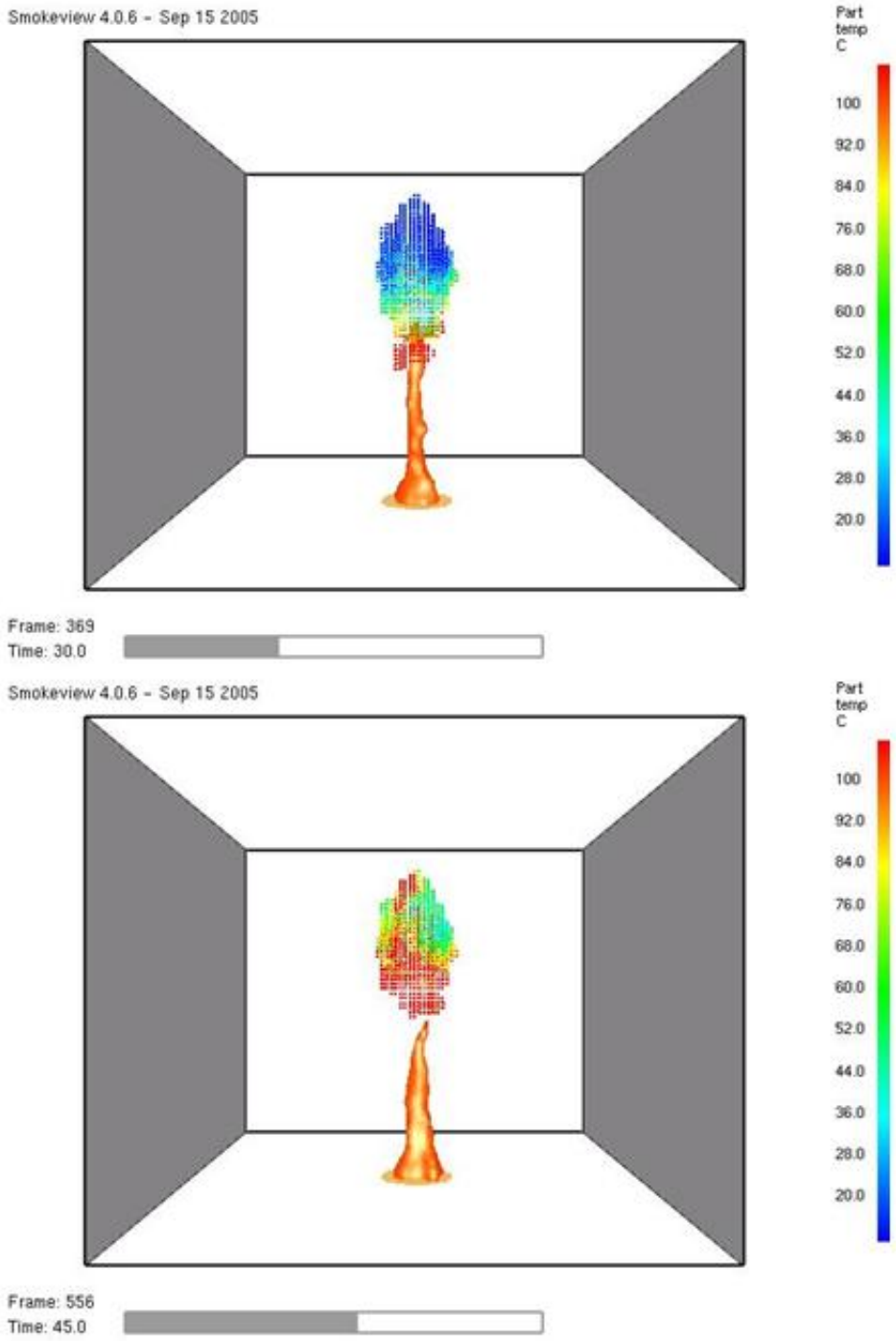

Figure 2- 15 Isosurfaces (three dimensional contours) on the mixture fraction, which is used to represent the flame structure in WFDS, at t=30 s(top) and t=45 s(bottom), along with the representation of the fuel elements, for the elliptical crown form tree.

In the section below I describe how the tree simulations differed from the no tree simulation and from each other.

Comparisons between simulations

mass loss data

Because there were no crown fuels in the no tree simulation comparison of mass loss is made for the tree simulations only. **Table 2-2**, below, lists the total fuel consumption for the tree simulations.

Table 2- 2 Percent fuel consumed over the course of each simulation.

Description	#	Total Fuel Consumed %
CONE HI NO WOODY	1	38.6
CONE LO NO WOODY	2	35.8
RAND HI NO WOODY	3	21.2
RAND LO NO WOODY	4	26.5
ELLPT HI NO WOODY	5	30.0
ELLPT LO NO WOODY	6	43.3
CONE HI W WOODY	7	32.2
CONE LO W WOODY	8	33.1
RAND HI W WOODY	9	20.8
RAND LO W WOODY	10	23.7
ELLPT HI W WOODY	11	38.6

ELLPT LO W WOODY	12	40.8
NO TREE SIMULATION	13	NA

For all tree simulations, fuel consumed was less than half of the total fuel available, so no crown was completely consumed. The highest percent fuel consumed was 43.3%, for the elliptical crown with lower crown base (4 m) and without large diameter woody biomass. The lowest percent fuel consumed was 20.8 %, for the random crown with higher crown base (7 m) and with woody biomass included. The range in fuel consumption was thus 22.5%.

Differences were observed in both the total fuel consumed (**Figure 2-16**) and in the timing in fuel consumption between the various simulations, with some simulations having fairly consistent rates of fuel consumption and others showing higher variability (**Figure 2-17**). In comparisons of fuel consumption across appropriate pairings (e.g. changing one factor while holding others constant), the largest differences in fuel consumption were between crown forms (e.g. . conical vs random); both crown form and the inclusion of woody mass had larger pairwise differences between simulations in mass loss than reduction in height to crown base.

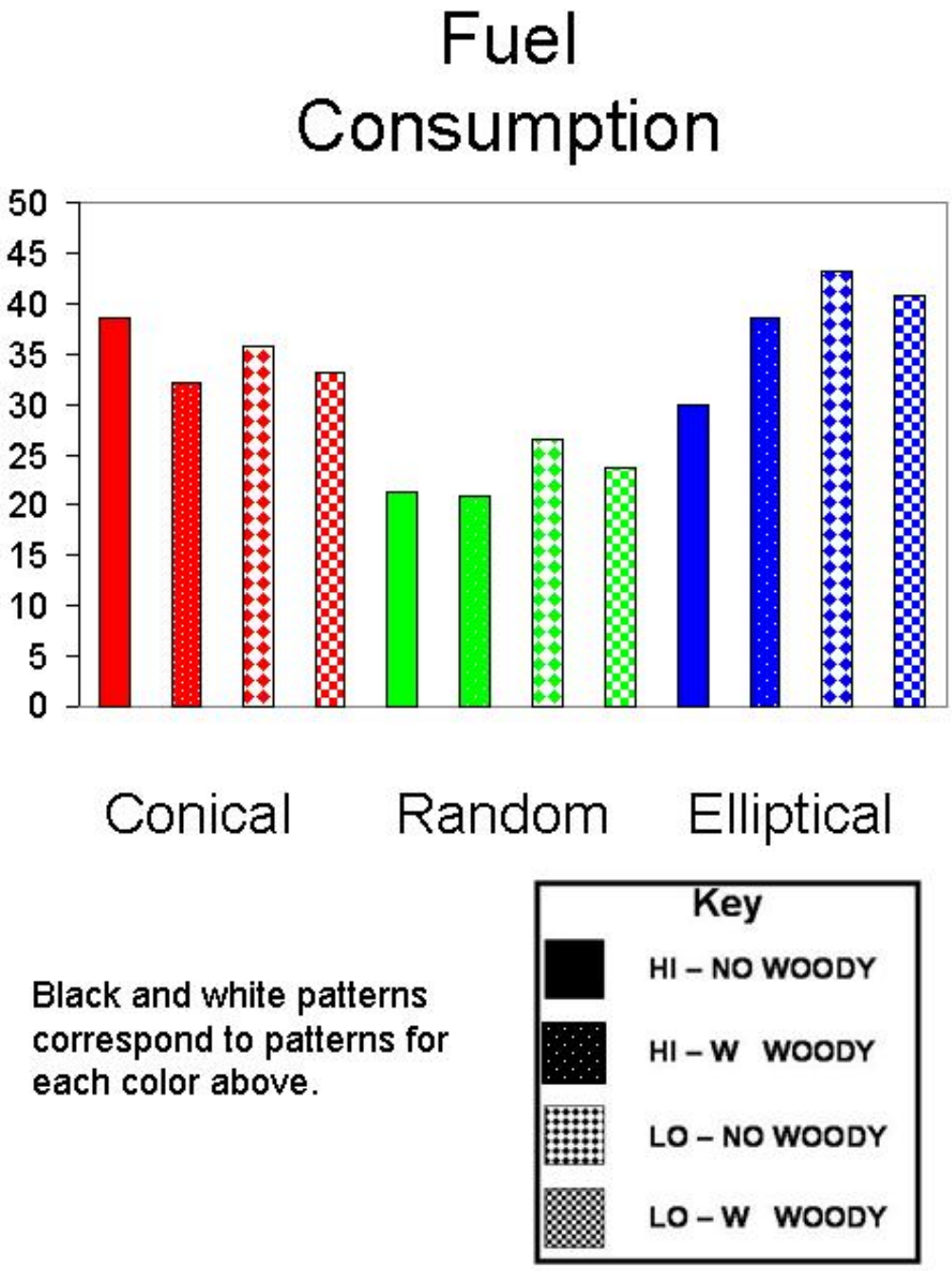

Figure 2- 16 Differences in fuel consumption between the various simulations. All bars of the same color share the same crown form. Patterns within a color indicate the other factors: height to crown base (HI = 7m, LO = 4m), and with and without woody biomass.

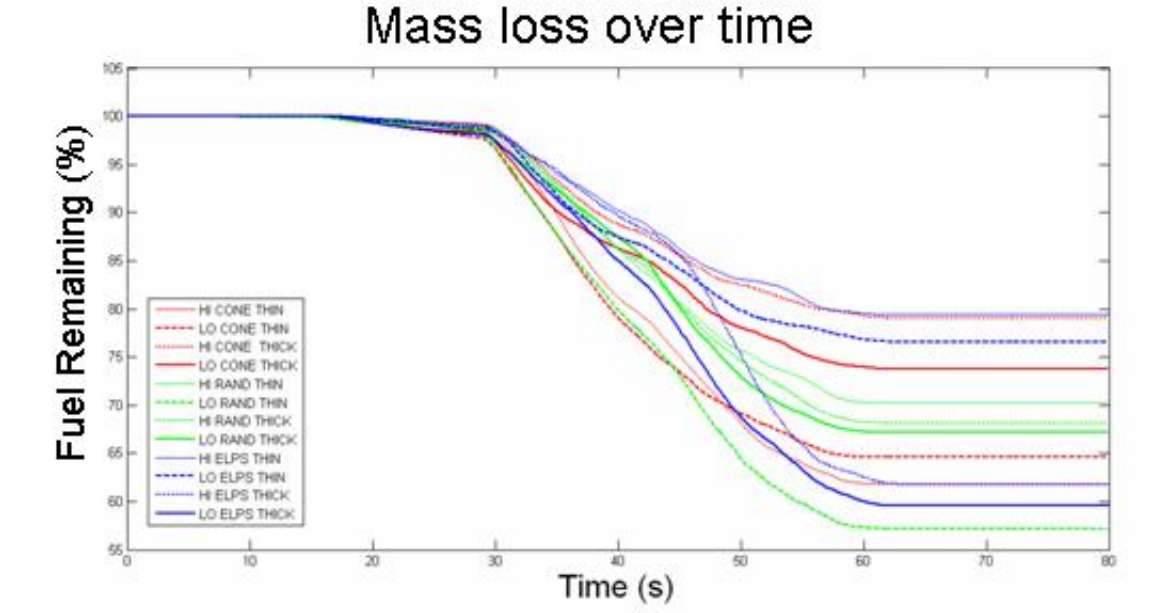

Figure 2- 17 Mass loss over time for each of the 12 tree burn simulations.

Some patterns in fuel consumption are suggested; inclusion of woody mass reduced fuel consumption in all but one case (Simulation 6 vs. Simulation 12), and lowering the height to crown base increased fuel consumption in all but one case (Simulation 1 vs. Simulation 2). The random crown form had the lowest fuel consumption in all cases.

Slice data

Comparisons of tree simulations vs no tree simulation

Although the temperature and wind are highly dynamic when viewed at particular moments in time, when viewed over a larger time span, such as the 30 second –averaged temperature and wind W slices for the no tree simulation, they show a very smooth and predictable pattern (**Figure 2-18**). **Figures 2-19, 2-20 and 2-21** illustrate how the patterns of time averaged temperature and wind W values were altered by the presence of the conical , random and elliptical trees, respectively. Figures shown are for simulations 1,3, and 5 (Table 2, below TAB) (the cases with high height to crown base (7 m) and without the inclusion of large diameter woody biomass). Qualitatively we see from these figures that the spatial pattern of temperature and wind is different between each tree and between each tree and the no tree simulation.

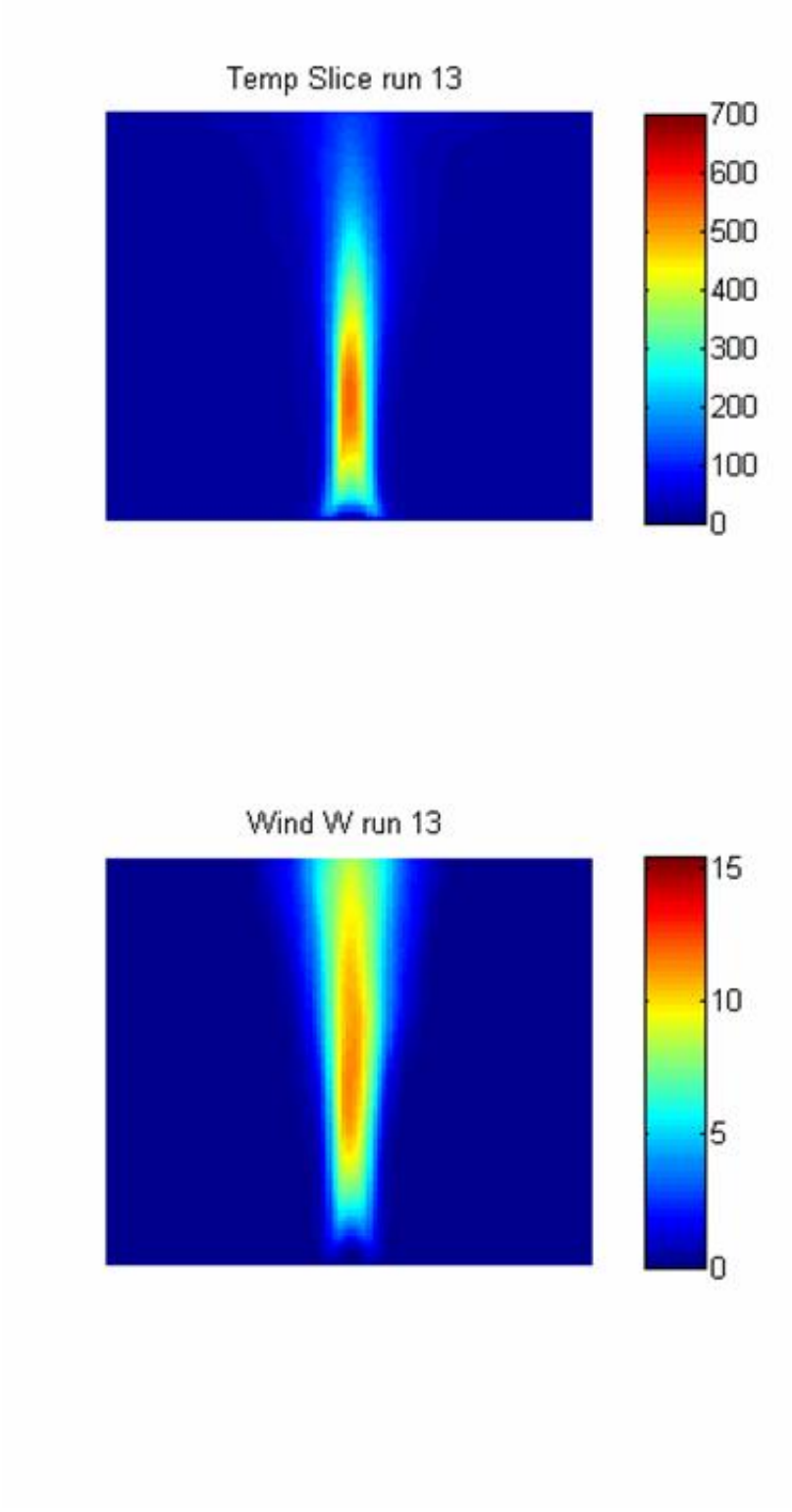

Figure 2- 18 Slices of temperature and W (vertical) component of the flow for the no tree simulation, averaged over the period t=30 to t=60, the period during which fuel consumption occurred in all the tree simulations.

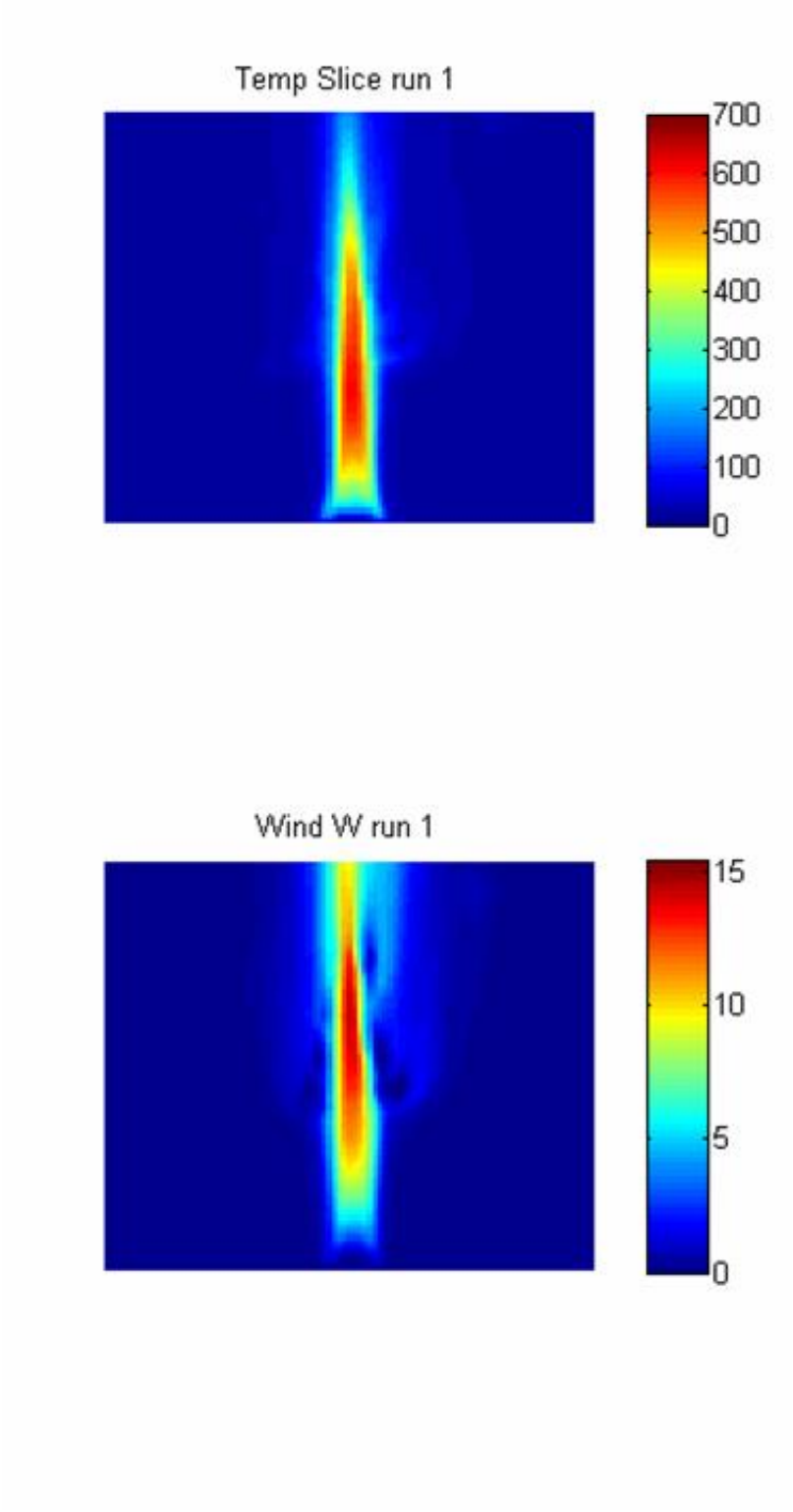

Figure 2- 19 Slices of temperature and W (vertical) component of the flow for the conical crown form tree simulation, averaged over the period t=30 to t=60, the period during which fuel consumption occurred in all the tree simulations.

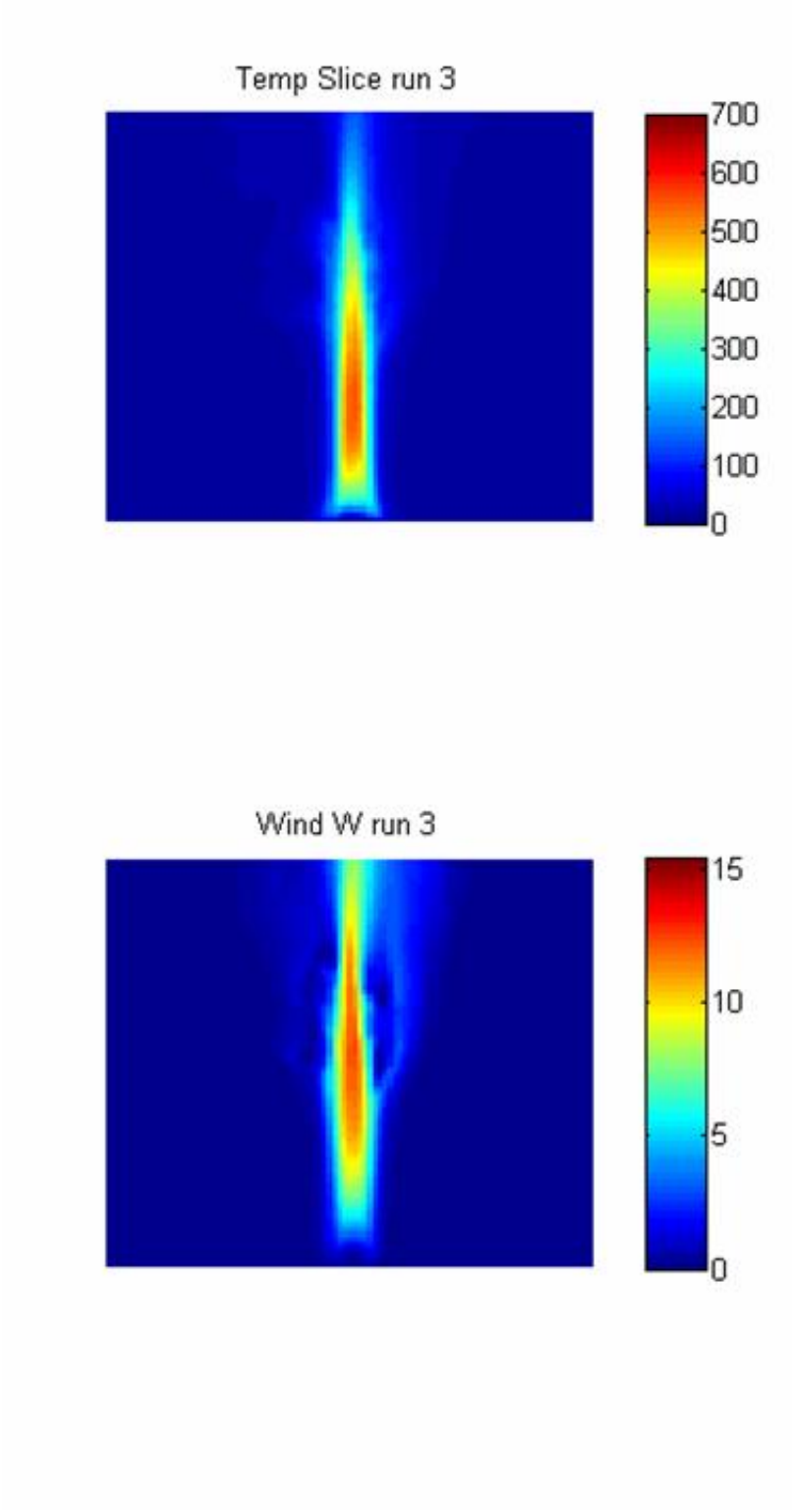

Figure 2- 20 Slices of temperature and W (vertical) component of the flow for the random crown form simulation, averaged over the period t=30 to t=60, the period during which fuel consumption occurred in all the tree simulations.

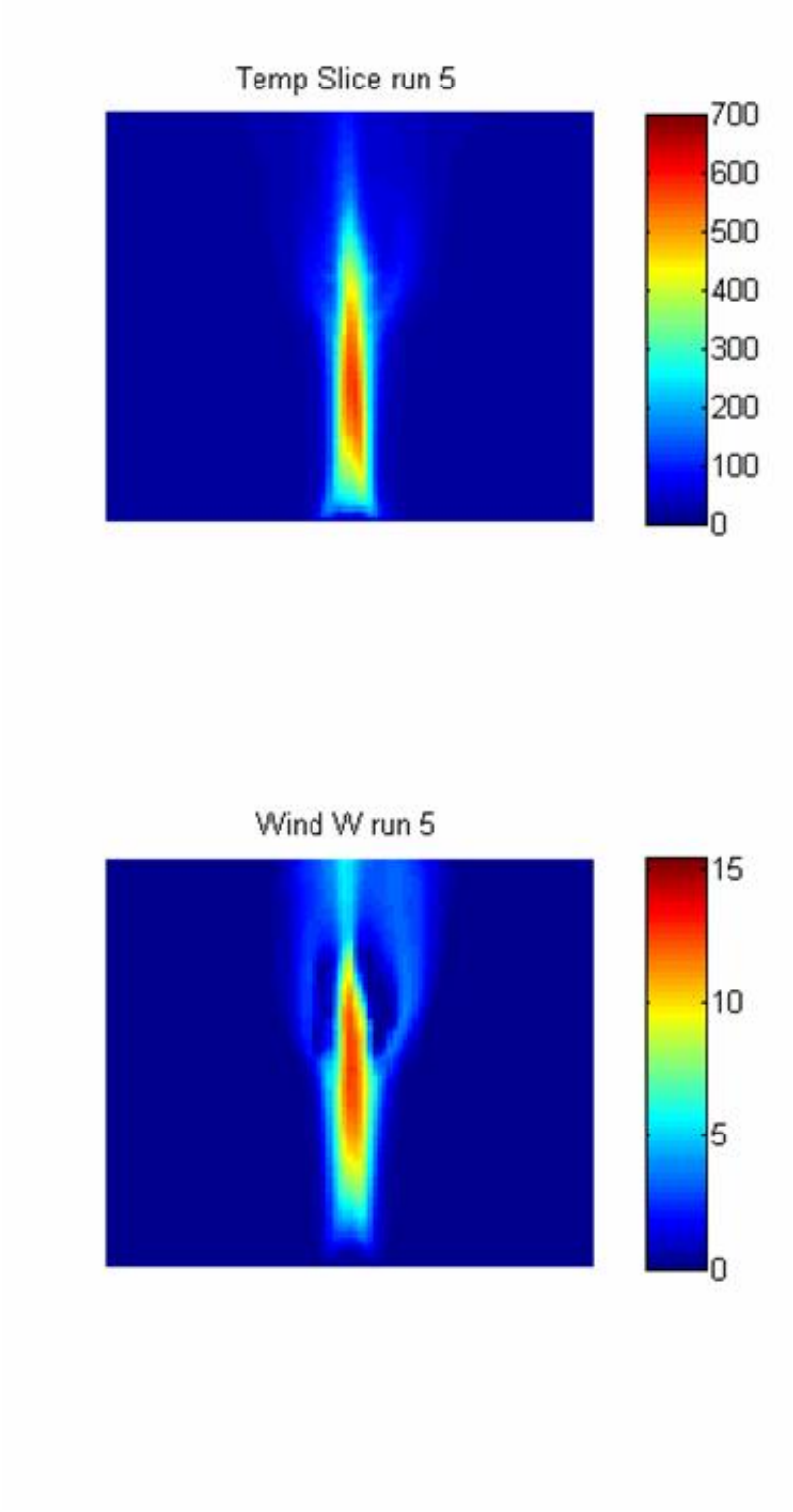

Figure 2- 21 Slices of temperature and W (vertical) component of the flow for the elliptical crown form simulation, averaged over the period t=30 to t=60, the period during which fuel consumption occurred in all the tree simulations.

Table 2-3, below, presents the contour areas from the slice data for the simulations.

Table 2- 3 Contour areas extracted at selected levels from 30 second time averaged two dimensional slices of temperature (levels T=300,T=400, and T=500) and wind W (levels W = 3, W = 6, and W = 9). Simulations are identified by name and by number.

Description	#	T300	T400	T500	W3	W6	W9
CONE HI NO WOODY	1	19.2	12.8	6.7	58.9	30.2	14.7
CONE LO NO WOODY	2	21.9	13.3	6.0	55.1	29.7	17.0
RAND HI NO WOODY	3	14.2	8.3	2.3	54.9	25.5	11.5
RAND LO NO WOODY	4	19.3	13.2	6.5	54.5	30.9	15.7
ELLPT HI NO WOODY	5	13.4	7.7	2.4	67.7	18.0	9.0
ELLPT LO NO WOODY	6	17.7	11.6	5.9	63.0	28.3	13.0
CONE HI W WOODY	7	18.0	11.8	5.8	57.5	25.8	8.0
CONE LO W WOODY	8	17.3	11.3	5.2	53.9	24.2	10.3
RAND HI W WOODY	9	15.8	8.6	4.5	56.0	22.2	4.6
RAND LO W WOODY	10	16.8	10.6	5.0	49.8	26.4	9.2
ELLPT HI W WOODY	11	16.1	10.3	4.5	68.4	17.2	4.8
ELLPT LO W WOODY	12	16.6	10.7	6.4	55.9	21.9	4.5
NO TREE SIMULATION	13	13.3	6.9	1.6	64.3	39.1	15.2

All tree simulations had larger temperature contour areas, for all three contour levels (T=300, T=400 and T=500). The majority of the tree simulation runs had smaller wind contour areas than the no tree run (two exceptions). These are intuitive results; larger temperature contours result when trees are burned because additional heat (above that of the ignitor rings) is generated from the burning of the crown fuels. Similarly, the smaller

wind W contour areas in the tree simulations arise because the wind field in the no tree simulation is unimpeded by crown fuels. Comparison between the no tree simulation and the tree simulations thus serves mostly to demonstrate an expected outcome that provides a context for comparisons between tree simulations.

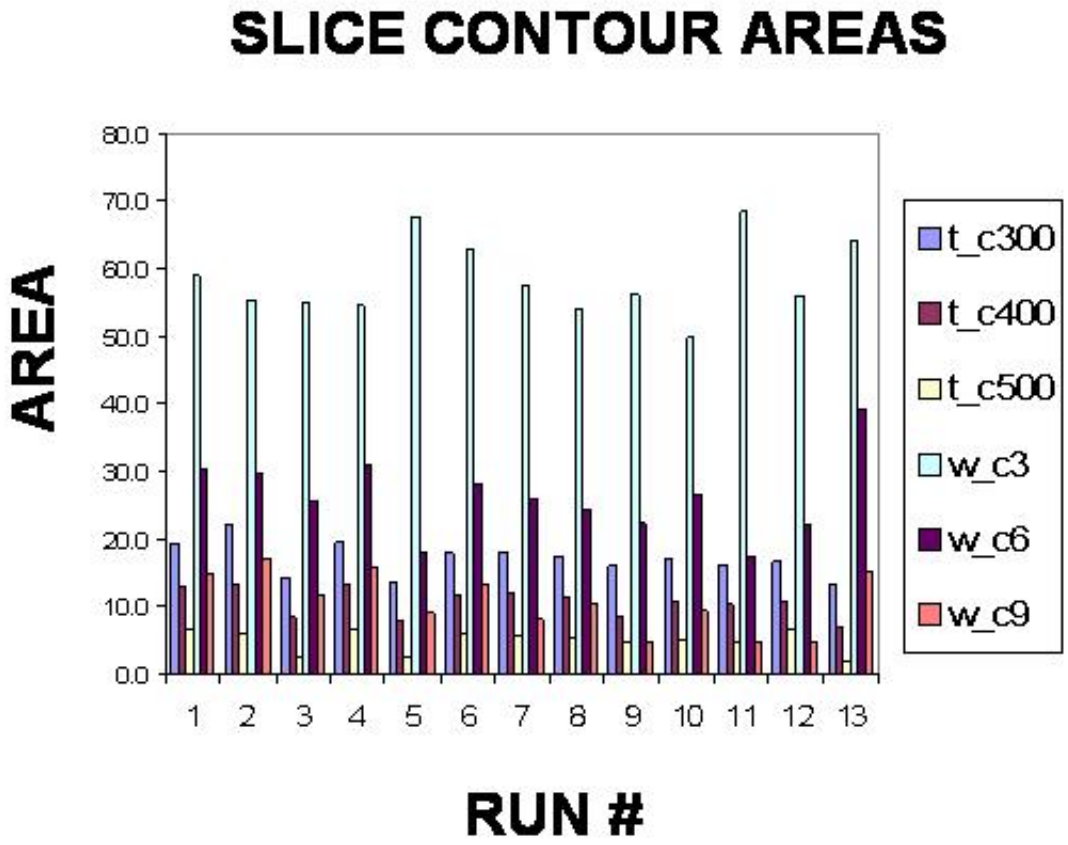

Figure 2- 22 Bar graph illustrating the contour areas for the time averaged slices of temperature and the W (vertical) component of the flow for all simulations.

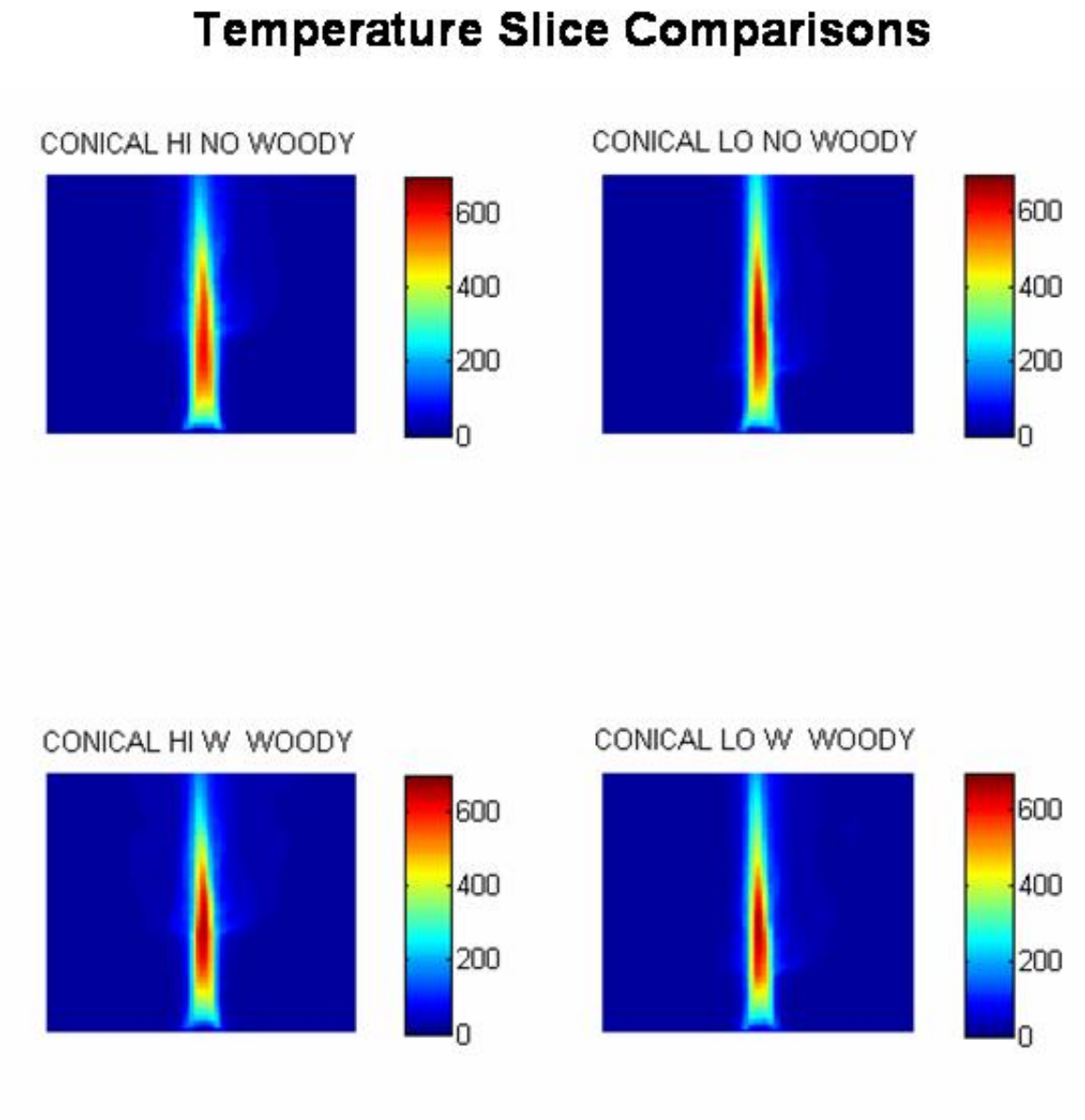

Figure 2- 23 Changes between simulations in the time averaged temperature slices for the conical crown form simulations.

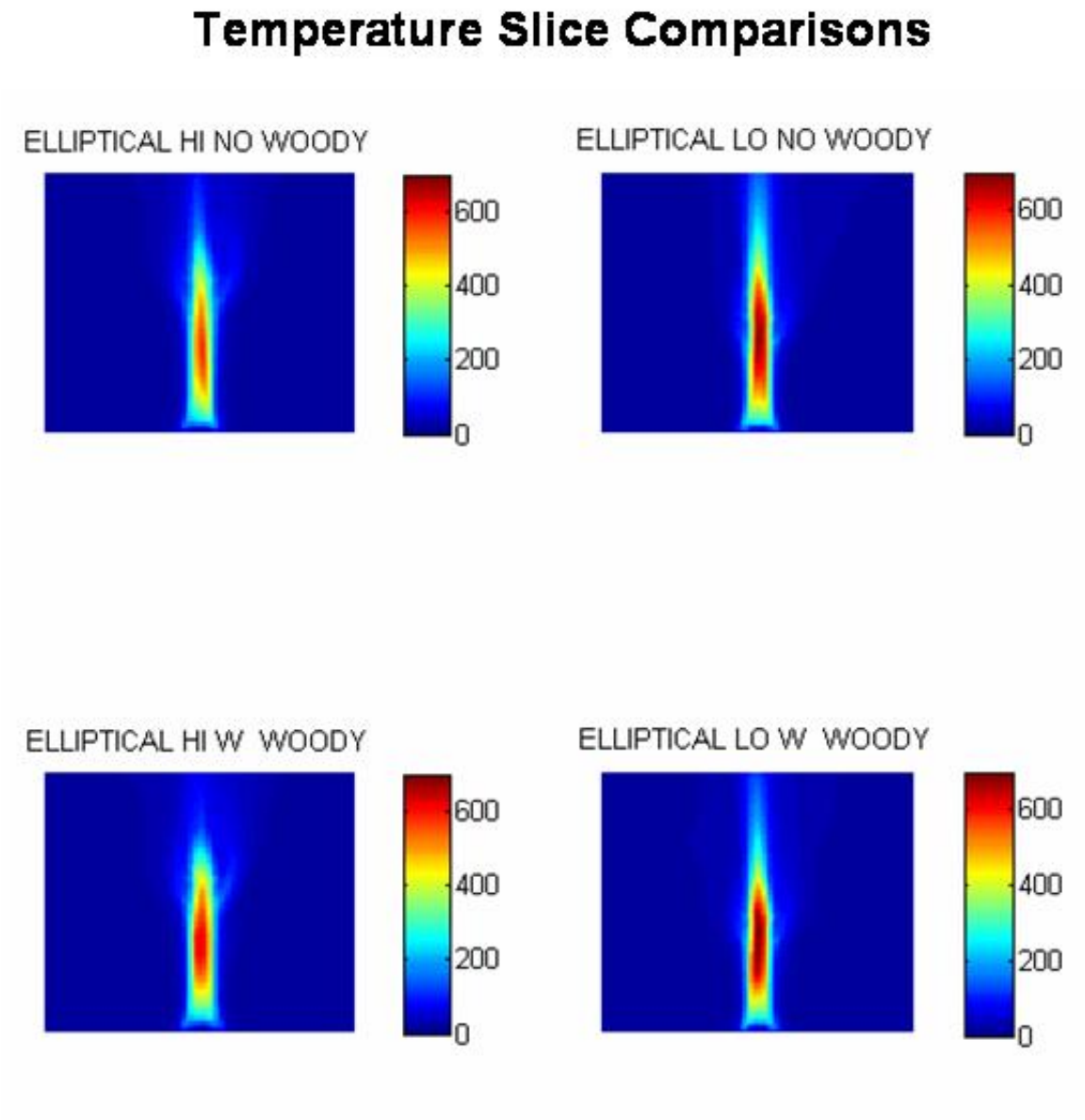

Figure 2- 24 Changes between simulations in the time averaged temperature slices for the elliptical crown form simulations.

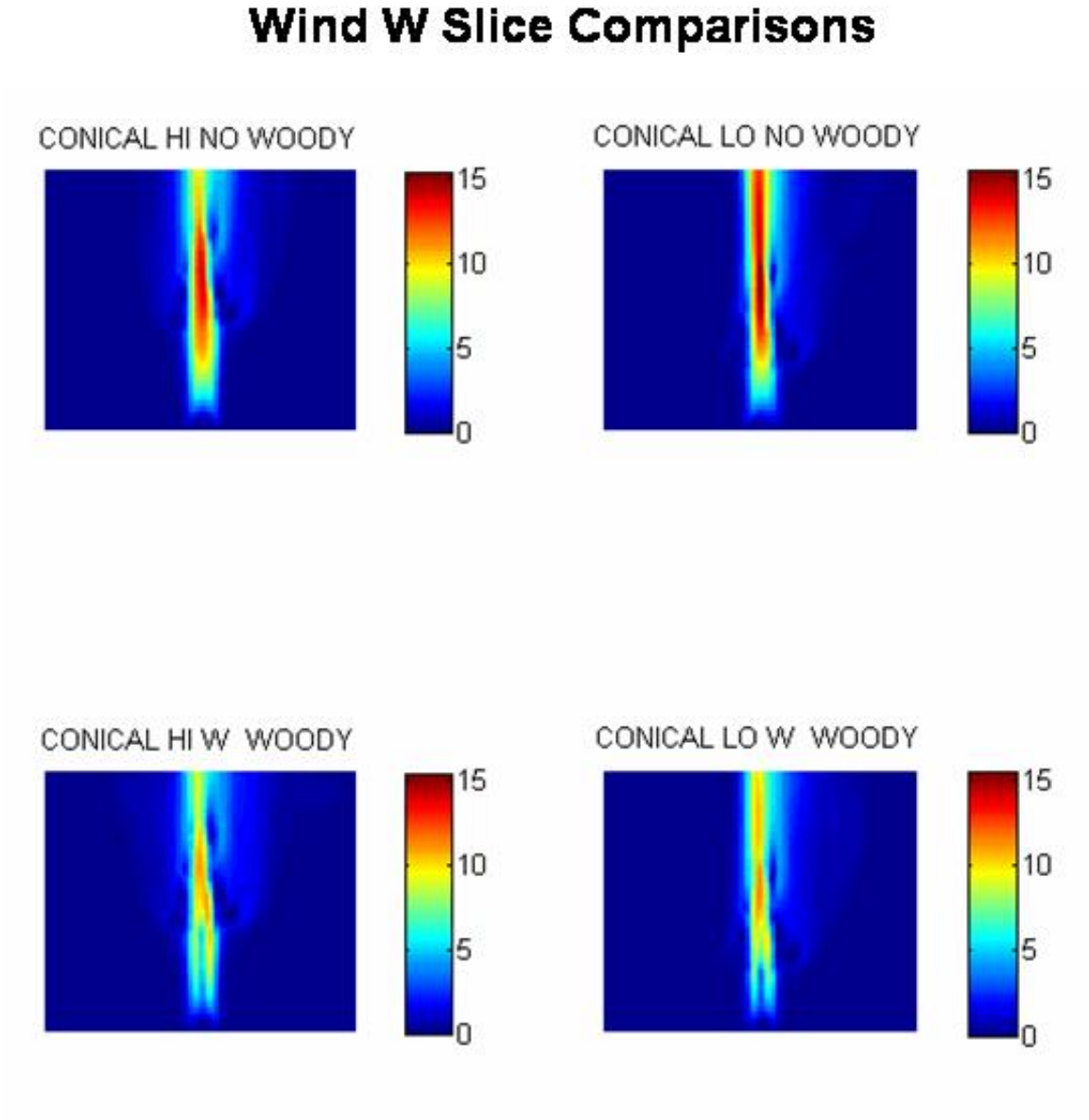

Figure 2- 25 Changes between simulations in the time averaged W (vertical) component of the flow slices for the conical crown form simulations.

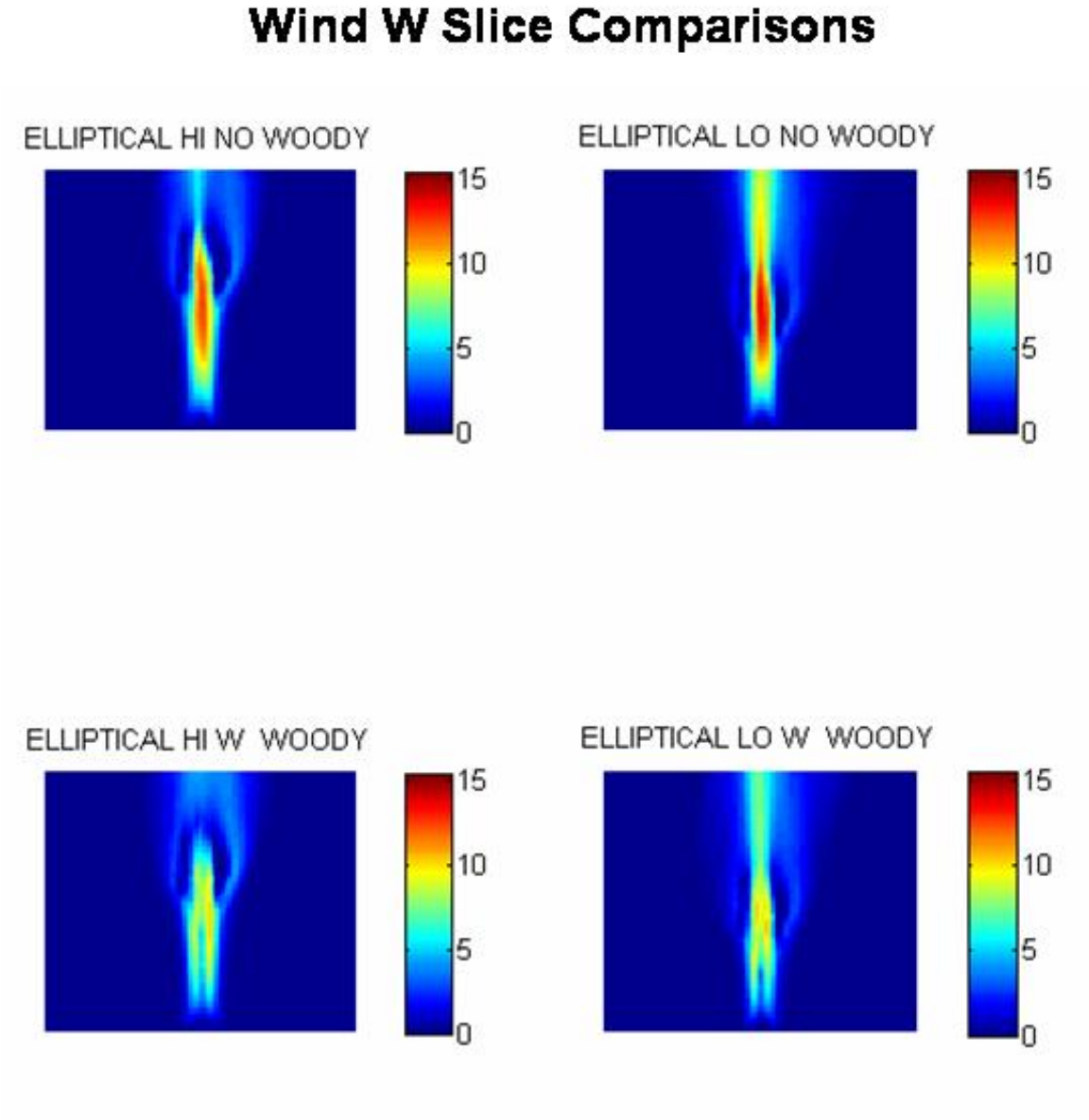

Figure 2- 26 Changes between simulations in the time averaged W (vertical) component of the flow slices for the elliptical crown form simulations.

Comparisons between tree simulations

Figure 2-22 presents a bar graph illustrating the contour slice areas for temperature and wind for all simulations. This same information is presented in **Table 2-3** above.

Figures 2-23 and 2-24 illustrate changes between simulations in the time averaged temperature slices for the conical and elliptical tree crown forms. **Figures 2-25 and 2-26** present the same comparison for the wind slice contour areas for the conical and elliptical tree crown forms.

In general, among the tree simulations, decreasing the height to crown base increased the temperature contour areas. This is intuitive because the fuel is closer to the heat source and corresponds with higher fuel consumption with lower height to crown base. Inclusion of woody biomass decreased the area of the temperature contours and of the wind W contours. These effects varied with crown form. For example, the wind field velocities were reduced more by the elliptical crown form than by the conical crown form at the lower crown base height. The conical crown form reduced the temperature more than the elliptical form but less than the random crown form; it had the least reduction of the wind field.

Individual cell data

The individual cell temperature data provide a complementary view of differences between simulations. The effects most clearly visible in these results are changes in the timing, magnitude and duration of heating within the crown. These effects were most

visible for the lower height to crown base simulations, in contrasts between simulations with and without the woody fuels.

Table 2- 4 Maximum temperatures recorded at individual cells, for five locations extending in a vertical line above the origin. Simulations are identified by name and by number.

Description	#	z = 2	z = 6	z = 10	z = 14	z = 18
CONE HI NO WOODY	1	579	973	1001	887	692
CONE LO NO WOODY	2	558	933	989	916	905
RAND HI NO WOODY	3	562	844	916	812	530
RAND LO NO WOODY	4	568	899	1003	905	879
ELLPT HI NO WOODY	5	573	865	970	667	332
ELLPT LO NO WOODY	6	547	888	947	908	743
CONE HI W WOODY	7	561	980	918	869	652
CONE LO W WOODY	8	521	883	944	905	808
RAND HI W WOODY	9	535	1036	952	874	471
RAND LO W WOODY	10	543	950	954	941	667
ELLPT HI W WOODY	11	563	947	961	884	264
ELLPT LO W WOODY	12	536	983	1044	837	547
NO TREE SIMULATION	13	514	636	865	872	470

Figure 2-27 shows an example of the individual cell values at a particular height (z =14 m) for all twelve tree simulations. In this figure, red lines are for simulations in which the woody mass was not included, and green lines are for simulations in which the woody mass was included. The inclusion of woody mass delayed heating, and shortened the

duration of heating, for the individual cell temperature at 14m for the lower height to crown base simulations (the lower three panels of each graph).

Figure 2-28 shows the maximum temperature for each individual cell (from a height of z = 1m to z = 18m) for each simulation. Again, green lines indicate simulations where woody mass was included and red lines where woody mass was excluded. Inclusion of woody mass reduced the maximum temperature recorded at individual cells over a range of heights for the conical and random crowns, particularly for the lower height to crown base simulations.

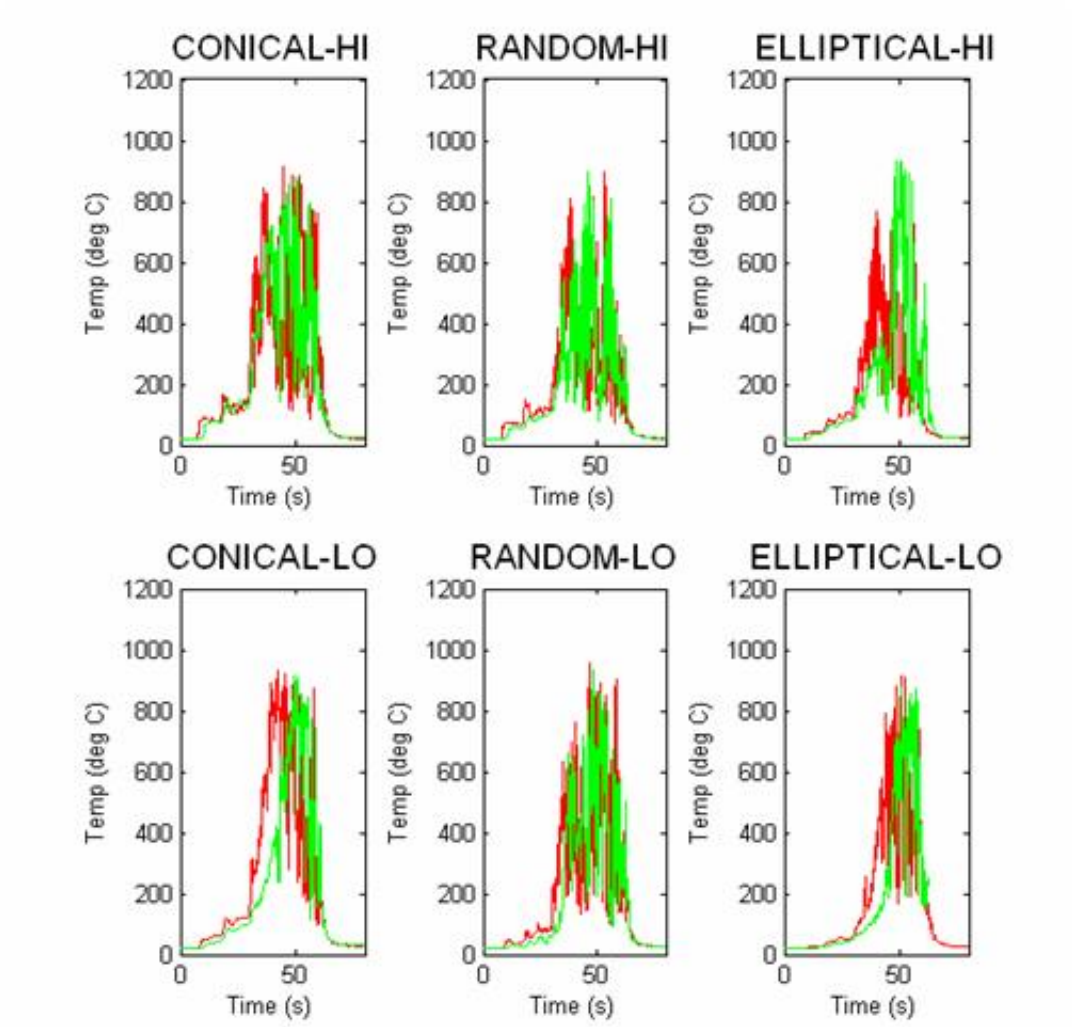

Figure 2- 27 Comparison of individual cell temperature records over time at z= 14m for all 12 tree burn simulations. Top panels: HI height to crown base (7 m), bottom: LO (4 m); red lines: woody biomass was excluded, green lines: woody biomass included.

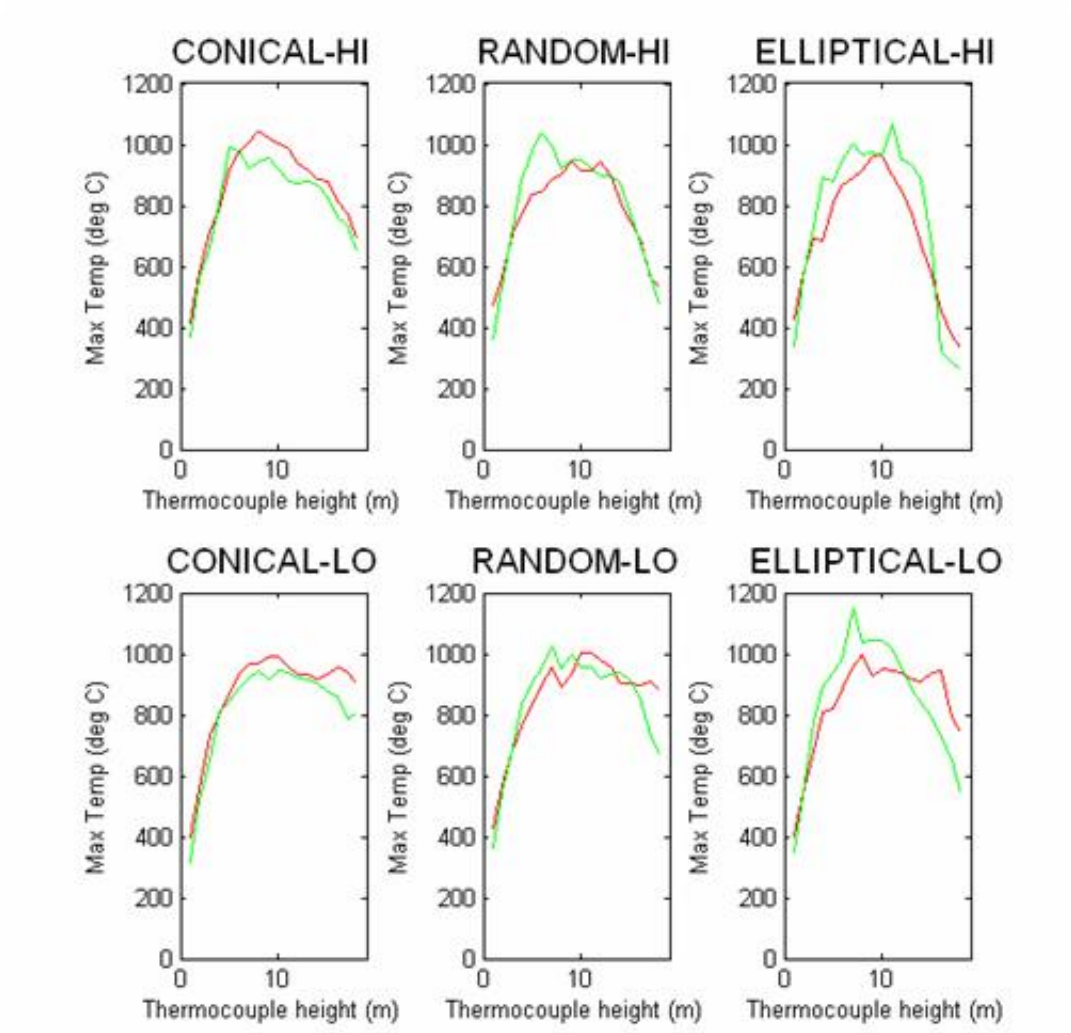
CONICAL-HI
RANDOM-HI
ELLIPTICAL-HI
CONICAL-LO
RANDOM-LO
ELLIPTICAL-LO
Max Temp (deg C)
Thermocouple height (m)
0
200
400
600
800
1000
1200
0
10

Figure 2- 28 Maximum temperature over time for individual cells located on the origin and extending up the z axis at 1 m intervals. Top panels: HI height to crown base (7 m), bottom: LO (4 m). Red lines: woody biomass excluded, green lines: woody biomass included.

DISCUSSION

In this study I carried out an exploratory analysis examining the effect of three factors, spatial configuration (crown form), height to crown base, and inclusion/exclusion of woody mass, on fine scale fire /fuel interactions, as described by patterns of fuel consumption, temperature and vertical component of the flow. All three factors affected both overall outcomes, such as the total fuel consumed or the time-averaged slices of temperature and wind, and how those quantities changed over time, such as the individual cell time traces and mass loss over time. Altogether, the overall result is that the specific spatial distribution of fuel, and the nature of that fuel, interacts with the specific geometry of the fire to determine not only what is burned but also how it burns. In these simulations this can be seen in the significant differences in fuel consumption, and temperature and wind effects between the different tree crowns. For example, the conical tree had greater fuel consumption with a height to crown base of 7 m than the random tree did with a height to crown base of 4 m.

All these factors relate to individual tree crown fuel properties. The spatial configuration of the crown, and the issue of inclusion of woody biomass in fire behavior modeling have not been considered previously. The height to crown base, however, is the primary driver in prediction of crown fire initiation in current operational models. The results presented here suggest that, while still important, height to crown base may not, in itself, be sufficient in prediction of crown fire initiation.

A basic problem with height to crown base is that, while it is easy to measure where the lowest live branch is, it is difficult to directly measure how crown biomass is distributed between the crown base and the top of the tree. A truly homogeneous crown volume is probably exceedingly rare in nature. Whether or not the height to crown base is relevant to the question of crown fire initiation, or of fire induced tree mortality, is dependent on knowledge of the nature of the distribution of crown fuel above that point; it is only directly related if the crown fuel is uniformly distributed (i.e., a homogeneous volume). It is precisely for this reason that the FUEL3D model was developed: there is a significant need for a quantitative description of how fuel is distributed in space. Because of its flexible design FUEL3D should be capable of modeling a wide diversity of tree and shrub crowns, providing a detailed, spatially explicit description of both foliar and woody biomass within the crown.

Results presented here illustrate that even woody biomass that does not burn still may affect how a tree burns, shown here in alteration of the temperature and vertical flow. I did not conduct in-depth analyses to explain these effects but it seems likely that they arose from a combination of different physical mechanisms. Both the radiative and convective heat transfer within the tree crown are altered by the presence of the coarser woody biomass. First, the added woody biomass material shields the foliar biomass above it from radiative heat (radiative shielding) and serves as a heat sink, receiving heat that would otherwise be available for the foliage. The wind field flow velocity is likely due to a minor drag effect of the added material (which is of coarse diameter and so thus has a small surface area to volume) and also reduced from heat loss, which is coupled to

the wind flow. These effects, although subtle, suggest that an accurate depiction of the composition of fuels within the crown, may be helpful in this sort of modeling. The coarser woody components of the crown are generally ignored; these results suggest that perhaps they should be given more attention, both in description of the fuel bed and in modeling of fire interactions. Physical fire model developers are cognizant of the potential importance of the effect of different fuel components and are actively working on building the capability to deal with multiple fuels within the crown (Mell, pers. comm.. and Linn, pers. comm. 2007). The FUEL3D model is helpful in this regard because it can be used to quantify the properties of many different components of the crown fuels, with individual summations of material by different size classes or types of material.

The work presented here is exploratory in nature, and intended to suggest possible avenues for future work rather than to test a particular hypothesis. No replication (through multiple simulations) was carried out so no statistical inferences should be made. Nevertheless, this work represents an important step towards a more integrated fire and fuels modeling strategy, employing detailed spatial modeling of fuels in conjunction with physical fire behavior modeling.

In general the complex dynamics involved in crown fires tend to result in problems for which simple calculations, which can be done in a spreadsheet or via a nomogram, are inadequate. As computing resources have improved, simulations with computer models have played an increasingly important role as a laboratory in which robust experiments can be designed. In many cases such simulation experiments make it possible to carry out

tests that would otherwise be infeasible, such as burning the exact same tree crown under different conditions as was done in these experiments.

Employing this strategy of modeled fuels and physical fire models will likely be of use in a number of ways, of which a few examples are presented here. First, extending the experiments presented here, with a replicated set of tree crowns and to span a wider range of heat inputs, fuel moistures and fuel quantities could be used to determine when sustained torching in the crown occurred. This could facilitate estimation of thresholds for crown fire initiation. Further extensions could address different levels of wind speed or different vertical wind profiles to identify thresholds important to crown fire propagation. Similarly, the effect of different spatial configurations of multiple trees and fire scenarios could be useful in the design and testing of fuel treatments to accomplish particular objectives. Finally, incorporation of change in vegetation over time could be used in assessment of the effective duration of fuel treatments, and could provide insights as to the degree to which vegetation succession influences fire occurrence and behavior over larger time and space scales. Through incorporation of detailed modeling of wildland fuels and physical fire behavior modeling, linkages between fire behavior and fire ecology, which have so far been elusive, could be determined.

LITERATURE CITED

Albini, F. A., and B. J. Stocks. 1986. Predicted and observed rates of spread of crown fires in immature jack pine. Combustion Science and Technology **48**:65-76.

Anderson, H. E. 1982. Aids to determining fuel models for estimating fire behavior. Page 22. USDA Forest Service Intermountain Research Station, Ogden, Utah, USA.

Cheney, N. P., and J. S. Gould. 1995. Fire growth in grassland fuels. International Journal of Wildland Fire **5**:237-244.

Cheney, N. P., J. S. Gould, and W. R. Catchpole. 1993. The influence of fuel, weather and fire shape variables on fire-spread in grasslands. International Journal of Wildland Fire **3**:31-44.

Cruz, M. G., B. W. Butler, M. E. Alexander, J. M. Forthofer, and R. H. Wakimoto. 2006. Predicting the ignition of crown fuels above a spreading surface fire. Part I: model idealization. International Journal of Wildland Fire **15**:47-60.

Cunningham, P., and R. Linn. 2007. Numerical simulations of grass fires using a coupled atmosphere-fire model: Dynamics of fire spread. Journal of Geophysical Research **112**:D05108.

Dupuy, J.-L., and D. Morvan. 2005. Numerical study of a crown fire spreading toward a fuel break using a multiphase physical model. International Journal of Wildland Fire **14**:141-151.

Finney, M. A. 1998. FARSITE: Fire Area Simulator -- model development and evaluation. Page 47. United States Department of Agriculture, Forest Service Rocky Mountain Research Station, Ft. Collins, CO USA.

Forestry Canada Fire Danger Group. 1992. Development and structure of the Canadian forest fire behavior prediction system. Forestry Canada, Science and Sustainable Development Directorate, Ottawa, ON.

Forney, G. W., and K. B. McGrattan. 2004. User's Guide for Smokeview Version 4: A Tool for visualizing Fire Dynamics Simulation Data. NISTIR Special Publication. National Institute of Standards and Technology.

Keyser, T. L., F. W. Smith, L. B. Lentile, and W. D. Sheppard. 2006. Modeling postfire mortality of ponderosa pine following a mixed severity wildfire in the Black Hills: the role of tree morphology and direct fire effects. Forest Science **52**:530-539.

Linn, R., Cunningham, Philip. 2005. Numerical simulations of grass fires using a coupled atmoshphere--fire model: Basic fire behavior and dependence on wind speed. Journal of Geophysical Research **110**:19.

Linn, R., J. N. Reisner, J. Colman, and J. Winterkamp. 2002. Studying wildfire behavior using FIRETEC. International Journal of Wildland Fire **11**:233-246.

Linn, R., J. Winterkamp, J. Colman, C. Edminster, and J. Bailey. 2005. Modeling interactions between fire and atmosphere in discrete element fuel beds. International Journal of Wildland Fire **14**:37-48.

Linn, R. R. 1997. Transport model for prediction of wildfire behavior. Scientific Report LA-13334-T, 195pp. Los Alamos National Laboratory, Los Alamos, NM.

Mell, W., J. J. Charney, M. A. Jenkins, P. Cheney, and J. Gould. 2005. Numerical simulations of grassland fire behavior from the LANL-FIRETEC and NIST-WFDS models. Page 10. EastFIRE Conference, George Mason University, Fairfax, VA.

Mell, W., M. A. Jenkins, J. Gould, and P. Cheney. 2006a. A Physics-Based approach to modeling grassland fires. International Journal of Wildland Fire:59.

Mell, W., S. Manzello, and A. Maranghides. 2006b. Numerical modeling of fire spread through trees and shrubs in D. X. Viegas, editor. V International Conference on Forest Fire Research, Coimbra, Portugal.

Reinhardt, E. D., and N. L. Crookston. 2003. The fire and fuels extension to the forest vegetation simulator. Page 209 p. General Technical Report. USDA Forest Service, Rocky Mountain Research Station, Ogden, UT.

Reinhardt, E. D., R. E. Keane, and J. K. Brown. 2001. Modeling fire effects. International Journal of Wildland Fire **10**:373-380.

Rothermel, R. C. 1983. How to predict the spread and intensity of forest and range fires. General Technical Report. USDA Forest Service, Intermountain Forest and Range Experimental Station, Ogden, UT.

Ryan, K. C., and E. D. Reinhardt. 1988. Predicting postfire mortality of seven western conifers. Canadian Journal of Forest Research **18**:1291-1297.

Scott, J. H., and E. D. Reinhardt. 2001. Assessing crown fire potential by linking models of surface and crown fire behavior. Research Paper. USDA Forest Service,Rocky Mountain Research Station, Fort Collins, CO.

Susott, R. A. 1982. Characterization of the thermal properties of forest fuels by combustion gas analysis. Forest Science **23**:404-420.

Swetnam, T. W., and J. L. Betancourt. 1990. Fire-southern oscillation relations in the southwestern United States. Science **249**:1017-1020.

Van Wagner, C. E. 1964. History of a small crown fire. Forestry Chronicals **40**:202-205,209

Van Wagner, C. E. 1966. Three experimental fires in jack pine slash. Page 22. Canadian Forestry Service.

Van Wagner, C. E. 1968. Fire behavior mechanisms in a red pine plantation: field and laboratatory evidence. Can. Dep. For. Rural Develop.

Van Wagner, C. E. 1973. Height of crown scorch in forest fires. Can. J. For. Res. **3**:373-378.

Van Wagner, C. E. 1977. Conditions for the start and spread of crown fire. Canadian Journal of Forest Research **7**:23-34.

Wade, D. D., and D. E. Ward. 1973. An analysis of the Air Force Bomb Range fire. Research Paper. USDA Forest Service, Southeast Forest Range Experiment Station, Ashville, NC.

CHAPTER III: AN INVESTIGATION OF VARIABILITY IN FIRE SPREAD RATES WITH THE PHYSICAL FIRE MODEL, FIRETEC

ABSTRACT

Operational fire behavior models predict an overall average forward spread rate based on small scale test burns in homogenous fuel beds. A shortcoming of these models is that there is no way to estimate error in the model prediction; this represents a potentially substantial error term of unknown magnitude which may endanger firefighters. Here, a replicated set of fire behavior simulations was conducted to examine the effects of spatial fuel variability on the forward spread rate of a wildland fire. Using a three dimensional physical fire model, fires were simulated in four different general spatial patterns of fuels, in which tree crowns were randomly clumped into different numbers and sizes of clumps. Seven different replicates, or unique spatial configurations, were tested for each clumping group, for a total of 28 simulations. Analyses were conducted comparing spread rates between clumping groups, within groups and within individual simulations; significant variability in spread rates was observed at all levels. Results suggest that, while the nature of variability in spread rate may relate to the spatial scale of fuel variability, variability in spread rate can largely be attributed to fine scale fire-fuel-atmosphere interactions which are by their nature difficult to predict beforehand. This suggests a need for a paradigm shift in fire behavior prediction which more explicitly recognizes the intrinsic variability in inputs and outcomes. A strategy is proposed in which physical fire models are used in replicated simulations to identify the underlying drivers of variability and their magnitude at different spatial scales; once thus identified new operational models could be developed which are better equipped to accommodate heterogeneity in the fuel bed.

INTRODUCTION

Numerous fire researchers have remarked that even in relatively homogeneous fuel beds, such as pine needles, fire spread is not even, but is characterized by variability, sometimes described as a progression of "fits and starts" (Fons 1946, Catchpole et al.1998, Rothermel 1972). In truth, no natural fuel beds are actually homogeneous, but are rather composed of particles of various sizes and voids between them. Despite the presence of these voids these fuels are considered to be "continuous" because the size of the flame typically extends beyond the void space, such that flame contact can consistently be made throughout the bed (Cohen et al. 2006). In surface fires burning in such fuels, it may be practical to ignore this variability by calculating the spread rate at a larger, integral scale, at which fine scale variability might reasonably be considered as transient and might be expected to even itself out (**Figure 3-1**). In this paper I refer to this integral scale spread rate as the overall average spread rate, calculated as the complete distance traveled divided by the time taken to get there. This approach is attractive because it permits the use of empirical correlative relationships to describe the rate of spread rather than having to deal with the significantly greater complexity of describing all the mechanisms involved. This approach is used by the Rothermel fire spread model (Rothermel 1972) which serves as the basis for all operational wildland fire behavior prediction of surface fires in the United States (Finney 1998, Andrews et al 2005, Scott and Reinhardt 2001).

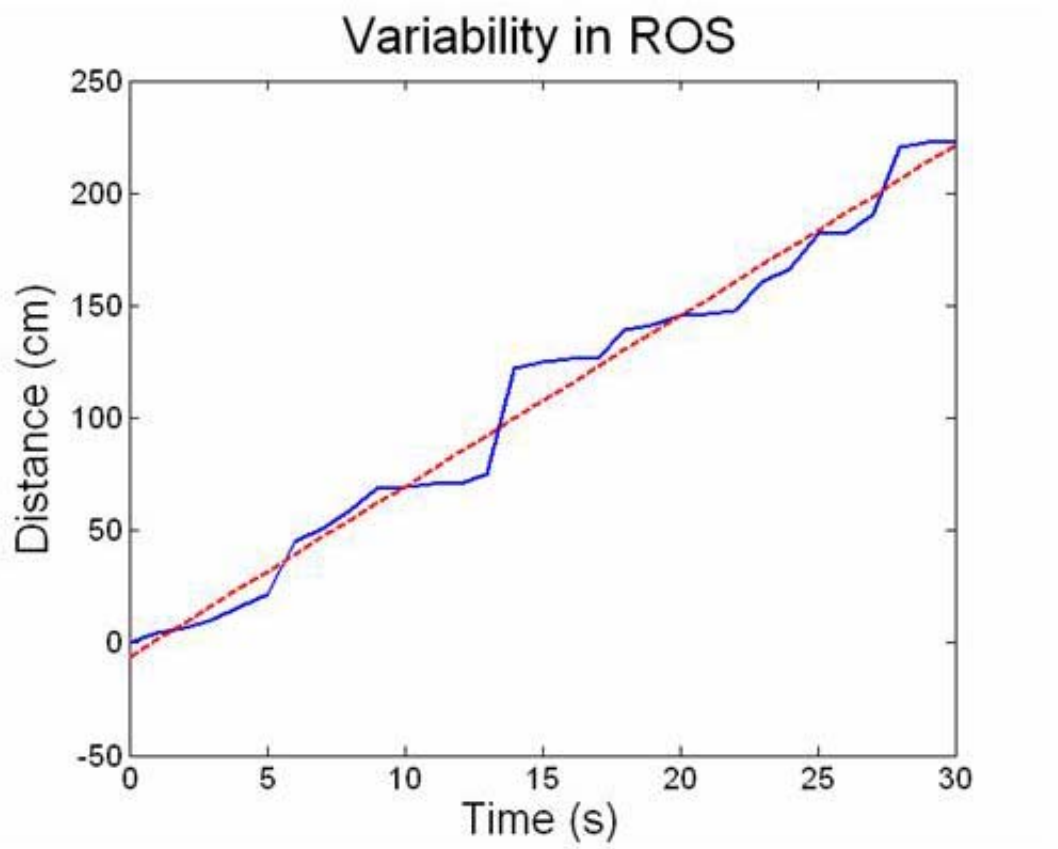

Figure 3- 1 Operational models predict an average rate of spread (red dash line) but not variability in spread rate (blue solid line). Variability in spread rate is important as accelerated spread rates (steep slope in center) may increase danger to firefighters.

Operational fire models then apply the same approach to predict crown fire spread using a correlative relationship identified from field observation of a small number of crown fires in different locations (Rothermel 1991). The correlative relationship used is a linear function of the spread rate predicted by the Rothermel surface fire spread model for Fuel Model 10 (timber, litter and understory), a common forest surface fuel (Anderson 1982). In this case the observed overall spread rates for crown fires were estimated over distance scales of miles traveled over hours; these distance and time scales are several orders of magnitude larger than the distance and time scales of meters over minutes that the original empirical litter and needle bed tests which the Rothermel model was based on.

A problem that arises with such predicted spread rate is that it is unclear at what spatial scale such predictions of an overall average spread rate are expected to be relevant. The overall average spread rate is essentially the slope of the trend line fitted to a graph in which time is on the x axis and distance is on the y axis (**Figure 3-1**). In ordinary empirical studies the variability around the trend line, or error term, associated with the data fitting, would be evident and would be quantified in some typical way (i.e. R^2 or Chi square). However, the formulation of the Rothermel model is such that this information is not available. It is clear from **Figure 3-1** that the adequacy of the overall average spread rate described by the trend line is not the same in all portions of the graph; the steep spread rate in the central portion of the graph represents a momentary accelerated rate which, while perhaps not significant when considered over a large time and distance scale, would be quite significant to a firefighter needing to evacuate an untenable fireline. The expression of an empirical spread rate without a corresponding expression of the

variability in that spread rate leads to a situation in which firefighters in the field may be exposed to danger because they rely on predictions of fire spread rate in which potentially significant sources of error are not considered.

One potential source of error or uncertainty in fire spread rates is the variability arising from heterogeneity within the fuel bed. Operational models assume homogeneous fuel beds and steady state spread rates, and thus do not address the potential effects of fuel bed heterogeneity in fire behavior calculations. Unlike operational fire behavior models, physics-based numerical fire behavior models (Linn 1997, Linn et al 2002, Mell et al 2005) have self-determining spread rates and thus are capable of addressing transitional behaviors and variability within the fuel bed; variability in spread rates is an emergent property of such models. Such models are thus ideally equipped to study the effects of spatial fuel variability on fire behavior.

One nuance of highly deterministic and dynamic models is that it is often difficult to generalize the observed outcomes, as to some degree what was observed may be sensitive to the particular spatial configuration of the fuels in a particular simulation. This sensitivity can be tested via replication, in which multiple simulations are carried out with unique spatial configurations. However, due to the high computational demands of physical fire models it is unusual to carry out large ensemble runs.

Objectives

The overall objective of this set of experiments was to use a detailed physical numerical fire behavior model, FIRETEC, to explore the effects of spatial variability in fuels on the forward rate of fire spread. Towards this aim, three sets of analyses were conducted.

The first analysis consisted of comparison of overall spread rates between four groups of simulations. Each group consisted of seven simulations in which fuels were clumped in a similar way but with unique spatial configurations. The clumping approach essentially spanned a range of numbers and sizes of clumps of trees. Altogether 28 simulations were carried out. This analysis thus tested whether differences in the overall average spread rate between simulations might be attributed to different clumping patterns.

The objective of the second analysis was to assess whether different clumping patterns influence the nature of the distributions of incremental spread rates within each of the 28 simulations described above.

The third and final analysis consisted of a case study in which two simulations from the same clumping group were subjected to a more detailed analysis exploring differences in spread rate.

METHODS

The FIRETEC model

FIRETEC/HIGRAD is similar to the WFDS model (described in Chapter II) in that both are Computational Fluid Dynamics (CFD) models which are driven by the principles of conservation of energy, mass, momentum and species. Both models distinguish different means of heat transfer (principally radiation and convection), address fire –atmosphere interactions (in which the vertical momentum equation includes a buoyancy term, so differences in local air pressure arising from the heat of the fire modify the wind field)

and fuel-atmosphere interactions (in which the quantity and geometrical properties of fuels in a particular location imposes drag on wind flows). Both models are built on the same general hydrodynamic theoretical basis, the Navier-Stokes equations. Beyond these similarities there are a number of ways in which the two models are different; most of these are rather technical in nature. In general, however, the differences between the two models reflect the history of their development. WFDS was developed from a structural fire background, and thus favors smaller spatial domains characterized by low-speed flows, and a more detailed treatment of combustion chemistry. In contrast, the underlying hydrodynamic model of FIRETEC/HIGRAD, HIGRAD arose from a larger-scale atmospheric / meteorological science background and thus is best applied over larger spatial domains; while its treatment of combustion and fuel properties is somewhat simpler than in WFDS it has in general a more involved treatment of atmospheric interactions. Fluid dynamics in FIRETEC are modeled with full compressibility, which allows for accurate wind field predictions even in complex conditions involving topography, fire and fuel interaction. Both models are in active development.

The simulations

The simulations carried out in this project are described below. The table below provides links to digital files of animations comparing two sets of two simulations; while the two simulations shown are discussed in more detail later in this chapter (in the case study) they are presented here as examples to aid the reader in visualizing the nature of these simulations. In the file names below, L7 and L3 are two simulations from the “LARGE”

clumping group (explained in more detail below) and S6 and S3 are two simulations from the "SMALL" clumping group.

Table 3- 1 Animations of stand Scale fire simulations with FIRETEC.

Hyperlink to File
Oblique_view_comparison_L7_vs_L3
Top_view_comparison_L7_vs_L3_winds
Oblique_view_comparison_S6_vs_S3
Top_view_comparison_S6_vs_S3_winds

Spatial domain and resolution

The numerical experiments were set up with the same rectangular spatial domain consisting of 160 cells in the x direction, 80 cells in the y direction, and 41 cells in the z direction. Cellsize in x and y was fixed at 2 m but z was transformed with a sigma transformation (**Figure 3-2**), in which a cubic polynomial is used to systematically increase the cell dimensions with increasing z. This has the effect of providing sufficient spatial detail near the ground (~ 1.5m) while ensuring that the top boundary is far enough away from the surface that boundary condition effects are minimized; the larger cell sizes toward the top boundary also reduce the computational demands as fewer cells are needed. Each simulation was set to run for 12000, 0.02 s time steps, for a total simulation time of 240 s, or 4 minutes. In all figures which follow in which references to simulation time are made, a difference of 1000 time steps is equivalent to 20 seconds.

Boundary conditions and layout

In computational fluid dynamics models, essentially all cells are interconnected and interact and influence each other. Just as a pebble tossed into a still pool causes ripples that extend for some distance, a change in pressure in one location, perhaps as a result of

added buoyancy from the heat of the fire, will cause subtle changes throughout the spatial domain. For this reason the definition and handling of the boundary conditions is one of the more difficult parts of setting up a simulation.

The same layout of specialized boundary conditions and related areas were used for all simulations (**Figure 3-3**). Each of these is described below; letters refer to the corresponding position in **Figure 3-3**.

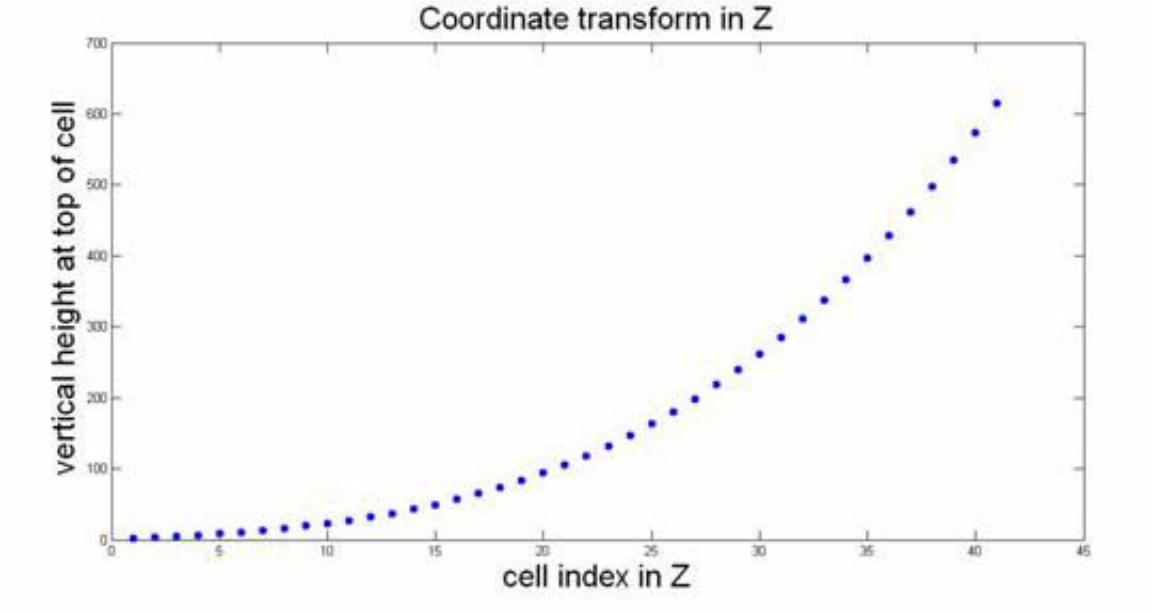

Figure 3- 2 The sigma transformation increases the height of the volume cells as you get closer to the top of the spatial domain to balance the need for higher resolution at the bottom against the need for sufficient space to avoid boundary condition effects.

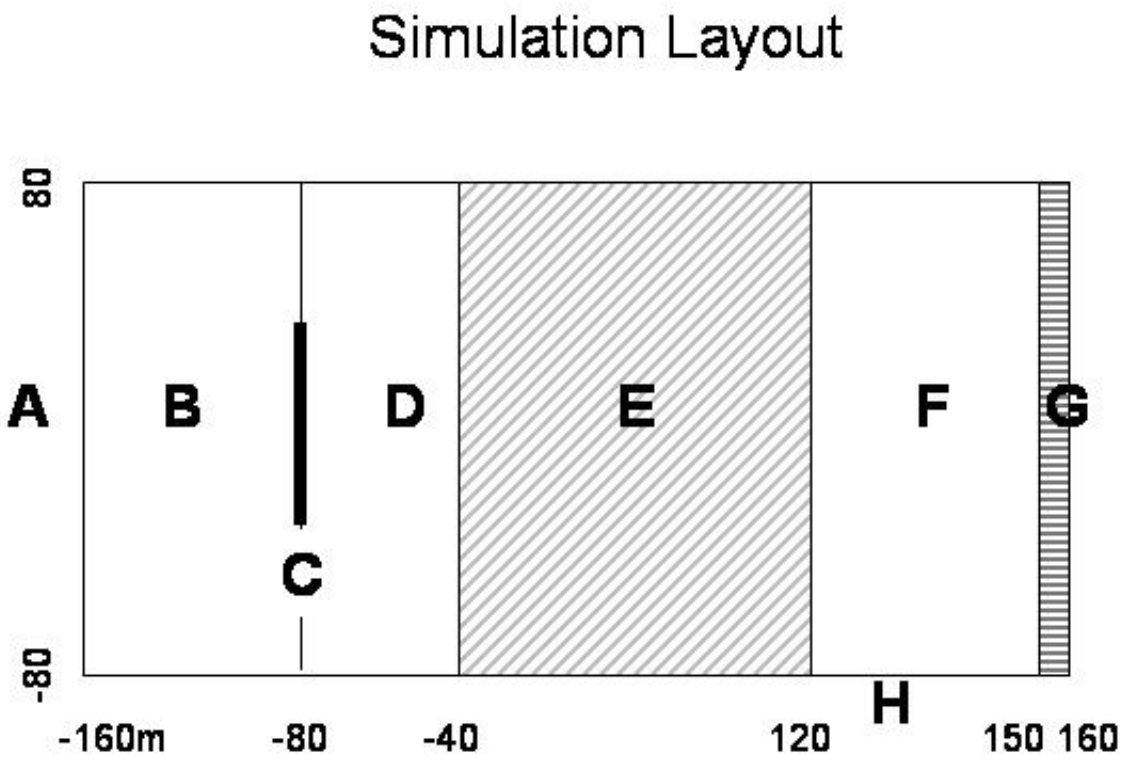

Figure 3- 3 The simulation layout. The simulation layout. The spatial domain measured 160 x 80 x 41 cells. Cells are 2m in x and y but increase in dimension with increasing z. A) predeveloped wind field enters as inflow B) Wind field entry zone C) Ignition strip D) Initial fire development zone E) Zone of fuel modification F) far end pre-boundary zone G) relaxation to outflow ambient windfield H) lateral relaxation boundary conditions.

A. pre-developed windfields as inflow

The sensitivity of CFD models to the nature of the flow requires careful handling. Inflow conditions that are too contrived and artificial can result in unrealistic outputs. For this reason, winds used in the simulations were developed beforehand by running FIRETEC/HIGRAD for the base case forest for a substantial period of time without a fire simulation. The forward wind speed was set at a constant 6 m/s above the top of the canopy and a defined vertical wind profile typical of real winds, where wind velocities decrease substantially from the top of the canopy to the forest floor as a result of increased drag. Over the course of this simulation a wind field developed that reflected the spatial structure of the base case forest. This pre-developed wind field was then used as inflow (winds flowing into the domain) for all cells on the left (x = -160m) boundary (**Figure 3-3 A**), as well as for outflow (winds flowing out of the domain) on the right boundary (**Figure 3-3 G**) (see below). The purpose of this complex and dynamic boundary conditions is that winds outside the domain have a significant amount of inertia that tends to influence flows within the domain to some extent.

B. Wind field entry zone

An area extending from this boundary to x = -80 was considered as the wind field entry zone. This area was designed to provide a reasonable distance over which the wind field could respond to the inhomogeneous fuels before the ignition strip.

C. Ignition strip

An ignition strip measuring 80 m in y by 2 m in x was defined at x = -80. This ignition strip was established with a time dependent ramp progression which increased from ambient temperature up to 1000 degrees and lasted for 50 seconds.

D. Initial fire development zone

An area extending from x = -80 to x = -40 and spanning the full dimension in y (160 m, from y=-80 to y = 80) was set aside for the initial development of the fire before entering the zone of fuel modification, described below. This provided a common fire start condition to all the simulations. Fuels within this area were identical for all simulations.

E. Zone of fuel modification

The only area within which the spatial configuration of fuels was permitted to be changed was called the zone of fuel modification. This area extended from x = -40 to x = 80, and the full dimension in y.

F. Far end pre-boundary zone

An area extending from x=80 to x = 140 was designated as the far end pre-boundary zone. This zone essentially ensured that changes in the fuels within the zone of fuel modification did not result in an abrupt transition near the boundary of the domain.

G. Relaxation to outflow ambient windfield

The ten cell wide strip from x = 150 to x = 160 was a special boundary zone, referred to as a 'relaxation' boundary condition, in which flow velocities and other quantities are incrementally modified to 'relax', or conform to values at the boundary. Here, the numerical values were relaxed to those of the outflow ambient windfield. This process is implemented to reduce the possibility of unexpected effects at the boundary, and is a commonly applied approach in CFD modeling.

H. Lateral Relaxation boundary

Along the lateral edges of the spatial domain a relaxation boundary condition similar to that at the end is implemented.

Fuels inputs

Surface fuels consisted of a homogeneous grass layer described with a fuel bed depth of 0.5 m, a fuel load of 0.45 kg m^{-2}, and a surface area to volume ratio of 4000 m^{-1}. This surface fuel layer is thus similar to the fuel model 3 (tall grass, Anderson 1982) but with a slightly lower fuel load, and fuel bed depth. Surface fuel moistures were set at ten percent of dry weight. For crown fuels, a base case forest was established consisting of 2000 individual, identical, trees randomly located within the entire domain. Trees were modeled as parametric volumes, consisting of two paraboloids, in which fuels are concentrated toward the outside edges (**Figure 3-4**) (Linn et al 2005). For each tree, the crown is confined to a volume described as :

$$\frac{h}{R^2}\left[r^2\right] + C \le Crown_{\text{int}erior} \le -\frac{d}{R^2}r^2 + H$$

Eqn. 3- 1

where H is the tree height, C is the height to crown base, and R is the maximum radius of the crown. All trees were identical, and values of 15, 3, and 2.5 were used for H, C, and R, respectively. The variables *h* and *d* correspond to the height of the upward facing bottom part of the crown and the downward facing top part of the crown, respectively. Within this volume, bulk density of crown fuel is modeled as:

$$\rho_{canopy} = \left[\frac{z - C + \frac{d}{R^2} r^2}{H - C} \right] \rho_{\max}$$

Eqn. 3- 2

where the maximum fuel density for any given cell, ρ_{max}, was set to a value of 0.48 kg m^{-3} (Linn et al 2005). This limit is intended to mimic shade intolerance, where the total amount of foliage in any particular cell is limited by available light.

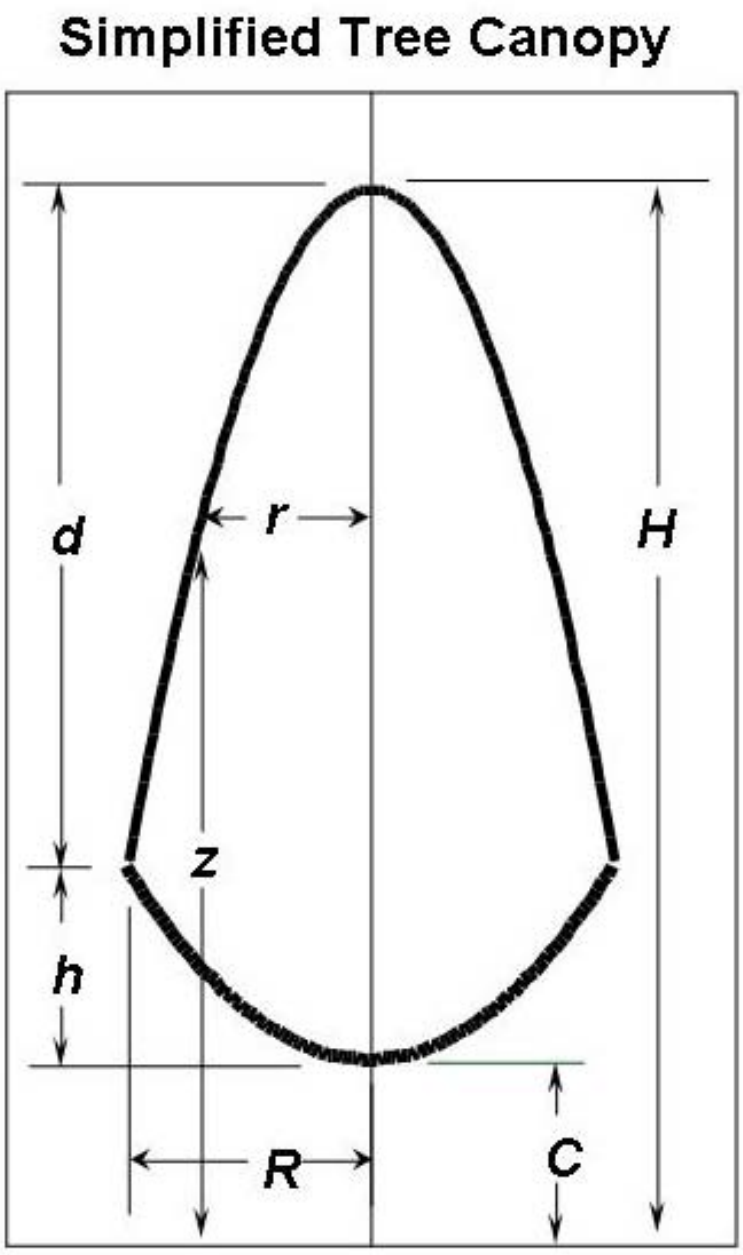

Figure 3- 4 The parametric description of tree and shrub canopies used to represent individual tree crowns in all simulations. The crown is envisioned as a double paraboloid in which the quantity of fuel increases smoothly towards the outer edge.

Generating forests with different spatial configurations

Four clumping groups were defined: random, small, medium and large. The first one had no explicit clumping; all trees were simply randomly located as in the base case forest. The other three clumping groups were each defined with a number of clump centroids and a specified radius. To generate the different clumping patterns, the trees located within the zone of fuel modification in the base case forest were randomly assigned to one of these centroids and their coordinates were translated to a new position randomly determined within the specified radius of that centroid. In each case the same set of simulated tree crowns was rearranged into clumps randomly. Fuels for each tree were partitioned among the appropriate set of three-dimensional cells (voxels) within which the volume of the tree crown was found. Cells located at the overlap of one or more trees received fuels from all contributing trees. However, if the total fuel in a given cell exceeded the allowable maximum value, ρ_{max}, that cell was set to the maximum. This prevented unnaturally high densities from occurring, and resulted in differences in overall crown bulk density between cluster groups. Output simulated forests ranged in overall bulk density from 0.007 to 0.0148 kg m-3; this is generally lower than most values reported for ponderosa pine in other studies (Reinhardt et al 2007, Cruz et al 2003) but differences in how void spaces between trees are accounted for make direct comparison difficult.

Simulation output

Simulations were run on a supercomputer at the Los Alamos National Laboratory, using typically 32 processors. A number of variables are output by the model at each time step; however due to the difficulties of transporting large volumes of data only a relatively

small subset of the data produced by the model was used. This data, which is what is typically used by most model users, included the U, V, and W components of the wind fields (corresponding to flow velocities along the x,y, and z axes, respectively), the potential temperature, theta, and fuel density rho. The potential temperature is the temperature that a parcel of fluid (or air) would have if adiabatically (no heat lost or gained) brought to a standard reference pressure of 1000 millibars. Potential temperature is preferred over actual temperature in many atmospheric science applications because it conveys more about the flow dynamics and is more straightforward to describe since interactions with pressure are eliminated by use of a constant reference pressure. All variables were output as binary 3D arrays with an output time step of every 2 seconds of simulation time. Data used in subsequent analyses comprised about 1.5 GB per simulation, for a total of 42 GB of data.

Analysis

quantifying spatial pattern of variability

I quantified the variability in the spatial pattern in the tree crowns for each simulation with the lacunarity curve (Plotnick et al 1993, Fraser et al 2005). Lacunarity is a scale dependent statistical measure of spatial heterogeneity, or texture. It can be thought of as describing the distribution of gap sizes across scales. In these calculations all tree crowns were identical, so the primary interest in capturing spatial variability was in the horizontal plane. Fuel density was thus summed vertically to create a two dimensional array of continuous (non integer) values representing the sum of fuel biomass in the vertical column of volume cells associated with that cell. Lacunarity was then calculated on the

80x 80 cell (160x160 m) square, two dimensional array of these cells containing the zone of fuel modification, for each simulation. Lacunarity was calculated at each box size, r, from r = 1 .. 80, using the gliding box algorithm (Plotnick et al 1993) as modified by Fraser et al. 2005, to accommodate continuous, rather than binary data:

$$\Lambda(r) = 1 + \frac{\sigma_Q^2(r)}{\left[Z_Q^{(1)}(r)\right]^2}$$

Eqn. 3- 3

where Λ(r) is the lacunarity statistic for boxes of size r, r is the size of each box, $\sigma_Q^2(r)$ is the sample variance associated with boxes of size r, and $Z_Q^{(1)}(r)$ is the mean of the frequency distribution (calculated in a histogram binning type operation) of the fuel being summed for box size r.

The logarithm of the lacunarity statistic is plotted against the logarithm of the box size to graphically represent the spatial variability across a range of spatial scales.

Assessing differences in spread rate between simulations

I examined differences in the overall spread rate between clumping groups, and in the nature of the distributions of incremental spread rates.

To test whether there were significant differences in the overall spread rate between the different clumping groups I used the Kruskal-Wallis test. The Kruskal-Wallis test is a non parametric equivalent to the classical one way Analysis of Variance (ANOVA), designed to compare samples from two or more groups. The test compares the medians of each group and calculates the probability for the null hypothesis that all samples are drawn from the same distribution. The Kruskal Wallis test assumes that all samples come from distributions with similar shape (but possibly different location or scale parameters).

To characterize the variability in surface spread rates within a simulation, it was necessary to calculate incremental spread rates. The calculation of incremental spread rates consisted of several steps. First, the maximum x coordinate where the fire had burned the surface fuels was extracted from each simulation output time step (every 2 seconds) by comparing the surface fuel values with the original, unburned state. Any surface cell in which fuel quantities had diminished by a minimum threshold value (0.005 kg/m^3) was considered to have burned. The cell with the maximum x coordinate thus identified represented the farthest point of spread at that time step.

Once each time step was associated with a particular position along the x axis representing the farthest point of spread at that point in time, incremental spread rates were calculated from the arrays of time and position. Due to the discretization of the spatial domain to 2 meter cells in x and y, it is possible that the fire may have more than one timestep associated with a particular coordinate in x. Similarly, because simulation outputs are written to files at a fixed interval (every 2 seconds) it is possible that between

output time steps the fire may have spread more than one cell. Incremental rates of spread were thus measured as the distance traveled (at least one cell) divided by the time taken. Each incremental rate of spread was recorded in an array for subsequent analysis.

The distribution of incremental spread rates within each simulation was described with skewness (described below), and a Kruskal-Wallis nonparametric test was used to compare these skewness values between clumping groups. Skewness is a nondimensional measure of the degree of the asymmetry in the shape of a distribution (Press et al. 1996), defined as

$$Skew = \frac{1}{N}\sum_{j=1}^{N}\left[\frac{x_j - \bar{x}}{\sigma}\right]^3$$

Eqn. 3- 4

where σ is the standard deviation of the distribution, x_j , (J= 1..N) are the individual incremental spread rates, N is the total number of spread rate values, and $\bar{x}$ is the average spread rate. Distributions that are symmetrical will have a skewness value close to zero; higher values greater than zero indicate a right tail, or high extreme values. Skewness should be interpreted with caution at low sample sizes, as even truly symmetrical data can have a non-zero skewness (Press et al 1996); here, distributions of incremental ROS had at least 50 observations in all cases.

Case study: comparison of two simulations

A case study was made of two runs from the same clumping group which had different overall rates of spread The objective of this case study was to explore the data in more depth to better understand the causal mechanisms behind the difference in spread rates. As a first step, I plotted the cumulative distance traveled by each fire over time to determine the time period when the two simulations diverged in spread rates. Once this period was identified, I extracted information from both simulations before the divergence in spread rates occurred and reconstructed what occurred through an iterative process of data exploration and visualization.

RESULTS

Quantifying spatial pattern of crown fuels

The approach used in generating different random fuel patterns was simple but effective. **Figures 3-5, 3-6, 3-7 and 3-8** illustrate, with two examples each, spatial patterns typical of each of the four clumping scenarios. The lacunarity curves plotted for each group in **Figure 3-9**(a) illustrate that, although each replicate has a unique spatial configuration, the overall spatial structure within each clumping group is quite similar, with the curves by group falling very closely together. The small and medium clumping groups were the most similar to each other in their spatial structure.

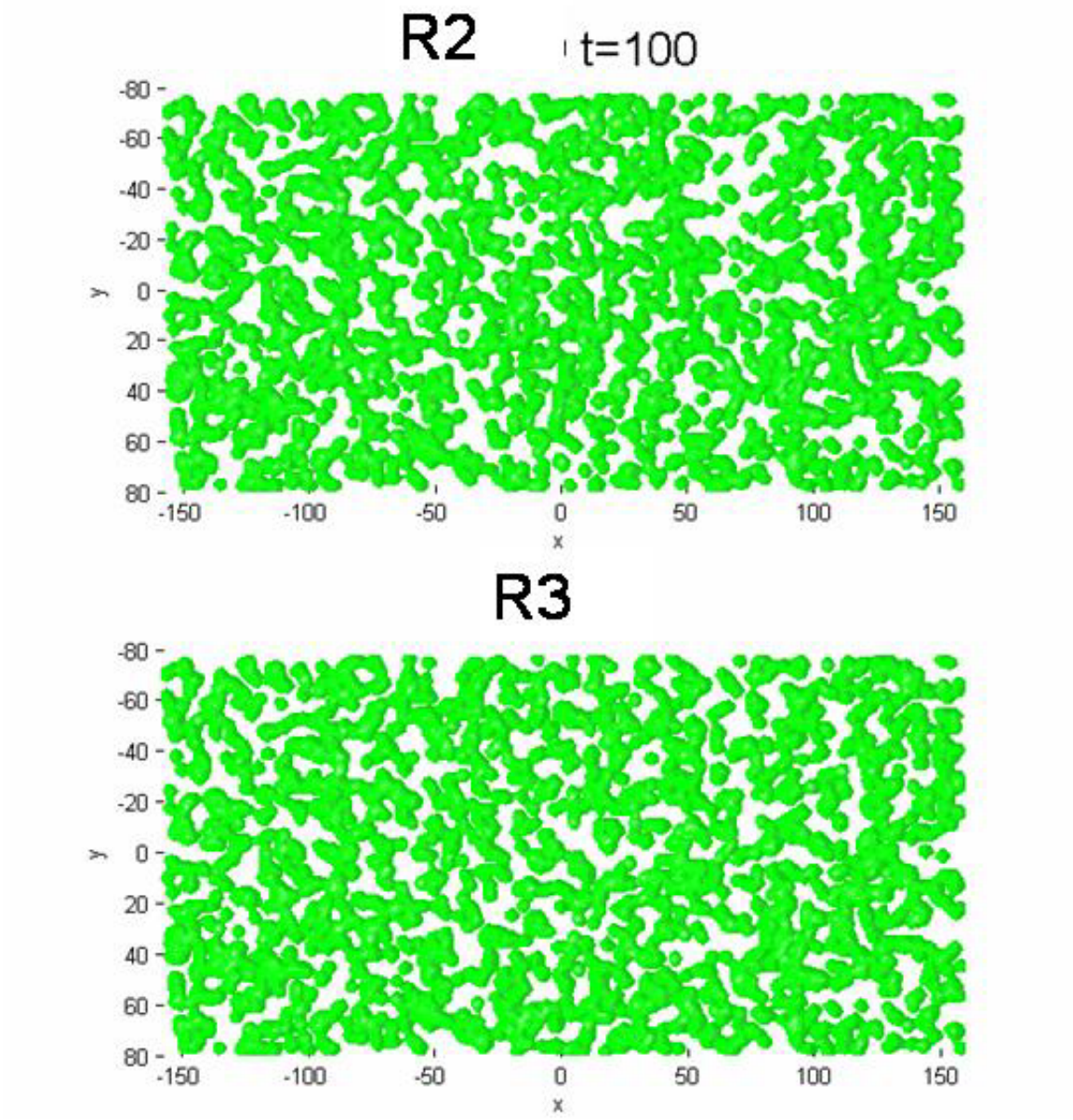

Figure 3- 5 Example spatial pattern of fuels in the RANDOM clumping scenario, in which no explicit clumping was imposed on the trees.

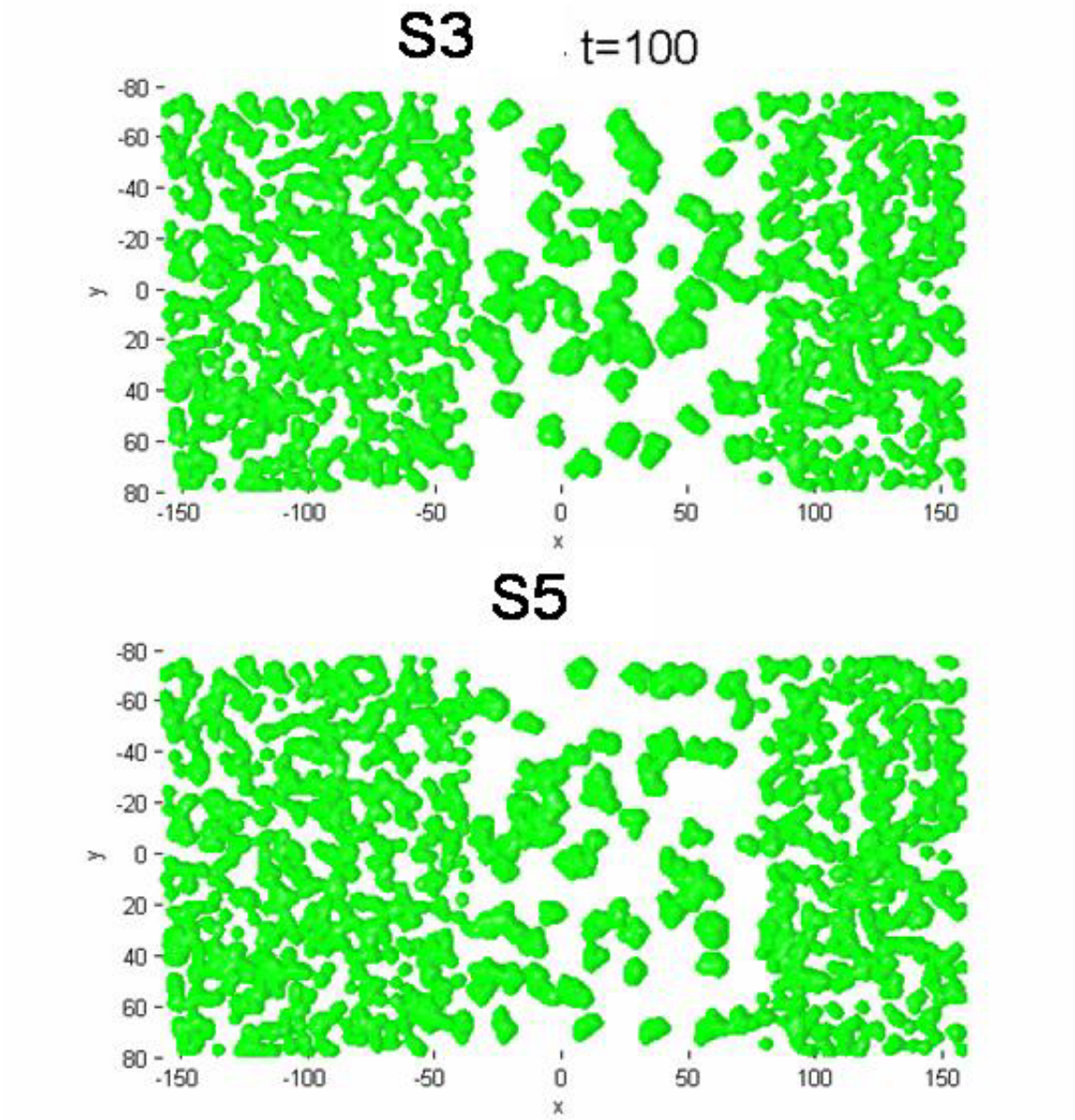

Figure 3- 6 Example spatial pattern from two different cases of the SMALL clumping group. The trees within the zone of fuel modification were translated in x and y according to membership in randomly determined small clumps.

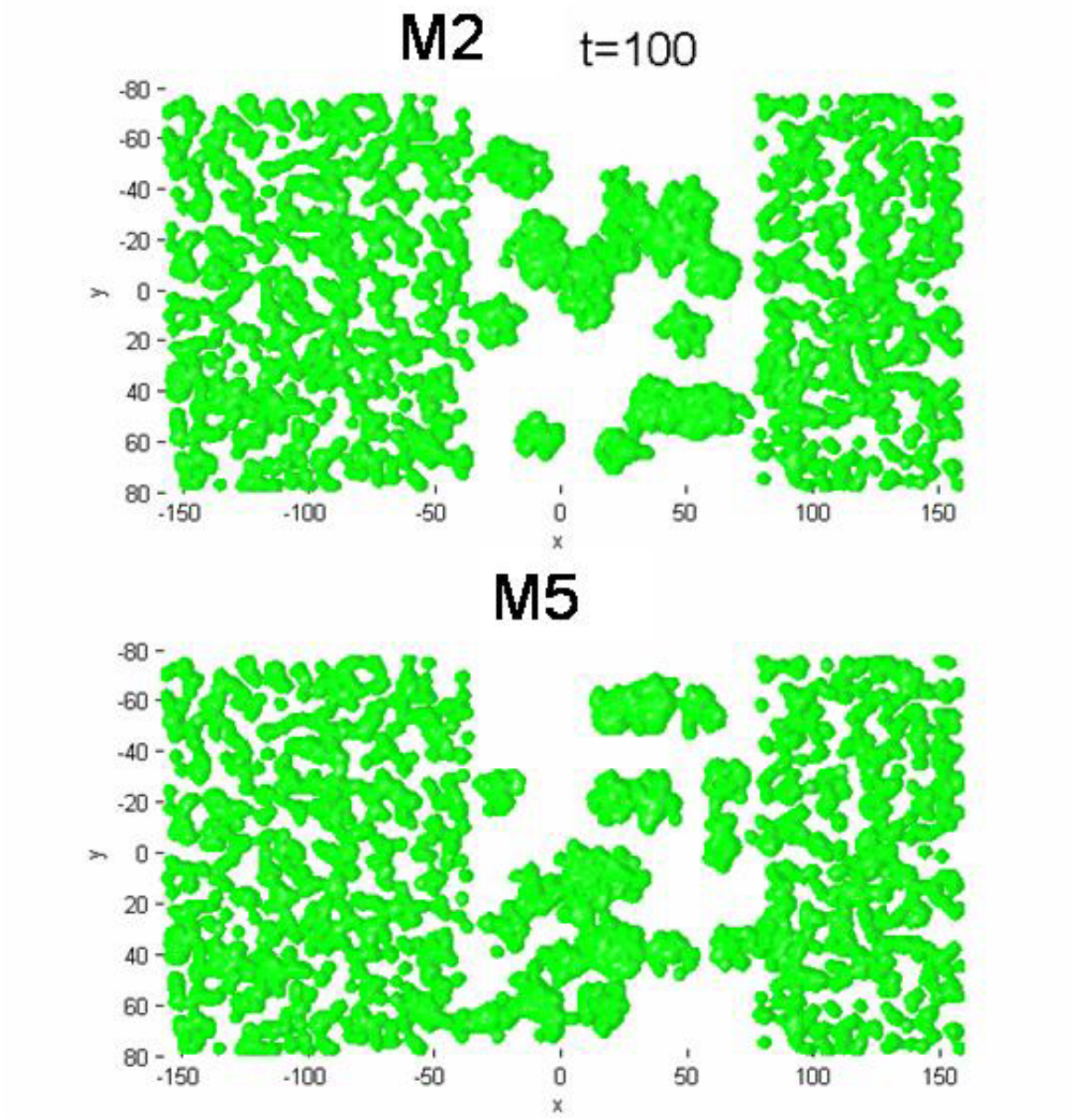

Figure 3- 7 Example spatial pattern from two different cases of the MEDIUM clumping group. The trees within the zone of fuel modification were translated in x and y according to membership in randomly determined medium sized clumps.

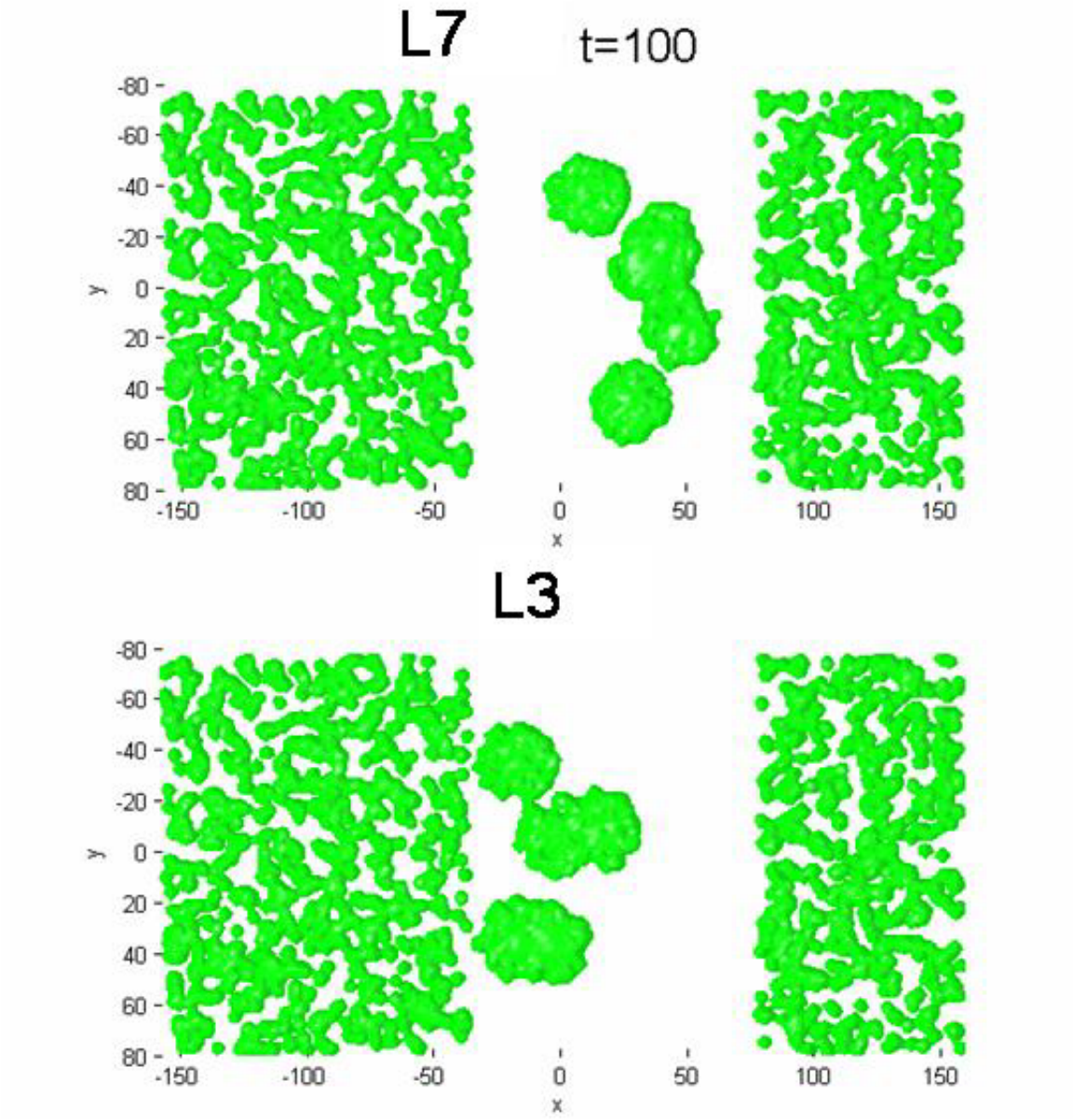

Figure 3- 8 Example spatial pattern from two different cases of the LARGE clumping group. The trees within the zone of fuel modification were translated in x and y according to membership in randomly determined large clumps clumps.

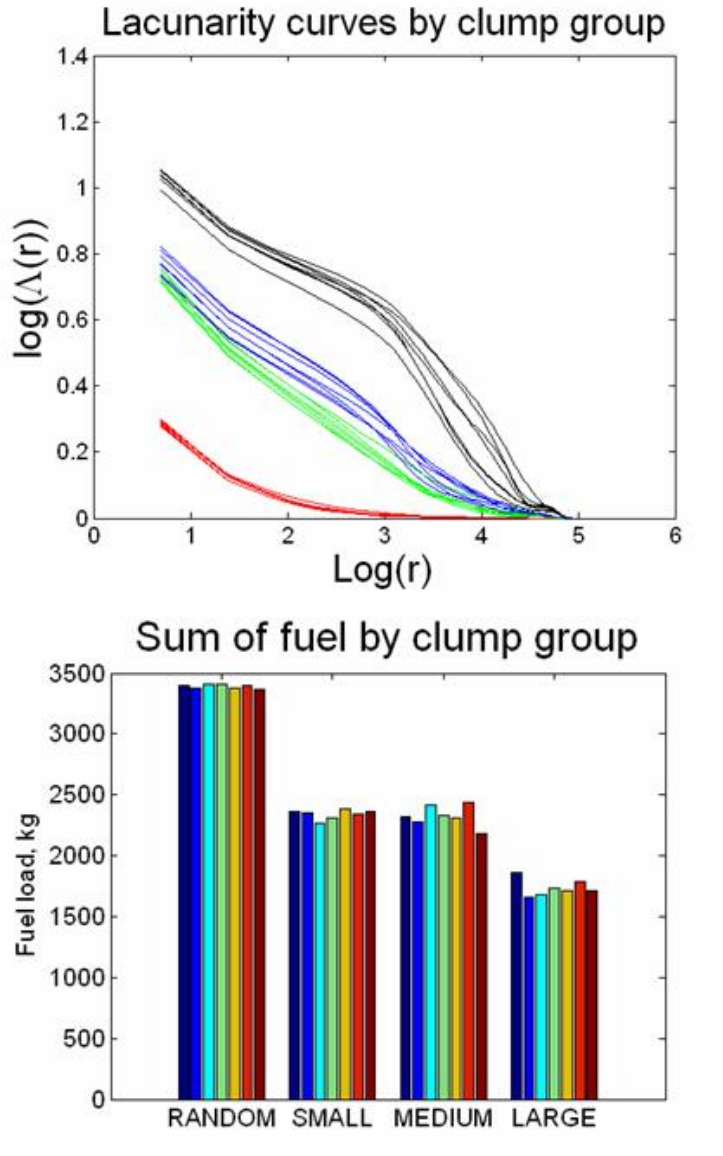

Figure 3- 9 Lacunarity curve plots which statistically describe the spatial variability in the fuel layers across spatial scales for the random (red), small(green), medium(blue) and large(black) clumping groups. Bottom: Bar charts of total canopy fuels in each simulation within the zone of fuel modification. Within group variability is low for both spatial pattern and fuel, while between group variability is fairly high. The small and medium clumping groups are quite similar in both spatial structure and fuel quantity.

Statistical tests assessing differences in median overall spread rates between clumping groups

Substantial variability was observed in the overall average spread rate across the 28 simulations (**Figure 3-10**). The average spread rate was 0.858 m/s (1.92 mph), with a standard deviation of 0.043 m/s (0.097 mph) and a coefficient of variation of 0.05. Within group variability (i.e., differences between unique spatial fuel configurations of the same kind) was higher than between group variability (i.e., random vs small clumping); no significant differences in the median overall spread rates were detected by the Kruskal Wallis test (**Table 2**, below). Variability was lower for the random clumping groups than for the others.

Table 3- 2 Results of Kruskal-Wallis non parametric comparison of differences in median overall spread rate between clumping groups.

Source	SS	df	MS	Chi-sq	Prob>Chi-sq
Groups	148.64	3	49.5476	2.22	0.5287
Error	1661.86	24	69.244		
Total	1810.5	27			

Analysis on incremental spread rates

Description of incremental spread rates

When considered not just as overall averages but as a series of incremental spread events, variability was considerably higher. The mean incremental spread rate across all simulations was 0.93 m/s (2.08 miles per hour), with an overall coefficient of variation of 0.545, an order of magnitude larger than the coefficient of variation calculated on the overall average spread rate. The higher variability at this scale is to be expected since the average spread rate is a measure of central tendency of the incremental spread rates. It is

important to remember, however, that what firefighters experience on a fire is not an overall average spread rate but the incremental spread rates.

Comparison of distributions of incremental spread rates

The nature of the variability in incremental spread rates, described with the skewness, was significantly different between clumping groups (Kruskal-Wallis p-value 0.0089), with more symmetrical distribution shapes for the random clumping groups than for the small, medium or large clumping groups, and the least symmetrical distributions for the medium clumping group (**Figure 3-11**). This suggests that, while the spatial structure of the fuels may not affect the median spread rate (as was found above), it may affect the predictability of spread rates; symmetrical patterns of variability, as observed in the random clumping group, are more easily described and accounted for because they are more similar to a Gaussian, or normal, distribution of errors.

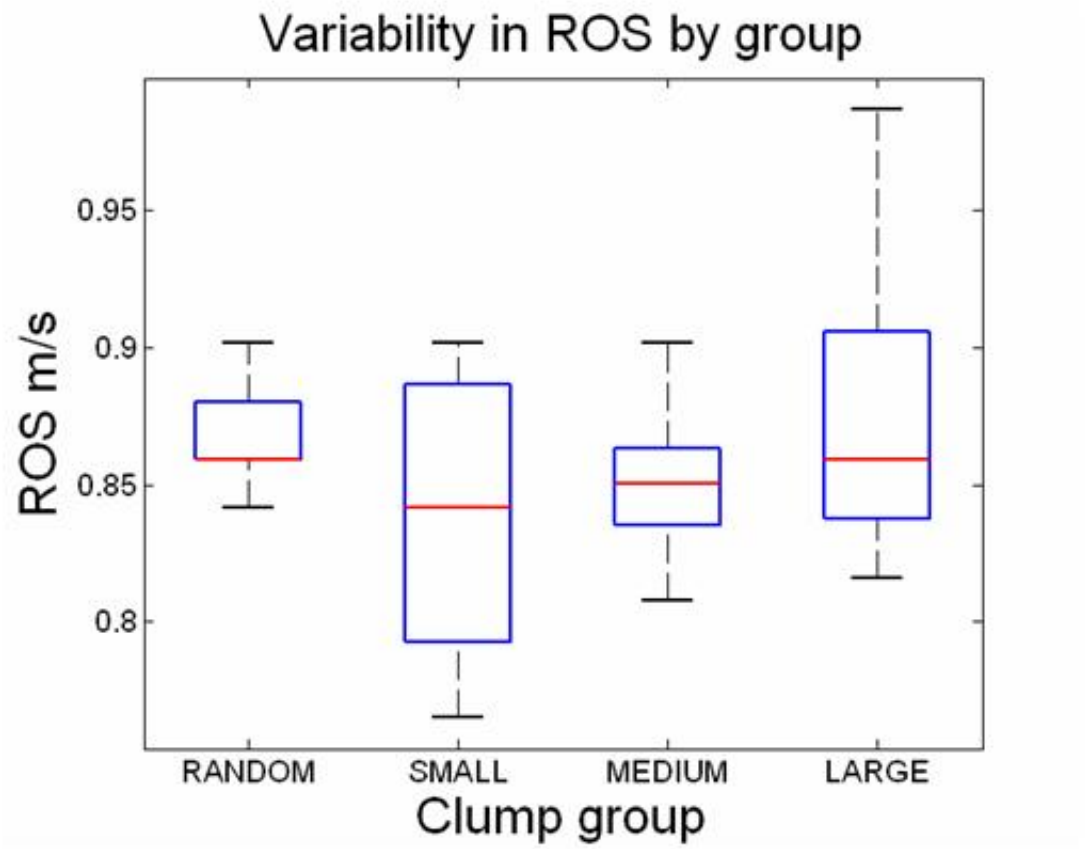

Figure 3- 10 Box plot illustrating distribution of overall average rates of spread between the four clumping groups. The blue box specifies the lower and upper quartile values, while the red line indicates the median value. The black lines show the extent of the rest of the data.

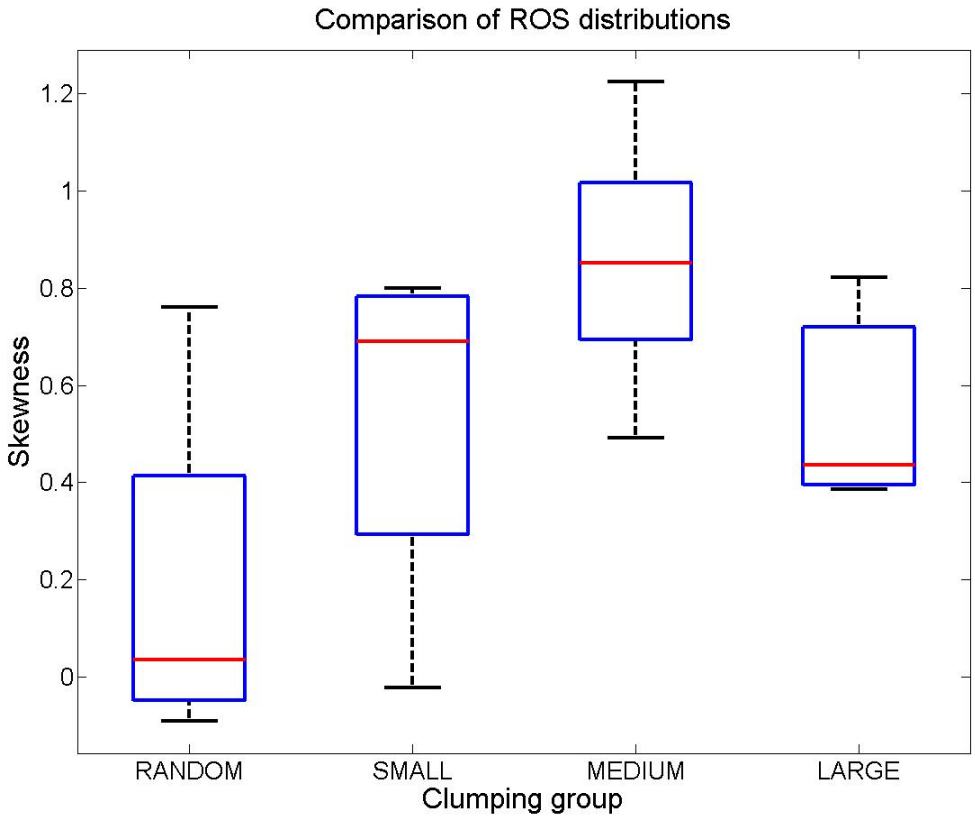

Figure 3- 11 Box plot illustrating that the nature of variability in incremental spread rates, described with skewness, varies between clumping groups (Kruskal-Wallis, p-value 0.0089). Each clump group consisted of seven different simulations. For each simulation, the distribution of incremental spread rates was extracted from the progression of the fire over time, and was described with the skewness, a nondimensional measure of degree of asymmetry in a distribution. Skewness values near zero are highly symmetrical; higher positive values of skewness indicate more extreme high values within the distribution.

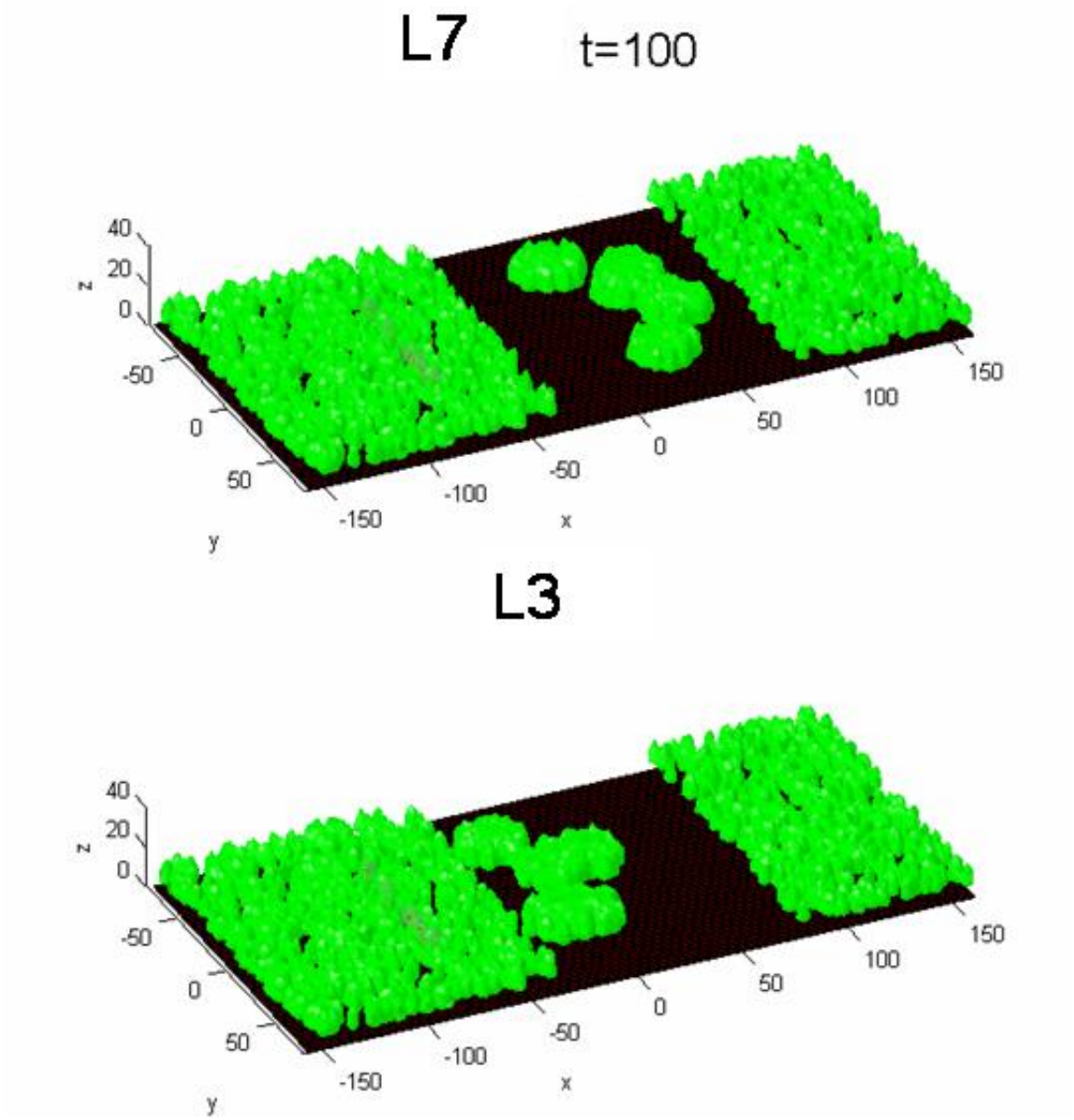

Figure 3- 12 Initial fuel configurations for the L7 (top) and L3 (bottom) simulations described in the case study comparison.

The case study

The two runs selected for more in-depth examination were the seventh and third simulations in the large clumping group, hereafter referred to as L7 and L3. **Figure 3-12** resents an oblique view of the spatial configurations of the two simulations near the beginning of the simulation. These two runs had the largest difference in overall spread rate, with 0.9872 (L3) and 0.8162 m/s overall (L7) (2.2 and 1.8 miles per hour, respectively). Examination of these runs provides useful insights into the mechanisms of variability in rate of spread. Animation files illustrating the progression of both simulations, as well as from a similar pair of simulations from the small clumping group (S3 and S6) are presented in **Table 3-1**.

The two simulations had identical spread rates for the first half of the simulation duration, until roughly t = 6000 (total time two minutes). (**Figure 3-13** and **Figure 3-14**) . At t = 5500, L7 had traveled a few cells farther than L3. Between t =6000 and t=6500 (a period of ten seconds) L3 (blue line) caught up with and then passed L7. Over the next 40 seconds, between t=6500 and t=10500, L3 generally maintains a higher rate of spread than L7, resulting in a significant gap in total distance traveled.

Figures 3-15 through Figure 3-21 present oblique views of the two simulations progressions between t=5000 and t=11000. Throughout this narrative, refer to **Figure 3-13** and **Figure 3-14** to see a clearer picture of the distance each fire traveled over time. At t = 5000 (**Figure 3-15**), the fires in both simulations have entered the zone of fuel modification and appear to have similar shape. In L3 (bottom panel) the distance between the fire and the clumps of trees is much shorter than in L7 (top panel). At t = 6000 (**Figure 3-16**) L3 has burned through the short gap between the unmodified random

forest and the tree clumps in the zone of fuel modification. The fire in L3 has actively engaged the trees within the clumps as evidenced by the tall flame structures visible in the lower panel. Simulation L7 meanwhile is burning in the homogeneous grass layer with a much lower intensity fire; there is some distance still remaining before it reaches its respective clumps of trees.

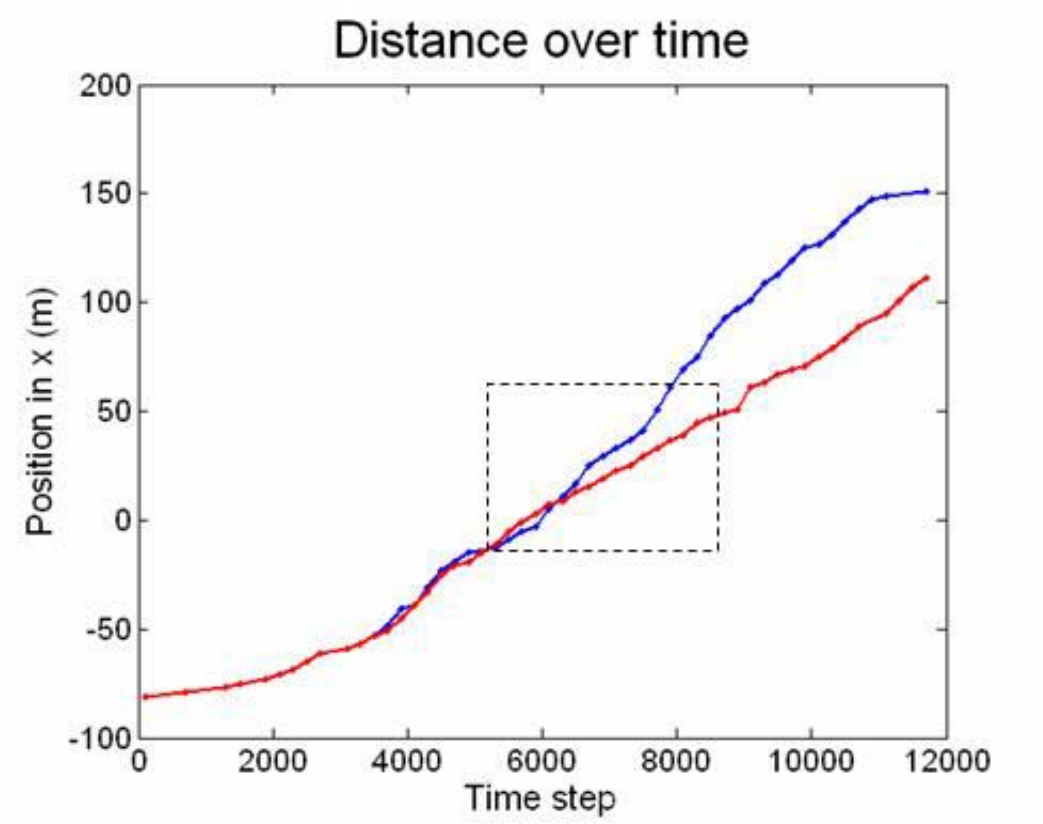

Figure 3- 13 Comparison of distance traveled over time by the fire in simulation L7 (red line) and the fire in simulation L3 (blue line), over the whole simulation duration of 4 minutes.The dashed box indicates the region of the graph shown in the next figure, which represents a period of time in which the two simulations diverged in their behavior.

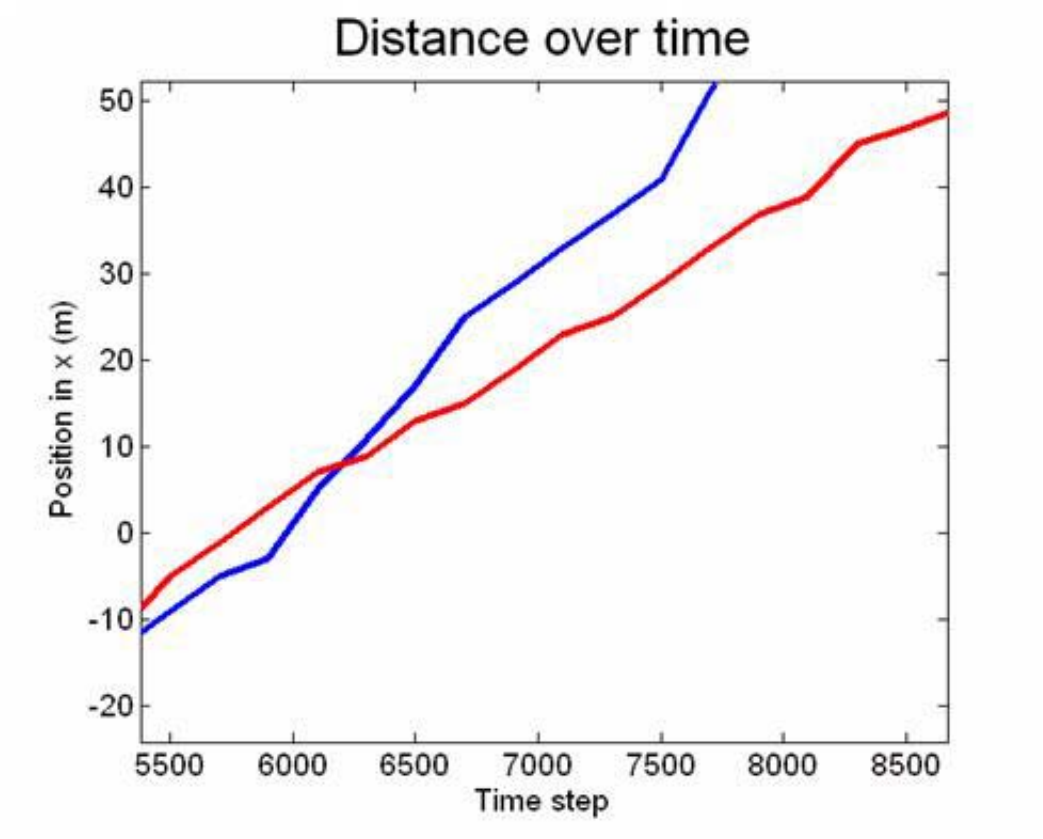

Figure 3- 14 A closer look at the distance over time plot shown in the previous figure, for the time period in which the two simulations, L3 and L7, diverged from each other.

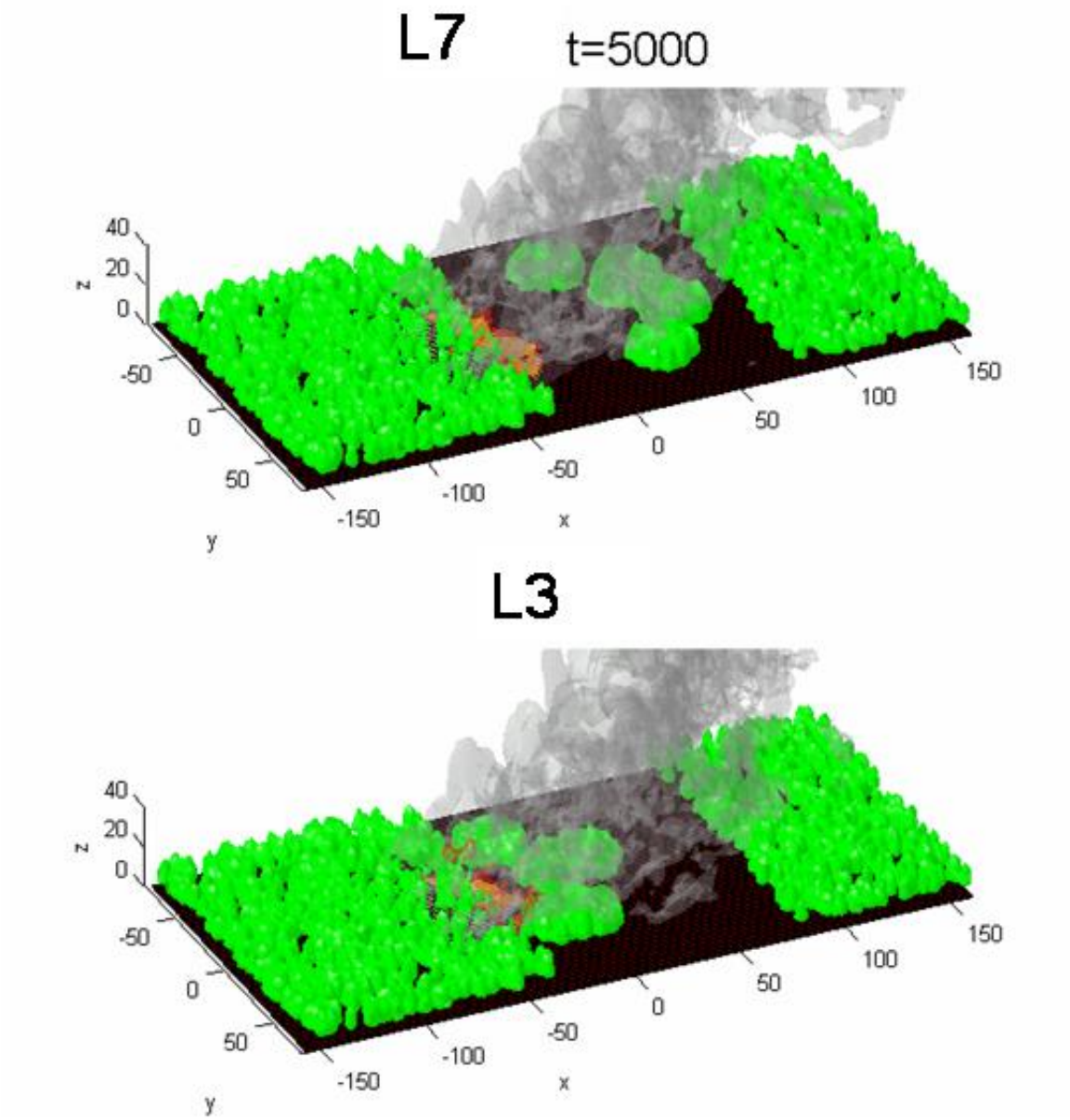

Figure 3- 15 Oblique view of fires in simulation L7 (top) and L3(bottom) at t=5000.

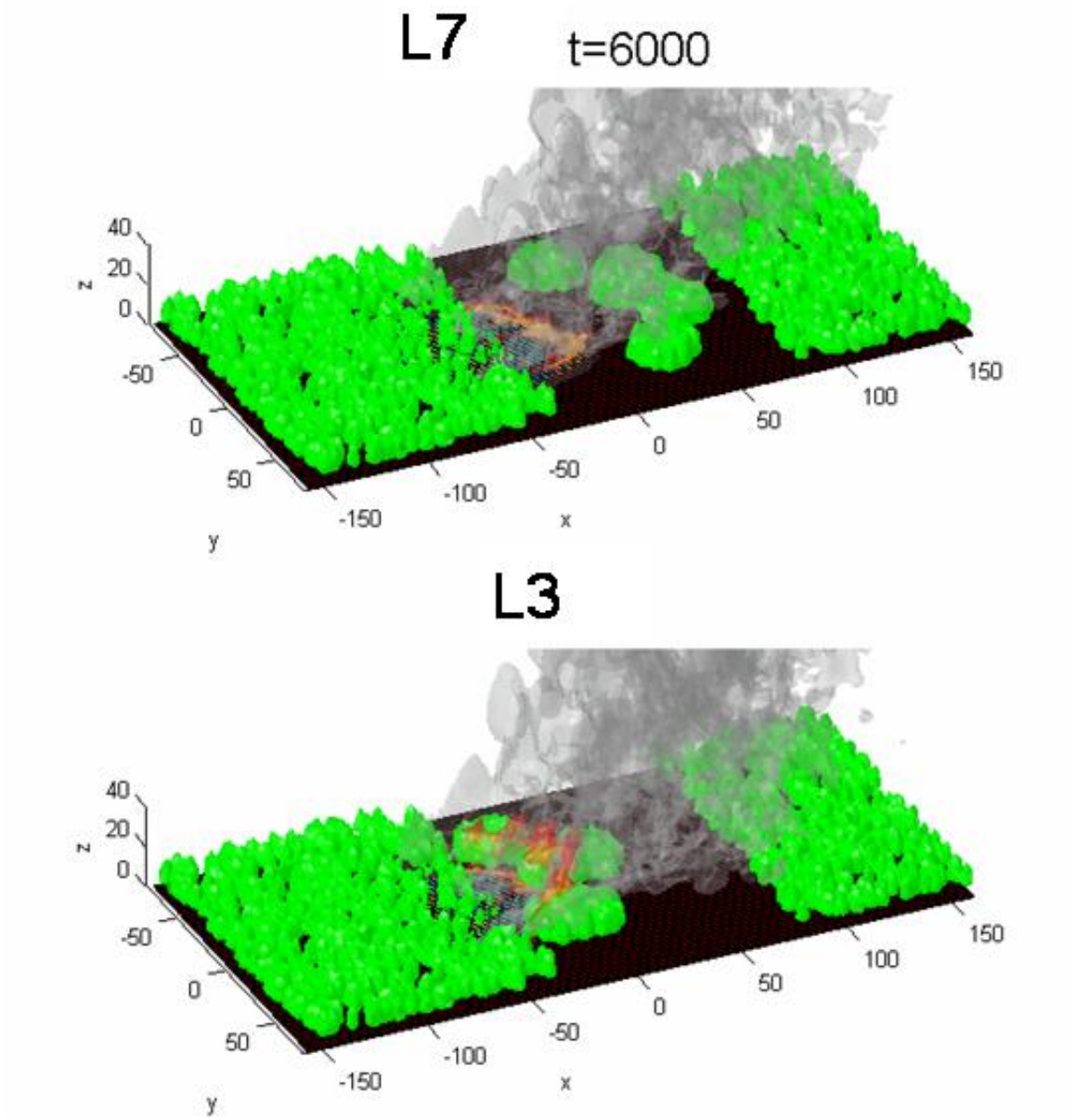

Figure 3- 16 Oblique view of fires in simulation L7 (top) and L3(bottom) at t=6000.

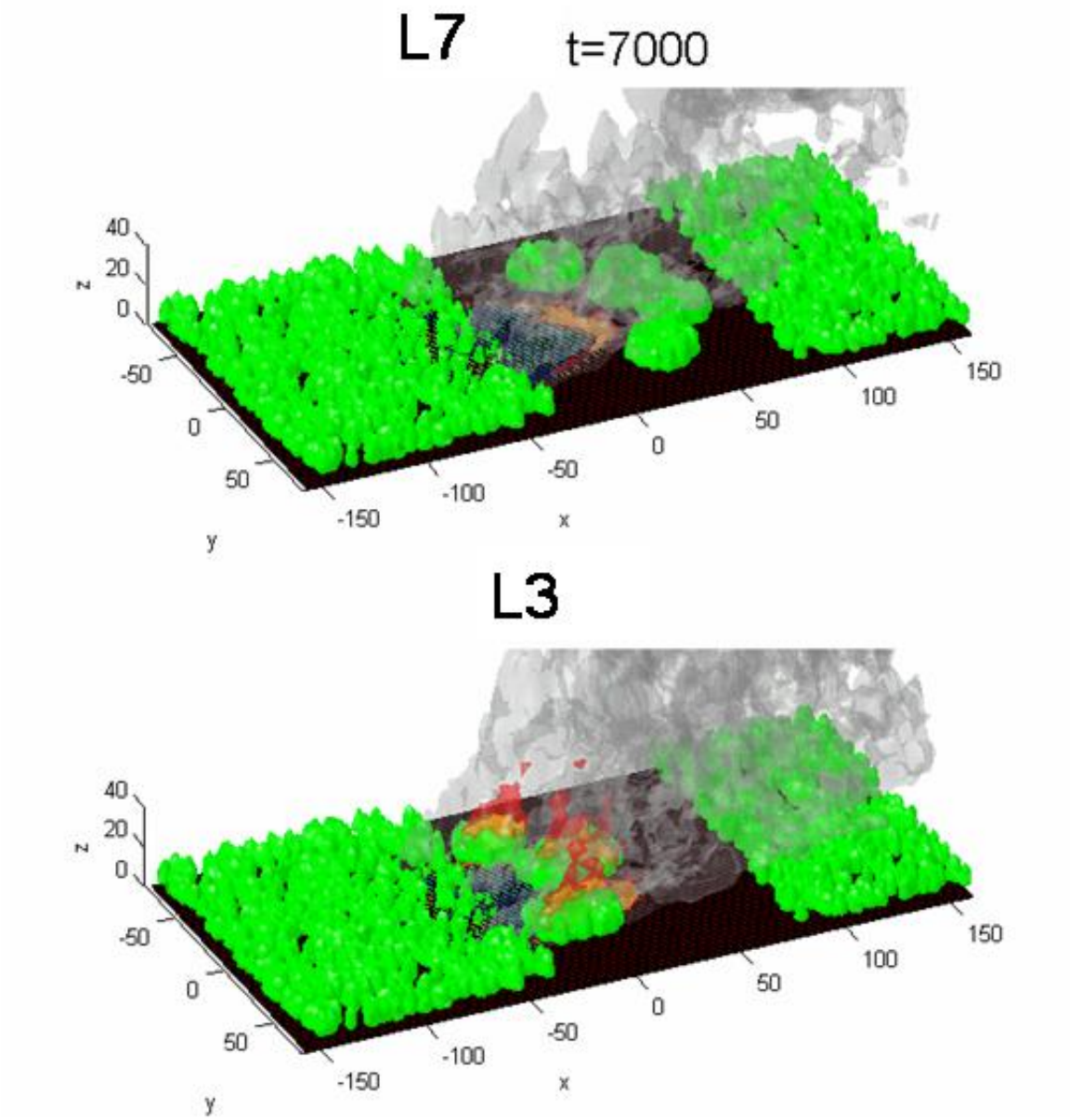

Figure 3- 17 Oblique view of fires in simulation L7 (top) and L3(bottom) at t=7000.

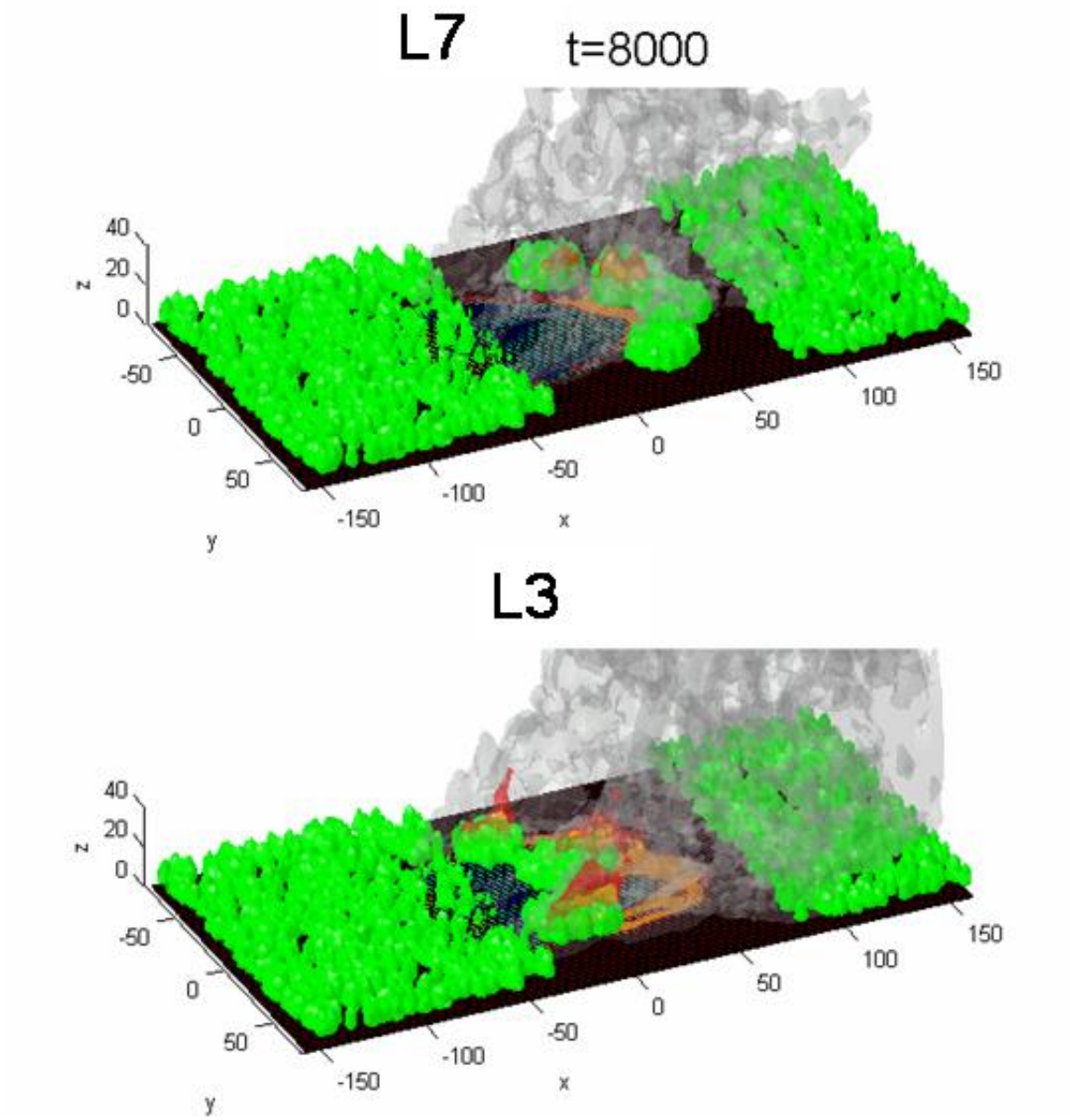

Figure 3- 18 Oblique view of fires in simulation L7 (top) and L3(bottom) at t=8000.

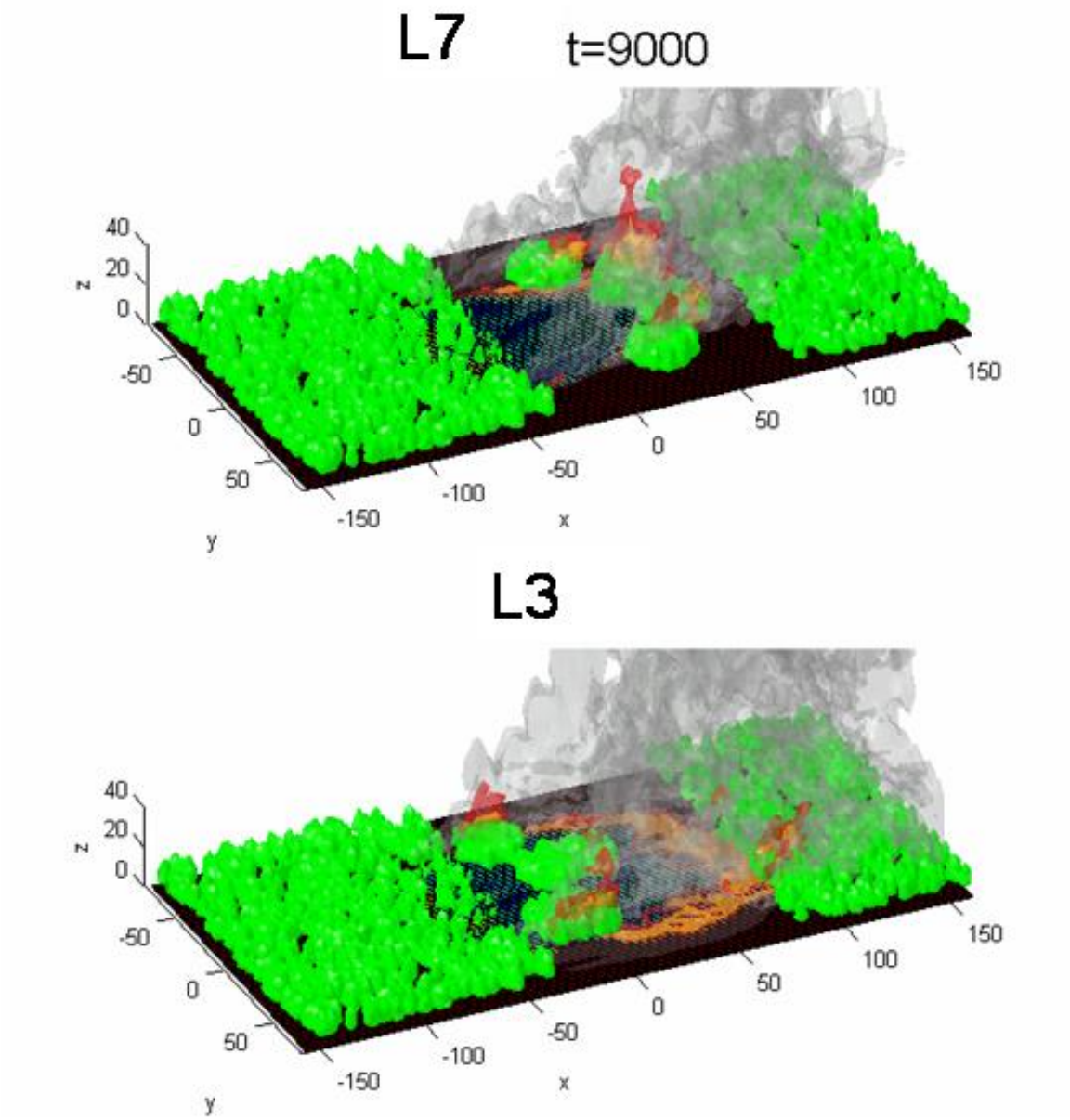

Figure 3- 19 Oblique view of fires in simulation L7 (top) and L3(bottom) at t=9000.

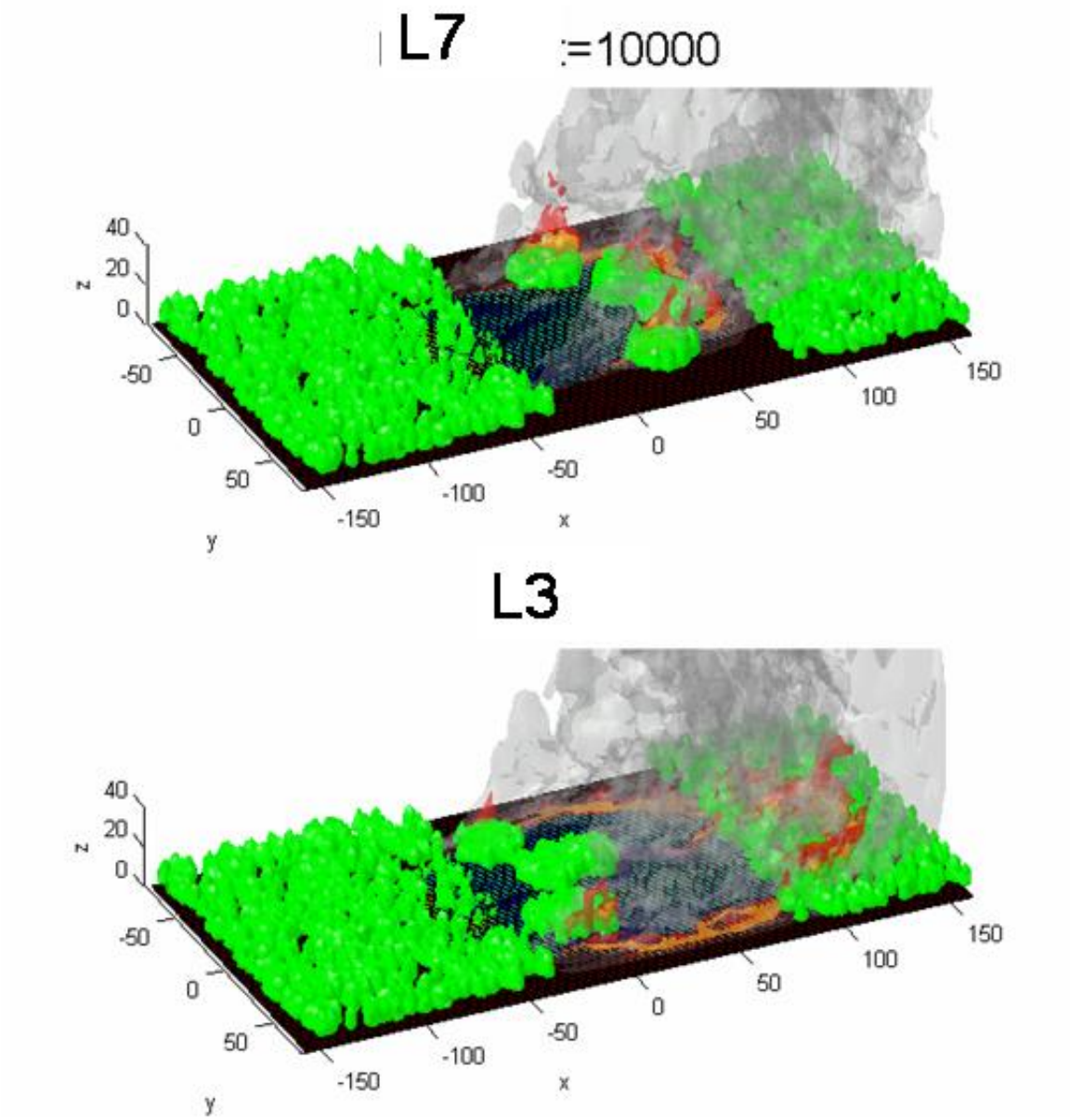

Figure 3- 20 Oblique view of fires in simulation L7 (top) and L3(bottom) at t=10000.

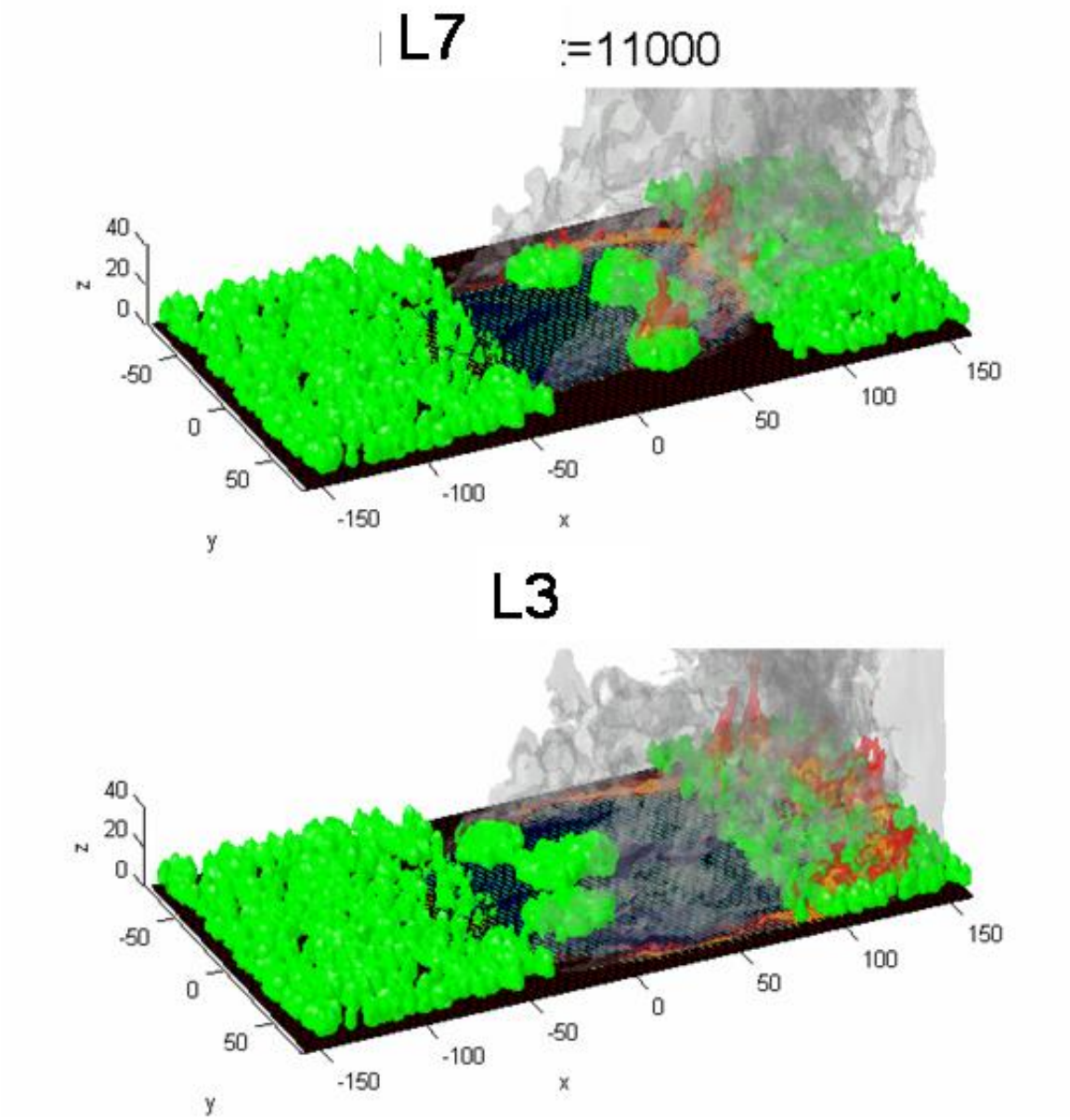

Figure 3- 21 Oblique view of fires in simulation L7 (top) and L3(bottom) at t=11000.

At t = 7000 (**Figure 3-17**) the fire in simulation L3 (bottom panel) is substantially enganged in the crown of the tree clumps and can be seen to extend slightly into the homogeneous grass fuel near the right edge of the tree clumps. The fire in simulation L7 (top panel) has not yet reached its tree clumps and is still moving through the grass fuels. At t= 8000 (**Figure 3-18**), the fire in simulation L3 (bottom panel) has extended well into the homogeneous grass fuel and had a wide flaming front. The fire in simulation L7 meanwhile has engaged the tree crowns in its tree clumps, but with generally less energy than was seen when L3 began burning the crowns of its tree clumps.

At t =9000 (**Figure 3-19**) simulation L3 (bottom panel) has burned across the wide area of grass fuels and has engaged the unmodified random forest on the other side. Simulation L7 is more engaged in the crowns of its tree clumps but does not appear to have significantly entered the grass fuels on the other side. At t=10000 (**Figure 3-20**) simulation L3 (bottom panel) has expanded its perimeter both laterally and farther into the unmodified random forest, and has an intense flame structure at the head of the fire. At t=11000 (**Figure 3-21**), the fire in simulation L3 has reached the damping layer in the last ten cells before the far side boundary and is thus prevented from moving further; this can be seen as a flattening out of the distance over time curve for that simulation in **Figure 3-13** (blue line). The fire in simulation L7 has entered the unmodified random forest on the other side of the zone of fuel modification.

This progression certainly shows variability in the forward spread rate and fire behavior in general, but it is not readily apparent why the two simulations might have such

differences in spread rate. The macroscopic spatial structure of the two simulations is very similar (as demonstrated by the lacunarity curves) as is the total quantity of fuel. Both simulations had the same, identical wind flow entering the spatial domain as well as the same ignition. The two spatial configurations are even similar, with a small gap between the random forest and the tree clumps on one side and a large gap on the other; if the fuels within the zone of fuel modification for simulation L7 were moved to the left, the two spatial configurations would be almost identical. Why, then, do the two simulations diverge in forward spread to such a degree?

Figures 3-22 through **3-32** shed light on this question. These figures present the same two simulations, again over time. The perspective has changed from an oblique angle to a planimetric view; the trees are shown with a higher transparency such that three dimensional cones representing a horizontal slice of the wind field at z = 3 m are emphasized.

Figure 3-22 begins at t=1000; this is only 20 seconds after the fire has initiated and has not yet advanced more than a few meters beyond the ignition strip. The fire is visible in the figures only through its effect on the windfield, which manifests itself with larger, reddish cones that (if you were to look at the figure with more magnification) are oriented more vertically, reflecting the buoyancy in the air induced by the heat of the fire. At this time the fire is clearly quite similar if not completely identical between the two simulations. However, some subtle differences exist. Note that the wind cones, which get larger, and change in color from blue to red with increasing magnitude, are visible mostly down the centerline of simulation L3, while there is a lull in the wind field down the

centerline in simulation L7; the windfield in L7 is more horseshoe shaped towards the left side of the domain. The lull in the winds extends through the center of the gap between the random forest and the tree clumps for L7. A small lull is also visible in L3 in its gap, but the wind cones indicate that the windfield has some magnitude near the center of the tree clumps and extending across the larger gap.

At t = 2000, (**Figure 3-23**), the lull in the winds in simulation L7 has gotten more pronounced; in L3, the centerline winds are still weak in magnitude but are clearly present. At t = 3000, (**Figure 3-24**) more activity from the fire is visible; the lull centered on the gap between the random forest and the tree clumps in L7 has gotten smaller but still exists in the vicinity of the center. In L3 (bottom panel), the wind flow has moved down from the centerline (negative in the y direction) to align with a gap between the tree clumps.

At t=4000, (**Figure 3-25**) the fire in both simulations has progressed to close to the edge of the zone of fuel modification. It is clear from the wind cones in the area of the fire that some subtle differences now exist between the two fires; the windcones near the center of the fire in L3 (bottom panel) are larger, indicating somewhat greater magnitude of velocity. The lull in the wind field is still present in L7. In L3, a stronger windfield has arisen extending in a curve near the bottom of the figure (around y = -60) upwards towards the centerline. In L7, the windfield has strengthened somewhat but is less coherent than in L3. So far this progression has still been earlier in time than the

sequence we saw in the oblique views (with the flames) in figures 15 to 21. Starting at t= 5000, we will see the same progression that we saw in figures 15 to 21.

At t = 5000 (**Figure 3-26**), the fires in both simulations have much stronger flames as evidenced by the larger red wind cones. The lull in the winds in L7 is quite small but still exists and is right at the centerline of the fire. In both simulations we see some increased wind velocities at the edges of the spatial domain. At t= 6000 (**Figure 3-27**), the fire in L7 has a much stronger wind field than the fire in L3. Recall from figure 14 that at t=6000, L7 (red line) had progressed slightly farther than L3 (blue line).

At t = 7000 (**Figure 3-28**), the fire in simulation L3 is engaged in the crowns of the tree clump, resulting in a strong wind field. A small lull in the wind field has appeared in L3 above the centerline and past the edge of the tree clumps, but the windfield near the gap between the tree clumps is fairly strong. In L7 (top panel) the fire is nearly at the tree clumps but has not reached them yet; the overall flow appears somewhat stronger than in L3 but the effects of the fire on the wind field are less pronounced.

At t= 8000 (**Figure 3-29**) we see a significant difference between the two simulations. L3 (bottom panel) shows a much stronger wind field at the outer edge of the tree clumps at the edge of the fire; a coherent flow pattern extends from within the gap between the random forest and the tree clumps, through the gap between clumps and into the larger grass fuel area to the right. The coherent flow appears to be funneled by interactions with the canopy, resulting in a higher velocity. Meanwhile, in simulation L7, the windfield has

lost intensity; the fire has entered the tree clump but is small. Small lulls are found in the wind field below the centerline in the gap between the random forest (to the left) and the tree clumps as well as in the smaller gap between the tree clumps and the random forest (to the right).

At t= 9000 (**Figure 3-30**) the coherent flow through the gap in the tree clumps in simulation L3 (bottom panel) has gotten much stronger as the fire runs across the grassy fuels and enters the random forest on the other side with force. The wind field is the strongest yet. In L7 (top panel) there is a lull near the centerline and the flow is split into two parts that go around the lull to either side; the fire seems to be oriented more towards the top of the figure (toward the y = 80 boundary).

At t = 10000 (**Figure 3-31**), the fire in simulation L3 is engaged in the crowns of the random forest near the right edge of the spatial domain. It has a coherent windfield behind it across most of its width and is mostly symmetrical. The fire in L7 is strongest towards the top edge (where y = 80) and is asymmetrical. There is a large lull in the wind field to the left of the tree clumps, as well as somewhat of a lull along the centerline extending into the random forest at the right.

Finally, at t = 11000 (**Figure 3-32**), the windfields for both fires have dropped in magnitude. The fire in simulation L3 is engaged with the majority of the random forest at the right edge of the spatial domain while the fire in L7 is entering the upper portion of that forest.

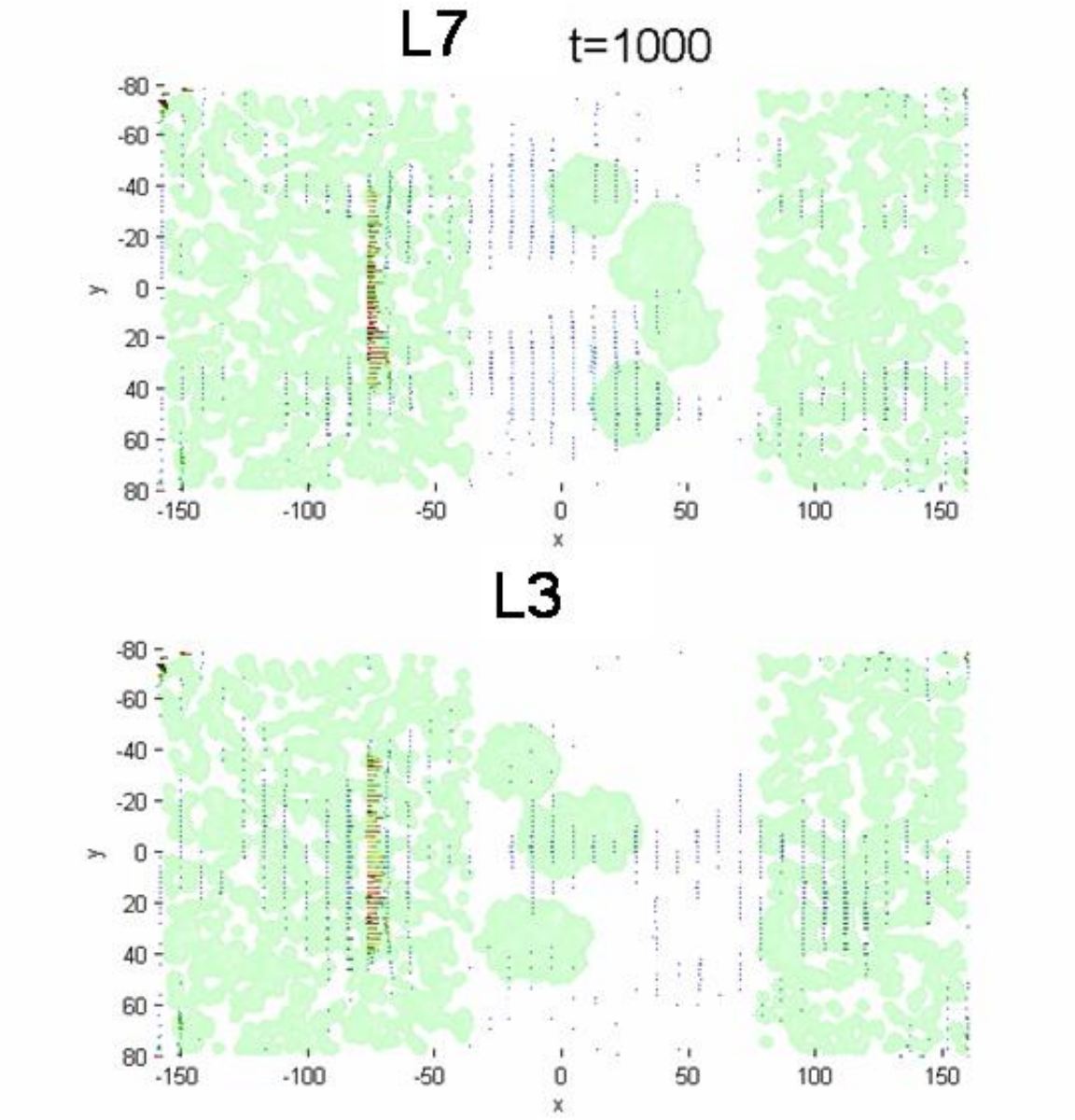

Figure 3- 22 Overhead perspective emphasizing differences in the wind fields between case study simulations L7 (top) and L3 (bottom) at t=1000.

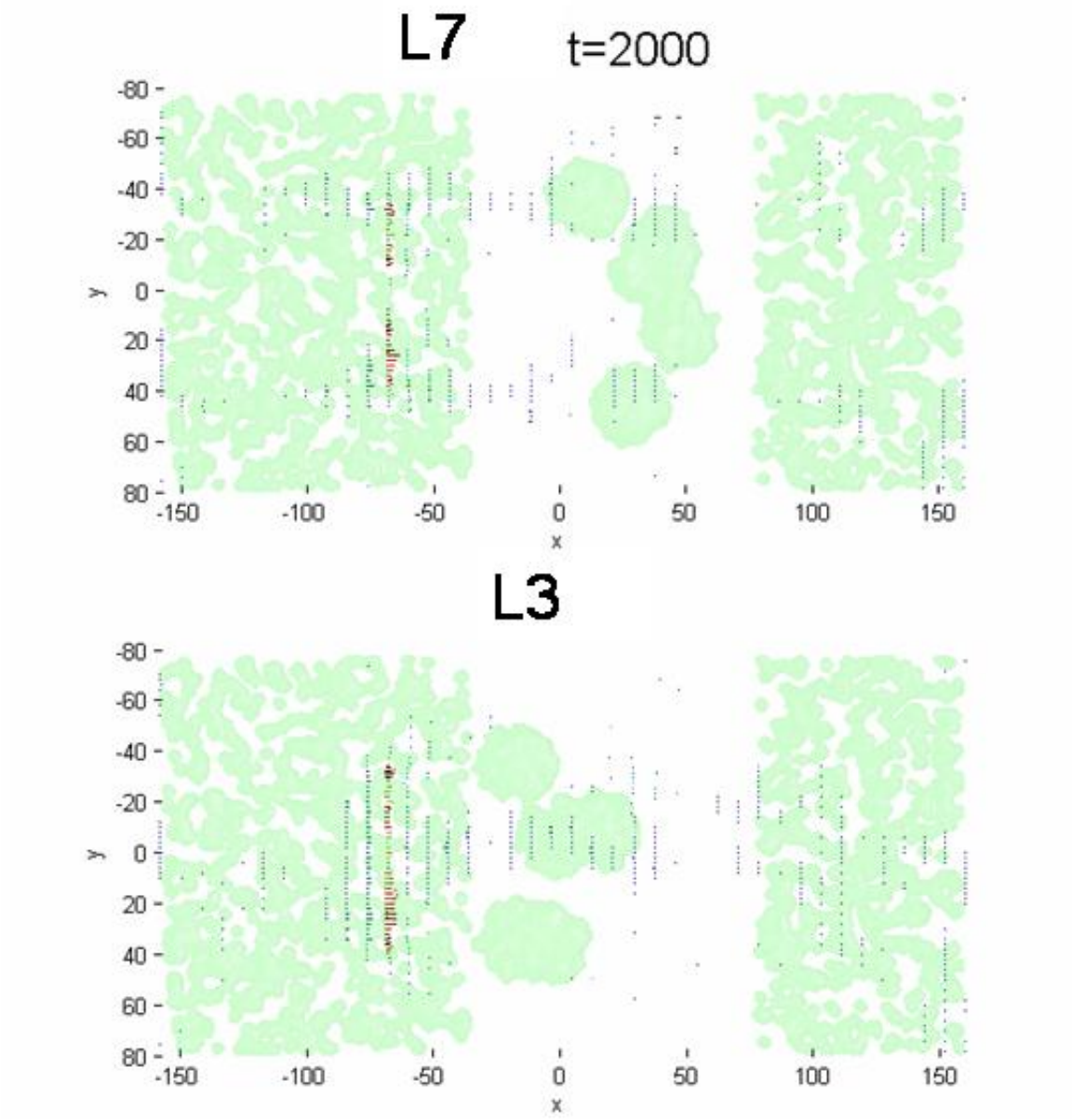

Figure 3- 23 Overhead perspective emphasizing differences in the wind fields between case study simulations L7 (top) and L3 (bottom) at t=2000.

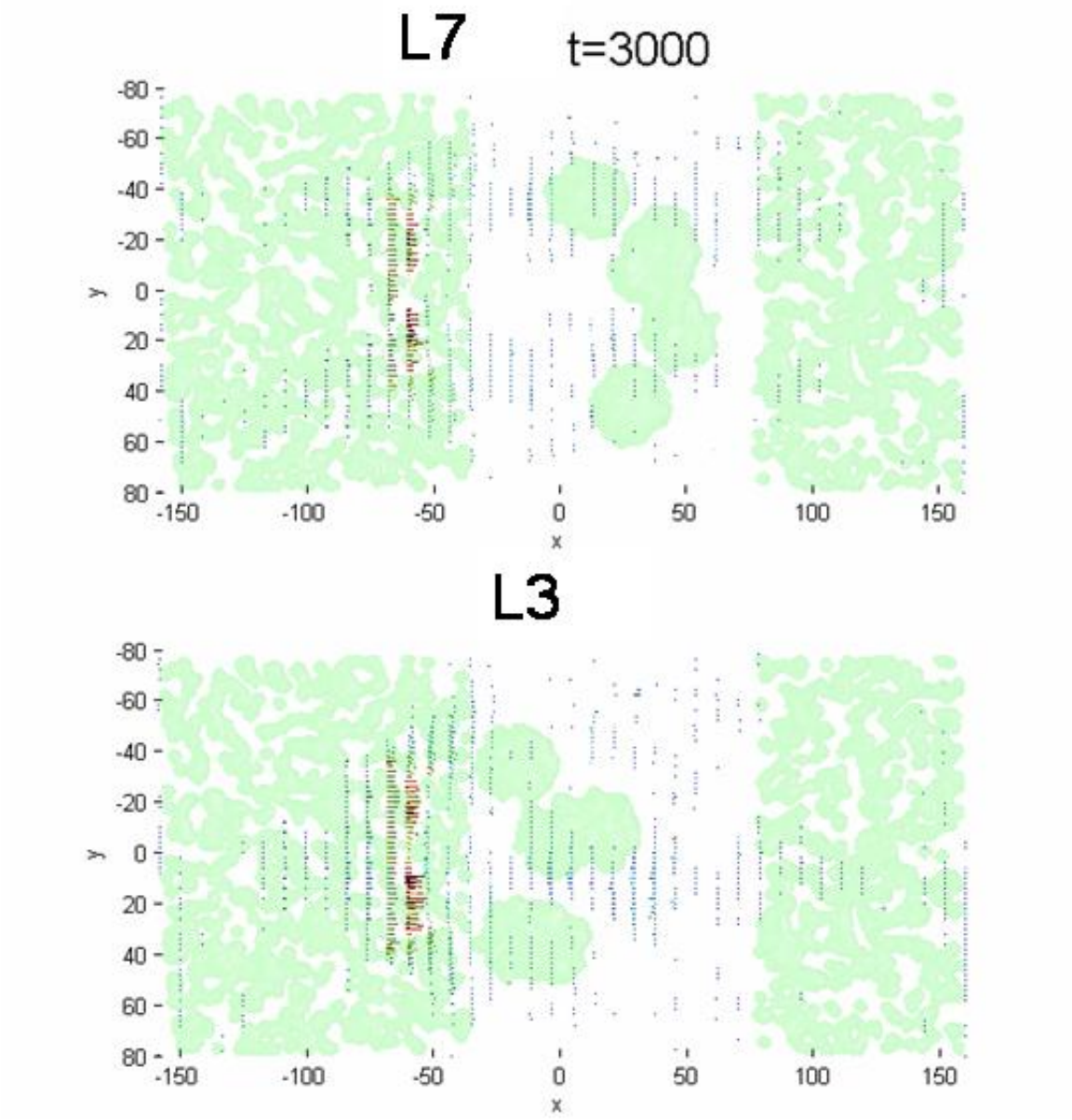

Figure 3- 24 Overhead perspective emphasizing differences in the wind fields between case study simulations L7 (top) and L3 (bottom) at t=3000.

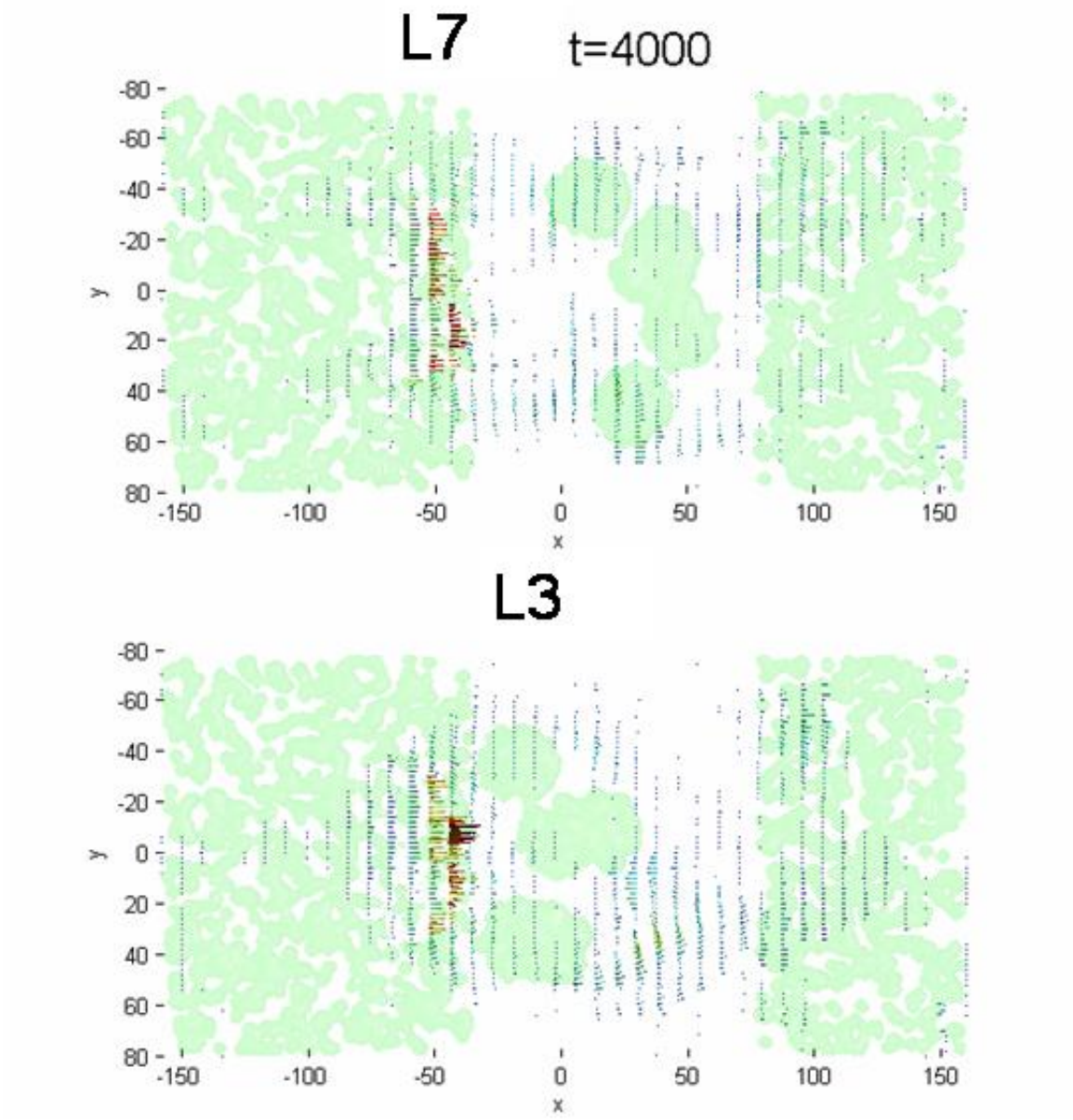

Figure 3- 25 Overhead perspective emphasizing differences in the wind fields between case study simulations L7 (top) and L3 (bottom) at t=5000.

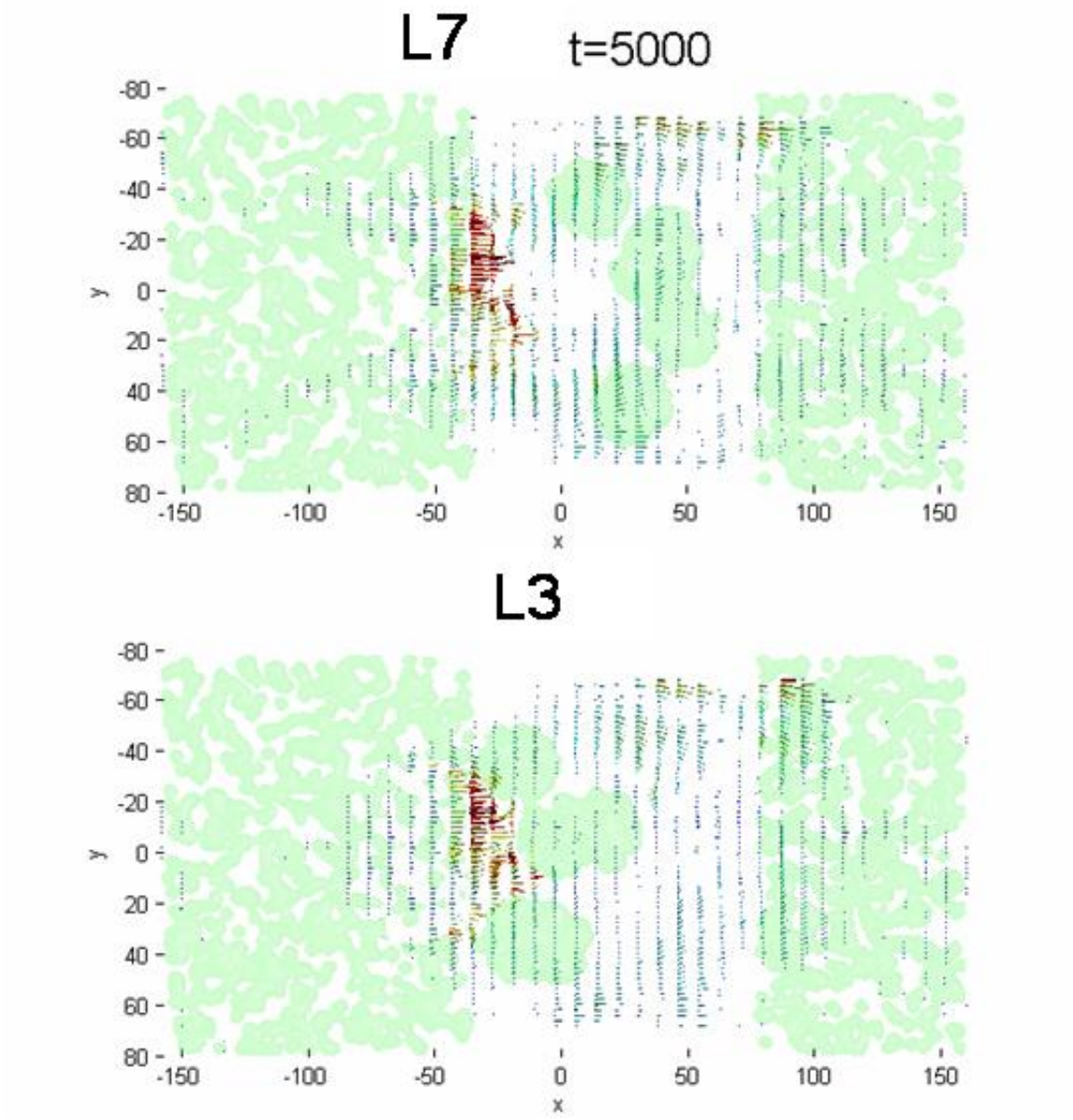

Figure 3- 26 Overhead perspective emphasizing differences in the wind fields between case study simulations L7 (top) and L3 (bottom) at t=5000.

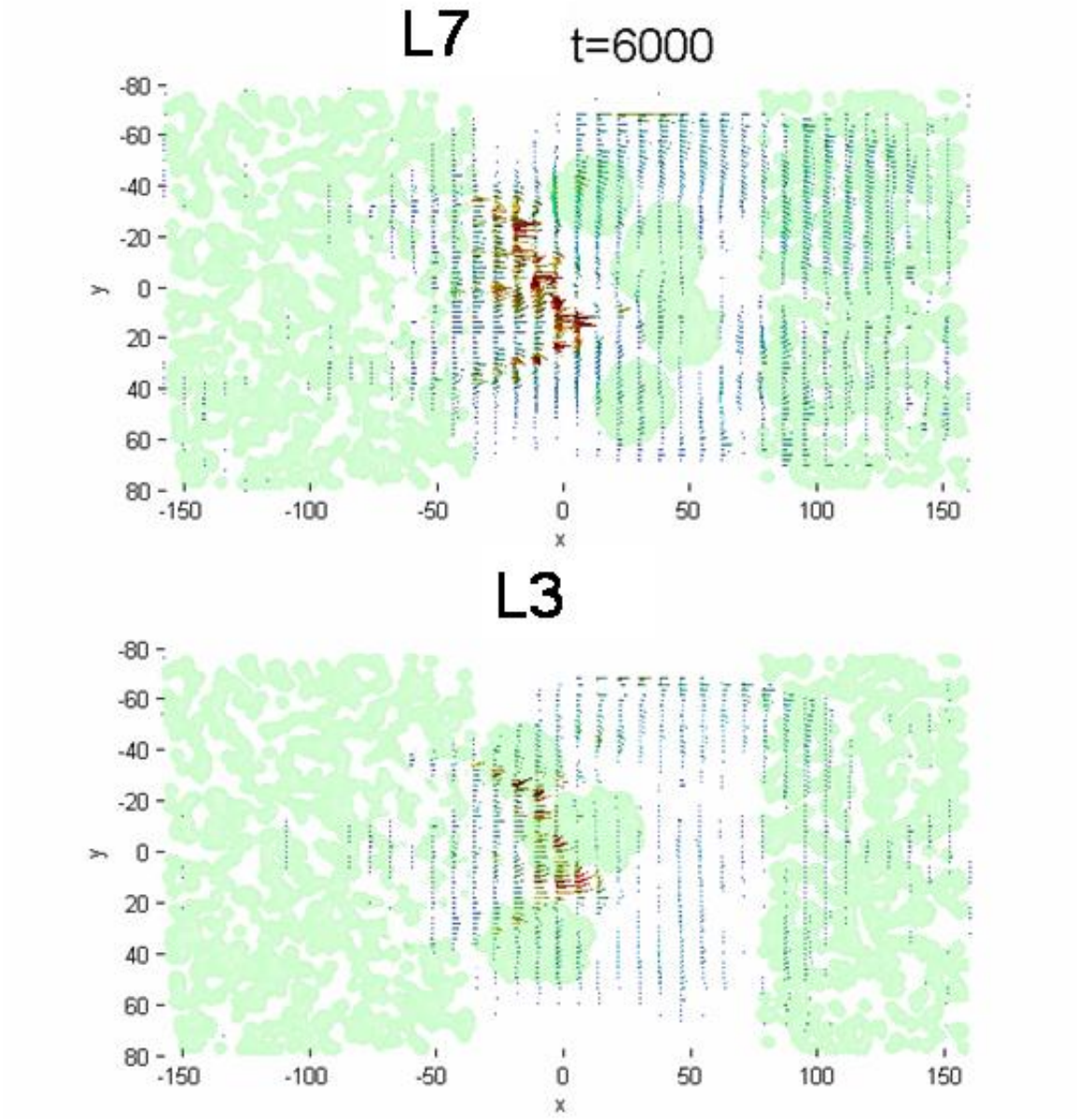

Figure 3- 27 Overhead perspective emphasizing differences in the wind fields between case study simulations L7 (top) and L3 (bottom) at t=6000.

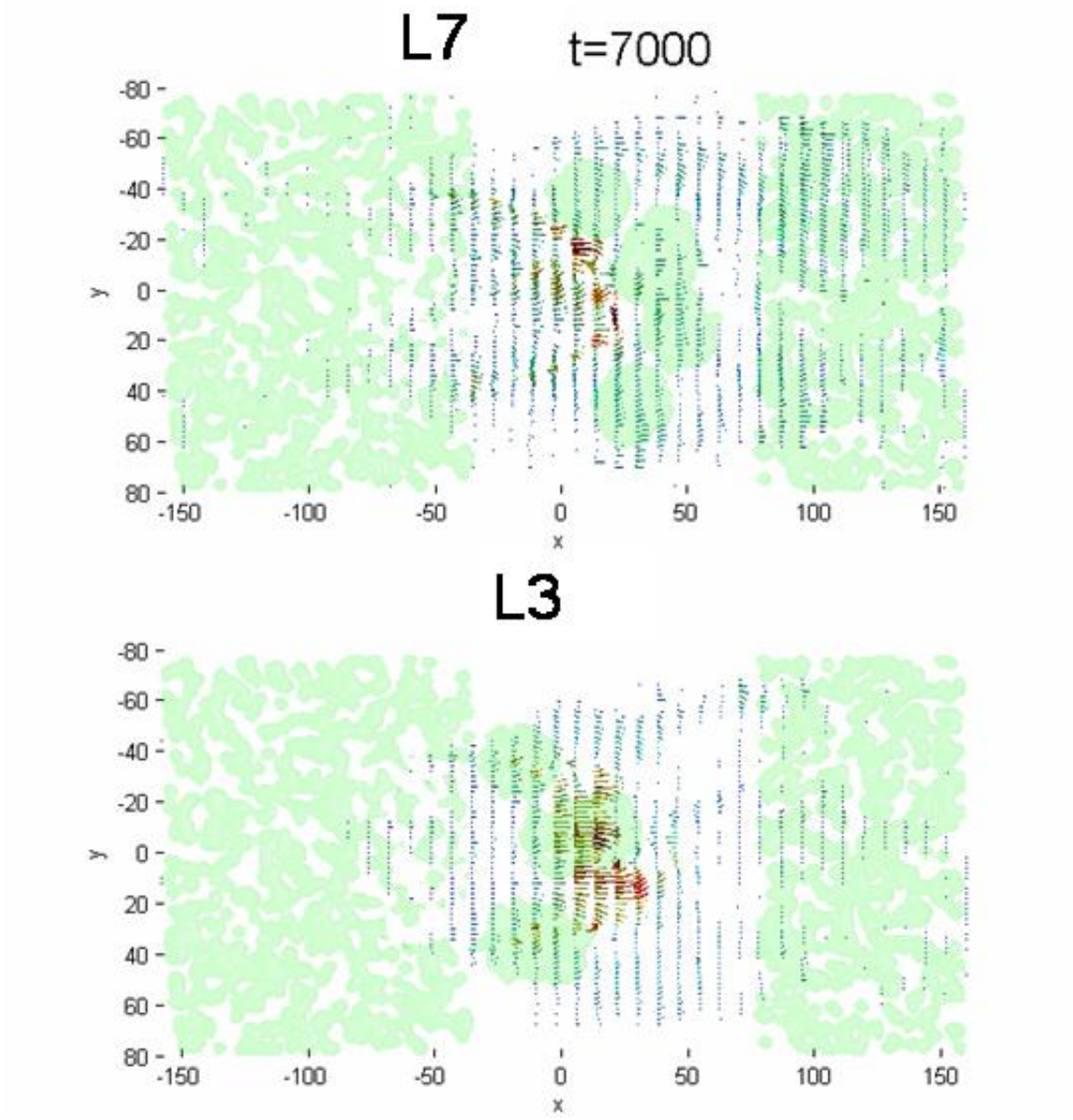

Figure 3- 28 Overhead perspective emphasizing differences in the wind fields between case study simulations L7 (top) and L3 (bottom) at t=7000.

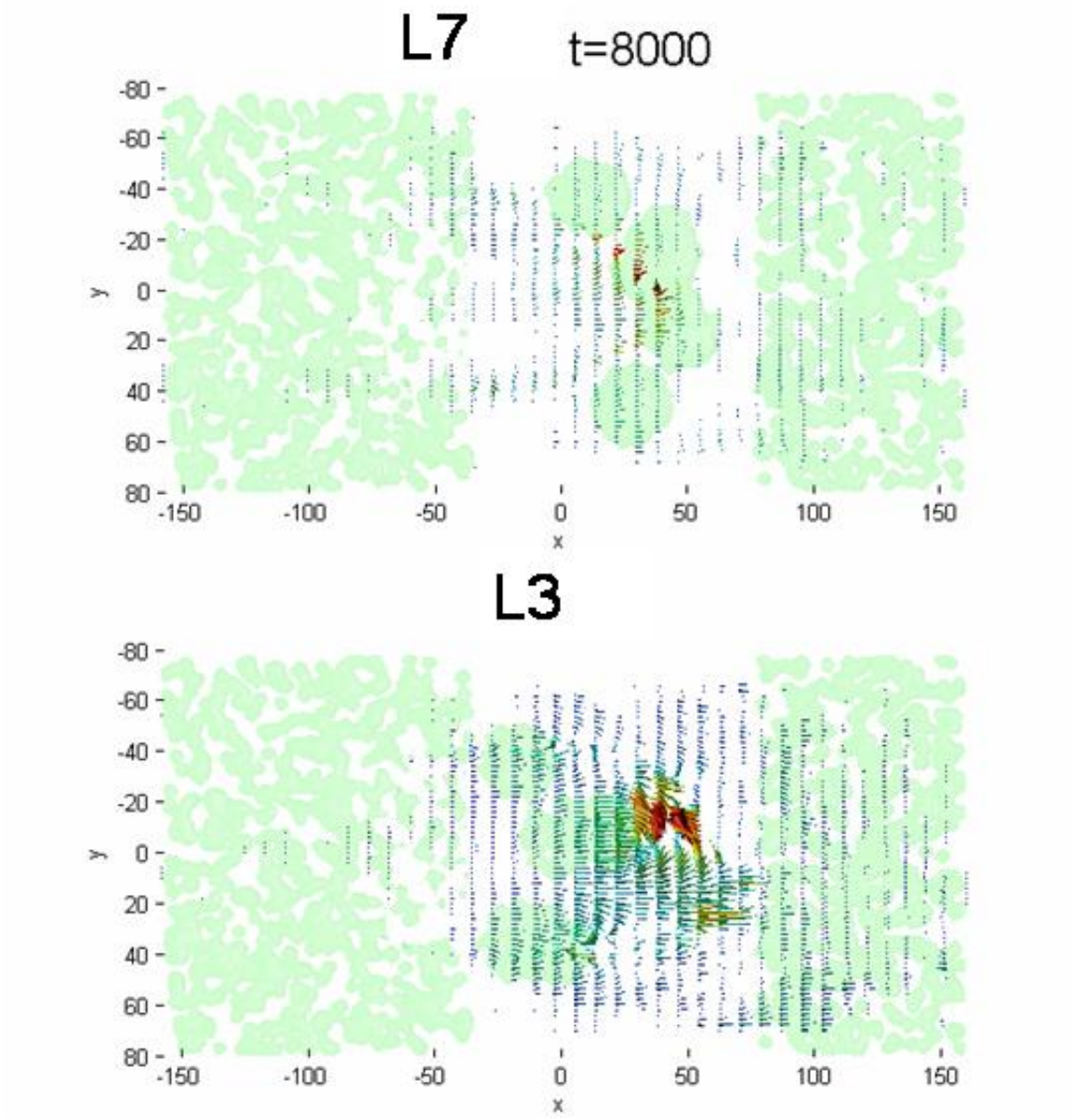

Figure 3- 29 Overhead perspective emphasizing differences in the wind fields between case study simulations L7 (top) and L3 (bottom) at t=8000.

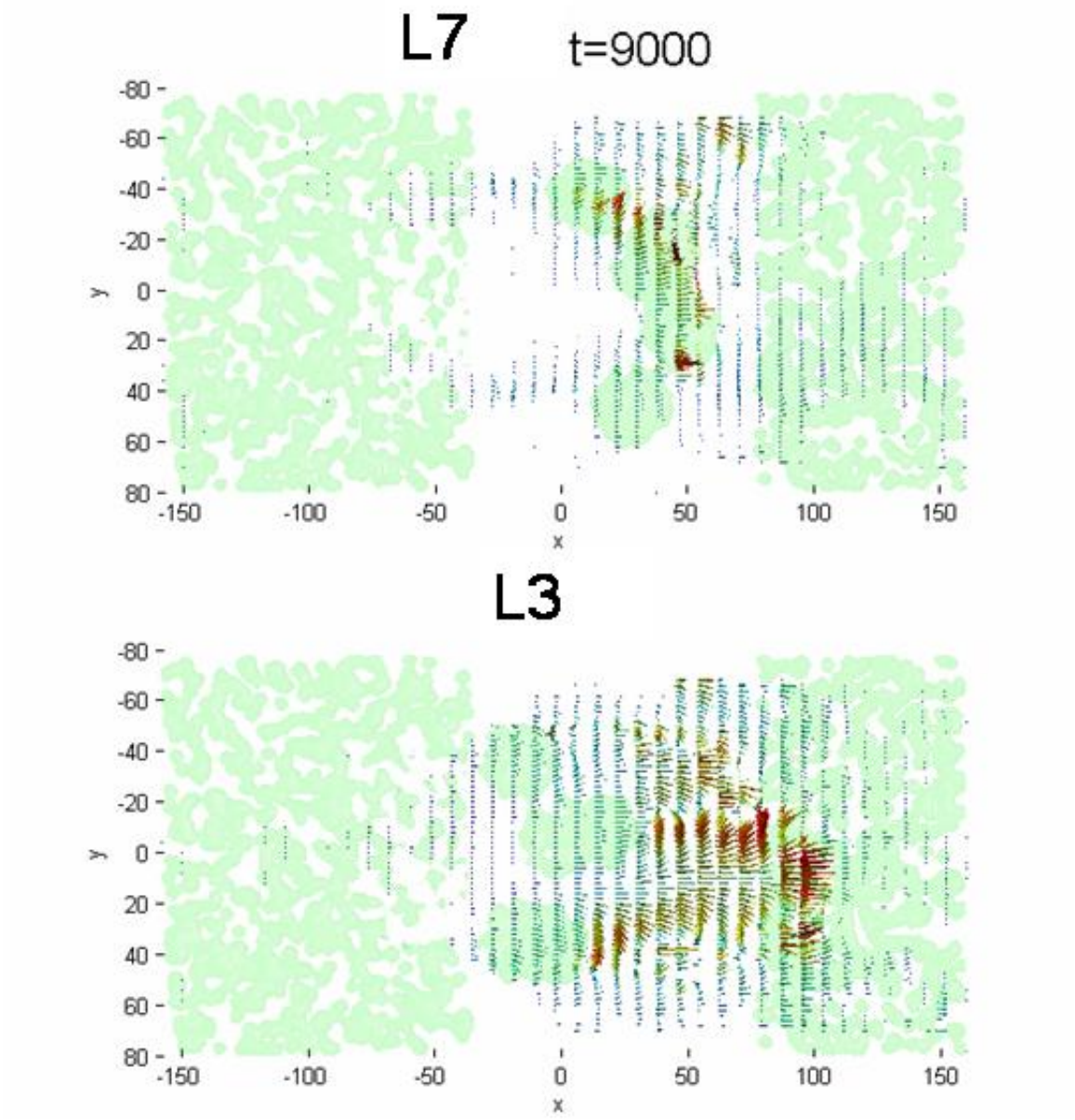

Figure 3- 30 Overhead perspective emphasizing differences in the wind fields between case study simulations L7 (top) and L3 (bottom) at t=9000.

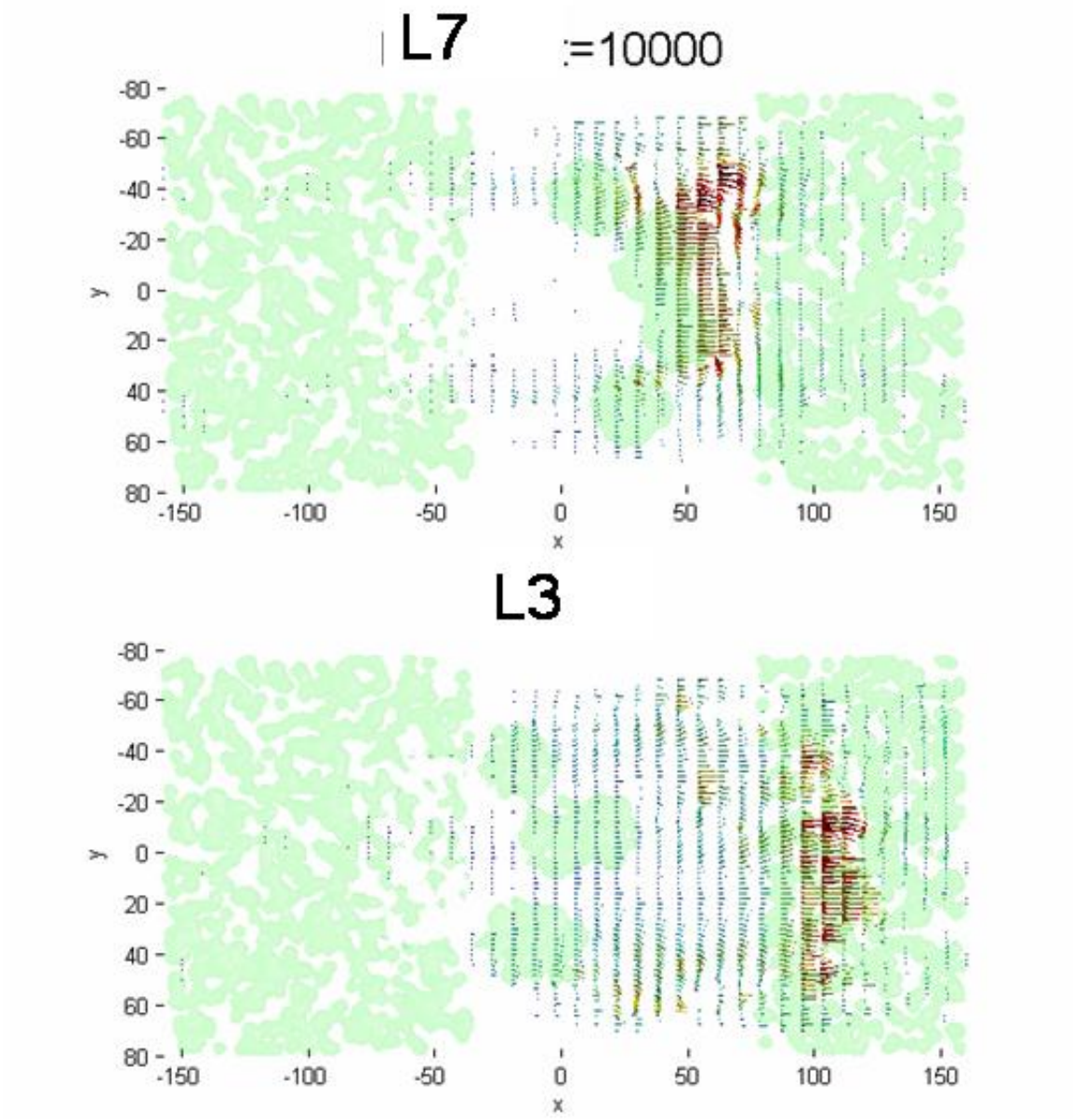

Figure 3- 31 Overhead perspective emphasizing differences in the wind fields between case study simulations L7 (top) and L3 (bottom) at t=10000.

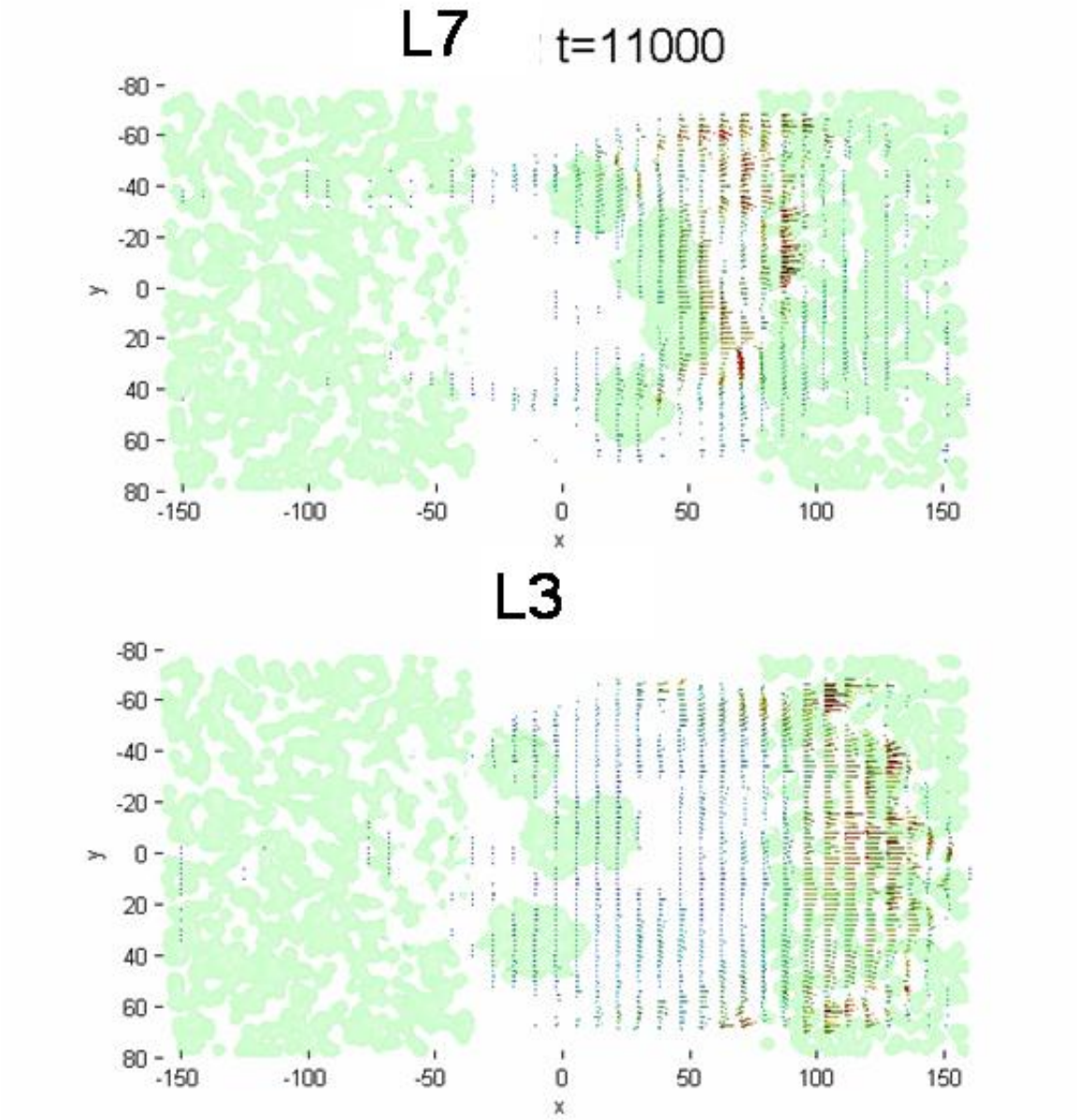

Figure 3- 32 Overhead perspective emphasizing differences in the wind fields between case study simulations L7 (top) and L3 (bottom) at t=11000.

DISCUSSION

The case study reveals that, despite similarities in the macroscopic spatial structure of fuels (as demonstrated by the nearly identical lacunarity curves and sum quantities of fuel), the significant differences that arose between the two simulations can be attributed to subtle fire-fuel-atmosphere interactions that occurred throughout the simulation. These interactions produced substantial differences in both incremental spread rates and in the overall spread rate.

In many cases these interactions developed over longer time and space scales but then manifested themselves in relatively short, discrete events. A significant turning point for the L3 simulation appears to have taken place around t=8000 where the wind field was accelerated by the burning crowns and channeled through the gap between the tree clumps. This event resulted in an accelerated incremental rate of spread that was more than three times the overall spread rate. For firefighters, an unexpected acceleration in fire spread can mean life or death; such an acceleration would not be addressed by operational fire models because the nature of their prediction of fire spread is only for a overall average rate of spread.

The fundamental problem with the overall average rate of spread used in operational fire models is that, without some knowledge of the variability around the average, and the spatial scale at which the average is expected to manifest itself, the overall average spread rate may be too vague to be of any value. In the approach used in operational models neither a characterization of the variability nor some description of the spatial scale in presented. This is a result of the approach used in constructing the Rothermel model, which required a reformulation of empirical results to a format more amenable to

use in fire danger indices (Rothermel 1972). It is curious to note, however, that an estimation of the variability around the average spread rate could be derived simply from the actual empirical data used in the development of the model. For example, a study detailing a large number of wind tunnel test burn experiments in four fuel types reported a coefficient of variation of 30% in the within-fire spread rate (Catchpole et al 1998).

It is important to realize that physical fire behavior models do not *predict* outcomes, but rather, they model the progression and *observe* the outcome. The dynamic factors involved belie prediction beyond generalizations which may or may not prove to be true given the potential impact of seemingly transient factors. In other words, physical models, given a set of initial and boundary conditions, are self-determining: they model fire behavior as it happens. It is not part of their architecture to concern themselves with what will happen: by their dynamics based nature they are capable of addressing what happens when it occurs. The overall spread rate is not stated in advance as a prediction but rather determined after the simulation is complete. Similarly, if given a detailed description of what happened in a given fire, a physical fire model could be used to determine why it happened. For this reason a simulation with a physical fire model is more akin to an actual test burn because no definitive expectation of results is explicitly stated beforehand.

A key finding of this study was that within-stand spatial variability in the fuels, which is currently not considered in any operational fire model, significantly influences the magnitude and nature of variability in fire spread rates. Variability in spread rates was

smallest, and most easily accounted for (i.e., normally distributed), when the fuels were not spatially clumped. As the spatial scale of clumping increased, variability in spread rates increased and the nature of the variability, measured with the skewness, changed. The higher skewness in the distributions of incremental spread rates in the more clumped fuels is problematic because it is less predictable. While the number of simulations in this study, and the duration of these simulations was too limited to broadly generalize, future testing with a larger sample size may reveal a stronger link between the spatial scale of fuel variability and variability in the spread rate. This suggests that it would be beneficial to begin developing a means for including some characterization of fuel spatial variability in maps of fuels. The lacunarity curve used here is appropriate for description of both landscape scale (Plotnick et al 1993) and within stand spatial variability (Fraser et al 2005); as it can easily be applied to remote sensing data, it shows some promise as a parsimonious measure of spatial variability which could be applied to wildland fuels. Further numerical and related field experiments are needed to explore these issues further.

The findings of this study have important implications for the role of modeling in fire management. Prediction of rate of spread has been the central emphasis in operational fire behavior for some time. The results of this study illustrate that prediction of rate of spread is of limited value without some characterization of the expected variability in that prediction. If prediction of rate of spread continues to be the focus, a paradigm shift may be needed in which greater emphasis is placed on the identification of the relative impact of different factors and on the range of potential outcomes that might arise. The results

presented here illustrate that ensemble or replicated simulations with physical fire models could be used to determine the magnitude of acceleration effects and their primary drivers, and thus identify the primary sources of variability in fire spread. The detailed mechanisms of fire behavior described by physical fire models could then provide guidance to simpler and computationally faster operational models which could leverage this information, statistically, to better account for variability in outcomes.

ACKNOWLEDGEMENTS

Material support for this work was provided by the USFS Rocky Mountain Research Station, Fire Sciences Laboratory. Significant support, both in terms of computing resources and in technical expertise was provided in this endeavor by Dr. Rod Linn and Jeremy Sauer at the Los Alamos National Lab, without whom this work could not have been completed.

LITERATURE CITED

Anderson, H. E. 1982. Aids to determining fuel models for estimating fire behavior. Page 22. USDA Forest Service Intermountain Research Station, Ogden, Utah, USA.

Andrews, P. L., C. D. Bevins, and S. R. C. 2005. BehavePlus fire modeling system, version 3: User's guide. General Technical Report. USDA Forest Service, Rocky Mountain Research Station, Fort Collins, CO.

Catchpole, W. R., E. A. Catchpole, B. W. Butler, R. C. Rothermel, G. A. Morris, and D. J. Latham. 1998. Rate of spread of free-burning fires in woody fuels in a wind tunnel. Combustion, Science and Technology **131**:1-37.

Cruz, M. G., M. E. Alexander, and R. H. Wakimoto. 2003. Assessing canopy fuel stratum characteristics in crown fire prone fuel types of western North America. International Journal of Wildland Fire **12**:39-50.

Finney, M. 1998. FARSITE: Fire area simulator--Model Development and Evaluation. United States Department of Agriculture, Forest Service Rocky Mountain Research Station, Research Paper RMRS-RP-4, Ogden, UT. 47pp.

Fons, W. L. 1946. Analysis of fire spread in light forest fuels. Journal of Agricultural Research **72**:93-121.

Fraser, G. W., M. A. Wulder, and K. O. Niemann. 2005. Simulation and quantification of the fine-scale spatial pattern and heterogeneity of forest canopy structure: a lacunarity-based method designed for analysis of continuous canopy heights. Forest Ecology and Management **214**:65-90.

Linn, R., J. N. Reisner, J. Colman, and J. Winterkamp. 2002. Studying wildfire behavior using FIRETEC. International Journal of Wildland Fire **11**:233-246.

Linn, R., J. Winterkamp, J. Colman, C. Edminster, and J. Bailey. 2005. Modeling interactions between fire and atmosphere in discrete element fuel beds. International Journal of Wildland Fire **14**:37-48.

Linn, R. R. 1997. Transport model for prediction of wildfire behavior. Scientific Report LA-13334-T, 195pp. Los Alamos National Laboratory, Los Alamos, NM.

Mell, W., J. J. Charney, M. A. Jenkins, P. Cheney, and J. Gould. 2005. Numerical simulations of grassland fire behavior from the LANL-FIRETEC and NIST-WFDS models. In Proceedings, EastFIRE Conference, George Mason University, Fairfax, VA. May 11-13, 2005.

Plotnick, R. E., R. H. Gardner, and R. V. O'Neill. 1993. Lacunarity indices as measures of landscape texture. Landscape Ecology **8**:201-211.

Press, W. H., S. A. Teukolsky, W. T. Vetterling, and B. P. Flannery 1996. Numerical Recipes in C: the art of scientific computing. Cambridge University Press, Cambridge, UK.

Reinhardt, E. D., J. H. Scott, K. Gray, and R. E. Keane. 2007. Estimating canopy fuel characteristics in five conifer stands in the western United States using tree and stand measurements. Can. J. For. Res. **36**:2803-2814.

Rothermel, Richard C. 1972. A mathematical model for predicting fire spread in wildland fuels. Res. Pap. INT-115. Ogden, UT: U.S. Department of Agriculture, Forest Service, Intermountain Forest and Range Experiment Station. 40 p..

Rothermel, R. C. 1991. Predicting behavior and size of crown fires in the Northern Rocky Mountains. Page 46. United States Department of Agriculture, Forest Service Intermountain Forest and Range Experiment Station, Ogden, Utah USA.

Scott, J. H., and E. D. Reinhardt. 2001. Assessing crown fire potential by linking models of surface and crown fire behavior. Research Paper. USDA Forest Service,Rocky Mountain Research Station, Fort Collins, CO.

APPENDIX A. LIST OF SYMBOLS AND THEIR MEANING, FOR THE FUEL3D MODEL

Table A- 1 List of Symbols and their meanings for the FUEL3D model.

Symbol	Description
	tree parameters
A_0	Stem cross sectional area at tree base
A_1	Stem cross sectional area at breast height
A_2	stem cross sectional area at crown base
A_3	minimum stem cross sectional
A_{BT}	sum of all branch basal cross sectional areas
A_{Bp}	cross sectional area of a parent segment
A_{Bi}	cross sectional area of a particular child segment at a branching node
D_0	Diameter at tree base
D_1	Diameter at breast height, cm
D_2	Diameter at crown base
D_3	Minimum stem diameter
D_B	diameter at base of a branch
H_1	breast height, = 1.37m
H_2	Height to live crown base,m
H_3	Crown length
H_T	Tree height,m
x_i	tree stem x coordinate for tree i
y_i	tree stem y coordinate for tree i
z_i	tree stem z coordinate for tree i
	Species and site parameters
ρ	average wood material density
ρ_f	average foliar material density
γ	ratio of child segment length to parent segment length
n	number of child branches at a branching node
C_1	coeff for folbm / xsa_hcb
C_2	coeff of sum branch xsa / xsa_hcb
C_3	crown heartwood taper form coefficient
C_4	crown stem wood taper form coefficient
C_5	Starter segment length / estimated total branch length
C_6	sum cross sectional area of child segments/ parent cross sectional area
C_7	proportion of biomass allocated dominant child at a branching node
ρ	average wood density
M_F	foliar biomass
M_1	woody biomass below crown base
M_2	woody biomass above crown base
M_{2s}	stem wood portion of woody biomass above crown base
M_{2b}	branch wood portion of woody biomass above crown base
M_{2bi}	branch biomass assigned to a particular branch
M_{fi}	foliar biomass assigned to a particular branch
V_1	Volume of wood below crown base
V_2	Volume of wood above crown base

V_{2s}	Volume of stem wood portion of crown
V_{2b}	Volume of branch wood portion of crown
L_T	predicted total branch length
l_o	initial segment length
l	a segment length
$\Re$	rotation matrix

Needle and foliar clump measurements

needle length	length of needle
needle radius	radius of needle
needle angle	angle between needles in a clump
n_needle	number of needles in a clump
fol_dens	material density of foliage
max_needle vertang	highest angle (where 90 is perpendicular to branch)
min needle vertang	smallest angle a needle has off the stem
between clump dist h	spacing of needle clumps along circumfrence
between clump dist v	spacing between whorls along the length of the branch

Branching control measurements

vert_nbr	n branches in a whorl on main stem
min_vertang	minimum vertical angle of branch, off stem
max_vertang	maximum vertical angle of branch, off stem
branch_angle	angle between branches
minr2	Lower limit on branch diameter
minr1	Diameter below which no branching occurs.
angvar	variability in angles

APPENDIX B: ANALYTICAL SOLUTION FOR THE DETERMINATION OF THE COEFFICIENTS OF THE QUADRATIC POLYNOMIAL FUNCTION DESCRIBING THE RADIUS OF THE TREE BOLE ABOVE THE CROWN BASE AS A TAPERING COLUMN.

The stem above the base of the tree crown is modeled separately from the branches in FUEL3D to facilitate flexibility in modeling of variability in branch size and geometry. This flexibility is essential in enabling the model to represent different species as well as for the representation of within-species variability in crown structure. Stem wood above the live crown base is modeled as a tapering column in which the change in radius over its length (from the base to the top) is described with a quadratic polynomial equation (Kozak et al 1969, Goulding and Murray 1975) of the form:

$$r = ax^2 + bx + c$$

Eqn. B- 1

where r is the radius of the tree bole, x represents height above height of the crown base and *a*, *b*, and *c* are coefficients of the polynomial. This is the same equation as presented in Chapter I, **Equation 1-14**. It is presented again here for the convenience of the reader.

The volume of stem wood above the crown base, to be modeled as a tapering column, is estimated by the equation below:

$$V_{2s} = \frac{C_4(H_3(A_3 + A_3 + (A_2 A_3)^{0.5}))}{3}$$

Eqn. B- 2

This equation is the same as in Chapter I, **Equation 1-15**. It is also presented here again for convenience. Since all inputs to the equation above are known, V_{2s} is determined. We rename V_{2s} as v here for convenience.

We then describe the volume v, in terms of the polynomial, above

$$v = \pi \int_0^h \left(ax^2 + bx + c\right)^2 dx$$

Eqn. B- 3

in which we integrate the circular cross section of the tree bole described by the circle with radius function r (described above, **Equation B-1**) over the crown length, *h*.

The radius at the base of this tapering column is known because the tapering column begins at the base of the live crown. This corresponds to the intercept coefficient, *c*.

We assume that the radius at the top of the tree, corresponds to a minimum radius defined as a species level parameter and determined from field sampling. We call this radius at the top of the tree *rh*.

We thus know 1) the radius at the bottom of the column, *c*, 2) the radius at the top of the column, *rh*, and the length between them, *h*.

We can then substitute these values into the equation for the polynomial and rearrange that equation such that parameter *b* is described in terms of *rh*, *c*,*h* (all of which are known), and *a* (still unknown):

$$rh = ah^2 + bh + c$$
$$rh = ah^2 + bh + r0$$
$$ah2 + bh = rh - r0$$
$$bh = rh - r0 - ah^2$$
$$b = \frac{rh - r0 - ah^2}{h}$$

Eqn. B- 4

As we know polynomial coefficient *c*, and we have rewritten coefficient *b* in terms of coefficient a, we need only to determine the value of polynomial coefficient *a*.

To do this we expand out the volume equation (**Equation B-3**), squaring the contents of the parentheses and combining like terms:

$$\nu = \pi \int_0^h \left(a^2x^4 + 2abx^3 + \left(2ac + b^2\right)x^2 + 2bcx + c^2\right)dx$$

Eqn. B- 5

We then integrate this equation

$$v = \pi\left[\frac{a^2x^5}{5} + \frac{2abx^4}{4} + \frac{\left(2ac+b^2\right)x^3}{3} + \frac{2bcx^2}{2} + c^2x\right]_0^h$$

Eqn. B- 6

Substituting known quantities, *rh* for *x*, and the known volume for the left hand side *v*, and rearranging the equation to solve for *a* gives us:

$$\mathrm{a} = \frac{\frac{1}{2}}{\frac{\pi}{h^3}}\left(5h\pi rh + 5\pi ch - \left(-15h^2\pi^2rh^2 + 10h^2\pi^2rhc - 15\pi^2c^2h^2 + 120\pi hv\right)^{\frac{1}{2}}\right)$$

Eqn. B- 7

At this point the polynomial function describes the radius of the tree in question from the base of the tree to the tree top, and subject to the constraints of measured species parameters such as wood density and minimum observed branch radius. This allows a precise determination of the volume, and associated woody biomass in any section described by lower limit h1 and upper limit h2 of this tapering column as

$$v_{\mathrm{sec}\,tion} = \pi\int_{h1}^{h2}\left(ax^2 + bx + c\right)^2 dx$$
$$m_{\mathrm{sec}\,tion} = v_{wection}\rho_{wood}$$

Eqn. B- 8

as well as the cross sectional area of the bole at any given height, x.

$$area = \pi\left(ax^2 + bx + c\right)^2$$

Eqn. B- 9

LITERATURE CITED

Goulding, C. J., and J. C. Murray. 1975. Polynomial taper equations that are compatible with tree volume equations. New Zealand Journal of Forest Science **5**:313-322.

Kozak, A., D. Munro, and J. H. G. Smith. 1969. Taper functions and their application in forest inventory. Forestry Chronicals **45**:278-283.

APPENDIX C: FIELD AND IMAGE PROCESSING BASED MEASUREMENT OF GEOMETRIC PARAMETERS.

DESCRIPTION OF FIELD STUDY

A field study was carried out at Ninemile on the Lolo National Forest near Missoula, Montana in July 2007 characterizing the whole tree and within branch geometry and allometric relationships needed for the FUEL3D model. This study was designed to complement an earlier study, called the crown fuels study (Scott and Reinhardt 2002, Reinhardt et al 2007), which emphasized biomass estimation but did not measure many geometric parameters. The 2007 field study was specifically designed to provide data needed to estimate geometric parameters. The field study consisted of destructive sampling of ten ponderosa pine trees, whole tree measurements, measurements on the whorls and branches.

Destructive sampling of trees

Ten Ponderosa pine trees were selected from the same stand. Several criteria came into play in the selection of these trees. A professional arborist assisted in the selection of all trees. First, all trees selected were qualitatively representative of the surrounding stand. An attempt was made to span a range of diameters but in general the stand was fairly homogeneous; the trees were thus of generally similar diameter and height Second, because the intention was to destructively sample the trees quickly but with minimal damage to the crown, each tree selected had to have at least one adjacent trees from which a restraining system (described below) could be established. Third, to minimize the aesthetic impacts of the tree removal, it was desirable that the trees removed be reasonably spaced from each other. When not in conflict with other criteria more central

to the study, trees were selected for removal such that other trees could be expected to benefit.

Once trees were selected, a professional arborist supervised the felling of the trees. Each tree was felled using a restraining system in which ropes and pulleys connecting the tree in question to one or more adjacent trees could be used to control the rate at which the tree came down. For additional control the cuts were made in such a way that a good deal of holding wood was left. This also slowed the trees fall. In several cases the trees descended slowly and did not actually hit the ground but were instead suspended from the ropes a short distance from the ground. The trees which were not suspended came to the ground slowly and with minimal impact. These careful measures ensured that the tree crowns were accessible for further measurement and processing but were undamaged.

Direct measurements

Once the trees were close to the ground, total tree height and height to the base of the live crown were directly measured on the tree with a tape held level and taut. Using the same tape, the height of each whorl was measured and tree diameter was measured, at breast height and at each whorl, with a standard metric diameter tape. The crown of each tree was then cut into smaller more workable sections one to three meters long, numbered and laid out in order.

Whorl measurements

On each section, measurements relating to the pipe model and allometric relationships were taken at each whorl. These measurements included the stem diameter below the whorl, the number of first order branches (which branch of the main tree stem), basal diameter of each branch, and the diameter of the stem above the whorl, angle from the vertical tree stem to each branch, total branch length, and the length on each branch between the branch base and the first branching node. Branch diameters were taken with metric digital calipers and angles were measured with transparent plastic angle gauges.

Branch measurements

Every third branch was cut off at the base, labeled and laid out in order on a tarpaulin for additional measurement and processing. These branch level measurements included counts of second order branches and of foliage clumps, branching angles and diameters at randomly selected branching nodes, and diameters at which foliage appeared on the branch.

Measurements made from digital images

These measurements served as a straightforward set of direct utility in the parameterization of the model. However, in many ways it is difficult to convey the whole pattern of a branching structure from just a few measurements. It is also prohibitively slow to carry out a great number of direct measurements on individual branches in the field. For this reason an apparatus was set up to facilitate recording using high resolution digital imagery (**Figure C-1**), and subsequent post field processing to aid in the quantification of branching patterns using semi-automated image processing procedures.

At the field site a 6 foot tall portable scaffold was leveled and secured with guy wires on a flat location.

Figure C- 1 Scaffold used to set up a downward facing digital camera for image processing based measurements of tree branch geometry.

Figure C- 2 An example branch image collected with the digital camera for the purpose of image-based branch measurements.

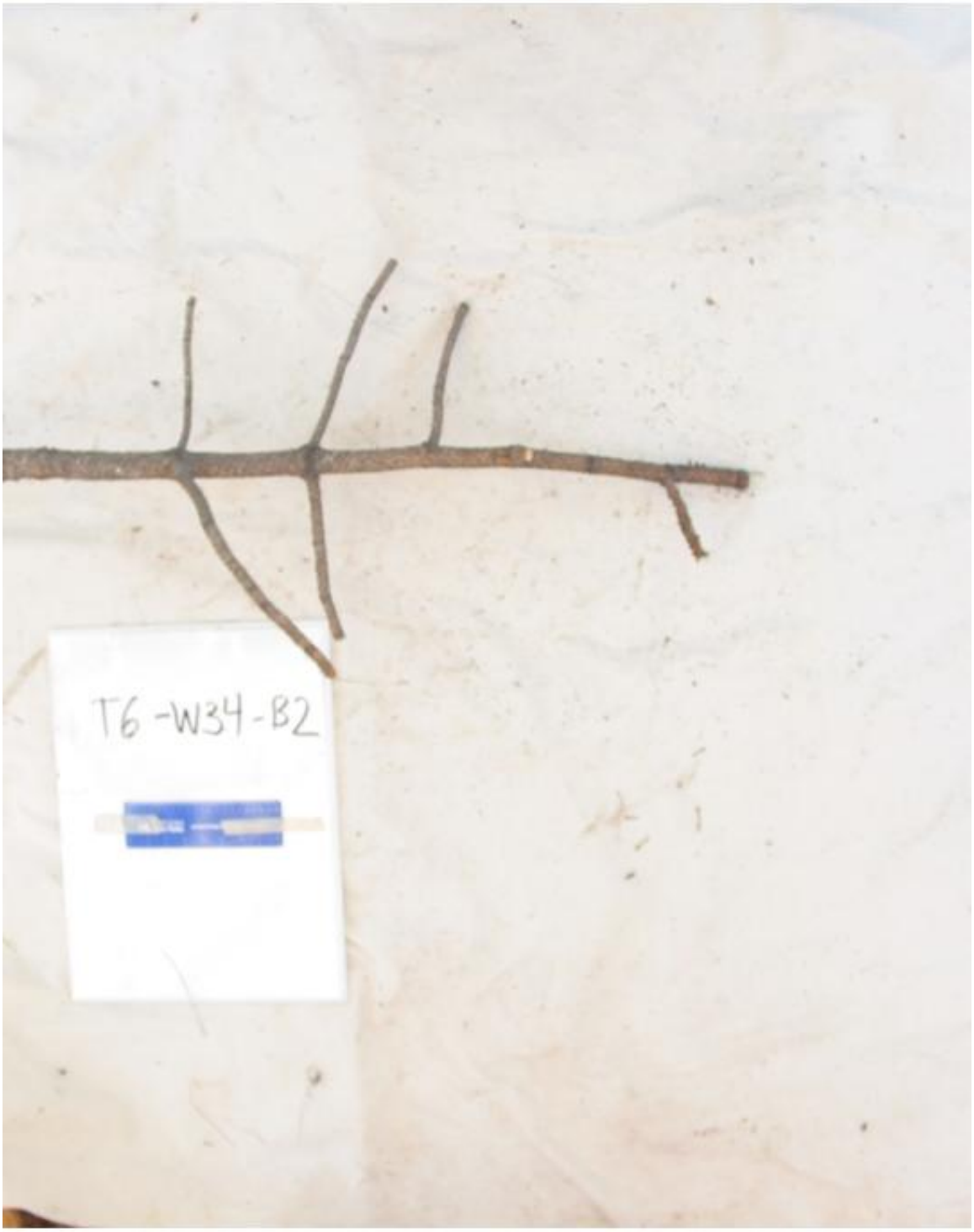

Figure C- 3 Example branch following clipping of foliage.

Securely clamped to the top of the scaffold was a device extending another 2 feet higher, and three feet outward from the scaffold, which was designed to hold a digital camera such that the camera is oriented directly downward (normal to the ground). A Canon PowerShotG5, 5.0 Megapixel digital camera was set on this device, leveled in two planes with carpenters levels, and also secured with guy wires to prevent lateral movement. A large canvas structure was set up to protect the equipment from the elements and to shade the area of the camera's view from direct sunlight. The camera was connected to a laptop computer via a USB cable and specialized software developed for use with the camera, PSRemote v1.54 (BreezeSys Software 2007 REF), was installed on the laptop. The specialized software allowed the camera to be operated remotely, including zoom and other adjustments, from the laptop, where what would be seen in the viewfinder would appears on the laptop screen. This arrangement was important to the image capture process because it enabled the field of view of the camera to be modified without having to climb up on the scaffold. A white canvas backdrop was set out on the flat area directly under the camera, and a dry erase board was used to include the appropriate labeling information in each branch image captured. Attached to the dry erase board was a high contrast ruler such that subsequent measurements made on the image could be calibrated to a known distance.

Before the branch was set up for digital image capture, it was stripped of moss. The backdrop was swept clean after each branch. Each sampled branch was then placed on the backdrop. A preview image of the branch was taken using the remote controlled digital camera and laptop to ensure that the branch was fully contained in the camera's

field of view. Two images were then taken for each branch. In the first image nothing was removed, so the entire pattern of foliage and material in the branch could be seen (**Figure C-2**). Then, holding the branch in the same position, foliage was clipped off, as well as any branches which extended vertically (towards the camera) (**Figure C-3**). Because material that extends vertically can result in distortions in image-based measurements (because the distance between the object and the camera is not consistent), branches that were retained were partly cut when necessary such that they could lie as flat as possible. In general no material extended vertically above the backdrop by more than 10 centimeters.

Subsamples of the branches were subjected to additional processing. Thirty smaller branches were placed in paper bags, labeled and taken in their entirety back to the lab. These samples were oven dried in the lab for 72 hours at 95 degrees Celsius, then weighed to determine dry weight of wood and foliage. Sections of woody components of these samples were cut into cylindrical pieces, the ends were sanded, and weighed. Measurements of all dimensions were made with digital calipers, two measurements for each of length, outside diameter at both ends and inside diameter at both ends (to determine bark thickness). The bark was then peeled off and the woody segments were then re-weighed and material density was calculated for wood directly and for bark by subtraction from the original volume.

Fifteen smaller branches which consisted of single woody section and a foliage clump were cut longitudinally such that the remaining foliage in the clump laid flat. Detailed

digital images were taken of these cut clumps, with the camera zoomed in to just a small area, for the description of needle dimensions and other properties of terminal structures, using the same general approaches as described above.

Image processing

The branch images with foliage were generally not used quantitatively as the foliage tended to obscure the structure of the branches. However, these images proved to be very useful in qualitative assessment of the overall geometry and pattern of the branches.

A semi-automated process was developed by which detailed measurements could be made from the digital images of the clipped branches. The process consisted of three stages: pre-processing, in which the digital images were prepared for the measurement process, basic measurements, and post processing, in which more involved measurements were assembled from the basic measurements.

Image preprocessing

The objective of preprocessing was to convert the full color field photos taken of individual tree branches to clean binary images which could then be analyzed more easily. Forested environments present challenges for any kind of photography because there is significant variability in the nature and quality of light, ranging from bright spots where sunflecks hit the forest floor to deep shadows. This variability in light intensity can be reduced by taking pictures at particular times of day, such as in the early morning, but it is not always feasible to restrict image capture to relatively narrow windows in time.

Images were taken in this study during daytime hours and under variable sunlight, so a number of preprocessing steps had to be done before the quantitative measurements could be done consistently on the images.

The first preprocessing step was to calibrate the image such that measurements made in pixel distances (i.e., some number of pixels between two points) could be converted to standard distance units (centimeters). This was done with on-screen digitization, by displaying the image on the computer, zooming in on the high contrast ruler located on the dry erase board, and interactively measuring the distance along the edge of the ruler (**Figure C-4**).

Figure C- 4 Calibration of distance in pixels on the image to distance in standard units (centimeters). Green plus signs indicate the portion of the image which was zoomed in interactively to facilitate precise on-screen digitization of the refererence scale.

Next the image was cropped to a smaller rectangle including the branch; this helped to improve the processing time as the overall image size was reduced. The image was then converted from 24-bit color to an unsigned 8-bit grayscale image by discarding information describing the hue and saturation of the image while retaining the luminance. Contrast was enhanced with a standard histogram stretching procedure. The cropped, higher contrast image was then converted to a binary (0's and 1's) image with a common thresholding procedure (Otsu 1979). The image was then reversed, such that the branch had a value of 1 (white) and the background was 0 (black). Speckling within the branch portion of the image was removed using the morphological reconstruction method (Soille 1999) (**Figure C-5**).

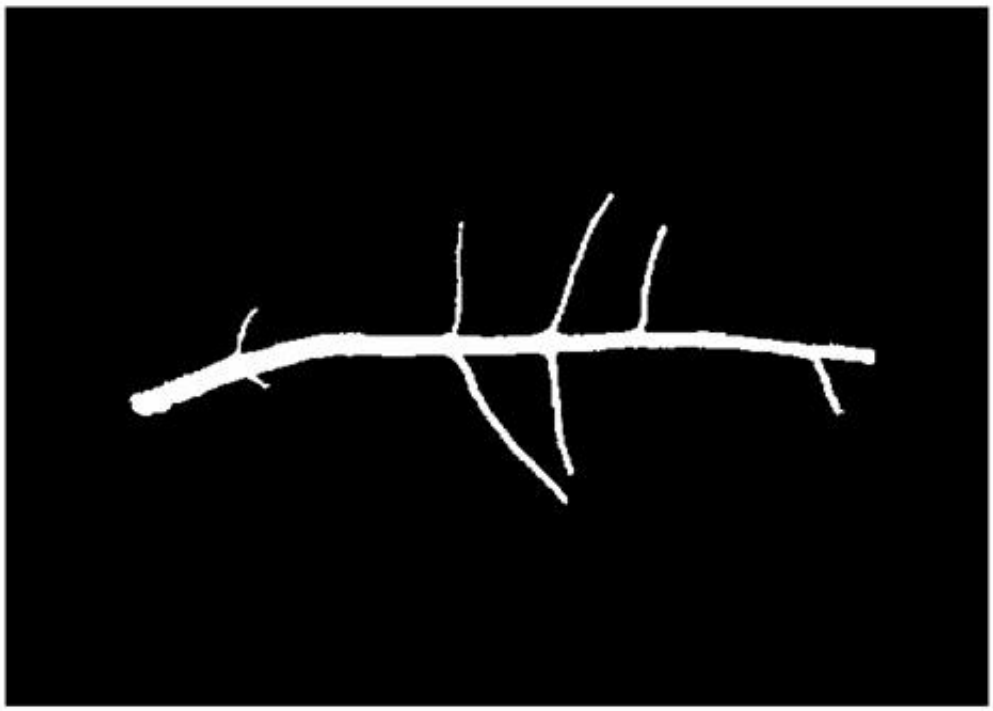

Figure C- 5 Example binary image of tree branch used in semi-automated image processing based measurement of tree branch geometry.

Finally, the edge pixels of the black and white image of the branch were smoothed out to eliminate fine scale features such as the scales in the bark. Earlier tests of the algorithm had determined that these small irregularities were problematic for processing because they made it more difficult to consistently identify branching nodes. This smoothing was accomplished with a two-stage dilation / erosion approach, in which the perimeter of an object in the image is iteratively expanded out (dilation) and then eroded inward (van den Boomgaard and van Balen 1992). When used in this manner, this approach does not affect the overall geometry or dimensions of objects in the image but the perimeter is smoother and easier to work with. The cells comprising the smoothed perimeter were extracted for use in image measurement algorithm, described below.

Algorithm for basic image measurements

The automated measurement process of the image begins at the cell on the perimeter closest to the upper left corner of the image. The algorithm deals with one perimeter cell and other cells in its local spatial context, then moves the calculation in a counter clockwise direction to another cell along the perimeter.

As the algorithm cycles through the cells along the perimeter, it tests for whether the cell in question can be considered as part of a branching node or not. This test is done by evaluating the intersection of an annulus (figure comprised of an outer and inner ring, like a tire or a donut) centered on the perimeter cell in question with the cells on the branch in the vicinity of the annulus. The cell in question is classified as being one of

three cases, based on the number of discrete regions identified by the annulus. The first case is a branch tip, in which there is only one region within the annulus. The second case is that of a point along the length of a branch, in which two regions are identified from the annulus intersection. The third case, a branching node, is identified if more than two distinct regions are found to intersect the annulus. The outer and inner dimensions of the annulus are set as a user specified parameter.

If the cell in question is identified as being a point along the length of the branch, the width of the branch (from the cell in question across to the other side of the branch) is measured. To do this a set of nearby cells along the perimeter and on the same side of the cell in question are sampled (a total number of such cells and an interval between them are specified by the user). The equation for the line best representing the coordinates and passing through the cell in question is determined by least squares. This fitted line represents a straight line generally parallel to the edge of the branch and which is tangent to the cell in question. From this line the equation for the line perpendicular to this line is determined. The algorithm then searches for the intersection of the cells comprising the perimeter and this perpendicular line. The coordinates of the closest intersection are recorded, and from these coordinates the width of the branch along that perpendicular line is calculated. A midpoint is determined between the two points and is saved in an array for processing in subsequent steps. This process is repeated until the entire

perimeter is spanned.

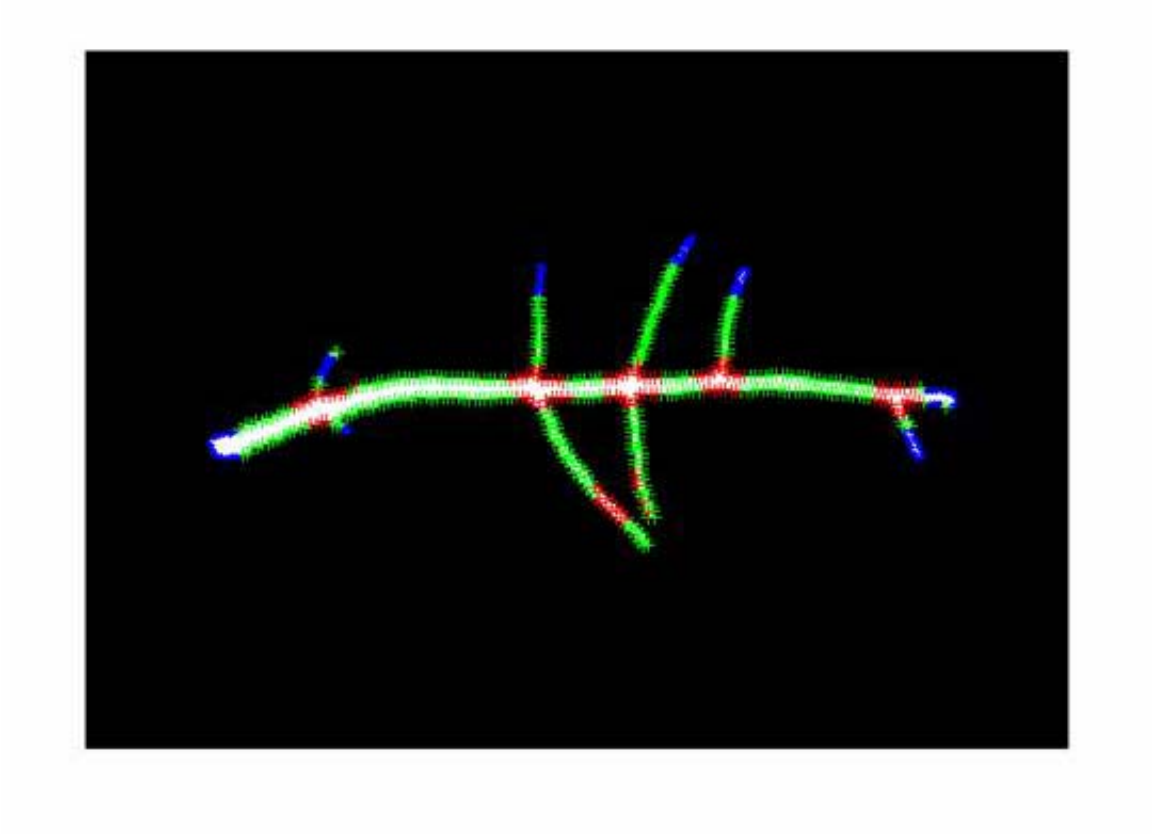

Figure C- 6 Example branch image processed with the following features identified: green – portions along the length of a branch where diameter measurements can be made. Blue: portions near branch ends where diameter measurements may be suspect. Red: portions near branching nodes where diameter measurements are likely to be suspect. For the most part the automated process correctly identified these regions; erroneous identifications, such as the branching nodes (red) on the lower two second order branches, were later removed manually.

inventory of branching nodes

Before proceeding further, the algorithm assembles a list of the perimeter coordinates which qualified as being portion of a branching node. The algorithm then assigns a temporary identifier to each set of perimeter cells which are spatially contiguous.

Subsequent steps consolidate these sets into groups which together lie around a common node and assign a unique node identifier to those cells. Additional testing is done to eliminate false nodes which can arise due to the peculiarities of the geometry of a branch (**Figure C-6**).

A centroid coordinate is calculated from the perimeter cells common to each branching node.

Calculation of angles and lengths

Angles are calculated between each set of three midpoints. Angles between such midpoints along the length of the branch are used to estimate curvature, while angles in the vicinity of branching nodes are used to estimate angles between branches.

Similarly, lengths are calculated over each branch section (between branching node centroids, and farthest branch tip cells). Angles and lengths are assembled in an array for further analysis in post processing.

post processing

In the post processing stage each branching node is associated with a group of measurements, including angles, lengths and widths. Altogether these assembled branching nodes then describe ‘branching objects’ used as basic building blocks in the FUEL3D model.

Determination of geometric parameters from field and image processing based measurements

Once the measurements were assembled from direct measurement and from the image processing based measurements, most of the parameters are simple ratios or other basic calculations made from those measurements. The majority of parameters were simply determined with simple descriptive statistics (i.e mean, μ and standard deviation, σ) of those calculations over a number of sample measurements.

A table presenting these straightforward measured values, as well as more detailed descriptions of calculations made in the parameterization of the model for ponderosa pine is presented in **Appendix D**, below.

LITERATURE CITED

BreezeSys_Software. 2007. PSRemote v1.54. Software which permits remote operation of a Canon PowerShot Digital Camera from a computer via a USB cable.

Otsu, N. 1979. A threshold selection method from Gray-Level histograms. IEEE Transactions on Systems, Man, and Cybernetics **9**:62-66.

Reinhardt, E. D., J. H. Scott, K. Gray, and R. E. Keane. 2007. Estimating canopy fuel characteristics in five conifer stands in the western United States using tree and stand measurements. Can. J. For. Res. **36**:2803-2814.

Scott, J. H., and E. D. Reinhardt. 2002. Estimating canopy fuels in conifer forests. Fire Management Today **62**:45-50.

Soille, P. 1999. Morphological image analysis: principles and applications. Springer-Verlag.

van den Boomgard, and v. Balen. 1992. Image transforms using bitmapped binary images. Computer vision, graphics and image processing: Graphical models and image processing **54**:254-258.

APPENDIX D: MODEL PARAMETERIZATION FOR PONDEROSA PINE

The FUEL3D model requires parameters describing the geometry of each species. The model was parameterized for Ponderosa pine from measurements made in two separate studies. The first study, known as the Crown Fuels Study, took place from 2000 to 2002 and consisted of destructive sampling of all trees within sample plots in five locations in the western United States. This study is described in detail in several publications (Scott and Reinhardt 2002, Reinhardt et al 2007). Of the five locations, three had data for ponderosa pine (Flagstaff, AZ,, Ninemile, MT, and Blodgett, CA). Data from the Flagstaff and Ninemile locations in the in the early stages of development of the FUEL3D model, as well as for parameterization of several important quantities and relationships, described below. The second study was carried out in Montana in 2007 and was designed to provide information not available from the Crown Fuels Study needed to parameterize geometry of Ponderosa pine trees.

Parameterization from Crown Fuels Study

Prediction of total branch length

FUEL3D requires an empirical equation for the total branch length, L_T, as a function of the basal diameter of a branch, D_B (here in cm). Initial inquiries with this data, consisting of 2207 individually measured branches on 78 trees determined this relationship as a power function relationship of the form

$$L_T = 0.47 D_B^{0.99}$$

Eqn. 1- 33 $R^2 = 0.77$

However subsequent work determined that a number of the branches used in that analysis were dead or otherwise unsuitable; analysis on more refined data determined a relationship with improved fit as

$$L_T = 0.6369 D_B^{0.8909}$$

Eqn. 1- 34 $R^2 = 0.968$

Beta parameters describing the distribution of branch basal diameters

The Beta distribution is used in FUEL3D to allow flexibility in the number and size of branches on a tree, so the parameters used in the model serve as a user input. To determine a range of reasonable values for the Beta distribution, maximum likelihood estimation procedures were used to fit the Beta distribution to the distribution of branch diameters on each tree (Hahn and Shapiro, 1994). The parameter values were variable and appear to vary with the competitive status of the tree (i.e. dominant, suppressed). Average values for the *v* and *w* parameters, of 2.35 and 74.1, respectively, are used as default values for the model.

Site level parameters

Additionally, the detailed biomass estimation from that study was used to determine two site level parameters, C_1 and C_2, which relate the foliar biomass MF, and the sum branch cross sectional area, to the cross sectional area at the base of the live crown, A_2 , respectively. For each tree, the individual values of parameters C_1 and C_2, C_{1i} and C_{2i}, were calculated as follows:

$$C_{1_i} = \frac{M_{Fi}}{A_{2i}}$$

$$C2_i = \frac{A_{BTi}}{A_{2i}}$$

Eqn. 1- 35

where M_{Fi} was the total foliar biomass from the tree (from destructive sampling), A_{2i} was the estimated cross sectional area at the base of the live crown for that tree, and A_{BTi} is the total branch cross sectional area for that tree.

For the Flagstaff site the average value of C_1 was 519.34; for the Ninemile crown fuels site this value was 612.8, reflecting a higher site productivity at that location. Both values are similar to those reported in other studies for loblolly pine (Valentine et al 1994) and Scots pine (Berninger and Nikinmaa 1997). The value of C_2 for the two sites was 1.366 for the Flagstaff site and 1.582 for the Ninemile site.

Parameterization of tree geometry

The crown fuels study emphasized biomass estimation but did not address branch geometry. A second study was carried out at Ninemile on the Lolo National Forest near Missoula, Montana in July 2007 characterizing the whole tree and within branch geometry and allometric relationships needed for the FUEL3D model. The procedures used in collecting this data are new, and required development of a semi-automated image processing based system for measurement of branches.

Table D- 1 Parameters describing Ponderosa pine geometry for the FUEL3D model determined from field data.

Parameter / Symbol	Description	μ	σ	source
	Site Parameters			
C_1	foliar biomass to cross sectional area at base of live crown coefficient	519.6	9.1	1
C_2	sum branch cross sectional area to cross sectional area at base of live crown coefficient	1.38	0.15	1
	Species Parameters			
C_3	crown volume heartwood taper form	.5	--	3

	coefficient			
C_4	crown stem wood taper form coefficient	1.26	0.16	2
C_5	length to first 2nd order branch, as proportion of total branch length	0.2	0.03	2
C_6	ratio of sum child segment cross sectional area to parent segment cross sectional area	1.06	0.14	2
C_7	proportion of sum child segment cross sectional area allocated to dominant branch	0.65	0.04	2
n	Number of child segments at a branching node (see below)	2	--	2
branch_angle	angle between branches at a branching node	76	7.1	2
min_ diam1	Smallest branch diameter on a tree (cm)	0.41	0.04	2
min_diam2	Branch diameter below which no branching occurs(cm)	0.94	0.11	2
n branch_whorl	Number of branches at a whorl (see below)	2	--	2
min_ang_whorl	Smallest angle (vertical) of branch off stem at whorl	10	3.4	2
max_ang_whorl	largest angle (vertical) of branch off	110	12.1	2

	stem at whorl			
d_whorl	distance between whorls, m	0.148	0.04	2

Foliage Clump Parameters

n_needle_clump	Number of needles in a fascicle	3	--	2
needle_length	Length of a needle, cm	15	1.1	2
needle_radius	radius of a needle, mm	0.51	0.02	2
needle_angle	Angle between needles within a fascicle	5	0.4	2
min_v_angle	minimum angle of faciscle off stem of needle clump	10	0.4	2
max_v_angle	maximum angle of fascicle off stem of needle clump	75	5	2
clump_dist_h	distance between fascicles along branch circumference (mm)	4.1	0.3	2
clump_dist_v	distance between needle whorls (cm)	1.3		2

Source: 1 Crown fuels study (Scott and Reinhardt 2002) 2 Field study July 2007, detailed in Appendix C. 3 From literature: Makela and Valentine 2006

n: number of child branch segments at a branching node

At each branching node the number of child segments was counted. A histogram was then assembled over all branching objects. From this histogram a probability distribution

function was determined. FUEL3D uses this probability distribution function l to determine how many child branching segments to insert at each branching node. The number of child segments with the greatest frequency was 2.

nbranch_whorl: number of branches at a whorl, including the continuing mains stem.

Similar to the parameter, n, above, a histogram was assembled describing the number of branches at each whorl. FUEl3D uses this histogram to determine the number of branches at a whorl.

Coefficient C4: Crown stem taper form coefficient

The crown stem taper form coefficient, C_4, was determined from the whorl data collected in the 2007 field study. This coefficient describes the ratio of the volume of a tapering column, extending from the base of the live crown, to the top of the tree, and described with a quadratic polynomial, to the ratio of a truncated cone with the same end radii. The analytical solution for the quadratic polynomial taper is described in detail in **Appendix B**. This was calculated for each of the ten trees sampled in 2007. A quadratic polynomial taper was fit to the diameters measured at each whorl, and the resulting polynomial was then integrated to determine the volume. The coefficient C_4, was determined by dividing that volume by the volume of a truncated cone with the same base and top areas.

LITERATURE CITED

Berninger, F., and E. Nikinmaa. 1997. Implications of varying pipe model relationships on Scots Pine growth in different climates. Functional Ecology **11**:146-156.

Hahn, G. J., and S. S. Shapiro 1994. Statistical models in engineering. John Wiley & Sons

Makela, A., and H. T. Valentine. 2006. Crown ratio influences allometric scaling in trees. Ecology **87**:2967-2972

Reinhardt, E. D., J. H. Scott, K. Gray, and R. E. Keane. 2007. Estimating canopy fuel characteristics in five conifer stands in the western United States using tree and stand measurements. Can. J. For. Res. **36**:2803-2814.

Scott, J. H., and E. D. Reinhardt. 2002. Estimating canopy fuels in conifer forests. Fire Management Today **62**:45-50.

Valentine, H. T., A. R. Ludlow, and G. M. Furnival. 1994. Modeling crown rise in even-aged stands of Sitka spruce or loblolly pine. Forest Ecology and Management **69**:189-197.